INFORMATION TO USERS

This manuscript has been reproduced from the microfilm master. UMI films the text directly from the original or copy submitted. Thus, some thesis and dissertation copies are in typewriter face, while others may be from any type of computer printer.

The quality of this reproduction is dependent upon the quality of the copy submitted. Broken or indistinct print, colored or poor quality illustrations and photographs, print bleedthrough, substandard margins, and improper alignment can adversely affect reproduction.

In the unlikely event that the author did not send UMI a complete manuscript and there are missing pages, these will be noted. Also, if unauthorized copyright material had to be removed, a note will indicate the deletion.

Oversize materials (e.g., maps, drawings, charts) are reproduced by sectioning the original, beginning at the upper left-hand corner and continuing from left to right in equal sections with small overlaps. Each original is also photographed in one exposure and is included in reduced form at the back of the book.

Photographs included in the original manuscript have been reproduced xerographically in this copy. Higher quality 6" x 9" black and white photographic prints are available for any photographs or illustrations appearing in this copy for an additional charge. Contact UMI directly to order.

UMI

A Bell & Howell Information Company
300 North Zeeb Road, Ann Arbor MI 48106-1346 USA
313/761-4700 800/521-0600

Factors Influencing the Regiochemistry of Nucleophilic Addition to the Radical Cation of Alkenes and Dienes Studied in the Context of the Photochemical Nucleophile-Olefin Combination, Aromatic Substitution (Photo-NOCAS) Reaction

by

Mary S.W. Chan
B.Sc. (Hons.), Calgary

Submitted in partial fulfilment of the requirements
for the degree of Doctor of Philosophy

at

Dalhousie University
Halifax, Nova Scotia
January 1998

DALHOUSIE UNIVERSITY

FACULTY OF GRADUATE STUDIES

The undersigned hereby certify that they have read and recommend to the Faculty of Graduate Studies for acceptance a thesis entitled "Factors Influencing the Regiochemistry of Nucleophilic Addition to the Radical Cation of Alkenes and Dienes Studied in the Context of the Photochemical Nucleophile-Olefin Combination, Aromatic Substitution (Photo-NOCAS) Reaction"

by Mary S.W. Chan

in partial fulfillment of the requirements for the degree of Doctor of Philosophy.

Dated: January 26, 1998

External Examiner

Research Supervisor

Examining Committee

DALHOUSIE UNIVERSITY

DATE: February 3, 1998

AUTHOR: Mary S. W. Chan

TITLE: Factors Influencing the Regiochemistry of Nucleophilic Addition to the Radical Cation of Alkenes and Dienes Studied in the Context of the Photochemical Nucleophile-Olefin Combination, Aromatic Substitution (Photo-NOCAS) Reaction

DEPARTMENT OR SCHOOL: Chemistry

DEGREE: Ph. D. CONVOCATION: May YEAR: 1998

Permission is herewith granted to Dalhousie University to circulate and to have copied for non-commercial purposes, at its discretion, the above title upon the request of individuals or institutions.

[redacted]
Signature of Author

To the Canadian Tax Payers

Table of Contents

List of Figures

List of Tables

Abstract

The regiochemistry of nucleophilic addition to the radical cations of simple alkenes and dienes was studied. Three nonsymmetric dienes [4-methyl-1,3-pentadiene (**5**), 2,4-dimethyl-1,3-pentadiene (**6**) and 2-methyl-1,3-butadiene (**7**)] and two alkenes [2-methylpropene (**8**) and 2-methyl-2-butene (**9**)] were examined in detail with methanol or fluoride ion serving as the nucleophile. The regioselectivity of each alkene or diene was determined by the product ratio from the photochemical nucleophile-olefin, combination aromatic substitution (photo-NOCAS) reaction. The relative stabilities of the reaction intermediates were estimated with *ab initio* molecular orbital calculations.

Distonic radical cations are initially formed upon the addition of methanol to the alkene or diene radical cation. The relatively low energy of the bridged structure provides a pathway for the equilibration of the two alternative open structures at the distonic radical cation stage. The regiochemistry is determined by irreversible deprotonation from the oxygen to form β-alkoxyalkyl radicals. The product resulting from the more stable β-alkoxyalkyl radical is favored, implying that the regiochemistry of methanol addition is thermodynamically controlled.

The possibility of a bridged structure does not exist for β-fluoroalkyl radicals. This eliminates the opportunity for the equilibration of the radical intermediates. The addition of fluoride occurs in a single irreversible step. Therefore, the product distribution is not a reflection of the thermodynamic stability of these radical intermediates. There is evidence to suggest that polar and steric factors are important. This leads to the conclusion that the addition of fluoride is kinetically controlled.

Results from theoretical calculations show that the more heavily substituted β-substituted alkyl radical is not necessarily the more stable. Calculations for substituted alkanes suggest that alkyl substitution on the carbon bearing the functional group can have significant effects on the relative stability of these compounds. Studies involving the methoxy, fluoro, cyano and isocyano groups exhibit a correlation between the magnitude of this effect with the electron demand of the functional group. For the more electronegative substituents, stabilization by the alkyl groups on the carbon bearing the functional group becomes larger than on the carbon bearing the radical center, thus reversing the trend expected when considering radical stability alone.

List of Abbreviations

A	electron acceptor
a	encounter distance
Ar	4-cyanophenyl, unless otherwise noted
CRIP	contact radical ion pair
D	electron donor
d	doublet
δ	dimensionless (nmr) scale
dc/fc	dry column/flash chromatography
ΔG_{ET}	free-energy for electron transfer
e_o	elementary charge, 1.60219×10^{-19} C
eV	electron volt
ε	relative dielectric constant
ε_o	permittivity of vacuum, 8.854×10^{-12} $C^2N^{-1}m^{-2}$
$E_{o,o}$	electronic excitation energy
EA	electron affinity
FRI	free radical ions
gc/fid	gas chromatography/flame ionization detector
gc/ms	gas chromatography/mass selective detector
HOMO	highest occupied molecular orbital
HSAB	hard-soft-acid-base principle
IP	ionization potential
ir	infrared spectrum
K	proportionality coefficient, 8.988×10^9 Nm^2C^{-2}
LUMO	lowest unoccupied molecular orbital
m	multiplet

m/z	mass-to-charge ratio
nmr	nuclear magnetic resonance
photo-NOCAS	photochemical nucleophile-olefin, combination aromatic substitution
PET	photoinduced electron transfer
q	quartet
tlc	thin layer chromatography
s	singlet
SSIP	solvent separated radical ion pair
WCOT	wall coated open tubular

All other abbreviations are standard.

Acknowledgments

I would like to thank my research supervisor, Dr. Arnold, for his continued support and for showing me the true colors of academic research. My fellow labmates, Peter de Lijser and Dino Mangion, brightened my days in the lab with their eagerness to help and cheerful conversation. A special thanks to Kim McManus for putting up with my endless complaining, for sharing the good times as well as the bad, and for the yummy lunch outings.

The work presented in this thesis would not have been possible without the generous support of numerous people in the department of chemistry. I would like to express my gratitude to Dr. Boyd and his group (particularly Jian Wang, Jaime Martell and Kent Worsnop) for helping me with the theoretical calculations and solving my computer problems, to Drs. Hooper and Lumsden for helping me with obtaining and interpreting my nmr spectra, to Jurgen Müller for the interesting conversations and for keeping my glassware supply healthy, and to Dr. Kim for the exact mass measurements. I would also like to thank Drs. Pacey, Burford and Pincock for their helpful discussions regarding my research project.

A special mention is reserved for teddy, who kept me focused on my work with his endless support and encouragement. I will always remember and cherish his friendship and guidance. His help in reading this thesis and his willingness to share his computer resources are also much appreciated.

I am grateful for scholarships from the Natural Sciences and Engineering Research Council of Canada, the Izaak Walton Killam Memorial Foundation, the Walter C. Sumner Foundation and the Department of Chemistry at Dalhousie University.

Chapter 1

General Introduction

1.1 Photoinduced Electron Transfer

The transfer of an electron from one molecule to another is a fundamental process that promotes chemical reactivity, and for this reason, electron transfer processes have been studied extensively in many areas of chemistry. This process initiates chemical reactions by generating reactive radical ion pairs. There is a variety of methods for producing radical ions from neutral molecules. Chemical methods include the use of oxidants,[1] acids,[2] or halogens.[3] Radical ions can also be generated electrochemically[4] or in mass spectrometers.[5] More relevant to the work described in this thesis is the formation of radical ion pairs by photoinduced electron transfer (PET). PET is believed to be one of the fundamental process for photosynthesis and has attracted much attention from chemists as well as molecular biologists over the last few decades.[6] Applications of PET processes can be found in organic synthesis,[7] solar energy storage systems,[8] environmental decontamination methods,[9] photosynthesis,[10] and photodynamic therapy of tumors.[11]

The energetics of electron transfer between two molecules in the gas phase are governed by the ionization potential (IP) of the donor and the electron affinity (EA) of the acceptor. IP is defined as the energy required to remove an electron from the highest occupied molecular orbital (HOMO) of a molecule while EA is the energy gained by adding one electron to a molecule. Both of these processes refer to a molecule in the ground state and electron transfer is favorable when the EA of the acceptor is greater than the IP of the donor. Light absorption of an appropriate wavelength can promote one electron from the HOMO to the lowest unoccupied molecular orbital (LUMO). The effect of this excitation on the IP and EA of a molecule is depicted in Figure 1.1. Effectively,

photo excitation decreases the IP by $E_{0,0}$ (the HOMO-LUMO energy gap) if the molecule is acting as a donor, because the electron can now be removed from the LUMO of the ground state molecule instead of the HOMO. Similarly, the EA increases by $E_{0,0}$ if the molecule acts as an acceptor because the electron can be accommodated by the HOMO of the ground state molecule. Figure 1.2 shows the effect of photo excitation on the energetics of electron transfer between two molecules. The electron transfer is evidently much more favorable when one of the partners is in an excited state.

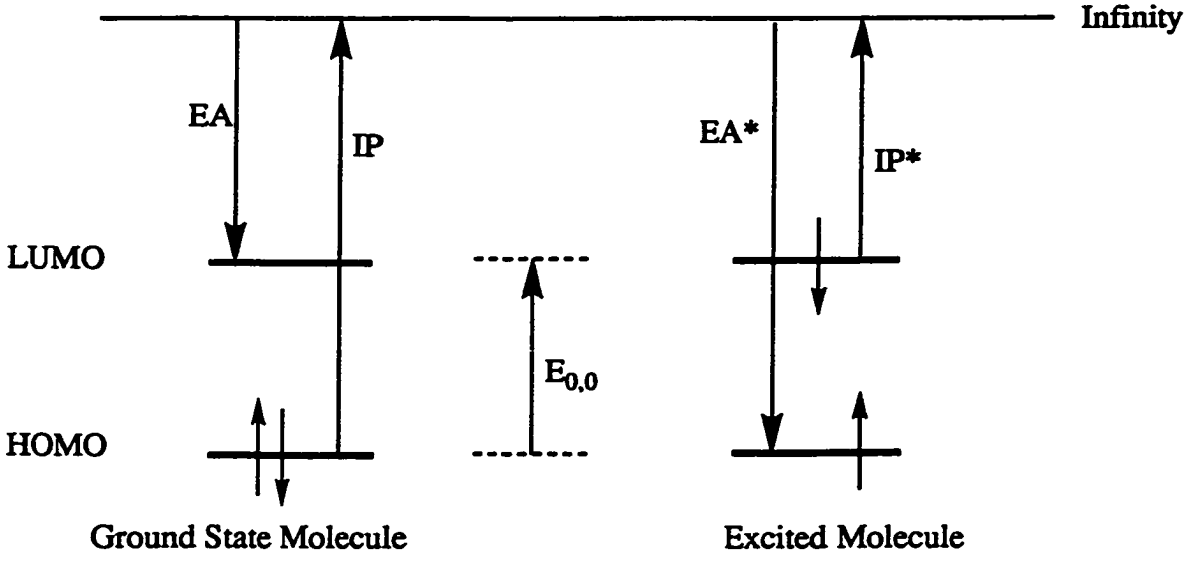

Figure 1.1: The Effect of Photo Excitation on Ionization Potential and Electron Affinity

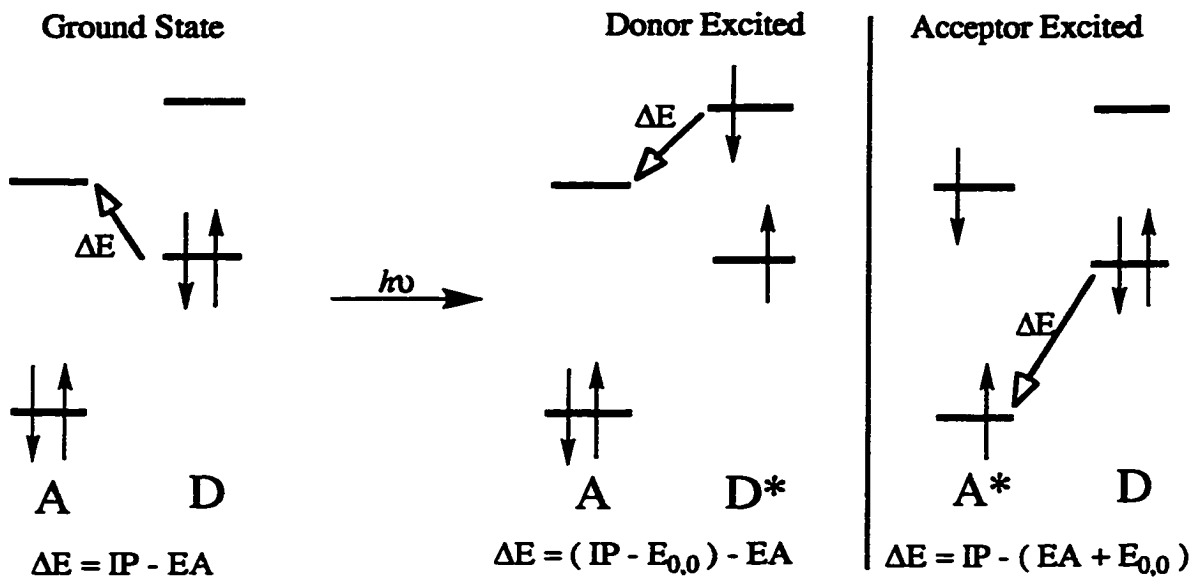

Figure 1.2: The Effect of Excitation on the Energetics of Electron Transfer

The ΔE shown in Figure 1.2 cannot be directly applied to photoinduced electron transfer in solution because it does not take into account solvent and Coulombic interactions. The Weller equation for electron transfer takes these factors into account.[12] The most practical and commonly used form of this equation is expressed by Equation 1.1. In solution, the ionization potential and electron affinity are replaced with oxidation and reduction potentials, respectively. The factor $e_o/\varepsilon a$ can be considered to be the free energy gained by bringing two radical ions to an encounter distance "a" in a solvent of dielectric constant ε.

$$\Delta G_{ET} = F\{E(D/D^+) - E(A/A^-) - Ke_o/\varepsilon a\} - E_{0,0} \qquad [1.1]$$

where:

ΔG_{ET} = free energy of electron transfer (J/mol)
F = Faraday constant (96 485 C/mol)
$E(D/D^+)$ = oxidation potential of the electron donor (V)
$E(A/A^-)$ = reduction potential of the electron acceptor (V)
K = constant of the Coulomb equation ($1/4\pi\varepsilon_o$)
ε_o = permittivity of vacuum (8.854×10^{-12} $N^{-1}m^{-2}C^2$)
e_o = charge of an electron (1.60219×10^{-19} C)
ε = relative solvent dielectric constant
a = separation distance of the radical ions (m)
$E_{0,0}$ = electronic excitation energy (J/mol)

Electron transfer will be feasible if ΔG_{ET} calculated from Equation 1.1 is negative.

Consequently, this equation states that photoinduced electron transfer in solution is

influenced by the electronic properties of the substrates and the polarity of the solvent. The more easily the donor is oxidized and the more easily the acceptor is reduced, the more electron transfer is thermodynamically favored. Polar solvents facilitate the formation of radical ions, whereas non-polar solvents increase the efficiency of back electron transfer, a process that returns the substrates to the ground state. Back electron transfer decreases the reaction efficiency and can be an important deactivating pathway for chemical reactions that occur via photoinduced electron transfer. Some practical methods used to reduce the rate of back electron transfer include the addition of salts or altering the electrostatic nature of the donor-acceptor pair in the ground state.[13] For example, if one started with either a charged donor or acceptor, then the species formed after electron transfer are not electrostatically attracted to each other. Examples of electron-donating carbanions and electron-accepting carbocations have been reported.[14]

The rate of electron transfer was determined to be a function of the free-energy. This process can be expected to occur at the diffusion-controlled rate if ΔG_{ET} calculated from Equation 1.1 is more negative than -17 kJ/mol.[15] Once electron transfer has taken place, a contact radical ion pair (CRIP) is initially formed. This can then be solvated to produce the solvent separated radical ion pair (SSRIP) if the conditions are favorable. The SSRIP can eventually diffuse apart to form the free radical ions (FRI). These labels describe the extent of separation between the radical cation and radical anion, and a pictorial representation of these ion pairs is shown in Figure 1.3.

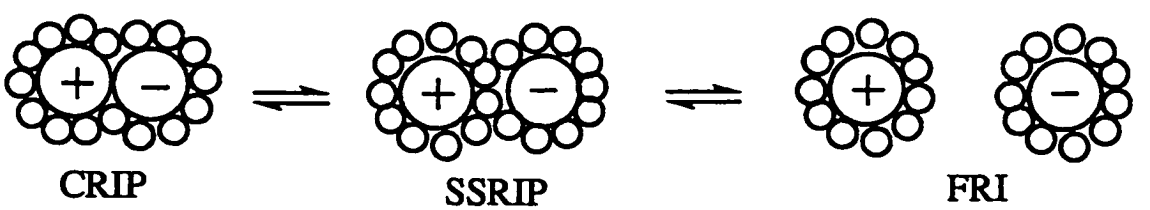

Figure 1.3: Pictorial Representation of the Types of Radical Ion Pairs.

The radical ions generated in this way can undergo a number of different chemical reactions. The product distribution of the reaction is generally dependent on which of these radical ion pairs dominate under the reaction conditions employed. Some examples of reactions involving radical ions include: E-Z isomerization,[16] ring opening,[17] deprotonation,[18] carbon-carbon bond cleavage,[19] cyclization,[20] nucleophilic addition[21] and dimerization.[22] The main focus of this research, however, was on identifying the factors that influence the regiochemistry of nucleophilic addition to the radical cations of simple alkenes and dienes. The investigations were carried out in the context of the photochemical nucleophile olefin combination, aromatic substitution (photo-NOCAS) reaction.

1.2 Addition Reactions to Alkenes

1.2.1 Electrophilic Additions

One of the fundamental reactions of alkenes is electrophilic addition. The mechanism requires the attack of an electrophilic species on an electron rich double bond to produce a positively charged intermediate. Combination of this intermediate with a nucleophilic species present in the reaction mixture produces the final addition product. Common electrophiles include mineral acids, water, alcohols, halogens and diborane. The regioselectivity of this addition usually gives Markovnikov-type products for all electrophiles except with diborane, where anti-Markovnikov products are obtained after oxidation of the boron intermediates. Markovnikov's rule was originally based on observations of the addition of hydrogen halides to non-symmetric alkenes. For electrophilic addition, Markovnikov's rule states the positive portion of the reagent goes to the side of the double or triple bond that has more hydrogens. This regioselectivity can be explained by the rationalization that the electrophile adds to the side that will give the more stable carbocation.[23] Of particular relevance to the work covered in this thesis is the addition of alcohols and fluorine to alkenes and conjugated dienes.

The addition of alcohols to double bonds can be achieved under acidic or basic conditions. In an acid catalyzed reaction, the mechanism is electrophilic with the proton being the attacking species and the resulting carbocation combining with another molecule of alcohol. As expected, the regiochemistry follows Markovnikov's rule.[24] The addition of alcohols to substituted cyclohexene and cycloheptenes is also observed to occur photochemically under neutral conditions.[25] The regiochemistry also follows Markovnikov's rule as shown by the example in Figure 1.4. It is postulated that this photochemical reaction also occurs through a carbocation intermediate.

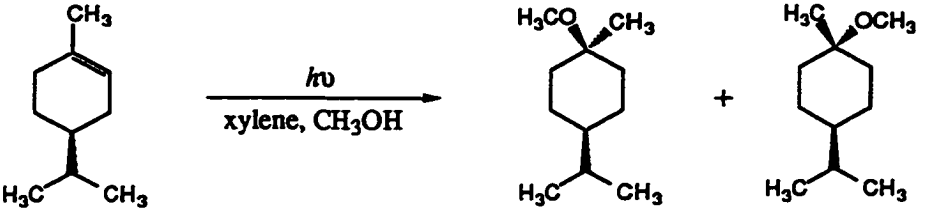

Figure 1.4: Photochemical Addition of Methanol to a Substituted Cyclohexene

The addition of fluorine to double bonds can be achieved in a number of ways depending on the substrate and the desired product. The addition of hydrogen fluoride across a double bond has been carried out with a large variety of compounds. This reaction occurs by the electrophilic mechanism and the orientation of addition is in accord with Markovnikov's rule.[26] However, selective fluorination using ordinary hydrogen fluoride or elemental fluorine is usually unsucessful because of their highly reactive, toxic and corrosive nature. As a result, the search for fluorinating agents that will promote selective fluorination of organic compounds has been subjected to intense research.[27] Both electrophilic and nucleophilic sources of fluorine have been investigated. Examples of nucleophilic sources of fluorine include tetraalkylammonium fluoride salts in combination with sources of positively charged halogens such as N-haloacetamides or N-halosuccinimides.[28] As shown by the examples in Figure 1.5, the reaction displays

Markovnikov-type regioselectivity when reacting with non-symmetric alkenes. These reactions were postulated to occur by the normal electrophilic addition mechanism where the halogen (bromine) adds as the electrophile followed by attack of fluoride anion on the carbonium ion intermediate.

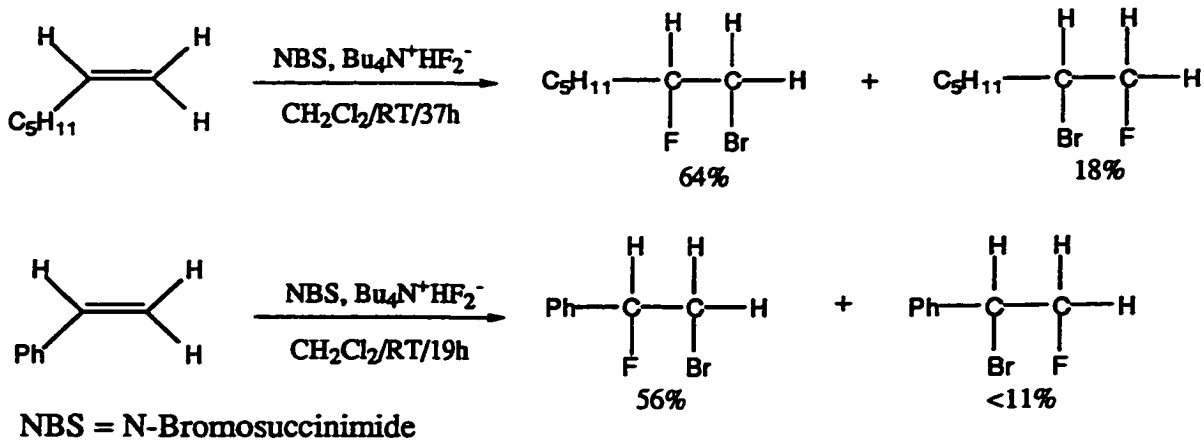

NBS = N-Bromosuccinimide

Figure 1.5: Examples of Reactions Involving Nucleophilic Sources of Fluorine

One class of electrophilic sources of fluorine involves the incorporation of a reactive N-F bond in various organic molecules. One such reagent is 1-fluoro-4-hydroxy-1,4-diazoniabicyclo[2.2.2]octane bistetrafluoroborate (1).[29] In the presence of an external nucleophile such as water, methanol or acetic acid, (1) reacts with non-symmetric alkenes to form vicinal fluoro-hydroxy, -methoxy or -acetoxy derivatives following Markovnikov-type regioselectivity. In the absence of added nucleophile, however, mono-fluorinated alkanes were isolated with certain substrates (Figure 1.6). They appear to be the result of *anti*-Markovnikov type addition, but the mechanism for the formation of these products has not been resolved.

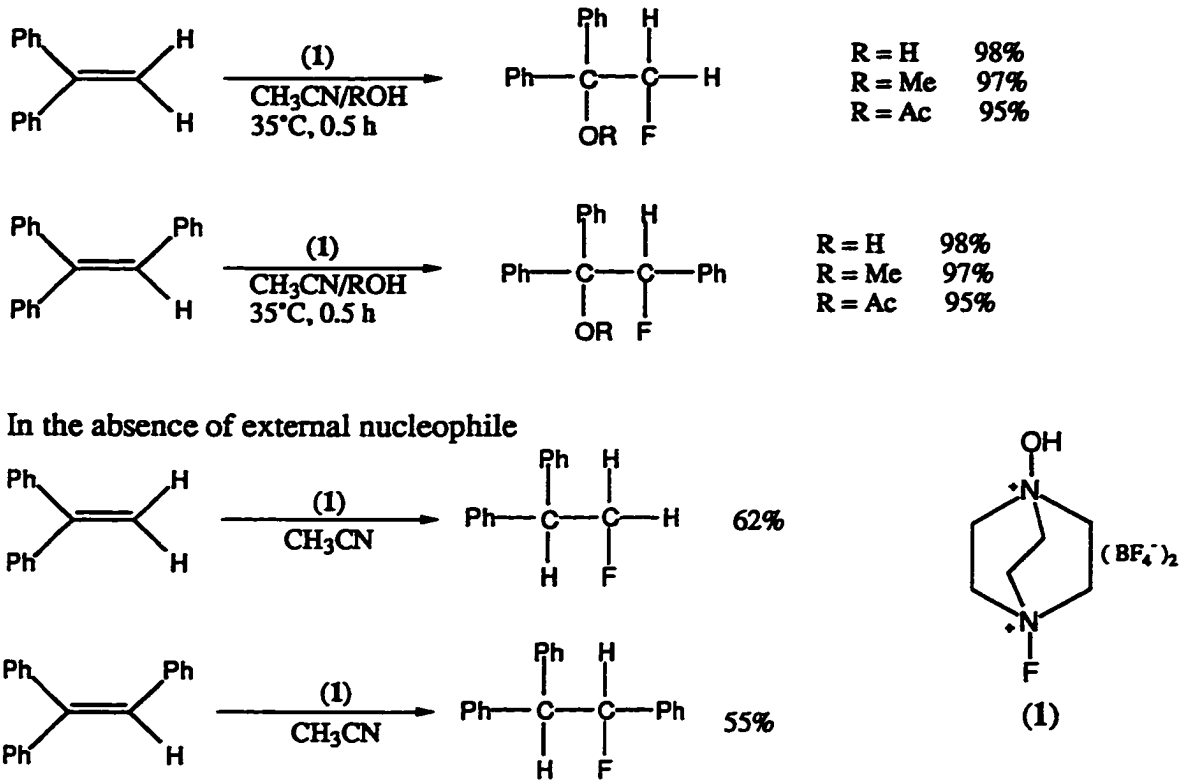

Figure 1.6: Reactive N-F Bonds as a Source of Fluorine

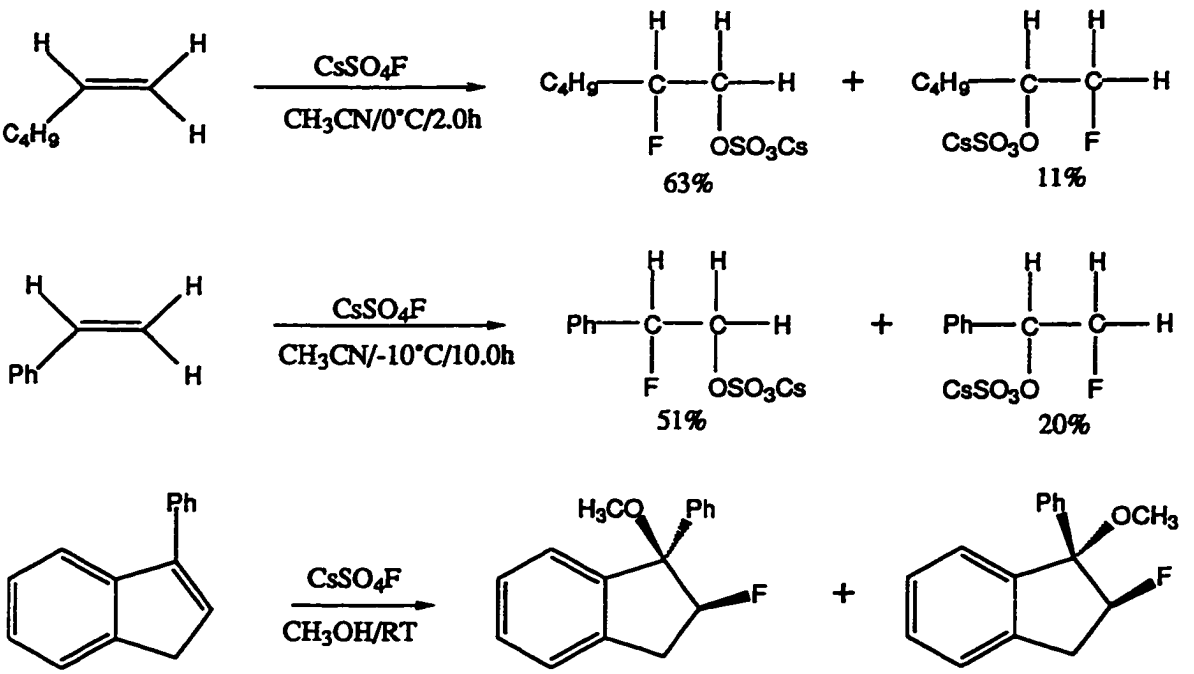

Figure 1.7: Cesium Fluoroxysulfate as a Source of Fluorine

Another fluorinating agent that has received a considerable amount of attention is cesium fluoroxysulfate.[30] Figure 1.7 shows some reactions of this reagent with a few non-symmetric alkenes. The regioselectivity appears to be following the Markovnikov mode of addition. However, as the regioselectivity is dependent on the substrate and the mechanism for this reaction has not been firmly established, it remains unclear what species is actually reacting as the electrophile.

1.2.2 Radical Additions

The addition of radicals to neutral alkenes is governed by a complex interplay of steric, polar and enthalpy factors. Which of these factors dominates is dependent on the specific substrate used. The reaction is often influenced by several factors whose effects are difficult to separate. Thus, the separation of the factors for specific substrates, using theoretical models and principal component analysis, is the focus of recent research in this area.[31] Even though the reaction is substrate dependent, some generalizations can be made about its regiochemistry. The regiochemistry is determined in the initial addition step, and the preferred orientation of addition for a free radical to non-symmetric alkenes is almost exclusively at the less substituted carbon of the double bond, giving *anti*-Markovnikov products. This regioselectivity is mostly attributed to the steric strain associated with the formation of the new bond,[32] and not to the relative stability of the radical intermediates as was originally postulated.[33] However, polar effects can be the deciding factor if there is no significant difference in the size of the substituents on the two ends of the double bond.

As mentioned in Section 1.1, radical ions can be generated by photoinduced electron transfer (PET). Some radical ions generated in this way can undergo bond cleavage to produce free radicals, which in turn, can participate in addition reactions in the presence of olefins.[34] The advantage of this method is that reactive (not resonance stabilized) alkyl radicals can be generated in organic solvents under mild conditions. As expected, the radical adds preferentially to the less substituted carbon when reacting with

non-symmetric alkenes. Under the reaction conditions studied, the adduct radical can be reduced to the anion by the radical anion of the photosenitizer. Proton abstraction by this anion gives *anti*-Markovnikov addition products (Fig. 1.8, path a). A side reaction of the adduct radical is coupling with the anion radical of the electron acceptor (usually an aromatic compound). This reaction pathway ultimately leads to aromatic substitution products and the acronym ROCAS (radical-olefin coupling aromatic substitution) has been used to describe this type of reaction (Fig. 1.8, path b).[34a]

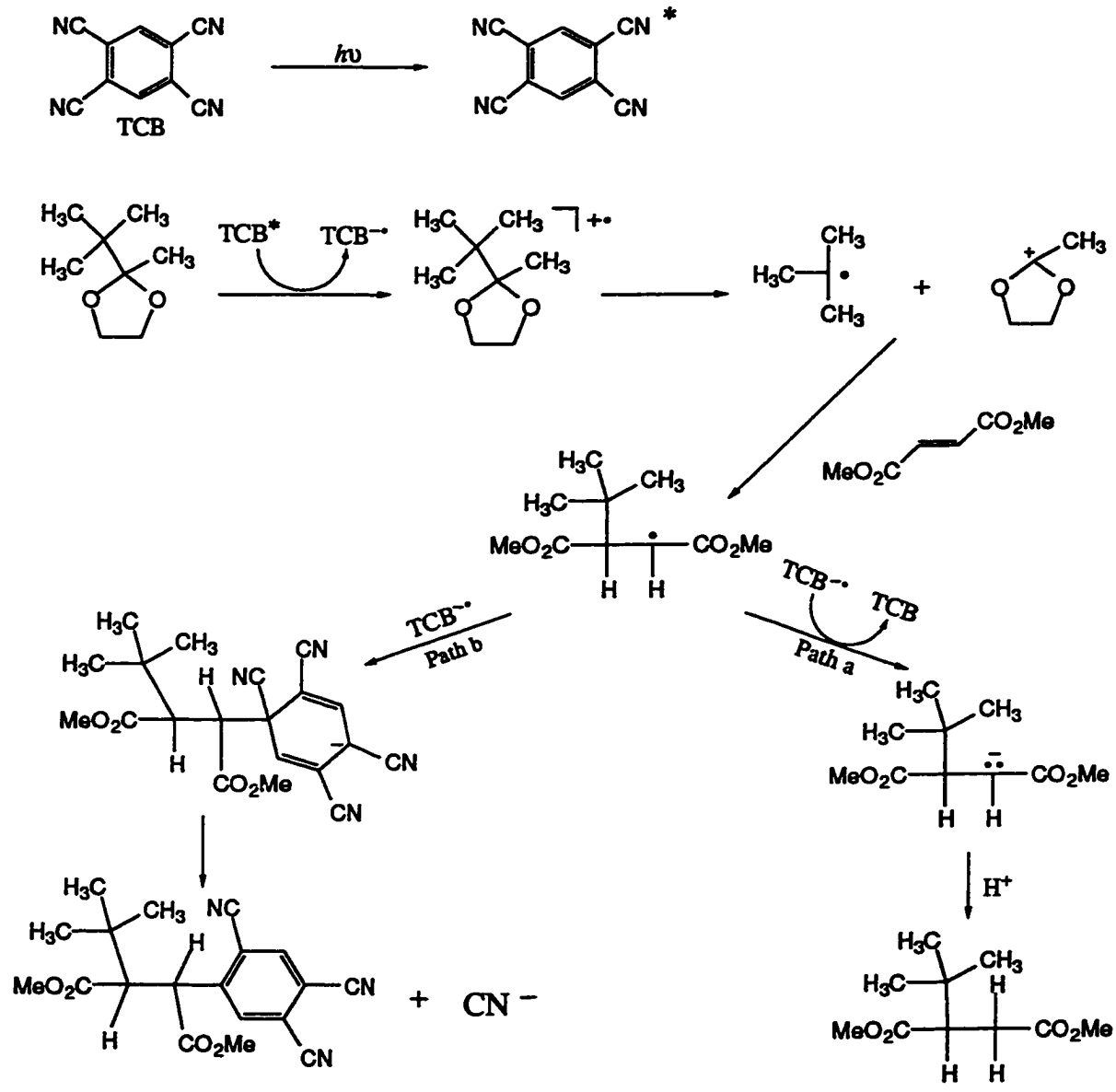

Figure 1.8: Reaction Pathways of Radicals Generated by PET

1.2.3 Nucleophilic Additions to Radical Cations

Radical cations of alkenes are susceptible to nucleophilic attack as ionization converts the alkene from an electron rich species to an electron deficient one. One way of generating radical cations in the presence of nucleophiles is by photoinduced electron transfer (PET). Additions of alcohols,[21,35] cyanide,[36] and ammonia[37] to the radical cation of a variety of alkenes generated in this manner have been investigated by product analysis. Laser flash photolysis studies have also been applied to the reaction of various nucleophiles with the styrene radical cation.[38] The regiochemistry of nucleophilic addition generally follow the *anti*-Markovnikov mode of addition. Attempts have been made to determine the factors that influence this regiochemistry with ammonia serving as the nucleophile. In the proposed mechanism for photoamination, the radical cation of the alkene is generated via PET. Nucleophilic addition of ammonia initially produces an aminated radical cation that deprotonates to give an aminated radical. This radical is then reduced to the anion, and this followed by reprotonation results in the aminated products. The reaction proceeds via three different types of intermediates: the radical cation of the alkene, the aminated radical and the aminated anion. Kojima and co-workers used PM3-HF calculations to determine the positive charge density distributions of the radical cations, the relative stability of the aminated radicals and anions for thirteen phenyl-substituted dienes.[37a] The relative stability of the aminated anions was the only property that agreed with experimentally determined product ratios for all of the dienes. These authors concluded that the regioselectivity was determined by the relative stability of the aminated anions.

The addition of water to the radical cation of small alkenes has been subjected to rigorous theoretical treatment as model systems to understand the mechanism of nucleophilic addition.[39] The latest treatment, by Zipse, maps the gas phase potential energy surface for the addition of water to the ethylene radical cation at the PMP4/6-311+G**//UMP2/6-31G* level.[39a] The essential points of the potential energy surface are

reproduced in Figure 1.9. The addition of water to the ethylene radical cation results in the open distonic radical ion (structure (2) in Figure 1.9) as the most stable species. However, the water molecule in this structure is only weakly bound, and it can easily move from one end of the ethylene moiety to the other through a low lying symmetrically bridged transition structure (structure (3) in Figure 1.9). All of the structures considered were much more stable than the sum of the energy of the isolated water molecule and ethylene radical cation. Attempts to locate a transition structure for the addition were unsuccessful beginning from a variety of geometries. It was concluded that the addition of water to ethylene radical cation is a highly exothermic process that occurs without a barrier in the gas phase.

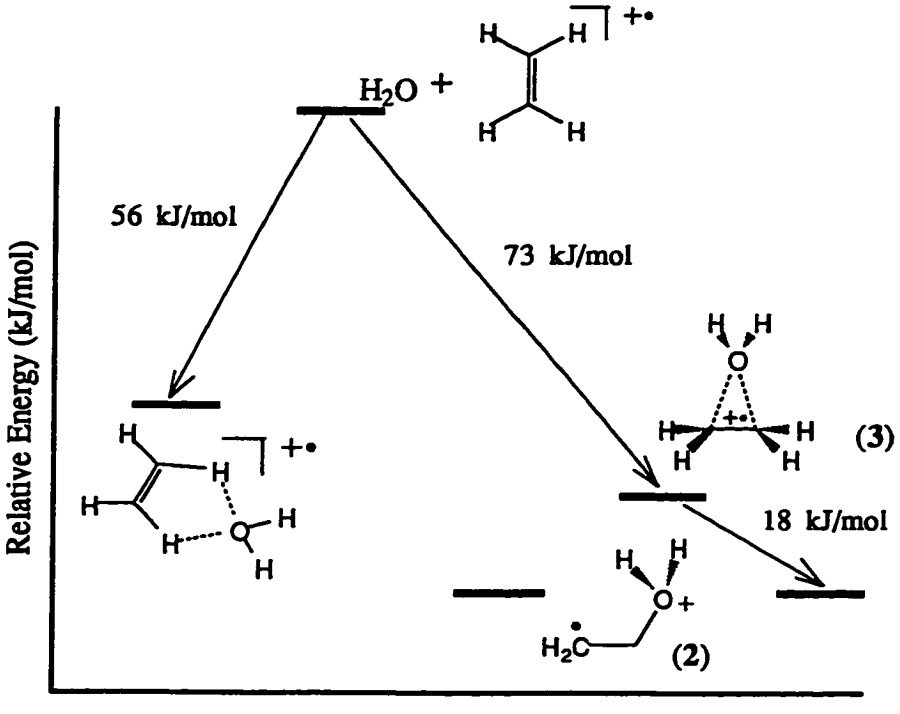

Figure 1.9: Gas Phase Potential Energy Surface for the Addition of Water to the Ethylene Radical Cation

The addition of water to small alkyl-substituted alkene radical cations such as propene and *trans*-butene have also been investigated.[39a,d] In general, it was found that

addition to alkyl-substituted alkenes is less exothermic than addition to ethylene. The increase in reaction enthalpy was attributed to the significant stabilization of alkene radical cations by alkyl substituents. Another observation was the preference of these substituted alkenes to form bridged structures rather than open distonic radical cations. In fact, the bridged structure was the most stable intermediate for the addition of water to the radical cation of *trans*-butene. It was not possible to obtain the geometry of an open distonic radical cation (analogous to structure (2) for ethylene) without restricting the C-O bond length. The species obtained in this manner is located 12 kJ/mol above that of the bridged structure.

1.3 The Photochemical Nucleophile-Olefin Combination Aromatic Substitution (photo-NOCAS) Reaction

The photo-NOCAS reaction achieves nucleophilic addition and aromatic substitution to produce a bifunctional compound starting from an olefin in one simple step. One of the first examples of this reaction was the combination of indene, 1,4-dicyanobenzene and alcohols observed by Majima and co-workers.[40] However, the product, 1-(4-cyanophenyl)-2-methoxyindan, was only isolated in low yields. The scope of the photo-NOCAS reaction, with respect to the olefin, has now been studied extensively.[19,20,21,41] Reasonable yields were obtained from a wide variety of olefins ranging from simple alkenes to terpenes and alkenols. Figure 1.10 shows a few examples of the photo-NOCAS reaction. The reaction, with respect to the aromatic species, has also been investigated, but it was concluded that 1,4-dicyanobenzene displays the most desirable photophysical properties to facilitate this reaction.[21e] The proposed mechanism, using 2,3-dimethyl-2-butene as a sample olefin, is shown in Figure 1.11. The reaction is initiated by photoinduced electron transfer, the resulting olefin radical cation is then attacked by the nucleophile to give a β-substituted radical. This radical then couples with the radical anion of 1,4-dicyanobenzene. Finally, rearomatization by the loss of cyanide

ion produces the photo-NOCAS product(s). The following sections contain a more detailed description of some of the more important processes involved in this mechanism.

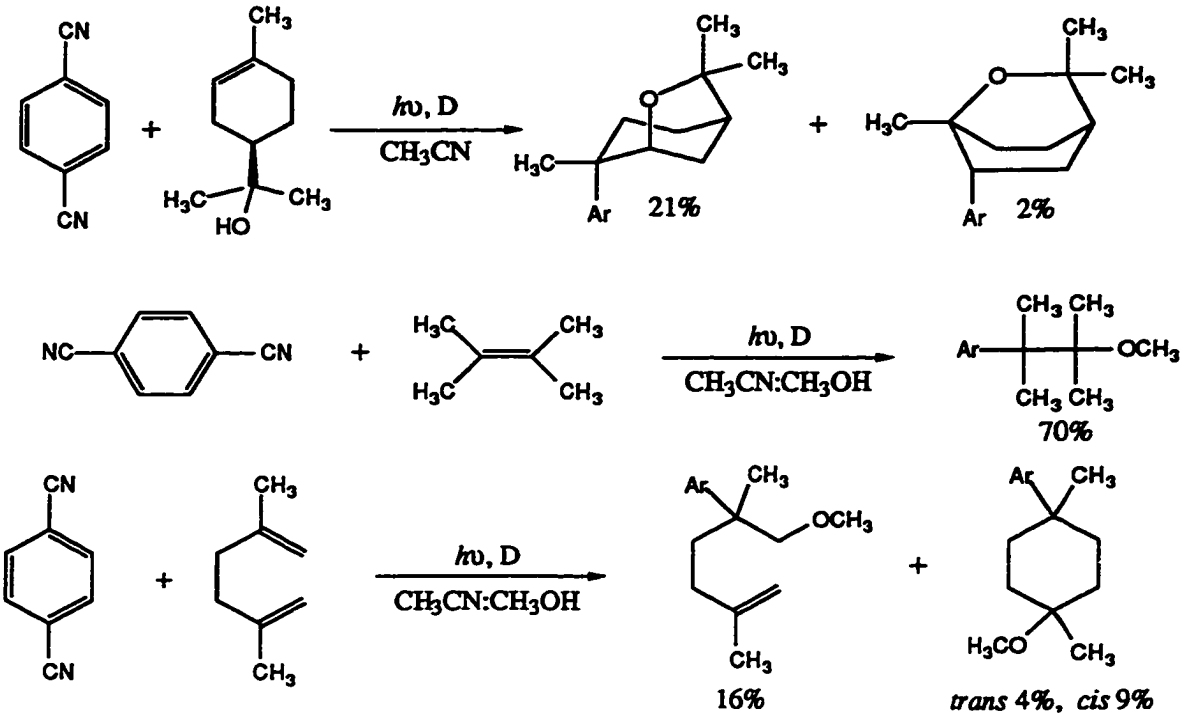

D = biphenyl Ar = 4-cyanophenyl

Figure 1.10: Examples of the Photo-NOCAS Reaction

a) Photoinduced Electron Transfer

In the first step of the photo-NOCAS mechanism, 1,4-dicyanobenzene (4), the principal light-absorbing species under these conditions, was promoted to the first singlet excited state upon irradiation. This conclusion was derived from fluorescence lifetime studies and Stern-Volmer plots, where the fluorescence of (4) was quenched by olefins at the diffusion-controlled rate in acetonitrile.[21b] The excited 1,4-dicyanobenzene behaves as an electron acceptor, and in the presence of a suitable donor such as a neutral olefin, PET occurs to produce the radical anion of (4) and the radical cation of the olefin. The details of PET have already been discussed in Section 1.1. The negative ΔG_{ET} calculated from Equation 1.1 lends further support for this electron transfer step (step 2 in Figure 1.11).

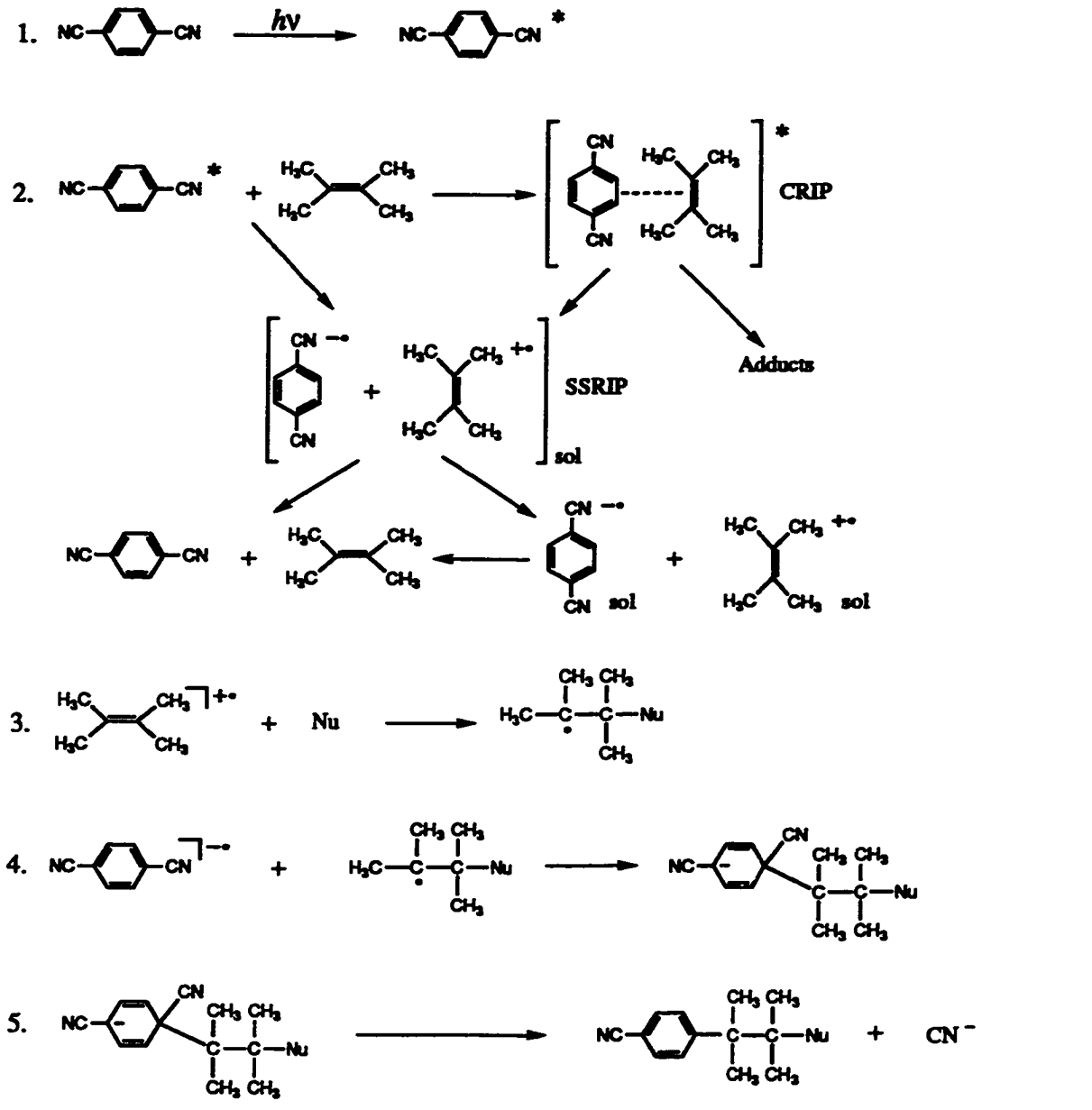

With the addition of biphenyl, a codonor

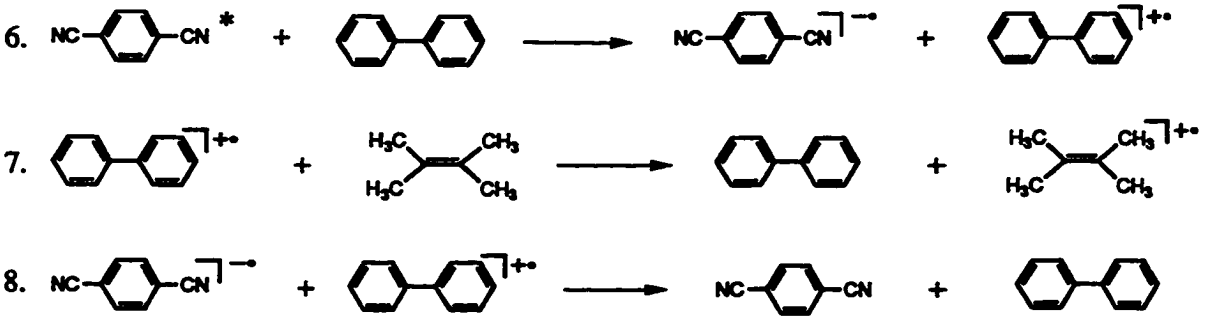

Figure 1.11: Mechanism of the Photo-NOCAS Reaction

b) Nucleophilic Addition

Step 3 in the proposed mechanism is the addition of a nucleophile to the radical cation of the olefin producing a distonic radical cation or a β-substituted free radical intermediate depending on the nature of the nucleophile. If a distonic radical cation results, deprotonation at this point leads to the β-substituted radical. The regioselectivity of nucleophilic addition to non-symmetric alkenes in the presence of (4) gave predominantly *anti*-Markovnikov photo-NOCAS products as exemplified by the reaction with 2-methylpropene (Figure 1.12).[21c] The designation of 2-(4-cyanophenyl)-methoxy-2-methylpropene as the *anti*-Markovnikov product is in accord with the Markovnikov rule of orientation for addition of hydrogen halides to olefins, where the anion (nucleophile) adds to the more heavily substituted carbon. However, no mechanistic information is implied by this designation. This regioselectivity suggests that nucleophilic addition occurs after the radical ion pairs have had a chance to diffuse apart. If the contact radical ion pair was stable, then coupling would be expected to occur before the addition of the nucleophile. This would lead to Markovnikov products due to the formation of the more stable zwitterionic or diradical intermediates as shown is Figure 1.12. The stabilization of the cation/radical by the methyl groups and steric effects determine the site of combination. However, the photo-NOCAS reaction does not occur through these intermediates because *anti*-Markovnikov products were isolated. The above experimental evidence confirm the order of steps 3 and 4 in the proposed mechanism.

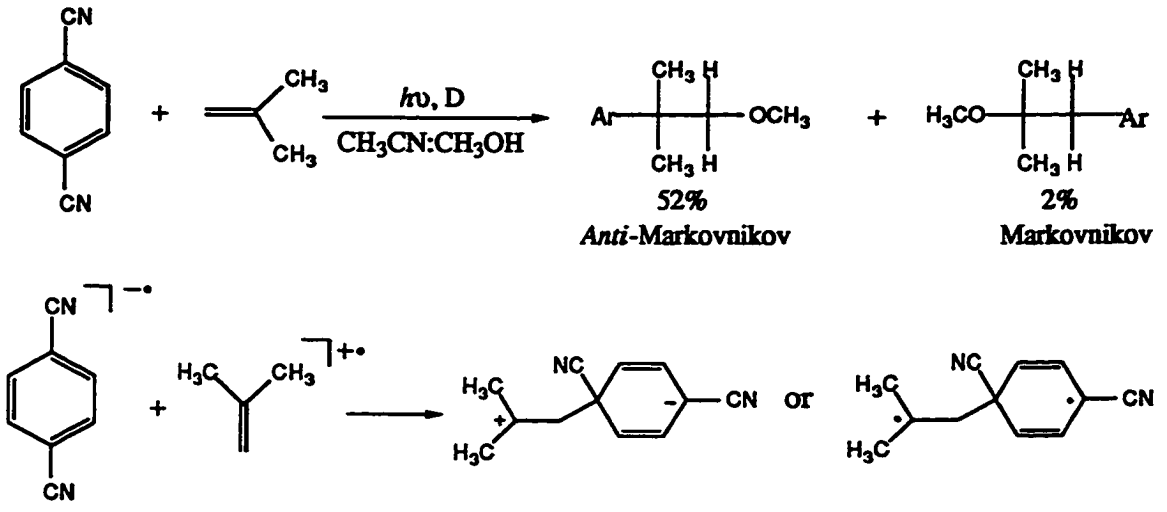

D = biphenyl Ar = 4-cyanophenyl

Figure 1.12: Zwitterionic or Diradical Intermediates from the Contact Radical Ion Pair

c) Combination of the β-Substituted Radical with the Radical Anion of 1,4-Dicyanobenzene

The stereoselectivity of the photo-NOCAS reaction is believed to be determined in this step (step 4 in Figure 1.11). *Ab initio* molecular orbital calculations of the interaction between radical cations and small neutral molecules showed that a bridged structure may be an important contributor of the distonic radical cation.[39] It is postulated that this bridging causes the predominant *trans* product observed in the photo-NOCAS reaction with cyclic compounds, since *anti*-addition of ($4^{\bullet-}$) to the bridging distonic radical cation would be favored.[21c] The reduction potential of the β-substituted radical formed in the previous step must be more negative than that of (4) in order for combination to occur. Otherwise, the radical would be reduced to an anion by ($4^{\bullet-}$). Protonation of this anion would then result in the formation of 1:1 (alkene: nucleophile) adducts instead of aromatic substitution products. Also, the site of coupling must be at the *ipso* position because attack at any other carbon on the aromatic ring would result in addition instead of substitution. This combination step, followed by re-aromatization with the elimination of a cyanide anion, completes the reaction sequence to produce the photo-NOCAS products.

d) Addition of a Sensitizer or a Codonor

In general, the addition of a sensitizer or a co-donor greatly improves the yield of the photo-NOCAS products. The term co-donor refers to a molecule that is not the major light absorbing species, but participates in electron transfer with the excited species in solution as shown in step 6 of Figure 1.11. When a co-donor such as biphenyl is added to the reaction mixture, it will undergo electron transfer with the excited state of (4), to produce a radical ion pair. The radical cation of the co-donor then oxidizes the olefin to produce the alkene radical cation. If phenanthrene is used, this compound will be the major light absorbing species and is therefore called a sensitizer. The excited state of the sensitizer is oxidized by (4) to generate a radical ion pair. The reaction then follows the same path as if a co-donor was added. The main consequence of the addition of a sensitizer/co-donor is that the radical cation of the olefin is generated at a distance away from ($4^{-\bullet}$) in step 7 instead of step 2.

Results obtained by Arnold and Snow lead to the conclusion that sensitizers/co-donors can improve the yield of photo-NOCAS products significantly even when the oxidation potential of these compounds is lower than that of the olefin by as much as 85 kJ/mol.[21c] This behavior suggests that a simple electron transfer process from the sensitizer/co-donor to the olefin is unlikely. Therefore, the formation of a bimolecular radical complex of the sensitizer-olefin/co-donor-olefin similar to the well-documented benzene-ethylene radical cation complex was postulated.[42] Nucleophilic addition may then occur via the small concentration of the olefin radical cation at equilibrium or it may involve nucleophilic attack on the complex directly. Another explanation is that the addition of these molecules decreases the efficiency of the deactivating back electron transfer process. For example, back electron transfer from the (4)/co-donor radical ion pair is believed to be slower than from the (4)/olefin pair.[20a]

1.4 Ab Initio Molecular Orbital Theory

Ab initio molecular orbital calculations are a useful tool to determine physical properties of reactive intermediates. Theoretical calculations have been used to map the reaction coordinates of numerous reactions involving reactive intermediates such as nucleophilic substitution on σ-cation radicals[43] and radical additions to alkenes.[31] The following section is a simplified description of *ab initio* molecular orbital theory to provide a brief background and to introduce the common terminology used in this field.[44]

Molecular orbital (MO) theory is concerned with predicting and describing molecular structure. This theory discards the idea that electrons are confined to specific atoms and develops a picture where electrons are distributed among a set of molecular orbitals with discrete energies. MO theory is based on quantum mechanics, in which the Schrödinger equation plays the central role. The familiar time-independent form is expressed in the following equation:

$$H\Psi=E\Psi \qquad [1.2]$$

In this expression, Ψ is a solution to the Schrödinger equation and is called a wave function. The wave function gives a complete description of the system, be it an atomic orbital, a molecular orbital, or an entire molecule. H is the Hamiltonian operator that contains energy terms relevant to the system being described. For a molecule, this would include expressions for the kinetic energies of the nuclei and electrons, as well as the potential energies for electron-electron repulsion, internuclear repulsion, and electron-nucleus attraction. E is a constant called an eigenvalue of Equation 1.2, and it represents the energy of the system. There are many possible solutions to Equation 1.2. Each of these solutions describes a different stationary state that can be occupied by the system. The corresponding eigenvalue is considered to be the energy for that state.

The complexity of the Schrödinger equation increases rapidly with the number of particles in the system. In fact, exact solutions are known only for simple systems like the hydrogen atom. Unfortunately, the systems that chemists wish to investigate are much more complicated. There are two approaches to solve this problem. The first is to simplify the Schrödinger equation itself and the second is to eliminate possible solutions that do not make physical sense until a reasonable set of wave functions can be obtained to use as initial guesses for iterative procedures. Both of these approaches are adapted by *ab initio* molecular orbital theory to make calculations on larger systems possible.

The Born-Oppenheimer approximation is the first of many steps to simplify the calculations. In this approximation, the nuclei are assumed to move very slowly compared to the electrons, so that electronic motion in a molecule is considered to occur in a field of fixed nuclei. This eliminates the kinetic energy term for nuclear motion in the Hamiltonian operator, and allows the treatment of electrons and nuclei to be separated.

The orbital approximation deals with the limits on the form of the many-electron wave function. This approximation states that the many-electron wave function can be taken as a product of one-electron wave functions called orbitals. This describes only the spatial distribution of the electrons. Therefore, a function describing the spin state of each electron must be added to the product for a complete description of the electrons. The Hartree product of spin orbitals takes the following form:

$$\Psi(1,2,...N) = \Psi_1(1)\alpha(1)\Psi_2(2)\beta(2)...\Psi_N(N)\beta(N) \qquad [1.3]$$

The quantity $\Psi^*\Psi$ is interpreted as the probability density of the electrons and in this case it is simply considered as the product of the one-electron densities as expressed in Equation 1.4.

$$P(1,2,...N)\Psi(1,2,...N)^*\Psi(1,2,...N) = \prod_{i=1}^{N} \Psi_i^*(i)\Psi_i(i) \qquad [1.4]$$

This interpretation is only valid when the probability distributions of the electrons are independent of one another. This is not a valid approximation for molecules, and methods of electron correlation such as configuration analysis and Møller-Plesset perturbation theory have been developed to correct for this problem.

Another effect of the definition of probability density is the antisymmetry principle. This stems from the fact that electrons are indistinguishable from one another, so that the many-electron probability density function expressed by Equation 1.4 must be unaffected by interchanging any two electrons. The consequence is that the total electron wave function must be either symmetric or antisymmetric with respect to interchanging any two electrons. This criterion is expressed mathematically by Equation 1.5.

$$\Psi(1,2,...i,j,...N) = \pm\Psi(1,2,...j,i,...N) \qquad [1.5]$$

Experimental evidence shows that the total electron wave function is antisymmetric with respect to interchanging any two electrons. Therefore, only the negative sign in 1.5 is correct for these purposes.

The product form of the wave function as shown in Equation 1.3 does not satisfy the requirements of the antisymmetric principle. Therefore, a new form of the wave function must be defined. This new form is called the Slater determinant, and the shorthand notation is given in Equation 1.6.

$$\Psi(1,2,...2N) = |\Psi_1(1)\alpha(1)\Psi_1(2)\beta(2)...\Psi_N(2N)\beta(2N)| \qquad [1.6]$$

The rows in the determinant are associated with the electrons and the columns are associated with orbitals. Expansion of this determinant generates all possible states of all the electrons in the molecular system. The properties of determinants guarantee that the antisymmetric principle is satisfied, because the sign of the determinant changes when any two rows are interchanged.

An acceptable form of the total electronic wave function is defined in terms of one-electron functions denoted by Ψ. It is thus necessary to find an acceptable expression for

these one-electron wave functions. For molecules, these functions are written as a linear combination of atomic orbitals as shown by Equation 1.7.

$$\Psi_i = \sum_{\mu} C_{\mu i}\varphi_{\mu} \qquad [1.7]$$

The variation principle states that the expectation value for the energy of any antisymmetric function will always be greater than the energy for the exact wave function . Applying this principle implies finding the set of molecular orbital expansion coefficients ($C_{\mu i}$) such that the energy is a minimum. This criterion is met when the coefficients satisfy the secular equations expressed by Equation 1.8, where N represents the number of atomic orbitals and ε_i is the one-electron orbital energy of Ψ_i.

$$\sum_{\nu} (F_{\mu\nu} - \varepsilon_i S_{\mu\nu})C_{\nu i} = 0 \qquad \mu = 1,2,...N \qquad [1.8]$$

The term $S_{\mu\nu}$ is an element of the overlap matrix representing the overlap between orbitals μ and ν. $F_{\mu\nu}$ is an element of the Fock matrix that represents the average effects of the field generated by all the electrons on each orbital. This term takes the form expressed by Equation 1.9.

$$F_{\mu\nu} = H_{\mu\nu} + \sum_{\lambda=1}^{N}\sum_{\sigma=1}^{N} P_{\lambda\sigma}\,[(\mu\nu|\lambda\sigma) - 1/2(\mu\lambda|\nu\sigma)] \qquad [1.9]$$

In equation 1.9 above, $H_{\mu\nu}$ is a one-electron Hamiltonian matrix element describing the motion of a single electron in the field of the bare nuclei. $P_{\lambda\sigma}$ is an element of the density matrix defined by Equation 1.10.

$$P_{\lambda\sigma} = 2\sum_{i=1}^{occ} C_{\lambda i}^{*}C_{\sigma i} \qquad [1.10]$$

The Fock matrix depends on the molecular orbital expansion coefficients through the density matrix. This implies that one must have an initial guess for this matrix before attempting to solve Equation 1.8. The procedure used in Hartree-Fock theory to solve this equation is an iterative approach called the self-consistent field (SCF) method, which involves the following steps:

1. Begin with an initial guess for the Fock matrix, usually approximated by $H_{\mu\nu}$, to solve for the set of expansion coefficients using Equation 1.8.
2. Form the density matrix.
3. Calculate the total electronic energy.
4. Reform the Fock matrix for the next iteration.

This procedure continues until the set of expansion coefficients no longer changes with additional iterations. At this point the energy is a minimum and the orbitals generate a field that produces the same orbitals, hence the term self-consistent field.

The atomic orbitals themselves are estimated by mathematical functions called basis functions. There are two types in common use, the Slater type orbitals (STOs) of the form $e^{-\xi r}$, and the Gaussian type orbitals (GTOs) of the form $e^{-\alpha r^2}$. GTOs are much easier to handle computationally, but STOs give a better representation of the actual shape of atomic orbitals. As a compromise between these two features, a combination of GTOs is used to approximate an STO function. This approach describes the basis functions of the type STO-NG, where N is the number of GTOs used to approximate the STO. The minimal basis set for *ab initio* molecular orbital calculations contains one of these basis functions approximating the 1*s* orbital for the first row atoms, and five of these basis functions to approximate the 1*s*, 2*s*, $2p_x$, $2p_y$, and $2p_z$ orbitals for the second row atoms. This minimal basis set can be expanded to introduce more flexibility. The double-zeta basis set simply doubles the number of basis functions for each atom. The split-valence basis set divides the valence shell orbitals into two basis functions to allow for size adjustments depending on the molecular environment. Split-valence basis sets are expressed in the form *k-lm*G, where *k* is the number of GTOs used to estimate the core orbitals, *l* is the number of GTOs used for the inner valence orbitals and *m* is the number of GTOs used to estimate the outer valence orbitals. These basis sets can be further expanded by adding polarization functions. These are six Cartesian d-type GTOs and three p-type GTOs that can be added to second row and first row atoms, respectively. These orbitals are denoted by adding a * or (d) in the expression for the basis set. Therefore, a 6-31G* basis set means that the core

orbitals are estimated by six GTOs, the inner valence orbitals are estimated by three GTOs, one GTO is used for the outer valence orbitals, and six d-type GTOs have been added to the second row atoms.

Chapter 2

The Regioselectivity of the Photo-NOCAS Reaction with Methanol Serving as the Nucleophile

2.1 Introduction

As was mentioned in Chapter 1, the regioselectivity of the photo-NOCAS reaction generally follows the *anti*-Markovnikov mode of addition, giving products where the nucleophile (methanol) has added to the less hindered end of the double bond. Examples of this reactivity can be seen in the isolated yields of simple alkenes subjected to typical photo-NOCAS reaction conditions. The photo-NOCAS products for 2-methylpropene and 2-methyl-2-butene are shown in Figure 2.1.

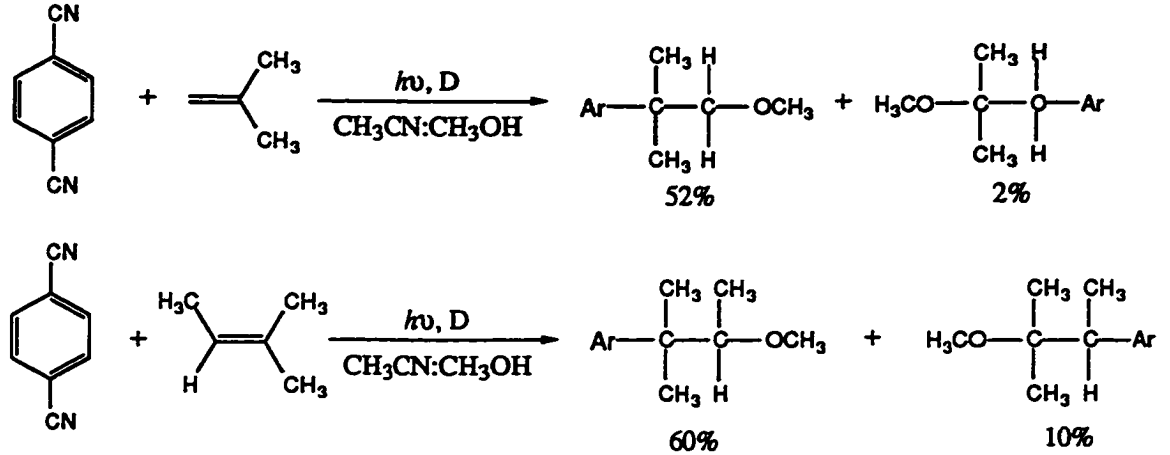

Figure 2.1: The Photo-NOCAS Reaction with Selected Alkenes

The definition of regioselectivity becomes more complicated when considering conjugated dienes. There is now the possibility of both 1,2- and 1,4-addition and products arising from both were isolated.[21f] The general trend observed from the various dienes considered was that the more heavily substituted dienes are more selective towards 1,4-

addition. The most heavily substituted diene studied, 2,5-dimethyl-2,4-hexadiene, gave exclusively 1,4-addition products. On the other hand, unsubstituted dienes such as 1,3-butadiene resulted in approximately equal amounts of 1,4- and 1,2-adducts. The selectivity between 1,2- and 1,4-addition is governed by step 4 in the photo-NOCAS reaction mechanism (Figure 1.11), where the allylic radical intermediate couples with the radical anion of 1,4-dicyanobenzene ($4^{\bullet-}$). This type of radical coupling is believed to be kinetically controlled as there is little or no activation energy. The transition state will resemble the starting materials (the radicals) according to the Hammond postulate.[45] Therefore, steric factors should direct the mode of coupling. For the less substituted dienes, both sites are equally favorable and equal amounts of 1,2- and 1,4-adducts are expected. The high selectivity observed in the more substituted dienes is a result of steric hindrance. In the case of 2,5-dimethyl-2,4-hexadiene, coupling to give the 1,2-adduct would be blocked by a neopentyl group (two β-methyl groups and one β-methoxy group). This type of steric hindrance is similar to the β-substituent effect in the S_N2 reaction.[46]

Initial attack of methanol generally occurs at one of the terminal positions (C_1 or C_4) of the conjugated dienes. Of the two terminal positions, the methanol adds preferentially to the less substituted carbon. If the two ends are identical, then addition occurs predominately at the terminal end of the more heavily substituted double bond. Product distributions for selected non-symmetric dienes are shown in Figure 2.2. It was suggested that the selectivity towards the less substituted olefinic carbon was influenced by a combination of steric factors, the relative stability of the allylic radical intermediates, and the positive charge distribution of the diene radical cations. However, no concrete evidence was collected to support this hypothesis. The experimental result that forced a re-examination of the factors that influence the regiochemistry is the photo-NOCAS reaction of 4-methyl-1,3-pentadiene (5) with methanol serving as the nucleophile. The isolated products and their yields for this reaction are shown if Figure 2.3.

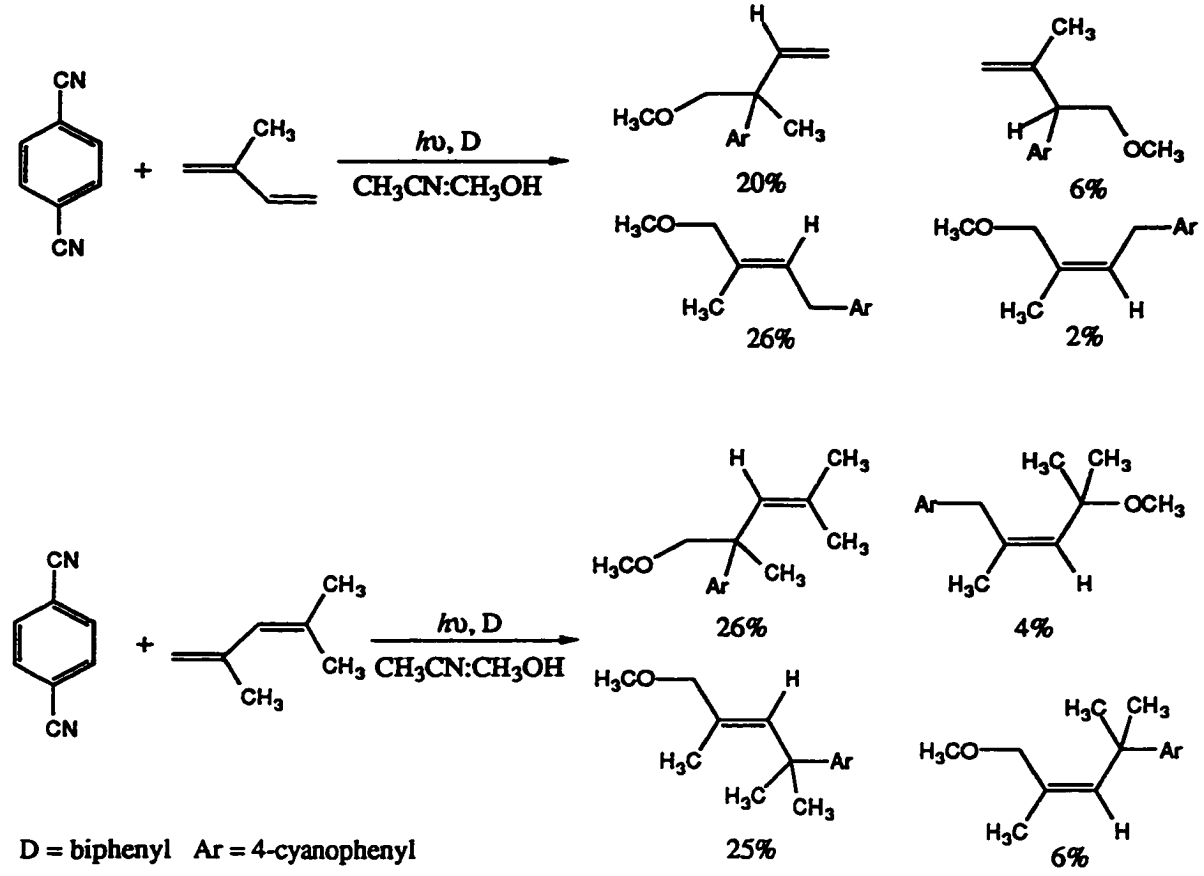

Figure 2.2: The Photo-NOCAS Reaction with Selected Dienes

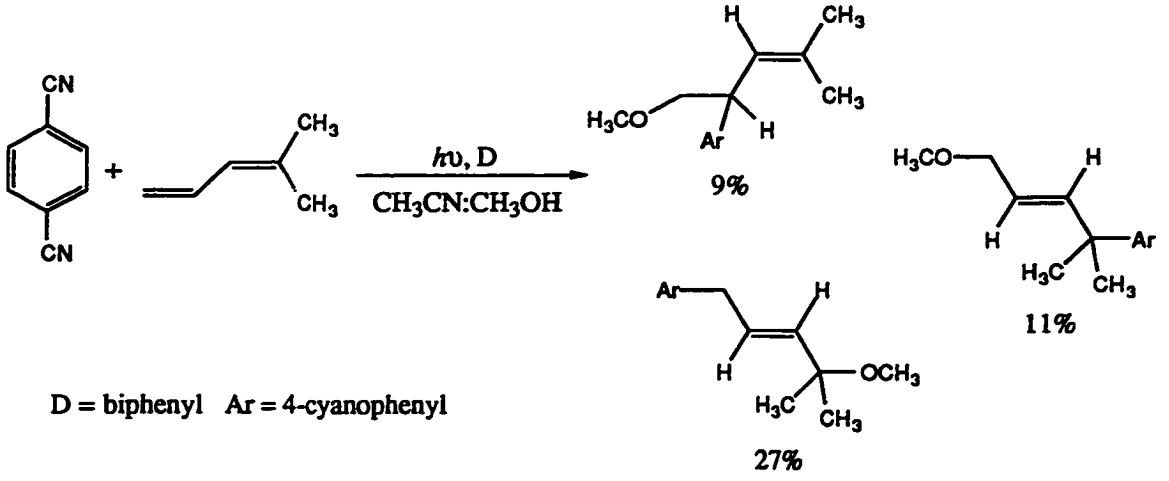

Figure 2.3: The Photo-NOCAS Reaction with 4-Methyl-1,3-Pentadiene

Clearly, the site of methanol addition is not determined by steric hindrance in this instance because the major product, (E)-1-(4-cyanophenyl)-4-methoxy-4-methyl-2-pentene (obtained in 27% yield), results from initial addition at the more substituted carbon. Furthermore, attack at this carbon atom ultimately leads to the less substituted of the two alternative allylic radical intermediates [(**5b**•) instead of (**5a**•) in Figure 2.4]. The relative stability of the allylic radicals also does not appear to influence the regiochemistry in this particular case; or, is it possible that (**5b**•) (a *mono*-substituted allylic radical) is more stable than (**5a**•) (a *tri*-substituted allylic radical)?

Figure 2.4: Allylic Radical Intermediates from 4-Methyl-1,3-Pentadiene

Obviously, further examination of the factors that determine the regiochemistry is required before an explanation for the product ratios can be formulated. The main objective of this project was to establish criteria useful for explaining/predicting the regiochemistry of the photo-NOCAS reaction, involving the combination of an alcohol (methanol) and the radical cation of an alkene or diene, substituting on 1,4-dicyanobenzene. The alkenes and dienes selected to provide a systematic study of the regioselectivity are: 4-methyl-1,3-pentadiene (**5**), 2,4-dimethyl-1,3-pentadiene (**6**), 2-methyl-1,3-butadiene (**7**), 2-methylpropene (**8**), and 2-methyl-2-butene (**9**).

Distonic radical cations are initially formed upon addition of methanol to the radical cation of an alkene or diene. *Ab initio* molecular orbital calculations on the addition of water to the ethylene radical cation have shown that this type of distonic radical cations can adopt an open or a bridged structure [species (**2**) and (**3**) in Figure 1.9]. Deprotonation

from the oxygen of the distonic radical cations leads to the β-alkoxyalkyl radicals, whose relative stability was postulated to influence the outcome of the regiochemistry. Evidently, information regarding the relative stability, geometry, charge and spin distributions of these reaction intermediates would help to determine the factors that influence regioselectivity. Therefore, the potential energy surface for the addition of methanol to each of the alkene or diene radical cations was investigated by theoretical calculations. Although nucleophilic addition to the radical cation of alkenes had already been examined theoretically, the calculations were of small molecules intended as reaction paradigms only. In addition, only symmetric molecules were studied, and as a consequence, no information regarding the regiochemistry could be obtained. Calculations on large systems such as those described here have not been attempted previously.

2.2 Computational Details

The Gaussian 92 package of programs was employed for the *ab initio* molecular orbital calculations in this project.[47] The geometries of the open shell systems were fully optimized at the unrestricted Hartree-Fock level with the 6-31G* basis set.[44] Single point energies were calculated to second order in Møller-Plesset perturbation theory (MP2) using the 6-31G* basis set at the HF/6-31G* optimized geometries,[48] and were corrected for spin contamination where appropriate. Unless otherwise noted, all of the structures were optimized using the Berny optimization procedure[49] without symmetry constraints and were confirmed, by harmonic frequency analyses, to be local minima on their respective potential energy surfaces. The charge and spin density distributions were obtained from Mulliken population analysis.[50]

2.3 Results

The issue of choosing an appropriate theoretical model has to be considered before calculations on the specific reaction intermediates can begin. The highest level employed for the water-ethylene system was PMP4/6-311+G**//UMP2/6-31G*, but the essential features of the potential energy surface was already well described at the PMP2/6-31G* level.[39] Such rigorous theoretical treatment is not practical for the large molecules proposed for this study. Some preliminary calculations were performed on smaller molecules with the aim of selecting the most appropriate theoretical model. The relative stability of the two alternative β-alkoxyalkyl radicals derived from methanol addition to the 2-methylpropene radical cation were evaluated at various theoretical levels. The results are summarized in Table 2.1. These two species were chosen to represent typical radical intermediates. The energy difference between 2,2-dimethyl-3-oxabutane and 4-methyl-2-oxapentane was also chosen to represent the ether functional groups in the compounds to be studied. The relative stability for the ethers at various theoretical levels are collected in Table 2.2. The data in these two tables show that the energy difference between the two molecules started to stabilize at the MP2/6-31G*//HF/6-31G* level. There was little advantage to optimization at the MP2 level or increasing the basis set to 6-311+G*. Therefore, all subsequent calculations were performed up to the MP2/6-31G*//HF/6-31G* level. Of the two empirical methods investigated, the results obtained from Benson's empirical rules were more consistent with the *ab initio* calculations. The agreement between the semi-empirical method AM1 and the *ab initio* results was poor for the relative stability of the compounds in question.

Table 2.1: Relative Stability of 1-Methoxy-2-Methyl-2-Propyl Radical (**8a**•) and 2-Methoxy-2-Methyl-1-Propyl Radical (**8b**•) Calculated at Various Theoretical Levels

Method	Total Energy of (**8a**•) (au)	Total Energy of (**8b**•) (au)	Difference (kJ/mol)
AM1	-0.06669	-0.04444	-58.4
Benson's Rules	-0.03173	-0.03241	1.8
HF/STO-3G//HF/STO-3G	-267.24569	-267.23509	-27.8
HF/3-21G//HF/3-21G	-269.05254	-269.05284	0.8
HF/6-31G*//HF/6-31G*	-270.54905	-270.54409	-13.0
MP2/6-31G*//HF/6-31G*	-271.35317	-271.35279	-1.3
MP2/6-31G*//MP2/6-31G*	-271.35728	-271.35666	-1.6
MP2/6-311+G*//MP2/6-31G*	-271.47432	-271.47387	-1.2

Table 2.2: Relative Stability of 2,2-Dimethyl-3-Oxabutane and 4-Methyl-2-Oxapentane Calculated at Various Theoretical Levels

Method	Total Energy of 2,2-Dimethyl-3-Oxabutane (au)	Total Energy of 4-Methyl-2-Oxapentane (au)	Difference (kJ/mol)
AM1	-0.10332	-0.11166	-21.9
Benson's Rules	-0.10916	-0.09817	28.9
HF/6-31G*//HF/6-31G*	-271.17563	-271.17495	1.8
MP2/6-31G*//HF/6-31G*	-272.01315	-272.00731	15.3
MP2/6-31G*//MP2/6-31G*	-272.01496	-272.00920	15.1
MP2/6-311+G*//MP2/6-31G*	-272.13546	-272.12944	15.8

The ionization potential of unsaturated molecules is another physical property that can be easily obtained both theoretically and experimentally. The calculated ionization potentials for the alkenes and dienes selected for this study are compared with experimental data in Table 2.3. The vertical ionization potential is defined as the energy absorbed by the molecule during the instantaneous removal of an electron. The geometry of the resulting ion does not have time to adjust, and as a result, it may still contain a large amount of vibrational energy.[51] The vertical ionization potential is obtained from the theoretical calculations by taking the negative of the eigenvalue of the HOMO in the neutral molecule. The adiabatic ionization potential is the energy absorbed when the electron is detached infinitely slowly and reversibly. The vibrational degrees of freedom of the molecule have time to adjust continually during ionization, and at the end of the process the ions is at its lowest vibrational state. The adiabatic ionization potential is calculated computationally by taking the difference between the total energy of the optimized neutral molecule and that of the radical cation.

Table 2.3: Ionization Potential of Selected Alkenes and Dienes

Alkene or Diene	Calculated Vertical IP [a] (eV)	Experimental Vertical IP [b] (eV)	Calculated Adiabatic IP [c] (eV)
2-Methyl-1,3-butadiene (7)	8.67	8.85	8.45
2,4-Dimethyl-1,3-pentadiene (6)	8.62	8.49	7.58
4-Methyl-1,3-pentadiene (5)	8.23	8.28	7.90
2-Methylpropene (8)	9.39	9.24	8.81
2-Methyl-2-butene (9)	8.93	8.68	8.27

[a]taken from the eigenvalue of the HOMO in the neutral molecule
[b]taken from reference 52
[c]taken as the difference in the calculated total energies (MP2/6-31G*//HF/6-31G*) of the fully optimized neutral molecule and the radical cation

2.3.1 Methanol Addition to Dienes

1) 2-Methyl-1,3-Butadiene

Geometry optimization of the 2-methyl-1,3-butadiene radical cation ($7^{+\bullet}$) gave the expected planar structure with the $C_1C_2C_3C_4$ dihedral angle at 180.0°. Selected geometrical parameters, charge and spin density distribution for this radical cation can be found in Figure 2.5. The calculated vertical ionization potential agrees well with the experimental ionization potential taken from the photoelectron spectrum. Also consistent with experimental results, the small difference between the vertical and the adiabatic ionization potential (0.22 eV) indicates very little geometrical change upon ionization.[53]

Two fully optimized structures were obtained from the addition of methanol to ($7^{+\bullet}$). They are consistent with methanol bonding to C_1 ($\mathbf{7a}^{+\bullet}$) and to C_4 ($\mathbf{7b}^{+\bullet}$) of the diene radical cation. Selected geometrical parameters, charge and spin density distributions for these two species are shown in Figures 2.6 and 2.7. These structures can be described as distonic radical cations in that the charge and spin are located in different parts of the molecule. The positive charge is largely associated with the ether moiety whereas the spin is located on the other three carbon atoms of the diene, forming an allylic radical. Deprotonation from the oxygen of ($\mathbf{7a}^{+\bullet}$) and ($\mathbf{7b}^{+\bullet}$) gave the allylic radicals ($\mathbf{7a}^{\bullet}$) and ($\mathbf{7b}^{\bullet}$), respectively. Selected geometrical parameters, charge and spin density distributions are summarized in Figures 2.8 and 2.9 for these two allylic radicals. The structure of the allylic radicals is very similar to the distonic radical cations. The only major structural change is the shortening of the carbon-oxygen bond from 1.54 Å in the distonic radical cation to 1.40 Å in the allylic radicals.

The gas phase potential energy surface for methanol addition to ($7^{+\bullet}$) is depicted in Figure 2.10. The total energy of the individual species are reported in Table 2.4. The distonic radical cation ($\mathbf{7a}^{+\bullet}$) is more stable than ($\mathbf{7b}^{+\bullet}$) by 7.3 kJ/mol, and both of these distonic radical cations are significantly more stable than the isolated methanol and diene

radical cation. The allylic radical (7a•) is more stable than the alternative structure (7b•) by 8.5 kJ/mol. For this diene, both the more stable distonic radical cation ($7a^{+\bullet}$) and the more stable radical (7a•) have methanol bonded to C_1 where the radical moiety is the more heavily alkyl-substituted. The major product isolated from the photo-NOCAS reaction of 2-methyl-1,3-butadiene (7) is consistent with the methanol attacking at the C_1 position.

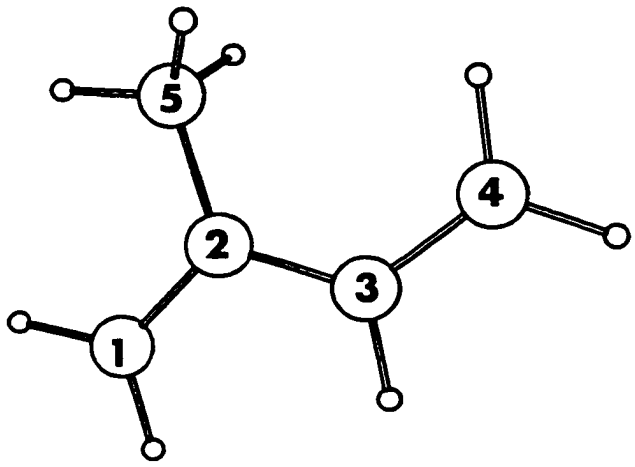

HF/6-31G* Optimized Geometrical Parameters

Interatomic Distance (Å)		Angles (deg)		Dihedral Angles (deg)	
C_1-C_2	1.400	$C_1C_2C_3$	116.5	$C_4C_3C_2C_1$	-180.0
C_2-C_3	1.408	$C_1C_2C_5$	120.4	$C_5C_2C_3C_1$	0.0
C_3-C_4	1.379	$C_2C_3C_4$	124.0		
C_2-C_5	1.505	$C_3C_2C_5$	123.1		

Charge and Spin Density Distributions from Mulliken Population Analysis

Atom Number	Charge[a]	Spin[a]
1	0.28	0.67
2	0.13	-0.06
3	0.13	-0.25
4	0.28	0.64
5	0.17	0.00

[a]All charge and spin density of directly bonded hydrogen atoms are summed into the carbon atoms

Figure 2.5: Selected Geometrical Parameters, Charge and Spin Density Distributions for the 2-Methyl-1,3-Butadiene Radical Cation ($7^{+\bullet}$)

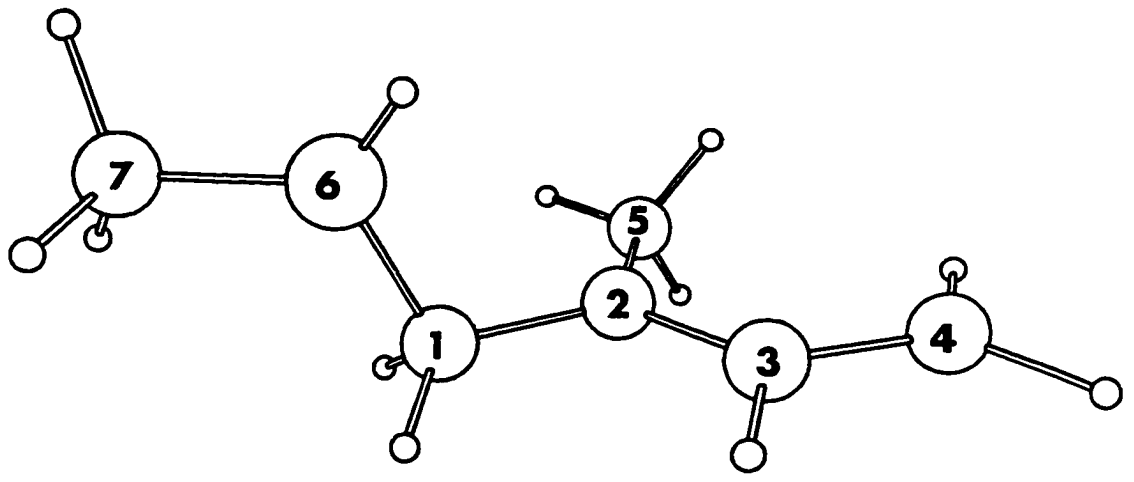

HF/6-31G* Optimized Geometrical Parameters

Interatomic Distance (Å)		Angles (deg)		Dihedral Angles (deg)	
C_1-C_2	1.481	$C_1C_2C_3$	118.1	$C_4C_3C_2C_1$	178.3
C_2-C_3	1.399	$C_1C_2C_5$	118.2	$C_5C_2C_3C_1$	178.2
C_3-C_4	1.389	$C_2C_3C_4$	125.3	$C_7O_6C_1C_2$	-178.2
C_2-C_5	1.517	$C_2C_1O_6$	107.9	$C_3C_2C_1O_6$	105.7
C_1-O_6	1.540	$C_1O_6C_7$	119.9		
C_2-O_6	2.442				
O_6-C_7	1.466				

Charge and Spin Density Distributions from Mulliken Population Analysis

Atom Number	Charge[a]	Spin[a]
1	0.42	-0.04
2	-0.01	0.91
3	0.04	-0.71
4	0.08	0.85
5	0.09	-0.05
6	-0.15	0.03
7	0.53	0.01

[a]All charge and spin density of directly bonded hydrogen atoms are summed into the carbon atoms

Figure 2.6: Selected Geometrical Parameters, Charge and Spin Density Distributions for ($7a^{+\bullet}$): 2-Methyl-1,3-Butadiene/Methanol Distonic Radical Cation, C_1 Bonded

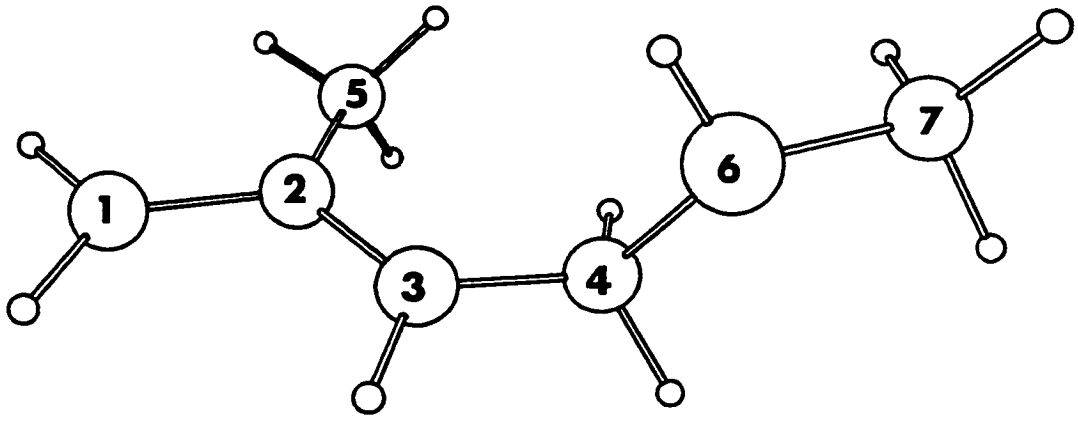

HF/6-31G* Optimized Geometrical Parameters

Interatomic Distance (Å)		Angles (deg)		Dihedral Angles (deg)	
C_1-C_2	1.397	$C_1C_2C_3$	118.7	$C_4C_3C_2C_1$	178.9
C_2-C_3	1.396	$C_1C_2C_5$	119.3	$C_5C_2C_1C_3$	178.7
C_3-C_4	1.476	$C_2C_3C_4$	124.4	$C_2C_3C_4O_6$	103.5
C_2-C_5	1.517	$C_3C_4O_6$	107.9	$C_3C_4O_6C_7$	-174.2
C_4-O_6	1.539	$C_4O_6C_7$	120.1		
C_3-O_6	2.437				
O_6-C_7	1.465				

Charge and Spin Density Distributions from Mulliken Population Analysis

Atom Number	Charge[a]	Spin[a]
1	0.06	0.86
2	0.09	-0.72
3	-0.02	0.83
4	0.45	-0.04
5	0.05	0.04
6	-0.15	0.03
7	0.52	0.01

[a]All charge and spin density of directly bonded hydrogen atoms are summed into the carbon atoms

Figure 2.7: Selected Geometrical Parameters, Charge and Spin Density Distributions for (**7b**$^{+\cdot}$): 2-Methyl-1,3-Butadiene/Methanol Distonic Radical Cation, C_4 Bonded

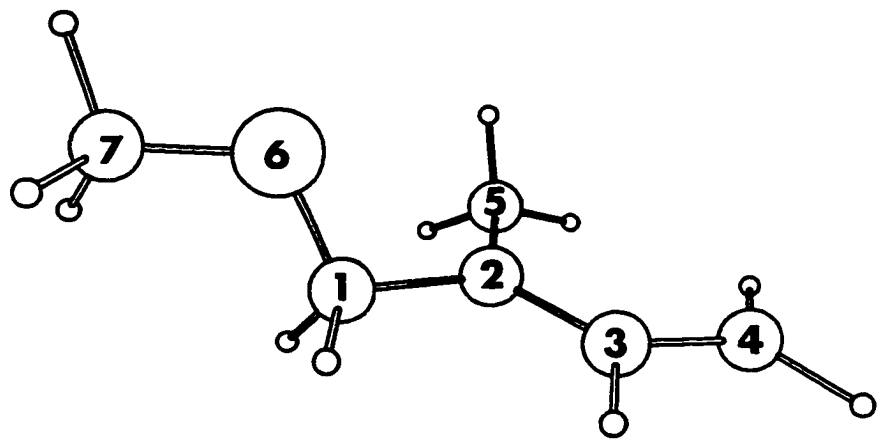

HF/6-31G* Optimized Geometrical Parameters

Interatomic Distance (Å)		Angles (deg)		Dihedral Angles (deg)	
C_1-C_2	1.504	$C_1C_2C_3$	119.9	$C_1C_2C_3C_4$	179.1
C_2-C_3	1.396	$C_1C_2C_5$	115.8	$C_5C_2C_1C_3$	-179.8
C_3-C_4	1.391	$C_2C_3C_4$	127.5	$C_2C_1O_6C_7$	-176.2
C_2-C_5	1.506	$C_2C_1O_6$	109.5	$C_3C_2C_1O_6$	125.2
C_1-O_6	1.400	$C_1O_6C_7$	114.1		
C_2-O_6	2.371				
O_6-C_7	1.392				

Charge and Spin Density Distributions from Mulliken Population Analysis

Atom Number	Charge[a]	Spin[a]
1	0.28	-0.07
2	0.04	1.00
3	0.00	-0.75
4	-0.03	0.87
5	0.02	-0.06
6	-0.61	0.01
7	0.30	0.00

[a]All charge and spin density of directly bonded hydrogen atoms are summed into the carbon atoms

Figure 2.8: Selected Geometrical Parameters, Charge and Spin Density Distributions for (7a•): 2-Methyl-1,3-Butadiene/Methanol β-Alkoxyalkyl Radical, C_1 Bonded

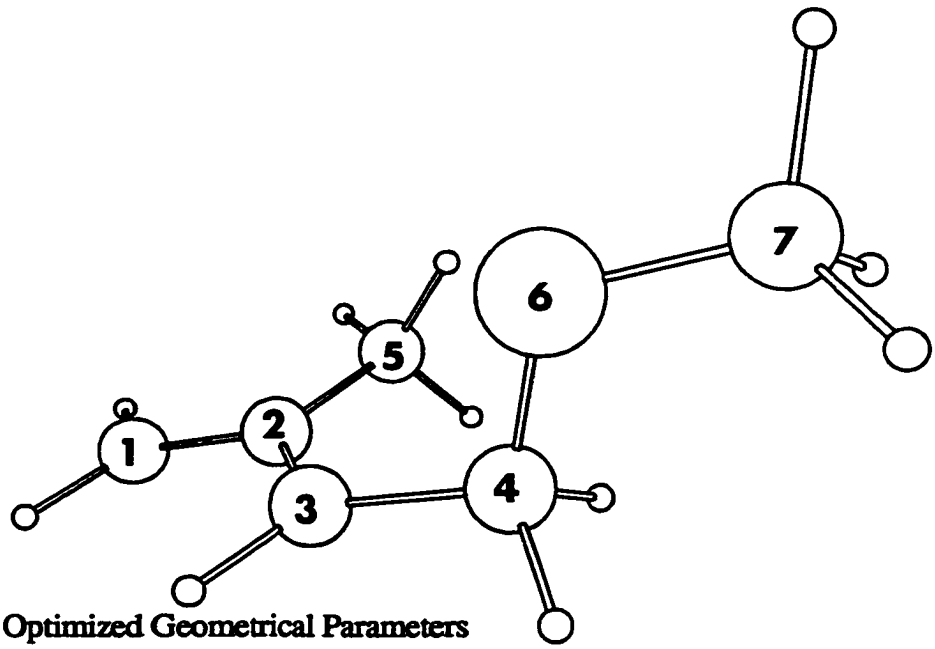

HF/6-31G* Optimized Geometrical Parameters

Interatomic Distance (Å)		Angles (deg)		Dihedral Angles (deg)	
C_1-C_2	1.390	$C_1C_2C_3$	120.2	$C_1C_2C_3C_4$	-178.1
C_2-C_3	1.403	$C_1C_2C_5$	119.6	$C_5C_2C_1C_3$	179.8
C_3-C_4	1.500	$C_2C_3C_4$	124.5	$C_2C_3C_4O_6$	78.3
C_2-C_5	1.516	$C_3C_4O_6$	109.9	$C_3C_4O_6C_7$	179.1
C_4-O_6	1.403	$C_4O_6C_7$	113.8		
C_3-O_6	2.377				
O_6-C_7	1.392				

Charge and Spin Density Distributions from Mulliken Population Analysis

Atom Number	Charge[a]	Spin[a]
1	-0.06	0.86
2	0.10	-0.80
3	-0.02	0.97
4	0.29	-0.09
5	0.00	0.04
6	-0.60	0.02
7	0.30	0.01

[a]All charge and spin density of directly bonded hydrogen atoms are summed into the carbon atoms

Figure 2.9: Selected Geometrical Parameters, Charge and Spin Density Distributions for (**7b**•): 2-Methyl-1,3-Butadiene/Methanol β-Alkoxyalkyl Radical, C_4 Bonded

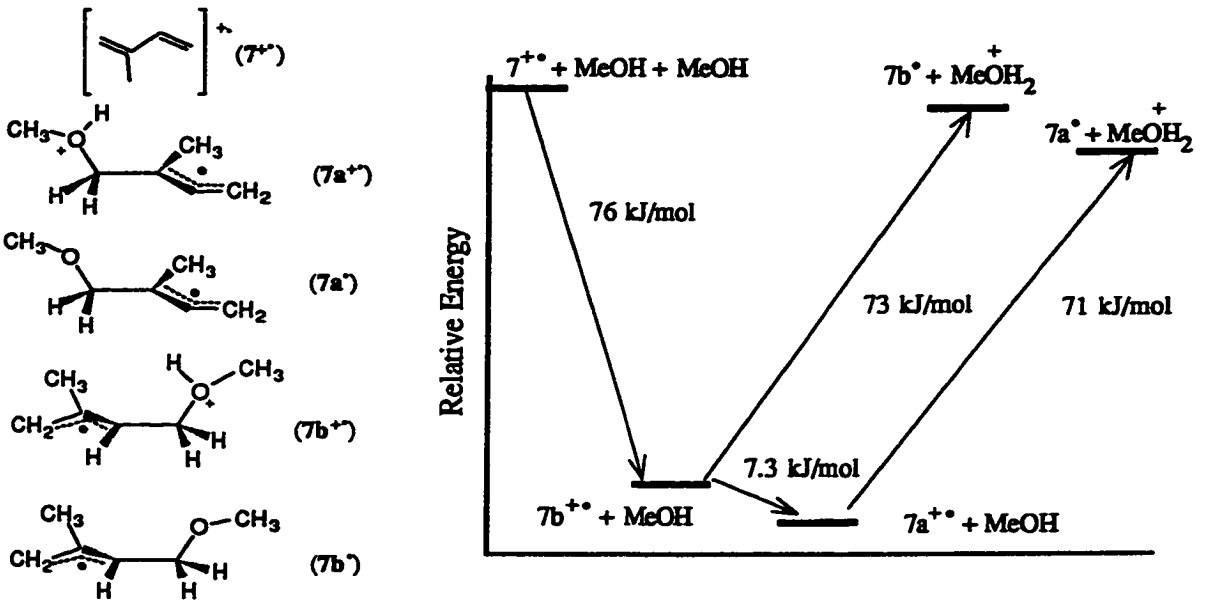

Figure 2.10: Potential Energy Surface of Methanol Addition to the 2-Methyl-1,3-Butadiene Radical Cation ($7^{+\bullet}$)

Table 2.4: Relative Total Energies for 2-Methyl-1,3-Butadiene Reaction Intermediates

Intermediate	Total Energy (au)	Total Energy (au)
($7^{+\bullet}$)	-194.29091	
Methanol	-115.34494	
Methanol	-115.34494	
Sum		-424.98079
($7a^{+\bullet}$)	-309.66773	
Methanol	-115.34494	
Sum		-425.01267
($7b^{+\bullet}$)	-309.66496	
Methanol	-115.34494	
Sum		-425.00990
($7a^{\bullet}$)	-309.34121	
Protonated Methanol	-115.64429	
Sum		-424.98550
($7b^{\bullet}$)	-309.33797	
Protonated Methanol	-115.64429	
Sum		-424.98226

2) 2,4-dimethyl-1,3-Pentadiene

As shown in Table 2.3, the calculated vertical ionization potential for 2,4-dimethyl-1,3-pentadiene (6) is in good agreement with the experimental results. The large difference (1.04 eV) between the vertical and adiabatic ionization potentials suggests notable geometrical changes upon ionization. There is convincing experimental evidence that the neutral molecule is significantly twisted from the s-*cis* conformer (dihedral angle $C_1C_2C_3C_4$ is ca. 50°).[54] Theoretical calculation (HF/6-31G) also found this s-*cis* twisted global minimum (dihedral angle of 52°) along with an *s-trans* conformer (dihedral angle of 180°) located 9.3 kJ/mol above the s-*cis* minimum.[55] In this study, identical results were obtained at the HF/6-31G* level, although the energy difference between the two conformers is now reduced to 7.9 kJ/mol. Selected geometrical parameters, charge and spin density distributions for the global minimum of the neutral dienes can be found in Appendix I. Geometry optimization of the radical cation gave a nearly planar s-*trans* minimum (dihedral angle of 179°). This structure contrasts markedly with the twisted geometry of the neutral molecule. Therefore, a thorough search was conducted for additional minimum structures on the radical cation potential surface. One other minimum was found, it is a slightly twisted *s-cis* conformer with a dihedral angle of 12°. However, this minimum is located 12.3 kJ/mol above the s-*trans* conformer. Details of structure, charge and spin density distributions for the radical cations of dienes are collected in Appendix II. The large difference in structure between the global minima of the neutral molecule and the radical cation matches the geometrical rearrangment suggested by the ionization potential results.

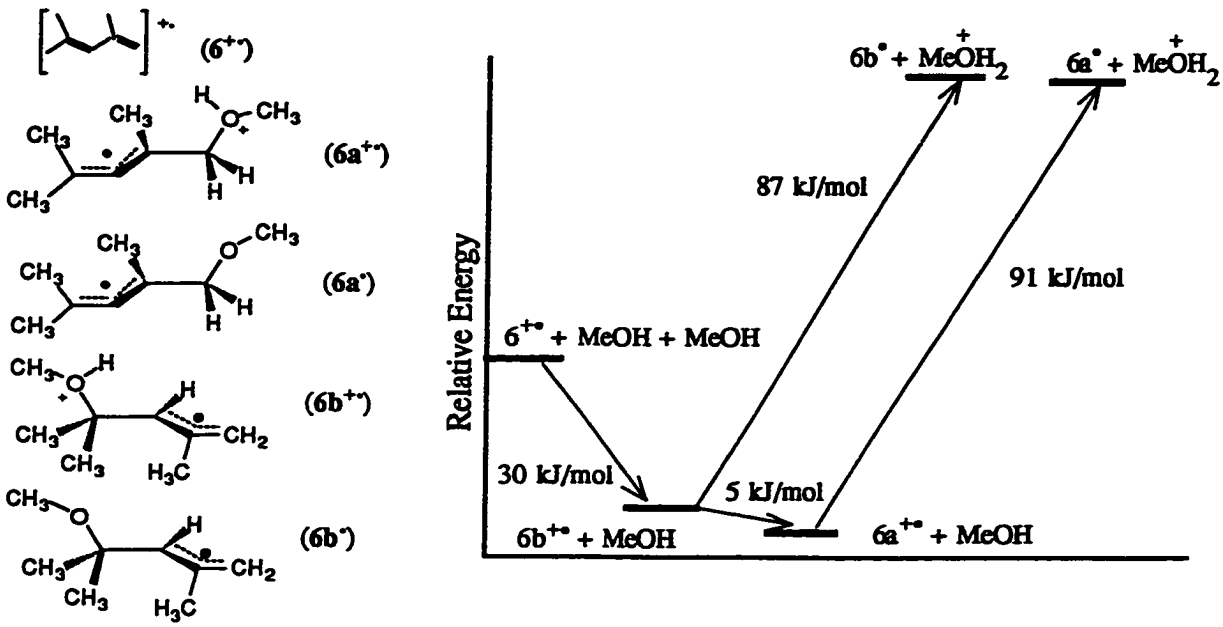

Figure 2.11: Potential Energy Surface of Methanol Addition to the 2,4-Dimethyl-1,3-Pentadiene Radical Cation ($6^{+\bullet}$)

Table 2.5: Relative Total Energies for 2,4-Dimethyl-1,3-Pentadiene Reaction Intermediates

Intermediate	Total Energy (au)	Total Energy (au)
($6^{+\bullet}$)	-272.65091	
Methanol	-115.34494	
Methanol	-115.34494	
Sum		-503.34079
($6a^{+\bullet}$)	-388.00920	
Methanol	-115.34494	
Sum		-503.35414
($6b^{+\bullet}$)	-388.00732	
Methanol	-115.34494	
Sum		-503.35226
($6a^{\bullet}$)	-387.67525	
Protonated Methanol	-115.64429	
Sum		-503.31954
($6b^{\bullet}$)	-387.67494	
Protonated Methanol	-115.64429	
Sum		-503.31923

The potential energy surface for methanol addition to the 2,4-dimethyl-1,3-pentadiene radical cation (**6**$^{+\bullet}$) appears in Figure 2.11. The total energy of the individual species are tabulated in Table 2.5. The structure of the intermediates are similar to those described above for the methanol/2-methyl-1,3-butadiene system. Therefore, the details of structure, charge and spin density for all subsequent intermediates are collected in appendices rather than incorporated into the main text. The distonic radical cation intermediates are collected in Appendix III and those of the β-alkoxyalkyl radicals in Appendix IV. As shown in Figure 2.11, the addition of methanol to this diene radical cation is an exothermic process. The distonic radical cation derived from methanol bonding at C_1 (**6a**$^{+\bullet}$) is relatively more stable than the one derived from methanol bonding at C_4 (**6b**$^{+\bullet}$). The relative stability of the β-alkoxyalkyl radicals also follows the same trend. The product distribution is consistent with the reaction following the more favorable energetic pathway.

3) 4-Methyl-1,3-Pentadiene

Figure 2.12 shows the potential energy surface of methanol addition to the 4-methyl-1,3-butadiene radical cation (**5**$^{+\bullet}$). The total energy of the individual species are reported in Table 2.6. The features of this potential energy surface are similar to those of the two other dienes studied. The structure of the distonic radical cation with methanol bonded to C_4 (**5b**$^{+\bullet}$) was easily obtained. The C_4-oxygen bond length is relatively long at 1.71 Å. The analogous structure with methanol bonded to C_1 (**5a**$^{+\bullet}$) was more difficult to obtain. The C_1-oxygen bond length had to be confined at 1.70 Å initially and the rest of the structure optimized. Relaxation of this constraint gave the fully optimized structure for the distonic radical cation (**5a**$^{+\bullet}$). Deprotonation from the oxygen of (**5a**$^{+\bullet}$) and (**5b**$^{+\bullet}$) gives the β-alkoxyalkyl radicals (**5a**$^{\bullet}$) and (**5b**$^{\bullet}$), respectively. Selected geometrical parameters, charge and spin density distributions for these intermediates are reported in Appendices III and IV.

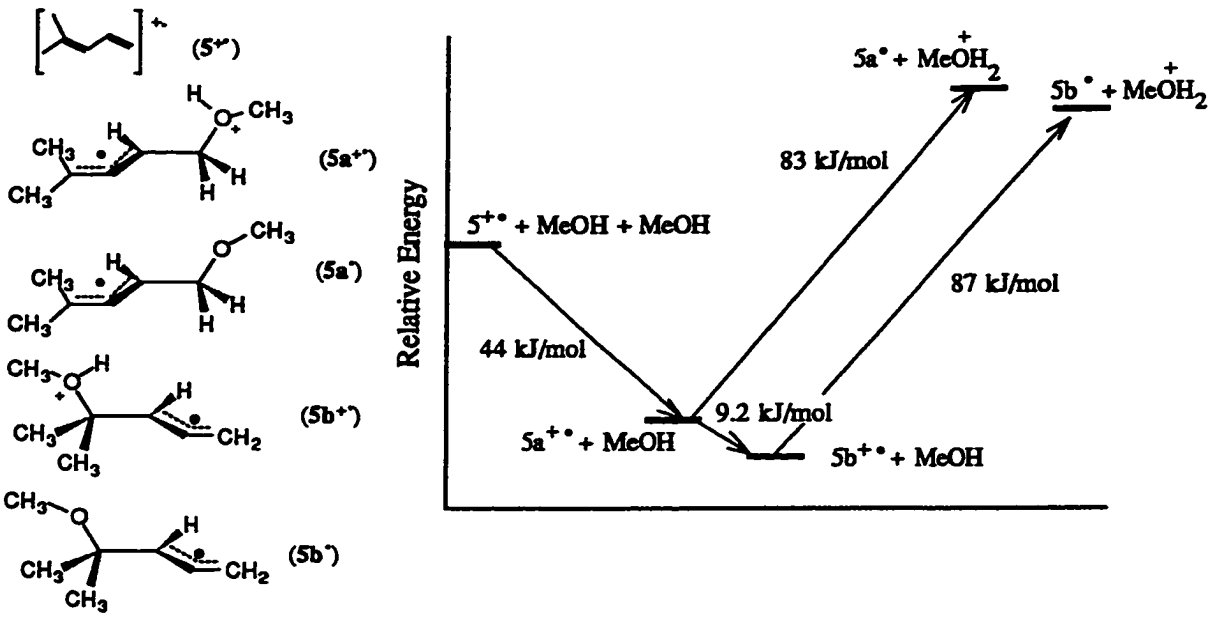

Figure 2.12: Potential Energy Surface of Methanol Addition to the 4-Methyl-1,3-Pentadiene Radical Cation ($5^{+\bullet}$)

Table 2.6: Relative Total Energies for 4-Methyl-1,3-Pentadiene Reaction Intermediates

Intermediate	Total Energy (au)	Total Energy (au)
($5^{+\bullet}$)	-233.47993	
Methanol	-115.34494	
Methanol	-115.34494	
Sum		-464.16981
($5a^{+\bullet}$)	-348.84162	
Methanol	-115.34494	
Sum		-464.18656
($5b^{+\bullet}$)	-348.84514	
Methanol	-115.34494	
Sum		-464.19008
($5a^{\bullet}$)	-348.51064	
Protonated Methanol	-115.64429	
Sum		-464.15493
($5b^{\bullet}$)	-348.51259	
Protonated Methanol	-115.64429	
Sum		-464.15688

Figure 2.12 shows that the intermediate with methanol bonded to C_4, [(**5b**$^{+\bullet}$) or (**5b**$^{\bullet}$)], is more stable than the alternative structure with methanol bonded at C_1, [(**5a**$^{+\bullet}$) or (**5a**$^{\bullet}$)]. This is contrary to established trends as the allylic radical moiety resulting from addition at C_4 is mono-substituted as compared to the tri-substituted allylic radical from addition at C_1. Clearly, there are factors other than radical stability that influence the relative stability of these reaction intermediates. The other obvious structural feature present in these intermediates is the ether functional group. The enthalpy change of isodesmic reactions were calculated to determine the influence of the ether moiety on the relative stability of the two alternative β-alkoxyalkyl radicals. The isodesmic reactions for the three dienes studied are shown in Figure 2.13. The "a" reactions are a direct comparison of the two alternative β-alkoxyalkyl radicals, whereas the "b" reactions attempt to separate the influence of the ether moiety from that of the radical moiety. For example, reaction 3a compares the two alternative β-alkoxyalkyl radicals from methanol addition to 4-methyl-1,3-pentadiene. The negative ΔH implies that (**5b**$^{\bullet}$), the radical resulting from addition at C_4, is more stable than (**5a**$^{\bullet}$), the radical resulting from addition at C_1. The left hand side of reaction 3b attempts to dissect (**5a**$^{\bullet}$) into two distinct molecules while trying to retain as much of the connectivity as possible. Ethyl methyl ether was chosen to represent the ether moiety. It was constructed by replacing the allylic radical portion of (**5a**$^{\bullet}$) by a methyl group. The radical part is represented by an allylic radical where the ether functional group in (**5a**$^{\bullet}$) had been replaced by a methyl group. The ether and allylic radical to represent (**5b**$^{\bullet}$) are constructed in a similar fashion. The isodesmic reaction 3b shows that a mono-substituted ether and a tri-substituted allylic radical is less stable than a tri-substituted ether and a mono-substituted allylic radical. It appears that alkyl substitution is more important on the carbon bearing ether functional group than on the radical moiety for this particular molecule. Structural details, spin and charge density distributions for the ethers and alkyl radicals are collected in Appendices V and VI, respectively.

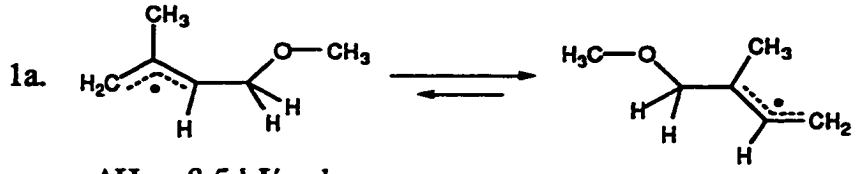

1a. $\Delta H = -8.5$ kJ/mol

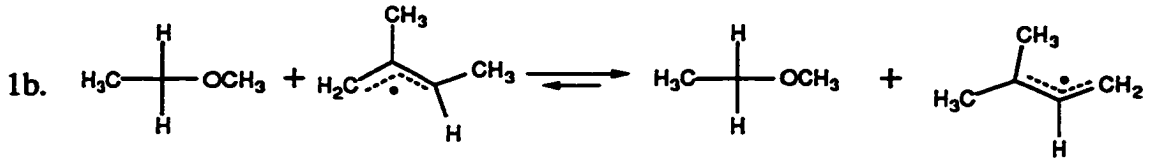

1b. $\Delta H = -6.7$ kJ/mol

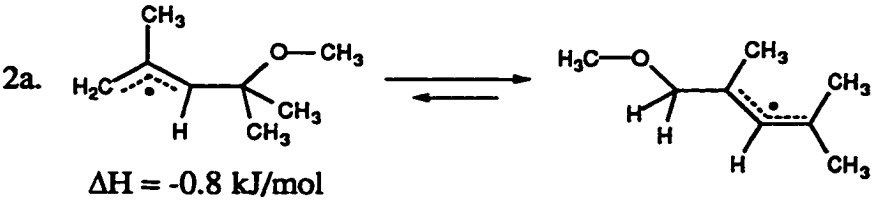

2a. $\Delta H = -0.8$ kJ/mol

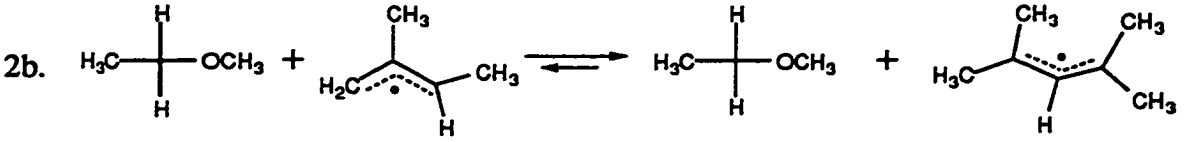

2b. $\Delta H = +8.7$ kJ/mol

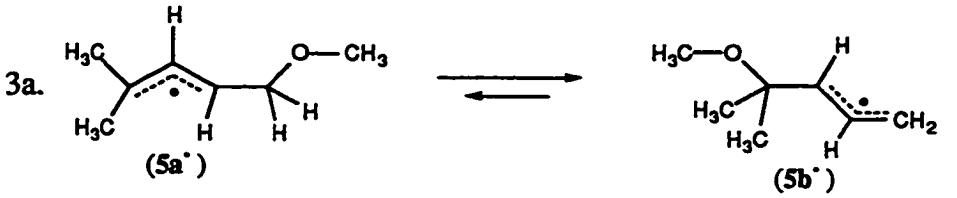

3a. $\Delta H = -5.1$ kJ/mol

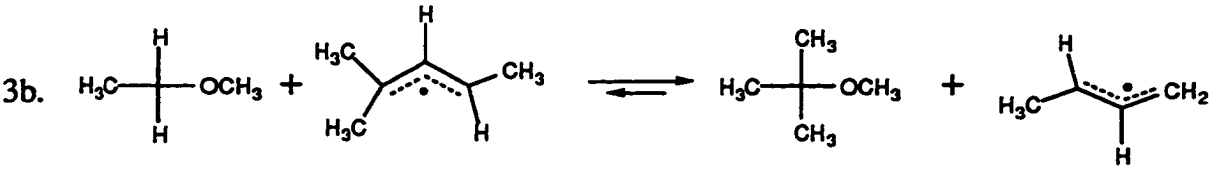

3b. $\Delta H = -2.0$ kJ/mol

Figure 2.13: Isodesmic Reactions to Evaluate the Relative Stability of β-Alkoxyalkyl Radicals

2.3.2 Methanol Addition to Alkenes

1) 2-Methylpropene

The potential energy surface for the addition of methanol to the 2-methylpropene radical cation ($8^{+\bullet}$) is depicted in Figure 2.14. The total energy for the individual reaction intermediates are shown in Table 2.7. Details on the geometry, spin and charge distributions for the distonic radical cations and β-alkoxyalkyl radicals can be found in Appendices III and IV, respectively. The structure of two distonic radical cations, consistent with methanol bonding to C_1 ($\mathbf{8a}^{+\bullet}$) and C_2 ($\mathbf{8b}^{+\bullet}$), was fully optimized without geometrical constraints. The C_1-O and C_2-O bond lengths are relatively long (1.57Å and 1.65Å respectively), suggesting that the methanol is only weakly bound to the alkene radical cation. However, a bridged structure ($\mathbf{8c}^{+\bullet}$) could not be obtained without restricting both of the carbon-oxygen bonds to equal bond lengths. This intermediate reverts to the more stable distonic radical cation ($\mathbf{8b}^{+\bullet}$) upon removing these structural constraints. Surprisingly, this bridged structure is a minimum with no negative vibrational frequencies. Therefore, it may be an intermediate, preceding formation of the distonic radical cations, or may form during the equilibration of the distonic radical cations. The energy of ($\mathbf{8c}^{+\bullet}$) would then set a lower limit (24-30 kJ/mol), presumably only slightly below the activation energy for the equilibration of the distonic radical cations. Deprotonation from the oxygen of ($\mathbf{8a}^{+\bullet}$) and ($\mathbf{8b}^{+\bullet}$) gives the β-alkoxyalkyl radicals ($\mathbf{8a}^{\bullet}$) and ($\mathbf{8b}^{\bullet}$), respectively. Notice that the relative stability of the intermediates is reversed upon deprotonation: *i.e.* ($\mathbf{8b}^{+\bullet}$) is more stable than ($\mathbf{8a}^{+\bullet}$), but ($\mathbf{8a}^{\bullet}$) is more stable than ($\mathbf{8b}^{\bullet}$).

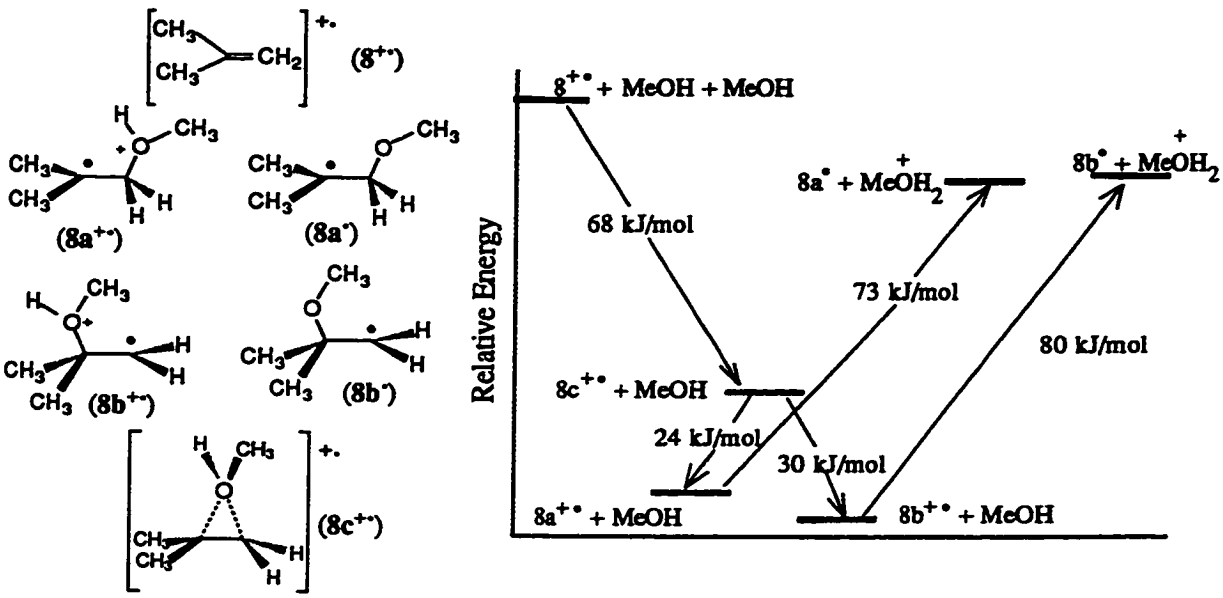

Figure 2.14: Potential Energy Surface of Methanol Addition to the 2-Methylpropene Radical Cation ($8^{+\bullet}$)

Table 2.7: Relative Total Energies for 2-Methylpropene Reaction Intermediates

Intermediate	Total Energy (au)	Total Energy (au)
($8^{+\bullet}$)	-156.30259	
Methanol	-115.34494	
Methanol	-115.34494	
Sum		-386.99247
($8a^{+\bullet}$)	-271.68225	
Methanol	-115.34494	
Sum		-387.02719
($8b^{+\bullet}$)	-271.68459	
Methanol	-115.34494	
Sum		-387.02953
($8c^{+\bullet}$)	-271.67327	
Methanol	-115.34494	
Sum		-387.01821
($8a^{\bullet}$)	-271.35528	
Protonated Methanol	-115.64429	
Sum		-386.99957
($8b^{\bullet}$)	-271.35479	
Protonated Methanol	-115.64429	
Sum		-386.99908

2) 2-Methyl-2-Butene

The potential energy surface for the addition of methanol to the radical cation of 2-methyl-2-butene (**9**$^{+\bullet}$) is shown in Figure 2.15. The total energy for the individual reaction intermediates are reported in Table 2.8. The structure of the open distonic radical cation with methanol bonded at C_3 (**9b**$^{+\bullet}$) converged without geometrical constraints. A structure for the bridged distonic radical cation (**9c**$^{+\bullet}$), located only 1.2 kJ/mol above (**9b**$^{+\bullet}$), was obtained without geometrical constraints. Calculations on the alternative open distonic radical cation with methanol bonded to C_2 (**9a**$^{+\bullet}$), converged only when the C_2-O bond length was held at 1.58 Å [the value obtained for the optimized structure of (**9b**$^{+\bullet}$)]. Removing this constraint from (**9a**$^{+\bullet}$) resulted in the optimized geometry for the bridged structure (**9c**$^{+\bullet}$). Nevertheless, this distonic radical cation is more stable than the alternative structure with methanol attached at C_3 (**9b**$^{+\bullet}$). As depicted in Figure 2.15, the differences in energy between the alternative distonic radical cations and this bridged radical cation are small. It seems likely that equilibration among these intermediates would be rapid. Deprotonation of the distonic radical cation (**9b**$^{+\bullet}$) leads to the tertiary β-alkoxyalkyl radical, (**9b**$^{\bullet}$), which is more stable than the secondary β-alkoxyalkyl radical (**9a**$^{\bullet}$) resulting from the deprotonation of (**9a**$^{+\bullet}$). Again, structural details, charge and spin density distributions can be found in Appendix III for the distonic radical cations and in Appendix IV for the β-alkoxyalkyl radical intermediates.

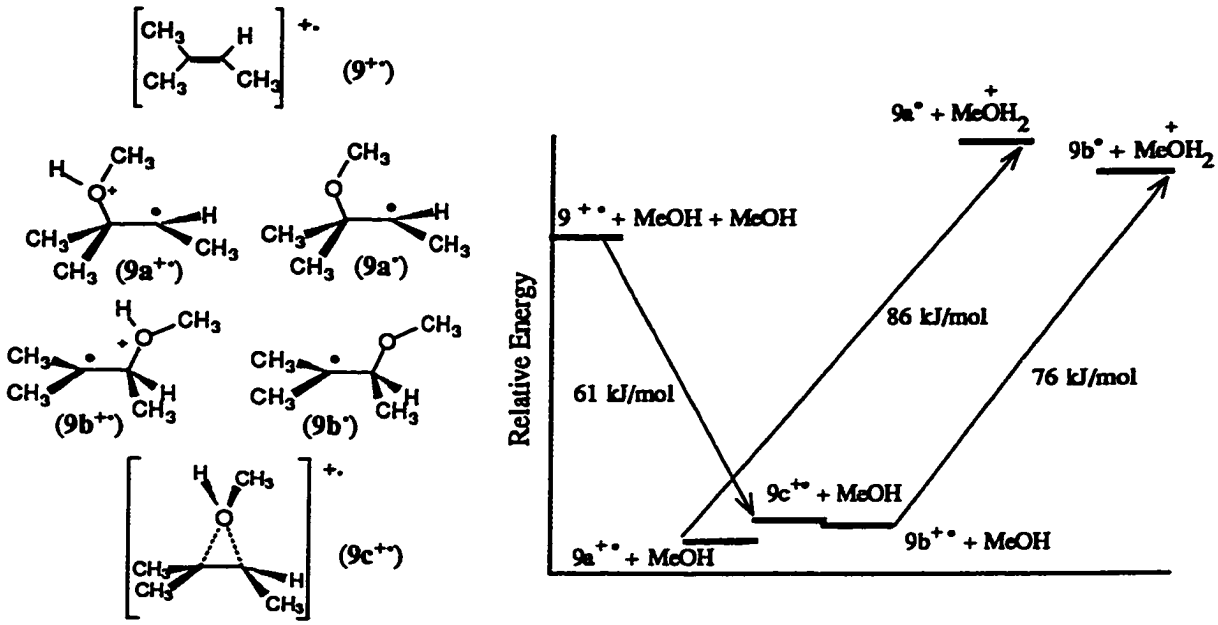

Figure 2.15: Potential Energy Surface of Methanol Addition to the 2-Methyl-2-Butene Radical Cation ($9^{+\bullet}$)

Table 2.8: Relative Total Energies for 2-Methyl-2-Butene Reaction Intermediates

Intermediate	Total Energy (au)	Total Energy (au)
($9^{+\bullet}$)	-195.48839	
Methanol	-115.34494	
Methanol	-115.34494	
Sum		-426.17827
($9a^{+\bullet}$)	-310.85828	
Methanol	-115.34494	
Sum		-426.20322
($9b^{+\bullet}$)	-310.85696	
Methanol	-115.34494	
Sum		-426.20190
($9c^{+\bullet}$)	-310.85651	
Methanol	-115.34494	
Sum		-426.20145
($9a^{\bullet}$)	-310.52614	
Protonated Methanol	-115.64429	
Sum		-426.17043
($9b^{\bullet}$)	-310.52857	
Protonated Methanol	-115.64429	
Sum		-426.17286

2.4 Discussion

2.4.1 The Influence of the Charge Distribution of the Radical Cations

The charge density distribution for the radical cations of the conjugated dienes studied are shown in Figure 2.16. In the case of the 2-methyl-1,3-butadiene radical cation ($7^{+\cdot}$), the charge density is identical for both terminal carbon atoms. Therefore, attack of methanol at either position would be equally probable if the regioselectivity is influenced by charge density. However, 89% of the products isolated arise from methanol attacking at the C_1 terminal position. For the 4-methyl-1,3-butadiene radical cation ($5^{+\cdot}$), 57% of the isolated products results from methanol attacking at the more hindered position, yet it carries less of the positive charge density than C_1. Finally, methanol prefers to bond with the more positively charged terminal carbon in the radical cation of 2,4-dimethyl-1,3-pentadiene, ($6^{+\cdot}$), as 93% of the isolated products arise from bonding at C_1. Obviously, the attack of methanol does not always occur at the more positively charged terminal carbon atom. Furthermore, there is no apparent correlation between charge density and the position of bonding observed in the reaction products. In light of these results, it can be concluded that the positive charge distribution in the diene radical cations does not influence the regioselectivity of methanol addition.

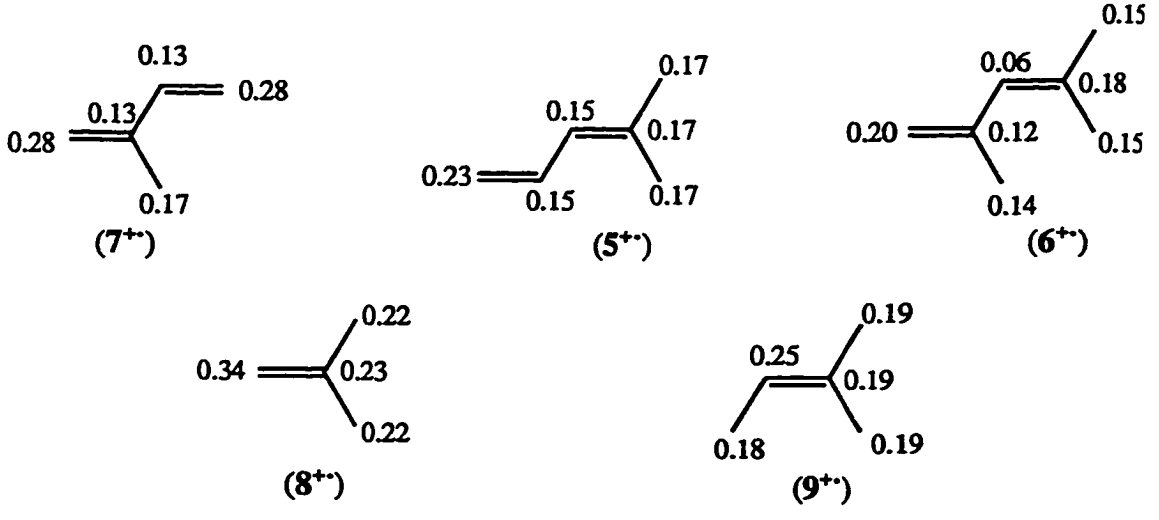

Figure 2.16: Charge Density Distribution of Radical Cations

The less alkyl-substituted olefinic carbon is associated with the higher positive charge density for the two simple alkenes studied [($\mathbf{8}^{+\bullet}$) and ($\mathbf{9}^{+\bullet}$) in Figure 2.16]. The product distribution of these alkenes shows that methanol consistently adds to the less hindered carbon. For the alkenes, the preferred site of bonding for methanol appears to be at the carbon bearing the more positive charge density in the radical cation. The positive charge density distribution in the radical cation may influence the regiochemistry of methanol addition for alkenes, but not for conjugated dienes.

2.4.2 The Influence of the Relative Stability of Reaction Intermediates

The relative stability between the two alternative distonic radical cations and β-alkoxyalkyl radicals, along with the isolated product distributions for the dienes and alkenes, are summarized in Table 2.9. The relative stability of the radical cation or radical intermediates that appear in columns two and three of Table 2.9 are calculated by subtracting the total energy of the intermediate with the less substituted radical moiety from the one with the more substituted radical moiety. For example, in the case of 2-methyl-1,3-butadiene, the total energy of the intermediate with methanol bonded to C_4 [($\mathbf{7b}^{+\bullet}$) and ($\mathbf{7b}^{\bullet}$)] was subtracted from the total energy of the intermediate with methanol bonded to C_1 [($\mathbf{7a}^{+\bullet}$) and ($\mathbf{7a}^{\bullet}$)]. In the case of the β-alkoxyalkyl radical intermediates, this can be considered as the enthalpy change for reaction 1a in Figure 2.13. Thus, a negative value means that the intermediate with the more heavily substituted radical moiety is more stable. In the isolated product ratio column, the relative amount the product derived from the intermediate with the more substituted radical moiety is listed on the left hand side. Therefore, negative values in columns two and three should correspond to larger percentages on the left hand side of column four if the product distribution is a reflection of the relative stability of the reaction intermediates.

Table 2.9: Relative Stability of Radical Intermediates and Isolated Product Ratios for Dienes and Alkenes

Diene or Alkene	Relative Stability of Distonic Radical Cations (kJ/mol)	Relative Stability of β-Alkoxyalkyl Radical (kJ/mol)	Isolated Product Ratio
2-Methyl-1,3-Butadiene (7)	-7.27	-8.51	89:11
2,4-Dimethyl-1,3-Pentadiene (6)	-4.94	-0.81	93:7
4-Methyl-1,3-Butadiene (5)	9.24	5.12	43:57
2-Methylpropene (8)	6.14	-1.29	96:4
2-Methyl-2-Butene (9)	3.46	-6.38	85:15

There are two observations that can be made from the data presented in Table 2.9. The first is that for the dienes investigated, the relative stability of the distonic radical cation intermediates follows the same trend as the β-alkoxyalkyl radicals. The major product isolated is consistent with the reaction proceeding via the more stable of these two types of intermediates. Therefore, the relative stability of the two alternative distonic radical cations as well as the β-alkoxyalkyl radicals can influence the regiochemistry of methanol addition for the dienes. The trend is reversed in the case of the alkenes: the more stable distonic radical cation deprotonates to give the less stable β-alkoxyalkyl radical. The major product isolated is consistent with the reaction proceeding via the more stable of the two alternative β-alkoxyalkyl radicals. Out of the five alkenes or dienes examined by *ab initio* molecular orbital calculations, the relative stability of the alternative β-alkoxyalkyl radicals is the only property that can consistently predict the experimental product ratio accurately.

2.4.3 Proposed Mechanism for Methanol Addition to the Radical Cations

The potential energy surfaces obtained from this study suggest that the deceptively simple representation of the initial bonding between the nucleophile (methanol) and the radical cations of the olefins (Figure 1.11, step 3) should be expanded. An extended

mechanism that is consistent with the information reflected in the potential energy surfaces is shown in Figure 2.17 with 2,3-dimethyl-2-butene as a sample olefin.

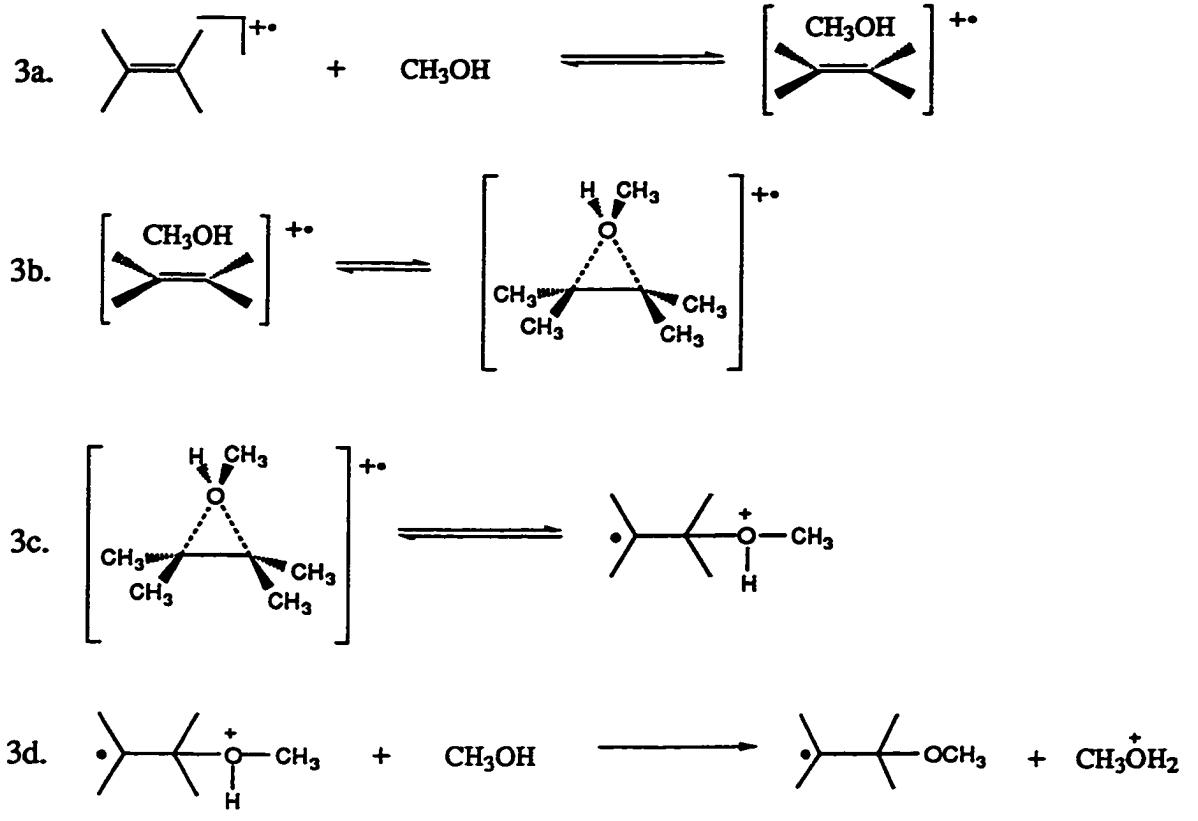

Figure 2.17: Extended Mechanism of Methanol Addition

In Figure 2.17, step 3a represents the initial formation of a dipole-induced radical-ion complex between the methanol and the radical cation of the alkene (or diene). In step 3b, the interaction between the nucleophile and the alkene radical cation increases to form a bridged distonic radical cation. This bridged structure collapses in step 3c to produce one of the two alternative distonic radical cations. Considering the small energy difference between the bridged and open distonic radical cations, it is plausible that rapid equilibration of the two alternative distonic radical cations proceeds through the bridged radical cation. Finally, irreversible deprotonation from the oxygen of the distonic radical cations yields the β-alkoxyalkyl radicals in step 3d. The irreversibility of the deprotonation is a logical

consequence of the low acidity of the media. The observed product regiochemistry reflects the relative rate of formation of the alternative β-alkoxyalkyl radicals; formation of the more stable β-alkoxyalkyl radical is preferred. The type of kinetic scheme proposed here is similar to the mechanism for the addition of alcohols to the silicon-carbon double bond of 1,1-diphenylsilene where primary deuterium kinetic isotope effects suggest that the proton transfer step is rate determining and is preceded by fast, reversible formation of the silene-alcohol complex.[56]

2.5 Conclusions

The regiochemistry of the photo-NOCAS reaction with methanol serving as the nucleophile, combining with the radical cations of an alkene or diene was examined through isolated product ratios. The relative stabilities of the reaction intermediates were estimated by *ab initio* molecular orbital calculations. It was postulated that the regioselectivity is established upon the addition of the nucleophile to the alkene (or diene) radical cation (step 3 of Figure 1.11). The theoretical calculations suggest that the addition process proceeds in a series of steps. Initial interaction between the nucleophile (methanol) and the radical cation leads to the formation of dipole-induced or bridged radical cation complexes. The carbon-oxygen interatomic distance is long (2.78 Å to 2.95 Å), suggesting that there is little covalent interaction. These radical cation complexes collapse to form two alternative distonic radical cations in the next step of the reaction sequence. The carbon-oxygen bond lengths in these distonic radical cations range from 1.55 Å to 1.71 Å, still long compared to the carbon-oxygen bond lengths of 1.42Å to 1.45 Å found in alkyl ethers determined from x-ray and neutron diffraction methods.[57] This implies that only partial carbon-oxygen bond formation has occurred and it is conceivable that the methanol molecule can move to the other carbon of the double bond via the bridged structure. Deprotonation from the oxygen of the distonic radical cations gives β-alkoxyalkyl radicals. The carbon-oxygen bond length in these radicals ranges from 1.39 Å

to 1.42 Å. The new carbon-oxygen bond formation is now complete, and the regiochemistry is established at this stage. The isolated product ratios are a reflection of the relative stability of the two alternative β-alkoxyalkyl radicals, with the formation of the more stable radical being favored. This suggests that enthalpy factors play an important role in determining the regiochemistry.

The regiochemistry is not influenced by steric factors as the methanol does not always add preferentially to the less hindered end of the double bond. Also, polar factors do not appear to play a significant role. The methanol does not always add preferentially to the carbon atom with the greatest positive charge density in the radical cation of the alkene or diene. This approach is a crude estimate of the polar effects. A better way to estimate the polar effects is to look at the change in the charge density distribution between the starting materials and the transition structures. An expansion of this study could include a search for the transition structures connecting the minima already identified on the potential energy surfaces. However, the evidence collected thus far lends support to the conclusion that the regioselectivity of methanol addition is thermodynamically controlled. There are low energy reaction pathways for the equilibration of the reaction intermediates, and the formation of the most stable β-alkoxyalkyl radical is favored. Steric and polar factors do not seem to influence the outcome of the regiochemistry.

An interesting consequence of this in depth study of the factors determining the regioselectivity is an understanding of how the regioselectivity of the photo-NOCAS reaction may be reversed. For example, the commonly observed regioselectivity of the photo-NOCAS reaction follows the *anti*-Markovnikov type addition, where the nucleophile adds preferentially to the less substituted olefinic carbon. Addition at this carbon produces the more heavily alkyl-substituted reaction intermediates. Only one exception to this selectivity was observed: the major product from the reaction with 4-methyl-1,3-pentadiene was a result of the methanol adding at the more substituted carbon. *Ab initio*

molecular orbital calculations indicated that the radical intermediate arising from addition at this carbon is the more stable of the two structures even though the radical moiety is less substituted. Preliminary results obtained from isodesmic reactions indicated that the unexpected stabilization was provided by alkyl substitution on the carbon bearing the oxygen of the ether function group. This observation suggests that the relative stability of radical intermediates can be controlled by changing the structure of the nucleophile. For example, the effect of the methoxy functional group was not large enough to reverse the relative stability of the radical intermediates for the two non-symmetric alkenes. Will other nucleophilies, such as fluoride or ammonia, behave differently? Will the effect of alkyl substitution on the carbon bearing these substituents be large enough to reverse the relative stability of the radical intermediates for the alkenes? And if so, will Markovnikov addition products be favored in the photo-NOCAS reaction with these nucleophiles? A natural extension of this study would be to carry out similar experimental and theoretical investigations with other nucleophiles to answer these questions.

Chapter 3

The Regioselectivity of the Photo-NOCAS Reaction with Fluoride Serving as the Nucleophile

3.1 Introduction

Organofluorine compounds can be found in a variety of industrial applications. Some of these include lubricants, coatings, propellants, pharmaceuticals, blood substitutes, liquid crystals and textile chemicals.[58] One of the more important uses for organofluorine compounds is isosteric replacement, the replacement of a hydrogen atom, hydroxyl group, or another halogen by a fluorine atom. The similarity in size of the fluorine and the hydrogen atom results in negligible steric effects, yet the significant difference in electronegativity produces pronounced effects on the electronic distribution within the molecule. These characteristics make isosteric replacement an ideal structural modification for altering the chemical and biological activities of organic compounds. For this reason, the selective formation of a carbon-fluorine bond has been, and continues to be, the focus of intensive research.[27c,d] Previous results have indicated that the photo-NOCAS reaction can be quite selective with methanol or cyanide reacting as the nucleophile. If the same selectivity exists with fluoride, selective carbon-fluorine bond formation can be achieved in one step. This, along with the ideas discussed in the conclusion of the last chapter, provided the impetus for the study of the photo-NOCAS reaction with fluoride serving as the nucleophile.

The proposed mechanism for the photo-NOCAS reaction, using 2,3-dimethyl-2-butene as the olefin, is shown in Figure 1.11 in Chapter 1. The scope and limitations of this reaction, with regard to the olefin in combination with alcoholic nucleophiles, have been extensively investigated; but only recently has this study been extended to other

nucleophiles.[59] Figure 3.1 summarizes the results of the reaction involving simple alkenes when methanol or cyanide anion serves as the nucleophile.

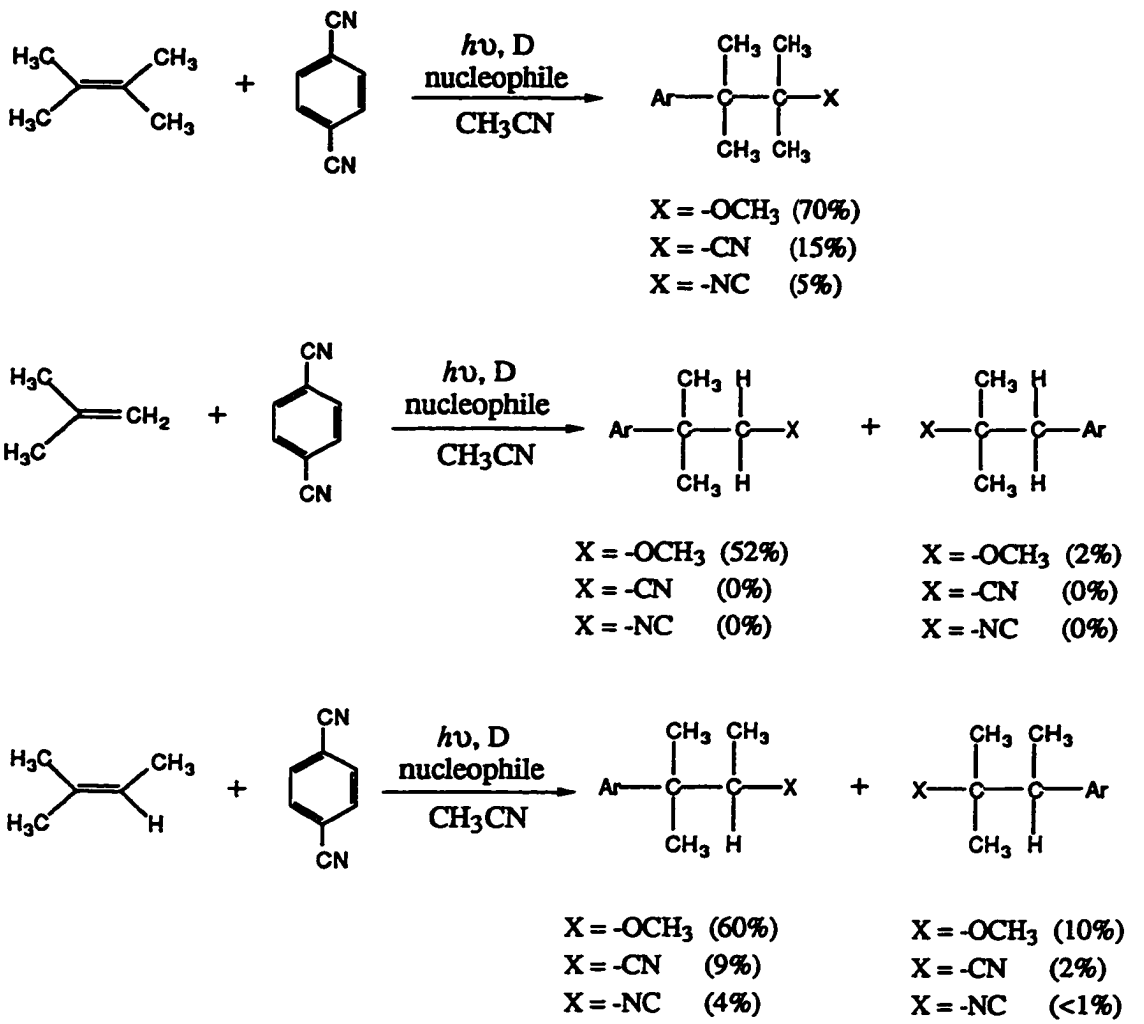

D = biphenyl Ar = 4-cyanophenyl

Figure 3.1: Isolated Yields of Photo-NOCAS Products with Methanol or Cyanide Serving as the Nucleophile

The regiochemistry in all cases can be considered as predominately *anti*-Markovnikov, where the nucleophile adds to the less substituted carbon of the double bond. The reasons for this preference have been rationalized. For alcoholic nucleophiles, the distonic radical cations that are initially formed can equilibrate via a relatively low

energy bridged structure. The regiochemistry is thermodynamically controlled and the product distribution is dependent on the stability of the β-alkoxyalkyl radical intermediates. However, when cyanide anion reacts as the nucleophile, the β-cyano or β-isocyano alkyl radicals cannot bridge, the regiochemistry is kinetically controlled, and hence steric factors dominate.[59] Experimental and theoretical investigations similar to those described in Chapter 2 were conducted to discover how the fluoride anion behaves in comparison with these other nucleophiles. The olefins chosen for this study were 2-methylpropene (**8**), 2-methyl-2-butene (**9**) and 2,3-dimethyl-2-butene (**10**).

3.2 Results

1) 2,3-Dimethyl-2-Butene

Irradiation of an acetonitrile solution of 1,4-dicyanobenzene (**4**), biphenyl (**11**), tetrabutylammonium fluoride (**12**), and 2,3-dimethyl-2-butene (**10**) resulted in one major 1:1 (alkene: 1,4-dicyanobenzene) adduct and one photo-NOCAS product (Figure 3.2). The 1:1 adduct, 3-(4-cyanophenyl)-2,3-dimethyl-1-butene (**13**), was obtained in 28% yield. The yield of the photo-NOCAS product, 3-(4-cyanophenyl)-2-fluoro-2,3-dimethylbutane (**14**), was 22%. The addition of the codonor, biphenyl, increased the efficiency of the reaction, but had no effect on the relative amounts of these reaction products.

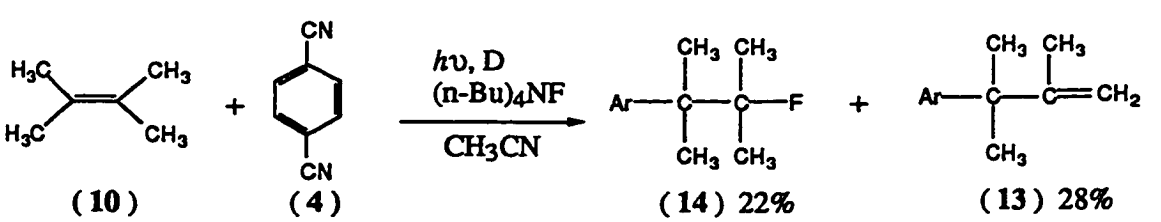

(**10**) (**4**) (**14**) 22% (**13**) 28%

D = biphenyl Ar = 4-cyanophenyl

Figure 3.2: Photo-NOCAS Reaction of 2,3-Dimethyl-2-Butene

The photo-NOCAS reaction of 2,3-dimethyl-2-butene (**10**) was also attempted using potassium fluoride as the fluoride ion source. These irradiations were identical to the ones involving (**12**) with the exception that equal molar amounts of KF and 18-crown-6 (1,4,7,10,13,16-hexaoxacyclooctadecane) were added instead. The use of KF as a source of fluoride ion did not affect the identity of the products, but significantly more 1:1 (alkene : 1,4-dicyanobenzene) adducts were observed. For this reason, tetrabutylammonium fluoride (**12**) was used in the subsequent large scale reactions to maximize the yield of the photo-NOCAS products.

2) 2-Methylpropene

A similar irradiation of an acetonitrile solution of (**4**), (**11**), (**12**), and 2-methylpropene (**8**) resulted in a 1:1 (alkene : 1,4-dicyanobenzene) adduct and two photo-NOCAS products (Figure 3.3). The 1:1 adduct, 3-(4-cyanophenyl)-2-methylpropene (**15**), was obtained in 8% yield. The *anti*-Markovnikov photo-NOCAS product, 2-(4-cyanophenyl)-1-fluoro-2-methylpropane (**16**), was isolated in 5% yield. A trace amount of the Markovnikov isomer, 1-(4-cyanophenyl)-2-fluoro-2-methylpropane, was identified (gc/ms, ^{1}H and ^{13}C nmr) but it was not isolated. Integration of a gc/ms chromatograph obtained from single ion monitoring for the molecular ion gave a ratio of 95 : 5 (*anti*-Markovnikov : Markovnikov) for the two photo-NOCAS products. This ratio remained constant as a function of irradiation time. Again, the addition of the codonor, biphenyl, increased the efficiency of the reaction, but did not have any effect on the product ratios.

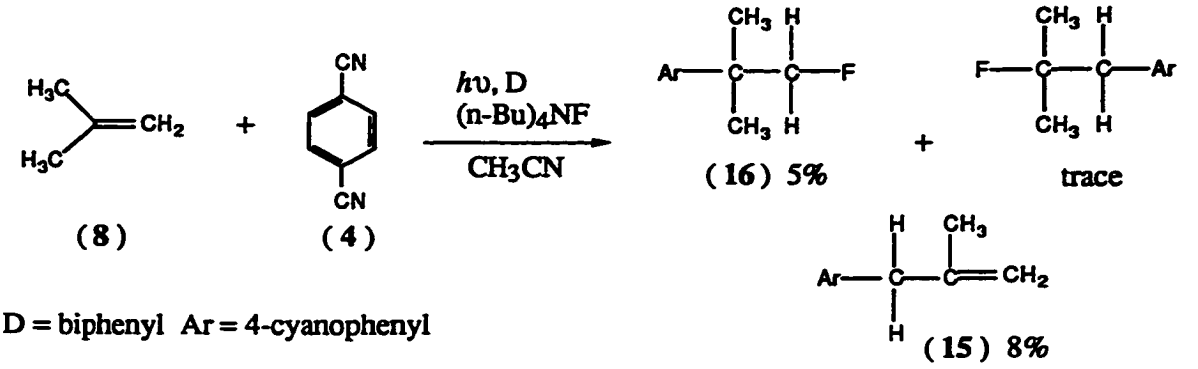

D = biphenyl Ar = 4-cyanophenyl

Figure 3.3: Photo-NOCAS Reaction of 2-Methylpropene

Theoretical investigations into the relative stability of the reaction intermediates involved calculations on fluoro-substituted radicals. The credibility of the MP2/6-31G*//HF/6-31G* level calculations was already established for radical intermediates in Chapter 2 (Table 2.1). However, the calculated thermodynamic stability of fluoro-substituted compounds has not been extensively investigated. Therefore, the influence of the theoretical model on the relative stability of two simple fluoro-substituted alkanes was examined and the results are summarized in Table 3.1. Including electron correlation (MP2) in the optimization and extending the basis set to 6-311+G* did not produce significant changes in the relative stability between these two compounds. These results are consistent with previous studies on fluorinated aromatic compounds where electron correlation and diffuse functions were not important for evaluating the enthalpy change of isodesmic reactions.[60] The data in Table 3.1 leads to the conclusion that the MP2/6-31G*//HF/6-31G* level is also sufficient for the fluoro-substituted compounds to be studied.

Table 3.1: Relative Stability of Fluoro-Substituted Alkanes Calculated at Various Theoretical Models

Theoretical Model	2-Fluoro-2-Methylpropane (au)	1-Fluoro-2-Methylpropane (au)	ΔH (kJ/mol)
HF/6-31G*//HF/6-31G*	-256.15900	-256.14810	28.62
MP2/6-31G*//HF/6-31G*	-256.85596	-256.84252	35.29
MP2/6-31G*//MP2/6-31G*	-256.85700	-256.84376	34.76
MP2/6-311+G*//MP2/6-31G*	-256.98841	-256.97513	34.87

Addition of the fluoride anion to the radical cation of 2-methylpropene produces β-fluoroalkyl radicals directly. The structure of the two possible radical intermediates for this reaction appears in Figure 3.4. Their relative stability was estimated by *ab initio* molecular orbital calculations. A comparison of the total energies obtained from MP2/6-31G*//HF/6-31G* calculations shows that the β-fluoroalkyl radical intermediate resulting from Markovnikov addition of fluoride to the radical cation (**8x**•) is 11.2 kJ/mol more stable than the alternative β-fluoroalkyl radical resulting from *anti*-Markovnikov addition (**8y**•). β-Fluoroalkyl radicals do not show a tendency to bridge,[61] and the results of the calculations were consistent with this. Geometry optimization starting from a symmetrically bridged radical converged to the more stable open radical (**8x**•). Details of structure, spin and charge density distributions for the β-fluoroalkyl intermediates discussed in this chapter can be found in Appendix IV.

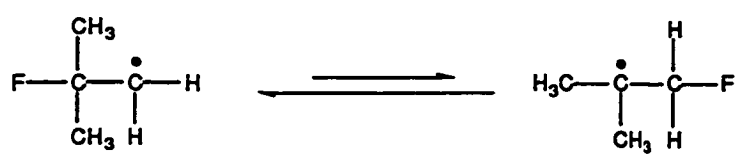

(**8x**•) (**8y**•)

ΔH = 11.2 kJ/mol

Figure 3.4: The Relative Stability of β-Fluoroalkyl Radical Intermediates from 2-Methylpropene

3) 2-Methyl-2-Butene

Irradiation of an acetonitrile solution of (4), (11), (12), and 2-methyl-2-butene (9) resulted in four 1:1 (alkene : 1,4-dicyanobenzene) adducts and two photo-NOCAS products (Figure 3.5). The combined yield of the four 1:1 adducts was 46%. The *anti*-Markovnikov photo-NOCAS product, 2-(4-cyanophenyl)-3-fluoro-2-methylbutane (17), was isolated in 22% yield; whereas the Markovnikov product, 3-(4-cyanophenyl)-2-fluoro-2-methylbutane (18), was obtained in only 2% yield. The ratio of *anti*-Markovnikov : Markovnikov products was found to be 89 : 11 by integration of a gc/ms chromatograph obtained by single ion monitoring for the molecular ion. This ratio was independent of irradiation time. The addition of a codonor, biphenyl, increased the efficiency of the reaction but had no effect on the product ratios.

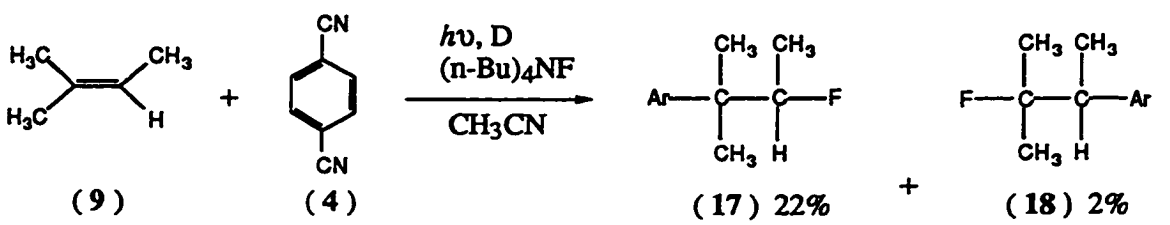

Figure 3.5: Photo-NOCAS Reaction of 2-Methyl-2-Butene

The relative stability of the radical intermediates for this reaction was also evaluated by *ab initio* molecular orbital calculations. The structure of the two alternative β-fluoroalkyl radicals are shown in Figure 3.6. A comparison of the total energies obtained from MP2/6-31G*//HF/6-31G* calculations show that the β-fluoroalkyl radical intermediates resulting from Markovnikov addition of fluoride to the radical cation (**9x**•) is 5.1 kJ/mol more stable than the alternative β-fluoroalkyl radical resulting from *anti*-

Markovnikov addition (**9y•**). Again, there was no evidence for bridging of the β-fluoroalkyl radical intermediate for this alkene.

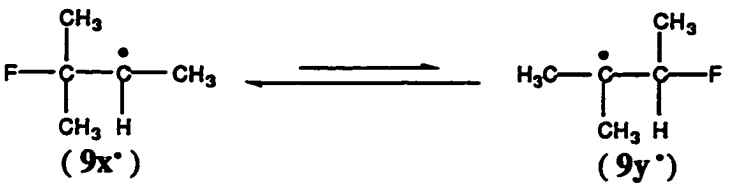

(**9x•**) (**9y•**)

$\Delta H = 5.1$ kJ/mol

Figure 3.6: The Relative Stability of β-Fluoroalkyl Radical Intermediates from 2-Methyl-2-Butene

4) Dienes

The feasibility of the photo-NOCAS reaction with fluoride anion serving as the nucleophile and conjugated dienes serving as the olefin was also investigated. The dienes investigated were: 1,3-butadiene, 2-methyl-1,3-butadiene, 4-methyl-1,3-pentadiene, 2,4-dimethyl-1,3-pentadiene, and 2,5-dimethyl-2,4-hexadiene. Irradiation of an acetonitrile solution of 1,4-dicyanobenzene (**4**), biphenyl (**11**), diene, and tetrabutylammonium fluoride (**12**) did not result in any photo-NOCAS products. The mass spectrum obtained from the gc/ms chromatographs of these reaction mixtures suggested that 1:1 (diene : 1,4-dicyanobenzene) adducts and dimers of the dienes were the major products from these reactions.

3.3 Discussion

The results of this study illustrated that the fluoride anion can react as a nucleophile in the context of the photo-NOCAS reaction. The photo-NOCAS products incorporating fluoride anion were obtained in reasonable yields with little attempt to optimize the reaction conditions. The nucleophilic nature of the fluoride anion has already been established. It serves as an effective nucleophile in nucleophilic substitution

reaction for a variety of organic substrates.[62] However, the fluoride anion was also observed to react as a base (pK_a of HF = 3.2).[63] Therefore, it is not surprising that deprotonation of the alkene radical cation, where the fluoride behaves as a base rather than a nucleophile, is a major competing pathway for the reactions under investigation. This kind of reactivity is also the major competing pathway in the preparation of alkyl fluorides by normal (S_N1, S_N2) nucleophilic substitution reactions.[62,64] Under the photo-NOCAS reaction condition, the basicity of the fluoride anion results in the formation of 1:1 (alkene: 1,4-dicyanobenzene) adducts. Figure 3.7 shows the mechanism for the formation of such adducts. These 1:1 adducts were the major product(s) in all of the reactions studied, indicating that the fluoride reacts more effectively as a base than as a nucleophile under the reaction conditions studied. This type of adduct is commonly observed when irradiations are carried out in the absence of a nucleophile.[65] Even though radical cations are known to be highly acidic species, there is direct evidence that the fluoride anion enhances the deprotonation step.[66] The radical cation of 2-methylpropene does not deprotonate easily, the resultant allylic radical is primary on both ambient ends. The 1:1 adduct (**15**) resulting from the deprotonation of the radical cation followed by coupling with the radical anion of the 1,4-dicyanobenzene is only observed in trace amounts in the absence of added base.[67]

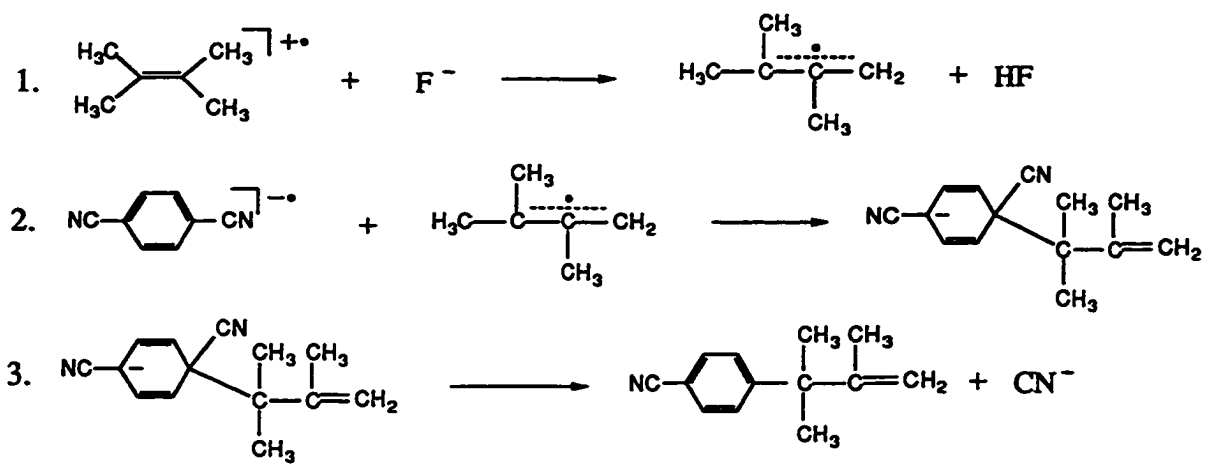

Figure 3.7: Mechanism for the Formation of 1:1 Adducts

Nucleophilic addition of fluoride anion to the radical cation of non-symmetric alkenes showed high regioselectivity. The regiochemistry can be described as predominately following the *anti*-Markovnikov mode of addition, where the nucleophile (fluoride) has added preferentially to the less substituted olefinic carbon. Addition at this end of the double bond produces the more heavily alkyl-substituted radical. At this point, one might be tempted to hypothesize that the regioselectivity is governed by the relative stability of the β-fluoroalkyl radical intermediates. However, results from theoretical calculations are contrary to this hypothesis. For both of the non-symmetric alkenes studied, the radical resulting from the Markovnikov addition of the fluoride anion is the more stable of the two alternative β-fluoroalkyl radicals. Therefore, enthalpy factors do not seem to influence the outcome of the regiochemistry. Steric factors, on the other hand, may be important as the fluoride consistently adds to the less substituted olefinic carbon. *Ab initio* molecular orbital calculations on the radical cations indicate that this carbon atom also carries the most positive charge density (see Figure 2.16). These experimental and theoretical results suggest that the fluoride anion behaves like the cyanide anion: the addition is kinetically controlled, with steric and polar factors dominating. This is in agreement with the highly exothermic nature of nucleophilic addition to the alkene radical cations found in Chapter 2 (see Figures 2.14 and 2.15). The large exothermic enthalpy results in an early transition state, and the product distribution is determined before the relative stability of the alternative β-fluoroalkyl radicals becomes important.

The attempted reactions with fluoride anion reacting as the nucleophile did not produce photo-NOCAS products when conjugated dienes were employed as the olefin. This behavior is related to that observed in the photo-NOCAS reaction with cyanide anion serving as the nucleophile. The nitrogen atom of the ambient cyanide anion reacts as a nucleophile to produce isonitrile products only with alkenes. No trace of the isonitrile products were found when conjugated dienes were used. This selectivity was

explained in terms of the hard-soft-acid-base (HSAB) principle. The fluoride anion falls into the hard category.[68] Relatively speaking, alkene radical cations can be considered as harder than those of conjugated dienes. Therefore, the hard fluoride anion nucleophile prefers to react with the harder alkene radical cations. The photo-NOCAS reaction incorporating fluoride as the nucleophile is then limited to hard electrophiles.

3.5 Conclusions

The fluoride anion can serve as an effective nucleophile in the photo-NOCAS reaction. The 4-cyanophenyl substituted fluoroalkanes were obtained in reasonable yields with alkenes. The reaction, however, is not effective with conjugated dienes. This reactivity can be explained in terms of the HSAB principle; the hard fluoride anion prefers to react with the relatively harder alkene radical cation. The classification of the alkene radical cations as "hard" and the diene radical cations as "soft" is only a qualitative division based on the conjugated nature of the diene. Other factors such as alkyl substitution may influence the hardness or softness of a radical cation. A quantitative scale for evaluating the hardness or softness of a radical cation would be a valuable tool for predicting its reactivity with a particular nucleophile. The need for a quantitative scale to evaluate the hardness and softness of a molecule or a particular site within a molecule has been previously recognized and methods for obtaining such scales have been developed. More recent developments involve the use of density functional theory.[69] Although such methodologies exist, there have been very few applications to real chemical systems. Further work on this project may include applying these methods to develop a quantitative scale to evaluate the hardness or softness of various olefins and nucleophiles.

The photo-NOCAS reaction with fluoride serving as the nucleophile is regioselective, with the fluoride anion adding preferentially to the less substituted end of a non-symmetric alkene. The product ratios were not a reflection of the relative

stabilities of the alternative β-fluoroalkyl radical intermediates, suggesting that enthalpy factors do not influence the regiochemistry. On the other hand, the fluoride anion adds consistently to the less substituted olefinic carbon, which is also the carbon atom bearing the greatest positive charge density in the radical cation of the alkene. These observations suggest that steric and polar factors are important and leads to the conclusion that addition is kinetically controlled. The product ratio is determined before the relative stability of the resulting β-fluoroalkyl radicals becomes important. This reactivity contrasts markedly with that observed when methanol reacts as the nucleophile, as discussed in the previous chapter, where the addition is thermodynamically controlled. Since the addition of methanol to the radical cation of the alkenes is also exothermic, it is conceivable that the less substituted reaction intermediate was initially formed. However, the bridged radical cation complex provides a low energy pathway for the methanol to migrate to the other side of the double bond. The same pathway for equilibration does not exist for the β-fluoroalkyl radicals as the fluorine atom is too small for the analogous bridging structure to be stable. Therefore, the β-fluoroalkyl radical initially formed goes on to produce photo-NOCAS product even though it is not the most stable intermediate.

Ab initio molecular orbital calculations indicate that the more stable of the two alternative β-fluoroalkyl radicals contains the less alkyl-substituted radical moiety for both non-symmetric alkenes examined. This is similar to the reversal of the relative stability of the β-alkoxyalkyl radicals observed for the nucleophilic addition of methanol to the 4-methyl-1,3-pentadiene radical cation. Therefore, the stabilization provided by alkyl substitution on the carbon bearing the functional group, the same factor that was responsible for the unprecedented order in the relative stability for the β-alkoxyalkyl radicals, can also be attributed to that observed in the β-fluoroalkyl radicals in the present study. Comparing the difference in relative stability of 11.2 kJ/mol between (**8x**•) and (**8y**•) vs. -1.3 kJ/mol for (**8a**•) and (**8b**•) , one can see that the magnitude of this stabilization is larger in the fluoride case. In fact, it is sufficiently large to cause a

primary β-fluoroalkyl radical to be more stable than a tertiary β-fluoroalkyl radical. This reversal of radical stability can have significant consequences on the outcome of reactions where the stability of radical intermediates is an important consideration. Therefore, a more detailed study on the effect of β-substituents on the stability of these radicals would be desirable. For example, more calculations could be performed to confirm that the extra stabilization is indeed due to alkyl substitution on the carbon bearing the substituent. The relative stability of substituted alkanes can be considered to determine if this effect is independent of the radical center. Studies conducted on different types of substituents would give an indication of the properties that govern the magnitude of this stabilization.

3.5 Computational Details

The Gaussian 94 package of programs was employed for the *ab initio* molecular orbital calculations.[70] The geometries of the open shell systems were fully optimized at the unrestricted Hartree-Fock level with the 6-31G* basis set.[44] Single point energies were calculated to second order in Møller-Plesset perturbation theory (MP2) using the 6-31G* basis set at the HF/6-31G* optimized geometries,[48] and were corrected for spin contamination where appropriate. Unless otherwise noted, all of the structures were optimized using the Berny optimization procedure[49] without symmetry constraints and were confirmed, by harmonic frequency analyses, to be local minima on their respective potential energy surfaces. The charge and spin density distributions were obtained from Mulliken population analysis.[50]

3.6 Experimental

3.6.1 General Information

Progress of the reactions was monitored by using a Hewlett-Packard (HP) 5890 gas chromatograph with a BD-1701 fused silica WCOT column (20 m x 0.25 mm, 0.4

μm film thickness) and a flame ionization detector (gc/fid). An HP 3392A integrator was interfaced with the gc/fid to obtain peak areas. An HP 5890 gas chromatograph with a 5% phenyl methyl silicone fused silica WCOT column (25 m x 0.20 mm, 0.33 μm film thickness) interfaced with an HP 5970 mass selective detector (gc/ms) was also used for product analysis. Exact mass determinations were obtained using a CEC 21-110 mass spectrometer. The mass spectra are reported as *m/z* (relative intensity). ^{1}H and ^{13}C nmr spectra were obtained from a Bruker 250 or 400 MSL spectrometer. Spectra were recorded in parts per million and the chemical shifts are relative to tetramethylsilane. Infrared spectra (ir) were recorded on a Nicolet 205 spectrometer and are reported in wave numbers (cm^{-1}). Separation of the reaction mixtures was carried out using a combination of the following chromatographic methods : preparative, centrifugally accelerated, radial, thin-layer chromatography (chromatotron),[71] using 1, 2 or 4 mm plates prepared with thin-layer chromatography (tlc) grade silica gel (with binder and fluorescent indicator, Merck 7749); dry column flash chromatography (dcfc)[72] packed with tlc grade silica gel (with binder, Rose Scientific Ltd. 81632); preparative thin-layer chromatography using pre-coated silica gel plates (2 mm thickness, Merck 5717).

3.6.2 Materials

Acetonitrile was distilled twice, first from sodium hydride and then from phosphorous pentoxide. It was then passed through a column of basic alumina, refluxed over calcium hydride for 24 h (under a nitrogen atmosphere), fractionally distilled, and stored over 3Å molecular sieves. 1,4-Dicyanobenzene (Aldrich) was purified by treatment with activated carbon in methylene chloride, followed by recrystallization from 95% ethanol. Biphenyl was recrystallized three times from methanol before use. Tetrabutylammonium fluoride (Aldrich) was dried at 55°C under vacuum for 24 h just prior to use. 2-Methylpropene (Matheson), 2,3-dimethyl-2-butene (Aldrich), and 2-methyl-2-butene (Aldrich) were used as received.

3.6.3 Irradiations

Irradiations were carried out on acetonitrile solutions of 1,4-dicyanobenzene (**4**), the alkene, tetrabutylammonium fluoride (**12**), and biphenyl (**11**) serving as a codonor. These solutions were irradiated in either 2 cm inner diameter Pyrex tubes or 5 mm Pyrex nmr tubes, which were deoxygenated by either nitrogen or alkene ebullition. The samples were irradiated at 10°C using a CGE 1kW medium-pressure mercury vapor lamp contained in a water-cooled quartz immersion well. The yields of the reaction products were calculated based on the amount of 1,4-dicyanobenzene consumed.

3.6.4 Reaction of 2,3-Dimethyl-2-Butene with 1,4-Dicyanobenzene and Tetrabutylammonium Fluoride

A solution of 1,4-dicyanobenzene (**4**) (1.0401 g, 0.0081 mol), biphenyl (**11**) (1.2151 g, 0.0079 mol) and tetrabutylammonium fluoride (**12**) (3.7161 g, 0.014 mol) in acetonitrile (160 ml) was deoxygenated by nitrogen ebullition. 2,3-Dimethyl-2-butene (**10**) (2.0 ml, 0.017 mol) was added to the reaction mixture, and the solution was irradiated for 24.0 h. Removal of the solvent yielded the crude photolysate. Initial separation of the irradiation mixture was achieved by dcfc using an ether/hexanes gradient. Further purification of the products 3-(4-cyanophenyl)-2,3-dimethyl-1-butene (**13**) and 3-(4-cyanophenyl)-2-fluoro-2,3-dimethylbutane (**14**) was carried out by repeated chromatography (chromatotron) using 100% hexanes as the eluant. Final separation of the 1:1 (alkene : 1,4-dicyanobenzene) adduct from the fluoride adduct was achieved by preparative tlc using a 2.5% ether/hexanes gradient (developed twice).

3-(4-Cyanophenyl)-2,3-Dimethyl-1-Butene (13)

The yield of (**13**) was 28%. The ^{1}H nmr spectrum agrees well with previously reported results.[7] ^{1}H nmr (250.13 MHz, $CDCl_3$) δ_{TMS}: 1.43 (s, 6H, H's of methyl groups adjacent to aryl-substituted carbon), 1.50 (s, 3H, H's of vinylic methyl group), 4.94 (d,

1H, $^2J_{H-H}$ = 1.2 Hz, vinylic hydrogen), 5.01 (d, 1H, $^2J_{H-H}$ = 1.2 Hz, vinylic hydrogen), 7.41 (d, 2H, $^3J_{H-H}$ = 8.5 Hz, H's adjacent to alkyl-substituted aryl carbon), 7.58 (d, 2H, $^3J_{H-H}$ = 8.5 Hz, H's adjacent to cyano-substituted aryl carbon); ^{13}C nmr (62.90 MHz, $CDCl_3$) δ: 20.09 (q, vinylic methyl group), 28.08 (q, methyl groups adjacent to aryl-substituted carbon), 44.42 (s, aryl-substituted carbon), 109.61 (s, quaternary aryl carbon, cyano-substituted), 110.78 (t, terminal olefinic carbon), 119.13 (s, CN), 126.98 (d, aromatic CH adjacent to alkyl-substituted aryl carbon), 132.02 (d, aromatic CH adjacent to cyano-substituted aryl carbon), 151.08 (s, quaternary aryl carbon, alkyl-substituted), 154.15 (s, alkyl-substituted olefinic carbon).

3-(4-Cyanophenyl)-2-Fluoro-2,3-Dimethylbutane (14)

The yield of (**14**) was 22%: infrared (Nicolet 205) υ: 2989(s), 2229(s), 1608(m), 1506(m), 1474(m), 1377(s), 1098(m), 844(s); ^{1}H nmr (250.13 MHz, $CDCl_3$) δ_{TMS}: 1.22 (d, 6H, $^3J_{H-F}$ = 22.0 Hz, H's of methyl groups adjacent to fluoro-substituted carbon), 1.42 (s, 6H, H's of methyl groups adjacent to aryl-substituted carbon), 7.55 (d, 2H, $^3J_{H-H}$ = 9.1 Hz, H's adjacent to alkyl-substituted aryl carbon), 7.60 (d, 2H, $^3J_{H-H}$ = 9.1 Hz, H's adjacent to cyano-substituted aryl carbon); ^{13}C nmr (62.90 MHz, $CDCl_3$) δ: 23.59 (q, d, $^2J_{C-F}$ = 24.8 Hz, methyl groups adjacent to fluoro-substituted carbon), 24.14 (q, d, $^3J_{C-F}$ = 5.7 Hz, methyl groups adjacent to aryl-substituted carbon), 45.12 (s, d, $^2J_{C-F}$ = 20.0 Hz, aryl-substituted carbon), 98.74 (s, d, $^1J_{C-F}$ = 175.5 Hz, fluoro-substituted carbon), 109.99 (s, quaternary aryl carbon, cyano-substituted), 119.04 (s, CN), 128.80 (d, aromatic CH adjacent to alkyl-substituted aryl carbon), 131.31 (d, aromatic CH adjacent to cyano-substituted aryl carbon), 151.61 (s, quaternary aryl carbon, alkyl-substituted); ms *m/z*: 40(25), 61(7), 116(30), 130 (20), 144(100), 145(95), 205(1); exact mass calcd. for $C_{13}H_{16}FN$: 205.1267; found: 205.1262.

3.6.5 Reaction of 2-Methylpropene with 1,4-Dicyanobenzene and Tetrabutylammonium Fluoride

2-Methylpropene (**8**) was bubbled into a solution of 1,4-dicyanobenzene (**4**) (1.5572 g, 0.012 mol), biphenyl (**11**) (1.9684 g, 0.013 mol) and tetrabutylammonium fluoride (**12**) (3.8249 g, 0.015 mol) in acetonitrile (240 ml). This reaction mixture was irradiated for 50.5 h. The solvent was then removed to afford the crude photolysate. Initial separation of the reaction mixture was achieved by dcfc using a solvent gradient of hexanes and ether. 1,4-Dicyanobenzene (**4**) (0.9318 g, 0.0073 mol) was recovered in this manner (40% conversion). Subsequent purification of the products 3-(4-cyanophenyl)-2-methylpropene (**15**) and 2-(4-cyanophenyl)-1-fluoro-2-methylpropane (**16**) were carried out by repeated chromatography (chromatotron) with 100% hexanes and 0.25% ether/hexanes as eluants, respectively.

A trace amount of 1-(4-cyanophenyl)-2-fluoro-2-methylpropane was also detected. Evidence for this compound consisted of a doublet at 2.95 ppm ($^3J_{H\text{-}F}$ = 21.7 Hz) in the ^{1}H nmr spectrum, indicative of the aryl-substituted methylene group, and, a doublet at 26.69 ppm ($^2J_{C\text{-}F}$ = 24.8 Hz) in the ^{13}C nmr spectrum, indicative of methyl groups adjacent to a fluoro-substituted carbon. Integration of a gc/ms chromatograph obtained from single ion monitoring mode for the molecular ion (*m/z* = 177) gave a ratio of 95 : 5 (*anti*-Markovnikov : Markovnikov) for the two photo-NOCAS products.

3-(4-Cyanophenyl)-2-Methylpropene (15)

The yield of (**15**) was 8%: infrared (Nicolet 205) υ: 3078(m), 2971(m), 2934(m), 2228(s), 1650(m), 1607(s), 1504(m), 1443(m), 1375(m), 897(s); ^{1}H nmr (250.13 MHz, $CDCl_3$) δ_{TMS}: 1.66 (s, 3H, CH_3), 3.36 (s, 2H, methylene group), 4.72 (s, 1H, vinylic hydrogen), 4.86 (s, 1H, vinylic hydrogen), 7.29 (d, 2H, $^3J_{H\text{-}H}$ = 8.5 Hz, H's adjacent to alkyl-substituted aryl carbon), 7.58 (d, 2H, $^3J_{H\text{-}H}$ = 8.5 Hz, H's adjacent to cyano-

substituted aryl carbon); ^{13}C nmr (62.90 MHz, $CDCl_3$) δ: 22.06 (q, CH_3), 44.64 (t, aryl-substituted methylene carbon), 110.07 (s, quaternary aryl carbon, cyano-substituted), 113.23 (t, terminal olefinic carbon), 119.09 (s, CN), 129.71 (d, aromatic CH adjacent to alkyl-substituted aryl carbon), 132.16 (d, aromatic CH adjacent to cyano-substituted aryl carbon), 143.56 (s), 145.44 (s); ms *m/z*: 63(6), 69(23), 89(8), 115(11), 116(10), 129(5), 142(100), 143(8), 156 (10), 157(67). These spectral data agree well with previously reported results.[73]

2-(4-Cyanophenyl)-1-Fluoro-2-Methylpropane (16)

The yield of (**16**) was 5%: infrared (Nicolet 205) υ: 2974(s), 2898(m), 2229(s), 1608(m), 1507(m), 1473(m), 1370(m), 1020(s), 839(s); ^1H nmr (250.13 MHz, $CDCl_3$) δ_{TMS}: 1.37 (d, 6H, $^4J_{H\text{-}F}$ = 1.8 Hz, H's of methyl groups), 4.38 (d, 2H, $^2J_{H\text{-}F}$ = 47.6 Hz, H's of fluoro-substituted methylene group), 7.49 (d, 2H, $^3J_{H\text{-}H}$ = 8.5 Hz, H's adjacent to alkyl-substituted aryl carbon), 7.63 (d, 2H, $^3J_{H\text{-}H}$ = 8.5 Hz, H's adjacent to cyano-substituted aryl carbon); ^{13}C nmr (62.90 MHz, $CDCl_3$) δ: 24.61 (q, d, $^3J_{C\text{-}F}$ = 5.8 Hz, methyl groups), 39.81 (s, d, $^2J_{C\text{-}F}$ = 18.1 Hz, aryl-substituted carbon), 90.65 (t, d, $^1J_{C\text{-}F}$ = 178.0 Hz, fluoro-substituted carbon), 110.35 (s, quaternary aryl carbon, cyano-substituted), 118.86 (s, CN), 127.02 (d, aromatic CH adjacent to alkyl-substituted aryl carbon), 132.12 (d, aromatic CH adjacent to cyano-substituted aryl carbon), 151.13 (s, d, $^3J_{C\text{-}F}$ = 2.9 Hz, quaternary aryl carbon, alkyl-substituted); ms *m/z*: 38(13), 40(12), 116(48), 144(100), 145(17), 177(32); exact mass calcd. for $C_{11}H_{12}FN$: 177.0954; found: 177.0955.

3.6.6 Reaction of 2-Methyl-2-Butene with 1,4-Dicyanobenzene and Tetrabutylammonium Fluoride

A solution of 1,4-dicyanobenzene (**4**) (1.6289 g, 0.013 mol), biphenyl (**11**) (1.8685 g, 0.012 mol) and tetrabutylammonium fluoride (**12**) (6.1549 g, 0.024 mol) in

acetonitrile (240 ml) was deoxygenated by nitrogen ebullition. 2-Methyl-2-butene (**9**) (3.0 ml, 0.028 mol) was added to the reaction mixture, and the solution was irradiated for 24.0 h. Removal of the solvent yielded the crude photolysate. Initial separation of the irradiation mixture was achieved by dcfc using an ether/hexanes gradient. 1,4-Dicyanobenzene (**4**) (0.4193 g, 0.0033 mol) was recovered in this manner (74% conversion). Four 1:1 adducts (combined yield of 46%) were also separated from the reaction mixture by dcfc. The identity of these products was deduced by the mass of the molecular ion (*m/z* = 171) and the fragmentation pattern in the mass spectrum. Subsequent purification of the fluoride adducts was carried out by repeated chromatography (chromatotron) using 100% hexanes as the eluant. Final separation of the two isomers was attempted by preparative tlc using a 1.0% ether/hexanes gradient (developed 12 times). Integration of a gc/ms chromatograph obtained from single ion monitoring mode for the molecular ion (*m/z* = 191) gave a ratio of 89 : 11 (*anti*-Markovnikov : Markovnikov) for the two photo-NOCAS products.

2-(4-Cyanophenyl)-3-Fluoro-2-Methylbutane (17)

The yield of (**17**) was 22%: infrared (Nicolet 205) υ: 2985(s), 2924(m), 2229(s), 1608(m), 1507(m), 1453(m), 1382(m), 1067(s), 841(s); ^{1}H nmr (250.13 MHz, $CDCl_3$) δ_{TMS}: 1.10 (d, d, 3H, $^3J_{H\text{-}H}$ = 6.1 Hz, $^3J_{H\text{-}F}$ = 24.4 Hz, H's of methyl group adjacent to fluoro-substituted carbon), 1.38 (s, 6H, H's of methyl groups adjacent to aryl-substituted carbon), 4.66 (q, d, 1H, $^3J_{H\text{-}H}$ = 6.1 Hz, $^2J_{H\text{-}F}$ = 47.0 Hz, methine proton), 7.50 (d, 2H, $^3J_{H\text{-}H}$ = 8.5 Hz, H's adjacent to alkyl-substituted aryl carbon), 7.61 (d, 2H, $^3J_{H\text{-}H}$ = 8.5 Hz, H's adjacent to cyano-substituted aryl carbon); ^{13}C nmr (100.61 MHz, $CDCl_3$) δ: 16.23 (q, d, $^2J_{C\text{-}F}$ = 24.2 Hz, methyl groups adjacent to fluoro-substituted carbon), 24.07 (q, d, $^3J_{C\text{-}F}$ = 5.3 Hz, methyl group adjacent to aryl-substituted carbon), 24.25 (q, d, $^3J_{C\text{-}F}$ = 4.7 Hz, methyl group adjacent to aryl-substituted carbon), 42.83 (s, d, $^2J_{C\text{-}F}$ = 18.7 Hz, aryl-substituted carbon), 96.36 (s, d, $^1J_{C\text{-}F}$ = 176.5 Hz, fluoro-substituted carbon), 110.48

(s, quaternary aryl carbon, cyano-substituted), 119.10 (s, CN), 127.89 (d, aromatic CH adjacent to alkyl-substituted aryl carbon), 132.10 (d, aromatic CH adjacent to cyano-substituted aryl carbon), 151.32 (s, quaternary aryl carbon, alkyl-substituted); ms *m/z*: 47(2), 104(8), 116(35), 144(100), 145(10), 191(8); exact mass calcd. for $C_{12}H_{14}FN$: 191.1110; found: 191.1105.

3-(4-Cyanophenyl)-2-Fluoro-2-Methylbutane (18)

The yield of (**18**) was 2%: Spectral information obtained from a 7:3 [(**18**):(**17**)] mixture. ^{1}H nmr (250.13 MHz, $CDCl_3$) δ_{TMS}: 1.26 (d, 6H, $^3J_{H\text{-}F}$ = 22.0 Hz, H's of methyl groups adjacent to fluoro-substituted carbon), 1.34 (d, 3H, $^3J_{H\text{-}H}$ = 7.3 Hz, H's of methyl group adjacent to aryl-substituted carbon), 2.96 (q, d, 1H, $^3J_{H\text{-}H}$ =7.3 Hz, $^3J_{H\text{-}F}$ = 19.5 Hz, methine proton), 7.35 (d, 2H, $^3J_{H\text{-}H}$ = 8.3 Hz, H's adjacent to alkyl-substituted aryl carbon), 7.59 (d, 2H, $^3J_{H\text{-}H}$ = 8.3 Hz, H's adjacent to cyano-substituted aryl carbon); ^{13}C nmr (62.90 MHz, $CDCl_3$) δ: 15.57 (q, d, $^3J_{C\text{-}F}$ = 5.7 Hz, methyl group adjacent to aryl-substituted carbon), 24.90 (q, d, $^2J_{C\text{-}F}$ = 24.7 Hz, methyl group adjacent to fluoro-substituted carbon), 25.76 (q, d, $^2J_{C\text{-}F}$ = 24.8 Hz, methyl group adjacent to fluoro-substituted carbon), 49.08 (s, d, $^2J_{C\text{-}F}$ = 21.7 Hz, aryl-substituted carbon), 96.51 (s, d, $^1J_{C\text{-}F}$ = 172.1 Hz, fluoro-substituted carbon), 110.49 (s, quaternary aryl carbon, cyano-substituted), 118.97 (s, CN), 129.67 (d, aromatic CH adjacent to alkyl-substituted aryl carbon), 131.85 (d, aromatic CH adjacent to cyano-substituted aryl carbon), 148.44 (s, quaternary aryl carbon, alkyl-substituted); ms *m/z*: 61(90), 77(20), 103(27), 116(21), 129 (19), 130(100), 156(34), 191(5).

Chapter 4

The Stabilizing Effect of Alkyl-Substitution on the Carbon Bearing Heteroatom Functional Groups

4.1 Introduction

The relative stability of the β-substituted alkyl radical intermediates arising from the nucleophilic addition to the radical cations of alkenes or dienes, estimated by theoretical calculations in Chapters 2 and 3, was not anticipated. The effect of the methoxy group on the relative stability of β-alkoxyalkyl radicals has already been alluded to in Chapter 2. In the most extreme case, the ether functional group caused a mono alkyl-substituted allylic radical to be more stable than a tri alkyl-substituted allylic radical. The relative stability of these radical intermediates was reflected in the product distribution of the photo-NOCAS reaction with 4-methyl-1,3-pentadiene. The effect of the β-substituent was also evident in the relative stability of fluoro-substituted radicals. In fact, the magnitude of this effect was so large that a primary β-fluoroalkyl radical becomes more stable than a tertiary β-fluoroalkyl radical as exemplified by those radicals studied in Chapter 3. This observation is contrary to the anticipated trend where the more heavily alkyl-substituted radical is expected to be the more stable. The influence of the relative stability of these β-substituted radical intermediates on the photo-NOCAS reaction has already been discussed. However, investigations into the thermodynamic stability of free radicals can have more general applications. For example, free radicals play an important role in basic processes such as air oxidation, thermal cracking, polymerization, aging and photosynthesis. The importance of free radical intermediates in organic reactions have also been well recognized and there is an abundance of literature regarding their structure, energetics and reactivity.[74]

One of the reactions that share the type of β-substituted intermediates studied in Chapters 2 and 3 is the addition of free radicals to alkenes. This reaction has been studied extensively due to its role as an important step in several industrial processes, and the complex combination of the factors that influence the product ratios and product yields of this reaction also provide an interesting challenge from an academic point of view. There has been continuous debate in the literature as to the nature of the factors that determine the rate and the regiochemistry of this reaction. There was evidence that enthalpic factors were not important and the reaction was thought to be kinetically controlled.[75] However, other studies provided evidence that the relative stability of the free radical intermediates play a prominent role in the addition of some radicals to substituted alkenes.[31] The current understanding is that each specific reaction is governed by a combination of polar, enthalpy, and steric factors.[76] The relative importance of these factors is unique and has to be determined for individual cases. A clear understanding of the factors that govern the relative stability of the β-substituted radicals is needed to predict the relative magnitude of the enthalpic factors for a given reaction. As a result, further investigations into the factors that determine the relative stabilities of these radical intermediates is warranted.

4.2 Computational Details

The Gaussian 94 package of programs was employed for all *ab initio* molecular orbital calculations.[70] The geometries of the open shell systems were fully optimized at the unrestricted Hartree-Fock level with the 6-31G* basis set.[44] Single point energies were calculated to second order in Møller-Plesset perturbation theory (MP2) using the 6-31G* basis set at the HF/6-31G* optimized geometries,[48] and were corrected for spin contamination where appropriate. Unless otherwise noted, all of the structures were optimized using the Berny optimization procedure[49] without symmetry constraints and were confirmed, by harmonic frequency analyses, to be local minima on their respective

potential energy surfaces. The charge and spin density distributions were obtained from Mulliken population analysis.[50]

4.3 Results

The theoretical calculations of the two alternative β-substituted radical intermediates that arise from nucleophilic addition to the radical cation of 2-methylpropene provide a comparison between a primary and a tertiary center. The isodesmic reaction 1a in Figure 4.1 shows the relative stability of two radicals substituted by cyano, isocyano, methoxy and fluoro groups evaluated at the MP2/6-31G*//HF/6-31G* level. Selected geometrical parameters, spin and charge densities for the β-substituted alkyl radicals are collected in Appendix IV, and those of the substituted alkanes in Appendix V. Regardless of the substituent, the enthalpy change is significantly less negative than when considering the relative stability of the alkyl radicals alone (-24.0 kJ/mol estimated by the isodesmic reaction 1c in Figure 4.2). The ΔH is fairly negative in the case of the cyano substituent, indicating that the tertiary alkyl radical is significantly more stable than the primary alkyl radical. However, the tertiary radical is only slightly more stable than the primary radical for the isocyano and methoxy substituted systems. The trend is reversed for the fluoro substituent where the primary radical is now 11 kJ/mol more stable than the tertiary radical, implying that replacing a hydrogen atom by a fluorine atom causes a change of 35 kJ/mol in the relative stability.

1a.

X = -CN	ΔH = -15.8 kJ/mol
X = -NC	ΔH = -2.0 kJ/mol
X = -OCH_3	ΔH = -1.3 kJ/mol
X = -F	ΔH = 11.2 kJ/mol

Figure 4.1: Relative Stability of β-Substituted Primary and Tertiary Alkyl Radicals

The enthalpy change of the isodesmic reactions 1b to 1e shown in Figure 4.2 were evaluated to confirm these dramatic substituent effects by attempting to separate the influence of the substituents in question from that of the radical moiety. Reaction 1b measures the relative stability of substituted alkanes independent of the radical center. The alkanes were chosen to be structurally similar to the original radicals and were derived by attaching a hydrogen atom to the radical center. The enthalpy for reaction 1b is positive for all substituents investigated, suggesting that all of the substituents prefer to be attached to the more heavily alkyl-substituted carbon. The isodesmic reaction 1c is designed to evaluate the effect of the radical moiety. The radical species were obtained by replacing the functional group in the original β-substituted radical by a hydrogen atom. It shows that a tertiary alkyl radical is more stable than a primary alkyl radical by 24.0 kJ/mol. This is consistent with expected trends and in general agreement with the literature value of 15.9 kJ/mol determined by experimentally measured heats of formation.[77] Reaction 1d is just the sum of reactions 1b and 1c. This isodesmic reaction illustrates the combined effect of substitution on the carbon atom bearing the functional groups as well as on the radical moiety. It can be viewed as an alternative method to measure the relative stability of the substituted alkyl radicals in reaction 1a.

The isodesmic reaction 1e depicted in Figure 4.3 is an alternative way of separating the radical center from the functional group. Instead of adding hydrogen atoms to radical centers or replacing functional groups with hydrogen atoms, only the connectivity at the carbon atom bearing the radical or functional group is retained while the other half of the molecule is replaced by a methyl group. The enthalpy change of this isodesmic reaction is similar to those obtained for reactions 1a and 1d. It is encouraging to find the general agreement between these three alternative methods of evaluating the same relative stability.

X = -CN ΔH = 8.4 kJ/mol
X = -NC ΔH = 21.6 kJ/mol
X = -OCH_3 ΔH = 15.3 kJ/mol
X = -F ΔH = 35.3 kJ/mol

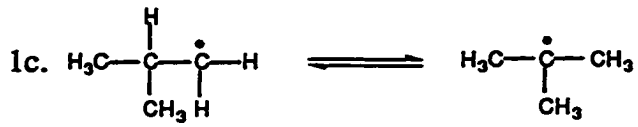

ΔH = -24.0 kJ/mol

X = -CN ΔH = -15.6 kJ/mol
X = -NC ΔH = -2.4 kJ/mol
X = -OCH_3 ΔH = -8.7 kJ/mol
X = -F ΔH = 11.3 kJ/mol

Figure 4.2: Relative Stability of Substituted Alkanes and Alkyl Radicals for Comparison between a Primary and a Tertiary Center

X = -CN ΔH = -8.3 kJ/mol
X = -NC ΔH = 4.9 kJ/mol
X = -OCH_3 ΔH = -2.9 kJ/mol
X = -F ΔH = 18.2 kJ/mol

Figure 4.3: Alternative Method for Evaluating the Relative Stability of β-Substituted Primary and Tertiary Alkyl Radicals

The theoretical calculations from 2-methyl-2-butene compare the relative stability of a secondary and a tertiary center. Reaction 2a in Figure 4.4 is a direct comparison of the two alternative β-substituted radical intermediates resulting from the nucleophilic addition

to the 2-methyl-2-butene radical cation. The values range from -6.4 kJ/mol for the methoxy substituent, where the tertiary radical is more stable, to 5.1 kJ/mol for the fluoro substituent, where the secondary radical is more stable.

X = -CN ΔH = -5.6 kJ/mol
X = -NC ΔH = 0.9 kJ/mol
X = -OCH_3 ΔH = -6.4 kJ/mol
X = -F ΔH = 5.1 kJ/mol

Figure 4.4: Relative Stability of β-Substituted Secondary and Tertiary Alkyl Radicals

The isodesmic reactions 2b and 2c, shown in Figure 4.5, were designed to separate the effect of the radical moiety from that of the functional groups. Reaction 2c indicates that a tertiary alkyl-substituted radical is more stable than a secondary alkyl-substituted radical by 9.8 kJ/mol. Reaction 2b eliminates the effect of the radical by adding a hydrogen atom to the radical center of the original β-substituted radical involved in reaction 2a. It measures the relative stability arising from the functional group alone. Again, the ΔH of this reaction is positive for all substituents, suggesting that it is energetically more favorable for them to be attached to the more heavily alkyl-substituted carbon atom. The ΔH of reaction 2d predicts the relative stability of the β-substituted radicals by combining the two effects exemplified by reactions 2b and 2c. In the case of the methoxy and cyano substituted radicals, the relative stability of the radical moiety dominates, and the overall reaction enthalpy is exothermic. When the radicals are substituted by an isocyano group the magnitude of the two effects is similar, and their combined result is almost thermo-neutral. The stabilizing effect of alkyl substitution on the carbon bearing the fluoro substituent is larger than that of alkyl substitution on a radical center. The overall result is

that the secondary β-fluoroalkyl radical is now more stable than the tertiary β-fluoroalkyl radical.

X = -CN ΔH = 3.5 kJ/mol
X = -NC ΔH = 9.5 kJ/mol
X = -OCH_3 ΔH = 5.0 kJ/mol
X = -F ΔH = 15.5 kJ/mol

ΔH = -9.8 kJ/mol

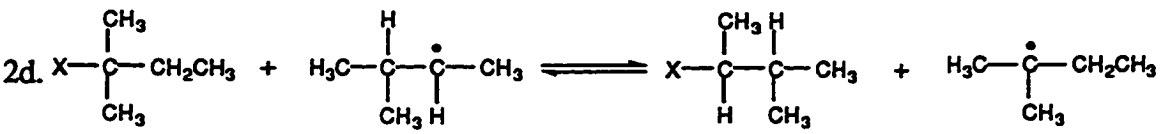

X = -CN ΔH = -6.3 kJ/mol
X = -NC ΔH = -0.3 kJ/mol
X = -OCH_3 ΔH = -4.8 kJ/mol
X = -F ΔH = 5.7 kJ/mol

Figure 4.5: Relative Stability of Substituted Alkanes and Alkyl Radicals for Comparison between a Secondary and a Tertiary Center

The isodesmic reaction 2e, depicted in Figure 4.6, represents an alternative method for separating the relative effects of the radical moiety and that of the substituents. In this strategy, the connectivity around the carbon bearing the substituent (or radical) is maintained and the other half of the molecule is replaced by a methyl group. The relative stability of the radicals and substituted alkanes measured in this manner are consistent with the previous results from reactions 2a and 2d.

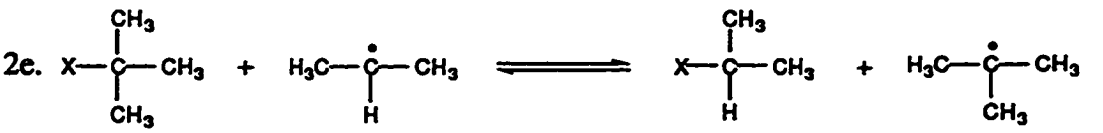

2e.

X = -CN ΔH = -3.5 kJ/mol
X = -NC ΔH = 2.0 kJ/mol
X = -OCH_3 ΔH = -4.1 kJ/mol
X = -F ΔH = 7.2 kJ/mol

Figure 4.6: Alternative Method for Evaluating the Relative Stability of β-Substituted Secondary and Tertiary Alkyl Radicals

4.4 Discussion

The general agreement between the reaction enthalpies of the isodesmic reactions 1a, 1d and 1e as well as those between 2a, 2d and 2e indicates that the relative stability of the β-substituted alkyl radicals is influenced by the relative stability of the appropriate alkyl radicals and the relative stability of the appropriate substituted alkanes. In some cases, alkyl substitution on the carbon atom bearing the substituent can have substantial effects on the relative stability of the whole radical species. The difference in energy between a primary and a tertiary substituted alkane is illustrated by the enthalpy change of the isodesmic reaction 1b. The effect of alkyl substitution on the carbon atom bearing the substituent ranges from 8.4 kJ/mol for the cyano group up to 35.3 kJ/mol for the fluoro substituent. The contribution from the radical moiety is the energy difference between a primary alkyl-substituted and a tertiary alkyl-substituted radical as illustrated in the isodesmic reaction 1c. The relative stability of the β-substituted alkyl radicals in reaction 1a is then a balance between two opposing trends: the stabilization provided by alkyl substitution on the carbon bearing the heteroatom substituent vs. the stabilization provided by alkyl substitution on the radical center. The enthalpy change of reaction 1a becomes positive when alkyl substitution on the carbon atom bearing the heteroatom substituent becomes more dramatic than alkyl substitution on the radical center (*i.e.* when the ΔH of reaction 1b is more positive than 24.0 kJ/mol). This is the case with the fluoro substituent

and as a result, the primary β-substituted alkyl radical is more stable than the tertiary β-substituted alkyl radical.

The enthalpy change for the isodesmic reaction 2b gives an indication of the energy difference between a secondary and a tertiary substituted alkane. As expected, the magnitude of the ΔH values are smaller than those from the isodesmic reaction 1b where the difference between a primary and a tertiary substituted alkane was compared. However, the ΔH is still always positive with the values ranging from 3.5 kJ/mol for the cyano substituent to 15.5 kJ/mol for the fluoro group. The relative stability of a secondary alkyl radical and a tertiary alkyl radical is estimated by the enthalpy change of reaction 2c. The excellent agreement between the ΔH values obtained from reaction 2a and 2d confirms that the relative stability of the β-substituted alkyl radicals is a competition between the stabilization by alkyl substitution at the heteroatom substituent and stabilization by alkyl substitution at the radical center. The fluoro substituent is the only group where alkyl substitution on the carbon atom bearing the functional group provides more thermodynamic stability than alkyl substitution on the radical center. Consequently, the secondary β-fluoroalkyl radical is more stable than the tertiary β-fluoroalkyl radical, as shown by the positive ΔH for the isodesmic reaction 2a.

The above analysis emphasizes the importance of alkyl substitution on the carbon atom bearing the heteroatom substituent. The ΔH of the isodesmic reactions 1b and 2b gives an indication of the magnitude of this effect for the four substituents studied. The idea that alkyl substitution may stabilize a carbon atom bearing certain types of functional groups may be intuitive. For example, one finds that *t*-butyl alcohol is more stable than methanol when considering their heats of formation.[78] However, the magnitude of this effect may not have been fully appreciated. Luo and Benson found a strong correlation between the quantity $\Delta H_f(t\text{-}C_4H_9X) - \Delta H_f(CH_3X)$ calculated from experimental heats of formation and the electronegativity of the heteroatom in the substituent X.[79] Further

investigations have shown that this correlation is also present for quantities such as $\Delta H_f(i\text{-}C_3H_7X) - \Delta H_f(CH_3X)$ and $\Delta H_f(C_2H_5X) - \Delta H_f(CH_3X)$. A study plotting the above values with 17 different electronegativity scales for X = F, OH, Cl, NH_2, Br, SH, I, CH_3 and H demonstrated that the best correlation was obtained with an electronegativity scale called the covalent potential, denoted by V_X.[80] A numerical definition for this electronegativity scale is expressed by Equation 4.1, where n_X is the number of valence electrons in the neutral atom X and r_X is the covalent radius of the heteratom in the substituent X. Thus, V_X measures the energy of attraction between an electron at the covalent radius and the nucleus, shielded by the core electrons.

$$V_X = n_X / r_X \qquad [4.1]$$

In the present study, the relative magnitude of the substituent effect reflected in the ΔH values of the isodesmic reactions 1b and 2b follows the order cyano < methoxy < isocyano < fluoro. The enthalpy changes of the isodesmic reactions 1b and 2b are similar to the enthalpy changes that Luo and Benson correlated to the electronegativity scale V_X, and therefore these values may also show a similar correlation. The ΔH values of these reaction and the V_X values for the corresponding central atom are listed in Table 4.1. A plot of these ΔH values vs. V_X is depicted in Figure 4.7.

Table 4.1: The Electronegativity Scale and Enthalpy Changes for Reactions 1b and 2b

Functional Group	V_X	ΔH (Reaction 1b, kJ/mol)	ΔH (Reaction 2b, kJ/mol)
-CN	5.19	8.4	3.5
-NC	6.67	21.6	9.5
$-OCH_3$	8.11	15.3	5.0
-F	9.915	35.3	15.5

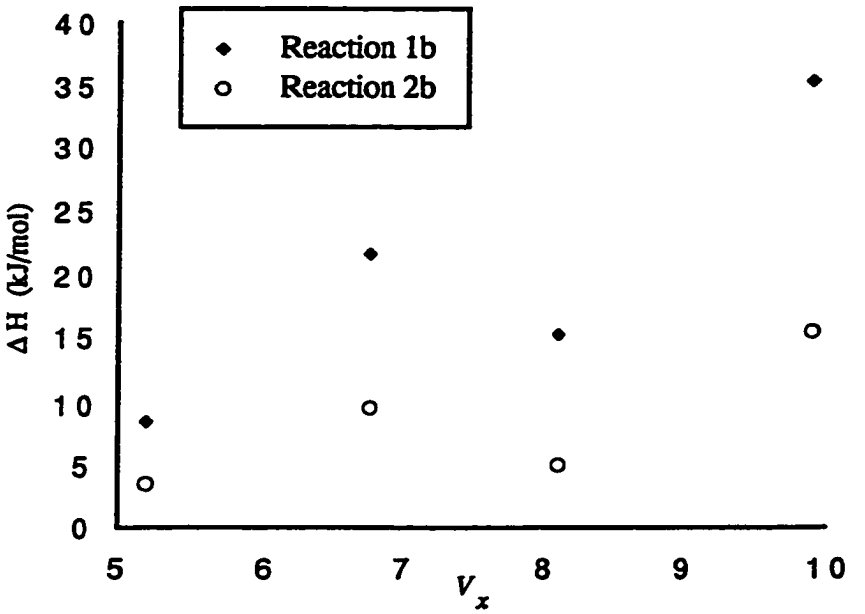

Figure 4.7: Enthalpy Change of Reactions 1b and 2b Plotted Against V_x

The results shown in Figure 4.7 and Table 4.1 indicate that there may be a correlation between the enthalpy change of the isodesmic reactions and the electronegativity of the centrally bonded atom. However, the order for the isocyano and the methoxy group is interchanged. The methoxy group is not making as much difference in the enthalpy change as predicted by the electronegativity of the oxygen atom and the isocyano group is causing too large a difference in the ΔH. This discrepancy could be a consequence of the fact that the V_x scale only addresses the electronegativity of the directly attached heteroatom, leaving the rest of the functional group unaccounted for. An explanation for the behavior observed with the isocyano and methoxy groups may be found by applying Laurencelle and Pacey's simple electrostatic model for the enthalpy of formation of substituted alkanes.[81] The model uses the difference in the electronegativity of two directly bonded atoms to calculate a charge transfer (q) along a covalent bond from Equation 4.2, where y is a proportionality constant and was found to be 0.33 times the charge on an

electron. The charge on a polyvalent atom is then taken as the sum of the charges contributed by the various bonds it forms and can be calculated by Equation 4.3.

$$q(\text{bond}) = y\,[V_X\,(\text{atom A}) - V_X\,(\text{atom B})] \qquad [4.2]$$

$$q\,(\text{atom}) = \sum_{\text{bonds}} q\,(\text{bonds}) \qquad [4.3]$$

The charge on the oxygen and the nitrogen atoms in the methoxy and isocyano groups can be obtained by applying this simple model. The oxygen atom in the methoxy is bonded to two carbon atoms, one to the methyl group and the other to the alkyl group, giving it a total charge of -5.84y. The nitrogen atom in the isocyano group has four bonds, three to the carbon in the isocyano group and one to the alkyl group, giving it a total charge of -5.92y. Details of these calculations are shown in Figure 4.8. These numbers suggest that the isocyano group should have a more dramatic effect on the enthalpy changes of reactions 1b and 2b than the methoxy group even though the nitrogen atom is less electronegative than the oxygen atom.

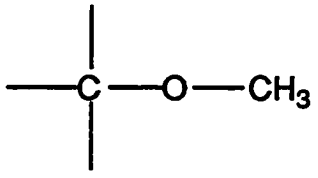

Total charge on Oxygen:

$$q\,(\text{C-O}) = y\,(5.19 - 8.11) = -2.92\,y$$

$$q\,(\text{O}) = 2\,[q(\text{C-O})] = 2\,(-2.92y) = -5.84y$$

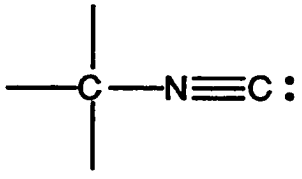

Total charge on Nitrogen:

$$q\,(\text{N-C}) = y\,(5.19 - 6.67) = -1.48\,y$$

$$q\,(\text{N}) = 4\,[q(\text{N-C})] = 4\,(-1.48y) = -5.92y$$

Figure 4.8: Charge Calculations for the Oxygen in the Methoxy Group and the Nitrogen in the Isocyano Group.

4.5 Conclusions

The results of the *ab initio* molecular orbital calculations presented in this study clearly illustrate the importance of substituent effects on the relative stability of β-substituted alkyl radicals. Alkyl substitution on the carbon atom bearing the functional group can cause significant changes to the relative stability of these reactive intermediates. In some cases, the stability provided by alkyl substitution on the carbon bearing the functional group is larger than that provided by substitution on the radical center. When this occurs, as in the case of the fluoro group, the less alkyl substituted radical becomes more stable. This suggests that the relative stability of these β-substituted radical intermediates is determined by a combination of influences from the radical center and the functional group. Consequently, one cannot automatically assume that the more heavily alkyl-substituted radical to be more stable; the whole structure of the intermediate must be considered.

The magnitude of the stabilization provided by alkyl substitution on the carbon bearing the functional group was estimated by isodesmic reactions of substituted alkanes. The ΔH values obtained from *ab initio* calculations for these reactions were dependent on the nature of the substituent. The data for the cyano, methoxy, isocyano, and fluoro substituents suggested that there may be a correlation between the amount of stabilization provided by the alkyl groups and the electron demand of the functional group. However, more data points are need to established a firm correlation (or to show the lack of one). A continuation of this project should included a more systematic study of different functional groups. For example, a study comparing the ΔH values with V_X for the series of halogens would provide more conclusive results.

Appendix I

Selected Geometrical Parameters and Charge Density Distribution

for

Neutral Alkenes and Dienes

2-Methyl-1,3-Butadiene (7)

HF/6-31G* Optimized Geometrical Parameters

Interatomic Distance (Å)		Angles (deg)		Dihedral Angles (deg)	
C_1C_2	1.326	$C_1C_2C_3$	119.7	$C_1C_2C_3C_4$	180.0
C_2C_3	1.477	$C_2C_3C_4$	126.1	$C_5C_2C_3C_1$	-180.0
C_3C_4	1.323	$C_1C_2C_5$	121.8		
C_2C_5	1.508	$C_3C_2C_5$	118.6		

Atomic Charge Density Distribution from Mulliken Population Analysis

Atom Number	Charge[a]
1	-0.09
2	0.10
3	0.04
4	0.05
5	0.00

[a]All charges of directly bonded hydrogen atoms are summed into the carbon atoms

Total Energy (MP2/6-31G*//HF/6-31G*): -194.59195au

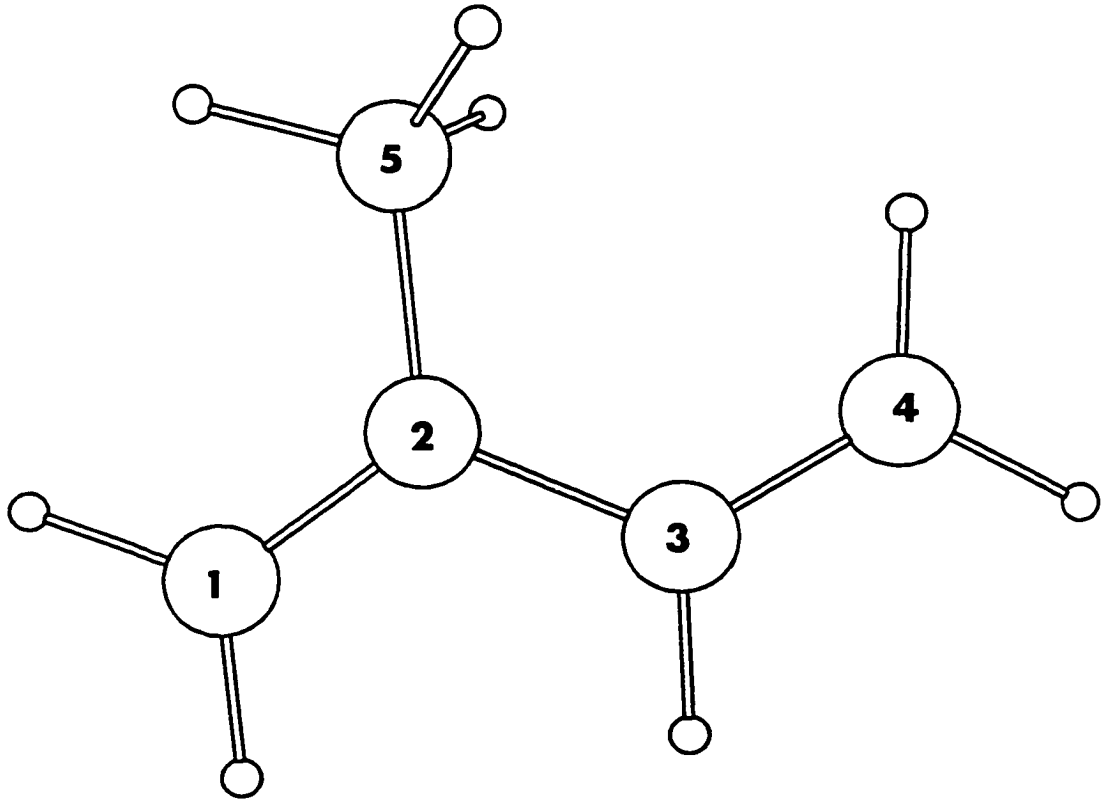

2,4-Dimethyl-1,3-Pentadiene (6)

HF/6-31G* Optimized Geometrical Parameters

Interatomic Distance (Å)		Angles (deg)		Dihedral Angles (deg)	
C_1C_2	1.324	$C_1C_2C_3$	123.1	$C_1C_2C_3C_4$	54.9
C_2C_3	1.486	$C_2C_3C_4$	128.6	$C_5C_4C_3C_2$	-179.9
C_2C_6	1.511	$C_1C_2C_6$	121.9	$C_6C_2C_1C_3$	-177.2
C_3C_4	1.327	$C_3C_4C_5$	120.6	$C_7C_4C_3C_2$	1.1
C_4C_5	1.510	$C_3C_4C_7$	125.1		
C_4C_7	1.509	$C_5C_4C_7$	114.3		

Atomic Charge Density Distribution from Mulliken Population Analysis

Atom Number	Charge[a]
1	-0.08
2	0.08
3	-0.08
4	0.08
5	0.00
6	0.00
7	0.00

[a]All charges of directly bonded hydrogen atoms are summed into the carbon atoms

Total Energy (MP2/6-31G*//HF/6-31G*): -272.92935 au

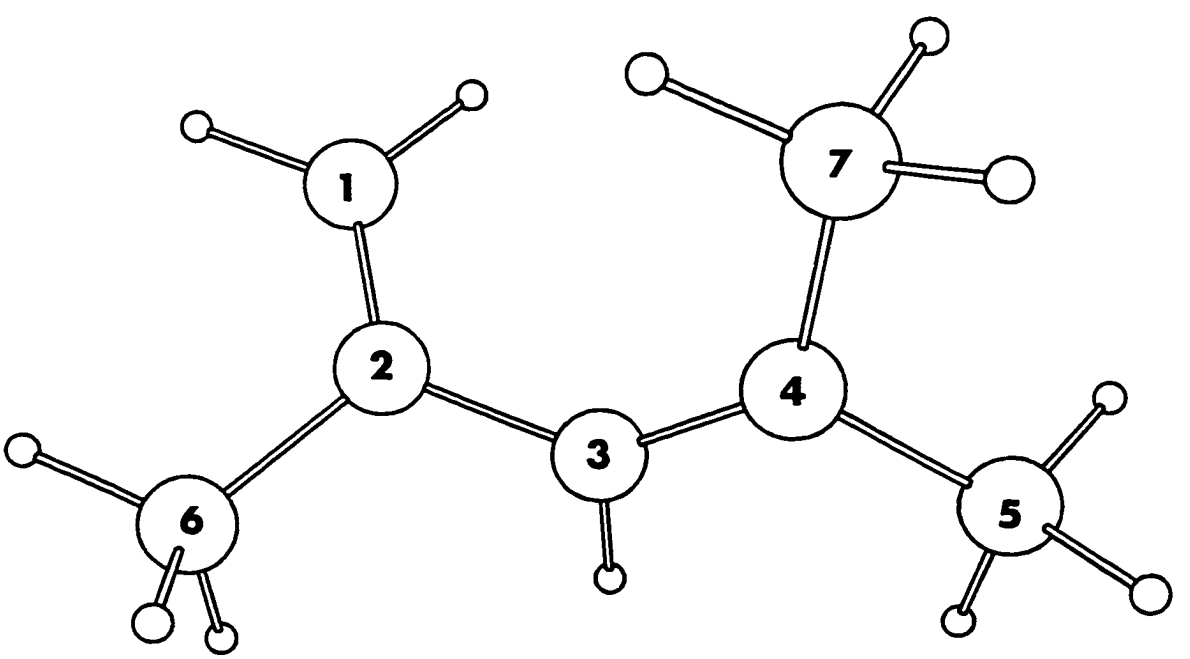

4-Methyl-1,3-Pentadiene (5)

HF/6-31G* Optimized Geometrical Parameters

Interatomic Distance (Å)		Angles (deg)		Dihedral Angles (deg)	
C_1C_2	1.321	$C_1C_2C_3$	123.4	$C_1C_2C_3C_4$	180.0
C_2C_3	1.468	$C_2C_3C_4$	127.8	$C_5C_4C_3C_2$	-179.9
C_3C_4	1.330	$C_3C_4C_5$	120.7	$C_6C_4C_3C_2$	0.0
C_4C_5	1.509	$C_3C_4C_6$	125.3		
C_4C_6	1.509	$C_5C_4C_6$	114.0		

Atomic Charge Density Distribution from Mulliken Population Analysis

Atom Number	Charge[a]
1	-0.07
2	0.06
3	-0.05
4	0.06
5	0.00
6	0.00

[a]All charges of directly bonded hydrogen atoms are summed into the carbon atoms

Total Energy (MP2/6-31G*//HF/6-31G*): -233.76185 au

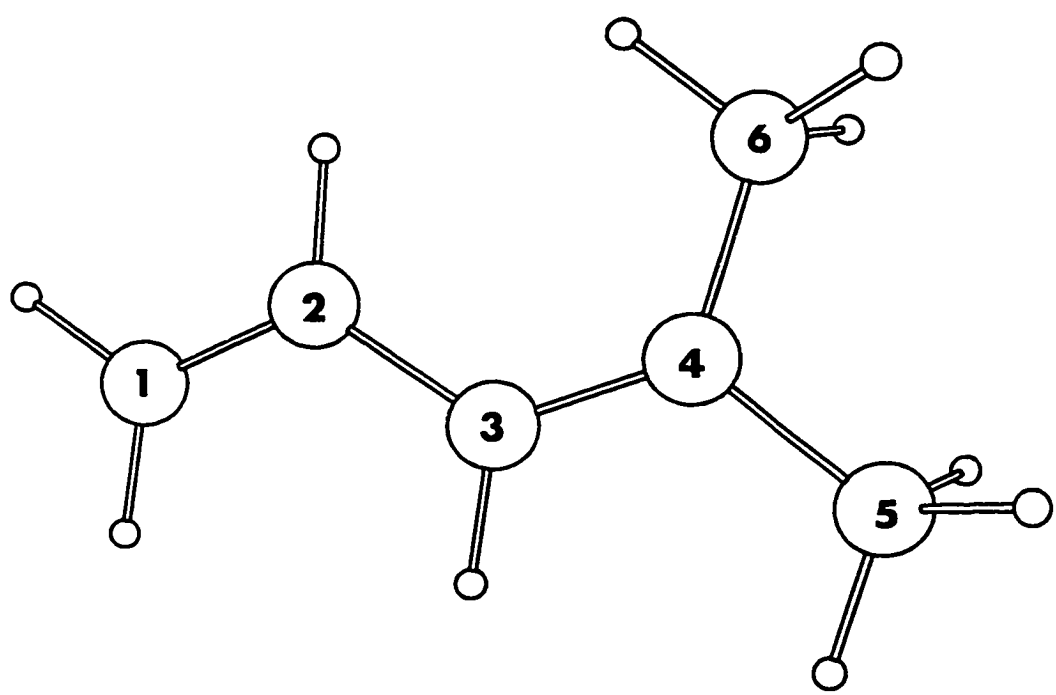

2-Methylpropene (8)

HF/6-31G* Optimized Geometrical Parameters

Interatomic Distance (Å)		Angles (deg)		Dihedral Angles (deg)	
C_1C_2	1.321	$C_1C_2C_3$	122.3	$C_1C_2C_3C_4$	180.0
C_2C_3	1.508	$C_3C_2C_4$	115.5		
C_2C_4	1.508				

Atomic Charge Density Distribution from Mulliken Population Analysis

Atom Number	Charge[a]
1	-0.10
2	0.11
3	0.00
4	0.00

[a]All charges of directly bonded hydrogen atoms are summed into the carbon atoms

Total Energy (MP2/6-31G*//HF/6-31G*): -156.62643 au

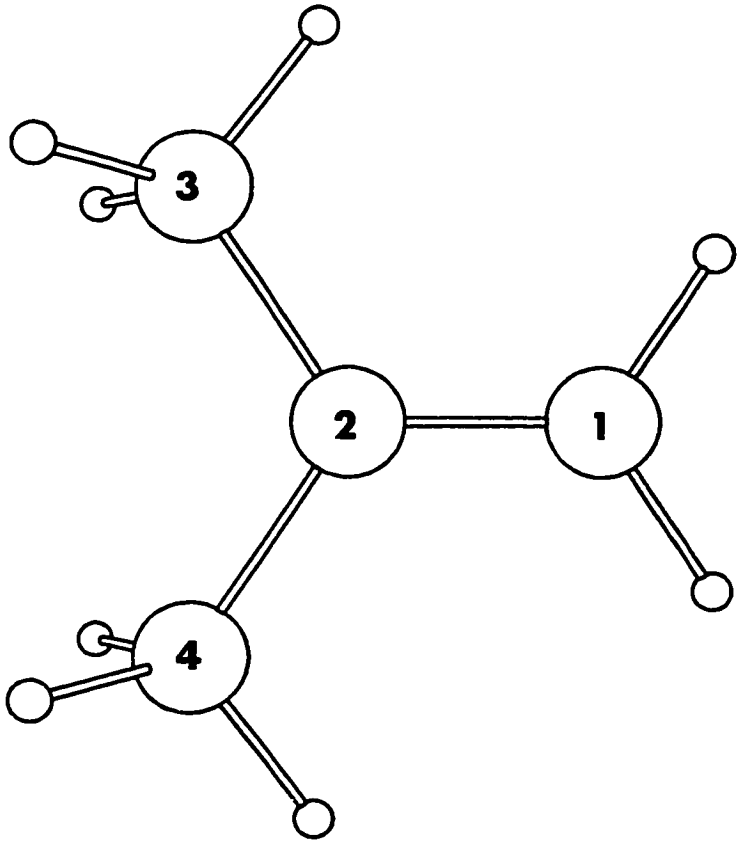

2-Methyl-2-Butene (9)

HF/6-31G* Optimized Geometrical Parameters

Interatomic Distance (Å)		Angles (deg)		Dihedral Angles (deg)	
C_1C_2	1.509	$C_1C_2C_3$	121.2	$C_1C_2C_3C_4$	180.0
C_2C_3	1.324	$C_1C_2C_5$	115.5	$C_1C_2C_3C_5$	180.0
C_3C_4	1.504	$C_2C_3C_4$	127.0		
C_2C_5	1.519	$C_3C_2C_5$	123.3		

Atomic Charge Density Distribution from Mulliken Population Analysis

Atom Number	Charge[a]
1	0.00
2	0.06
3	-0.04
4	0.00
5	-0.01

[a]All charges of directly bonded hydrogen atoms are summed into the carbon atoms

Total Energy (MP2/6-31G*//HF/6-31G*): -195.79227 au

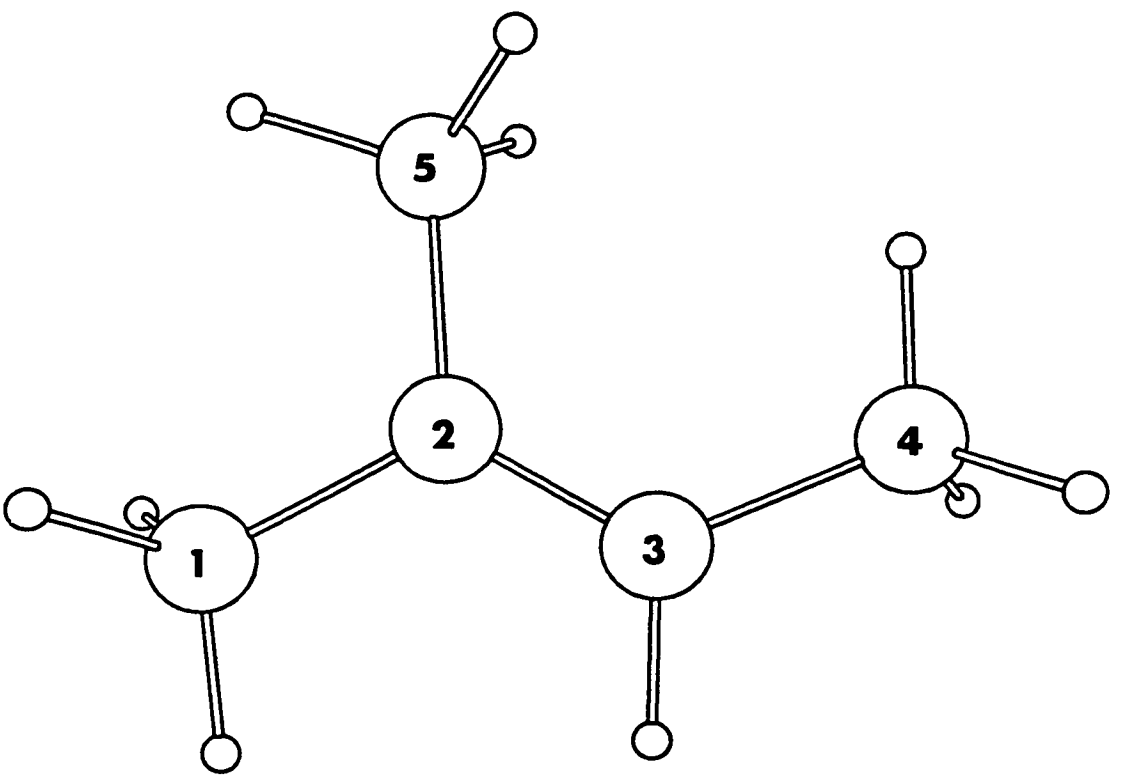

Appendix II

Selected Geometrical Parameters, Charge and Spin Density Distributions for the Radical Cations of Alkenes and Dienes

2,4-Dimethyl-1,3-Pentadiene Radical Cation ($6^{+\cdot}$)

HF/6-31G* Optimized Geometrical Parameters

Interatomic Distance (Å)		Angles (deg)		Dihedral Angles (deg)	
C_1C_2	1.399	$C_1C_2C_3$	115.4	$C_1C_2C_3C_4$	-179.2
C_2C_3	1.404	$C_2C_3C_4$	130.3	$C_5C_4C_3C_2$	178.3
C_2C_6	1.508	$C_1C_2C_6$	118.6	$C_6C_2C_1C_3$	-179.8
C_3C_4	1.398	$C_3C_4C_5$	118.4	$C_7C_4C_3C_2$	-1.5
C_4C_5	1.499	$C_3C_4C_7$	125.8		
C_4C_7	1.495	$C_5C_4C_7$	115.9		

Atomic Charge and Spin Density Distribution from Mulliken Population Analysis

Atom Number	Charge[a]	Spin[a]
1	0.20	0.86
2	0.12	-0.31
3	0.06	0.12
4	0.18	0.48
5	0.15	-0.05
6	0.15	-0.07
7	0.14	0.03

[a]All charge and spin densities of directly bonded hydrogen atoms are summed into the carbon atoms

Total Energy (MP2/6-31G*//HF/6-31G*): -272.65091 au

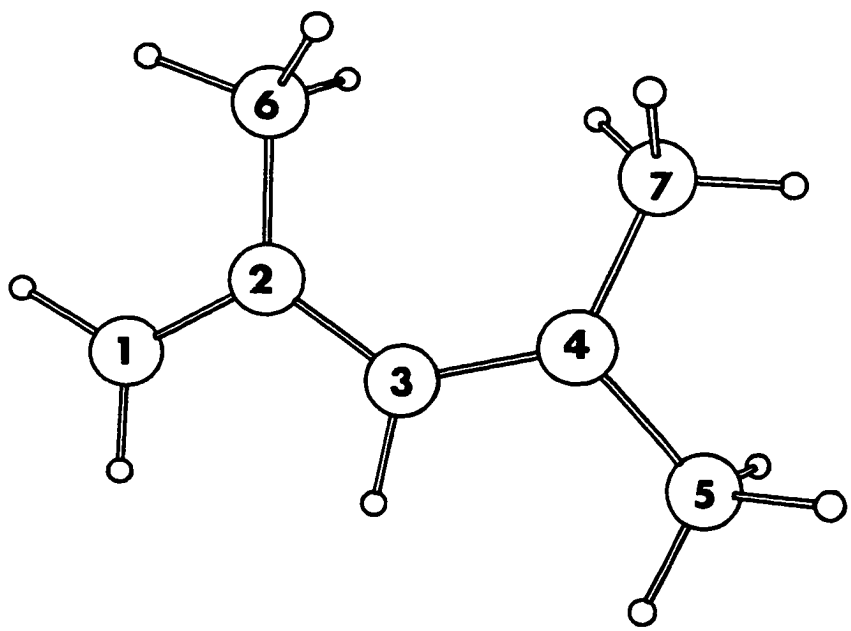

4-Methyl-1,3-Pentadiene Radical Cation ($5^{+\cdot}$)

HF/6-31G* Optimized Geometrical Parameters

Interatomic Distance (Å)		Angles (deg)		Dihedral Angles (deg)	
C_1C_2	1.384	$C_1C_2C_3$	121.2	$C_1C_2C_3C_4$	-180.0
C_2C_3	1.395	$C_2C_3C_4$	125.7	$C_5C_4C_3C_2$	-180.0
C_3C_4	1.402	$C_3C_4C_5$	119.2	$C_6C_4C_3C_2$	0.0
C_4C_5	1.494	$C_3C_4C_6$	124.5		
C_4C_6	1.494	$C_5C_4C_6$	116.2		

Atomic Charge and Spin Density Distribution from Mulliken Population Analysis

Atom Number	Charge[a]	Spin[a]
1	0.23	0.82
2	0.15	-0.37
3	0.11	0.24
4	0.17	0.46
5	0.17	-0.06
6	0.17	-0.06

[a]All charge and spin densities of directly bonded hydrogen atoms are summed into the carbon atoms

Total Energy (MP2/6-31G*//HF/6-31G*): -233.47993 au

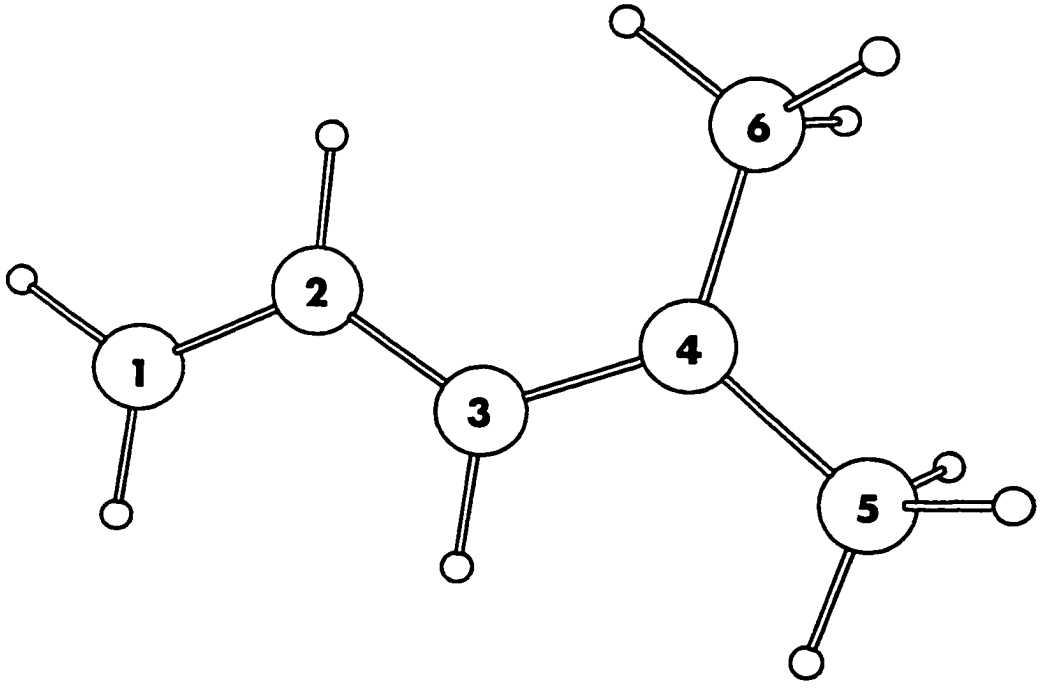

2-Methylpropene Radical Cation ($8^{+\cdot}$)

HF/6-31G* Optimized Geometrical Parameters

Interatomic Distance (Å)		Angles (deg)		Dihedral Angles (deg)	
C_1C_2	1.417	$C_1C_2C_3$	120.3	$C_1C_2C_3C_4$	180.0
C_2C_3	1.483	$C_3C_2C_4$	119.4		
C_2C_4	1.483				

Atomic Charge and Spin Density Distribution from Mulliken Population Analysis

Atom Number	Charge[a]	Spin[a]
1	0.34	0.82
2	0.23	0.31
3	0.22	-0.06
4	0.22	-0.06

[a]All charge and spin densities of directly bonded hydrogen atoms are summed into the carbon atoms

Total Energy (MP2/6-31G*//HF/6-31G*): -156.30259 au

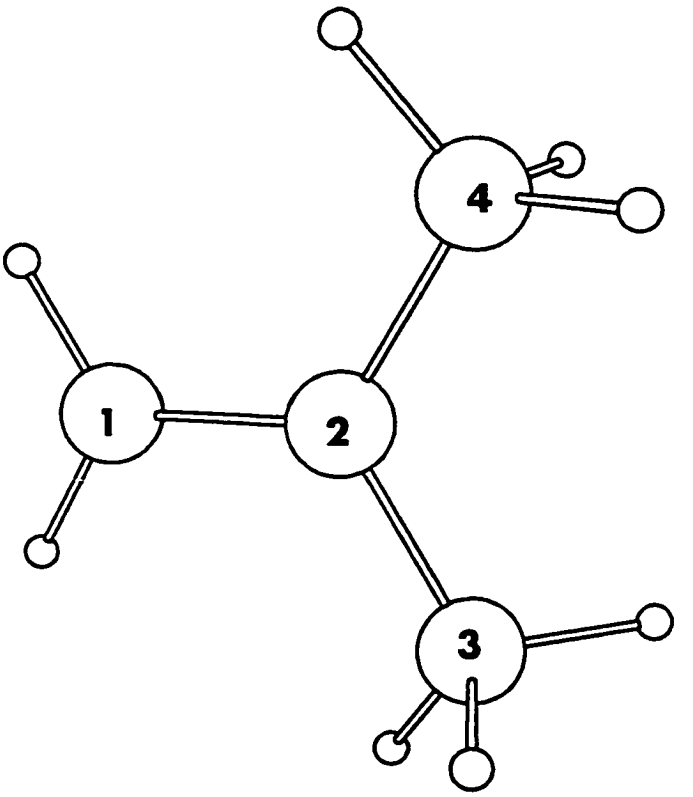

2-Methyl-2-Butene Radical Cation ($9^{+\cdot}$)

HF/6-31G* Optimized Geometrical Parameters

Interatomic Distance (Å)		Angles (deg)		Dihedral Angles (deg)	
C_1C_2	1.492	$C_1C_2C_3$	121.3	$C_1C_2C_3C_4$	0.0
C_2C_3	1.415	$C_1C_2C_5$	118.6	$C_1C_2C_3C_5$	180.0
C_3C_4	1.484	$C_2C_3C_4$	126.8		
C_2C_5	1.487	$C_3C_2C_5$	120.0		

Atomic Charge and Spin Density Distribution from Mulliken Population Analysis

Atom Number	Charge[a]	Spin[a]
1	0.19	-0.07
2	0.19	0.44
3	0.25	0.66
4	0.18	-0.09
5	0.19	-0.05

[a]All charge and spin densities of directly bonded hydrogen atoms are summed into the carbon atoms

Total Energy (MP2/6-31G*//HF/6-31G*): -195.48839 au

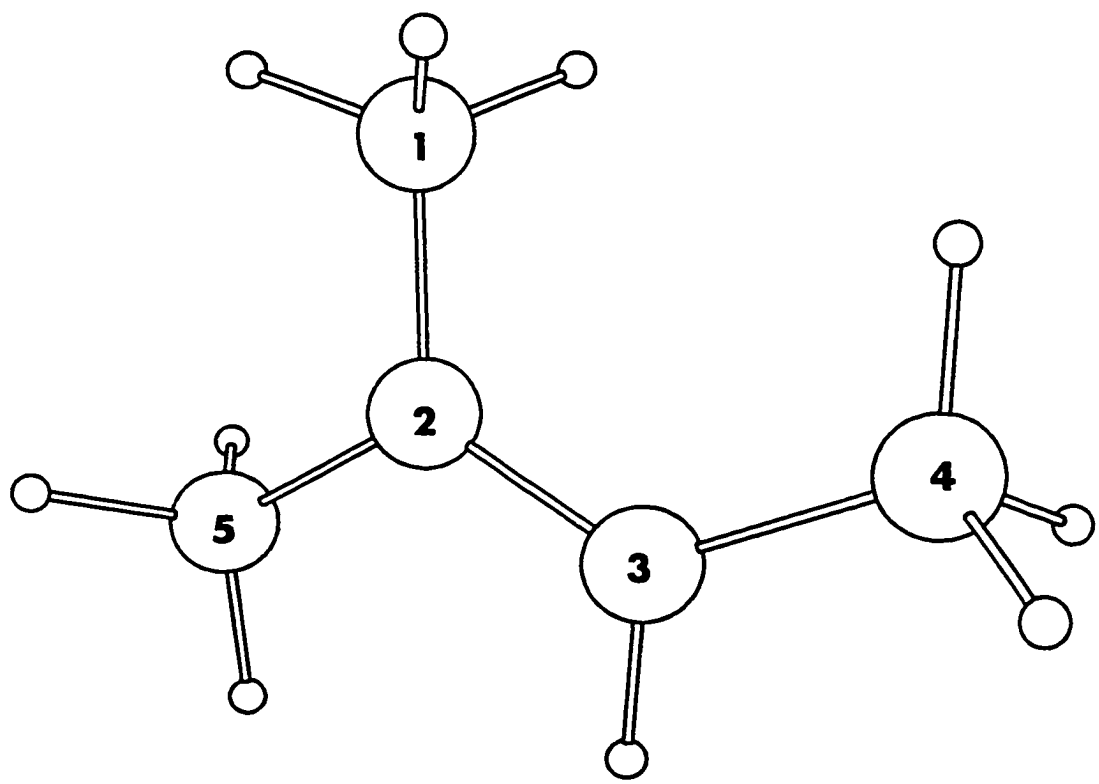

Appendix III

Selected Geometrical Parameters, Charge and Spin Density Distributions for Distonic Radical Cations

2,4-Dimethyl-1,3-Pentadiene/Methanol Distonic Radical Cation: C_1 Bonded, ($6a^{+\cdot}$)

HF/6-31G* Optimized Geometrical Parameters

Interatomic Distance (Å)		Angles (deg)		Dihedral Angles (deg)	
C_1C_2	1.480	$C_1C_2C_3$	116.2	$C_1C_2C_3C_4$	176.8
C_2C_3	1.402	$C_2C_3C_4$	131.2	$C_5C_4C_3C_2$	174.6
C_2C_6	1.512	$C_1C_2C_6$	116.7	$C_6C_2C_1C_3$	179.6
C_3C_4	1.395	$C_3C_4C_5$	125.8	$C_7C_4C_3C_2$	-4.0
C_4C_5	1.507	$C_3C_4C_7$	119.0	$C_3C_2C_1O_8$	-101.0
C_4C_7	1.507	$C_5C_4C_7$	115.3	$C_2C_1O_8C_9$	177.52
C_1O_8	1.554	$C_2C_1O_8$	107.8		
C_2O_8	2.451	$C_1O_8C_9$	119.9		
O_8C_9	1.463				

Atomic Charge and Spin Density Distribution from Mulliken Population Analysis

Atom Number	Charge[a]	Spin[a]
1	0.42	-0.04
2	-0.01	0.89
3	-0.03	-0.68
4	0.07	0.94
5	0.05	-0.05
6	0.09	-0.05
7	0.05	-0.05
8	-0.15	0.03
9	0.52	0.01

[a]All charge and spin densities of directly bonded hydrogen atoms are summed into the carbon atoms

Total Energy (MP2/6-31G*//HF/6-31G*): -388.00920 au

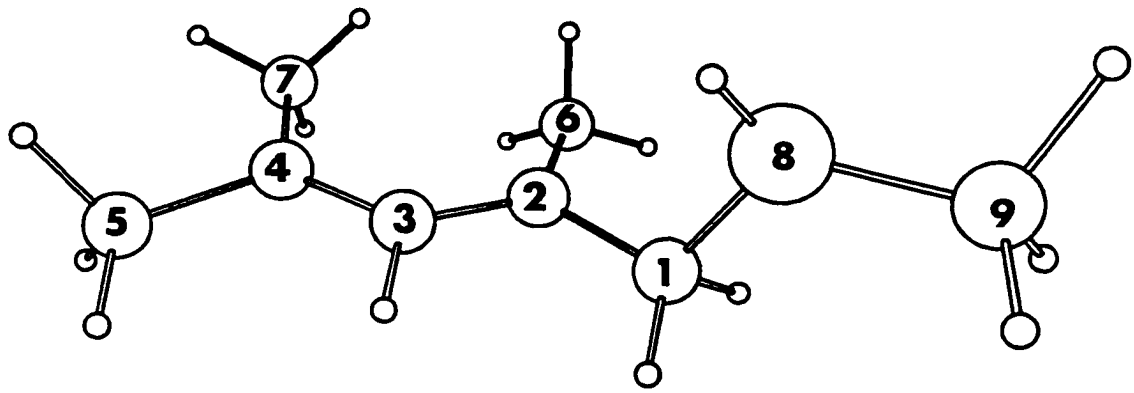

2,4-Dimethyl-1,3-Pentadiene/Methanol Distonic Radical Cation: C_4 Bonded, ($6b^{+\cdot}$)

HF/6-31G* Optimized Geometrical Parameters

Interatomic Distance (Å)		Angles (deg)		Dihedral Angles (deg)	
C_1C_2	1.401	$C_1C_2C_3$	127.1	$C_1C_2C_3C_4$	1.4
C_2C_3	1.397	$C_2C_3C_4$	132.1	$C_5C_4C_3C_2$	-1.4
C_2C_6	1.520	$C_1C_2C_6$	116.2	$C_6C_2C_1C_3$	-177.5
C_3C_4	1.481	$C_3C_4C_5$	112.6	$C_7C_4C_3C_2$	-141.8
C_4C_5	1.509	$C_3C_4C_7$	112.4	$C_2C_3C_4O_8$	110.9
C_4C_7	1.514	$C_5C_4C_7$	112.9	$C_3C_4O_8C_9$	-45.7
C_4O_8	1.711	$C_3C_4O_8$	104.1		
C_3O_8	2.520	$C_4O_8C_9$	123.3		
O_8C_9	1.451				

Atomic Charge and Spin Density Distribution from Mulliken Population Analysis

Atom Number	Charge[a]	Spin[a]
1	0.04	0.89
2	0.08	-0.75
3	0.00	0.83
4	0.22	-0.05
5	0.17	0.00
6	0.08	0.06
7	0.15	0.00
8	-0.22	0.03
9	0.48	0.00

[a]All charge and spin densities of directly bonded hydrogen atoms are summed into the carbon atoms

Total Energy (MP2/6-31G*//HF/6-31G*): -388.00732 au

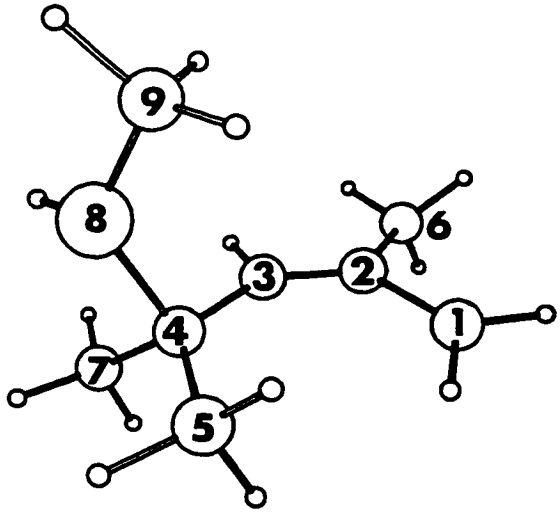

4-Methyl-1,3-Pentadiene/Methanol Distonic Radical Cation: C_1 Bonded, ($5a^{+\cdot}$)

HF/6-31G* Optimized Geometrical Parameters

Interatomic Distance (Å)		Angles (deg)		Dihedral Angles (deg)	
C_1C_2	1.472	$C_1C_2C_3$	120.8	$C_1C_2C_3C_4$	179.5
C_2C_3	1.391	$C_2C_3C_4$	127.3	$C_5C_4C_3C_2$	-178.3
C_3C_4	1.394	$C_3C_4C_5$	120.1	$C_6C_4C_3C_2$	0.6
C_4C_5	1.505	$C_3C_4C_6$	124.2	$C_3C_2C_1O_7$	98.2
C_4C_6	1.505	$C_2C_1O_7$	111.0	$C_2C_1O_7C_8$	82.0
C_1O_7	1.556	$C_1O_7C_8$	119.9		
C_2O_7	2.496				
C_8O_7	1.466				

Atomic Charge and Spin Density Distribution from Mulliken Population Analysis

Atom Number	Charge[a]	Spin[a]
1	0.43	-0.04
2	0.01	0.81
3	0.01	-0.63
4	0.07	0.93
5	0.06	-0.05
6	0.06	-0.05
7	-0.15	0.03
8	0.52	0.00

[a]All charge and spin densities of directly bonded hydrogen atoms are summed into the carbon atoms

Total Energy (MP2/6-31G*//HF/6-31G*): -348.84162 au

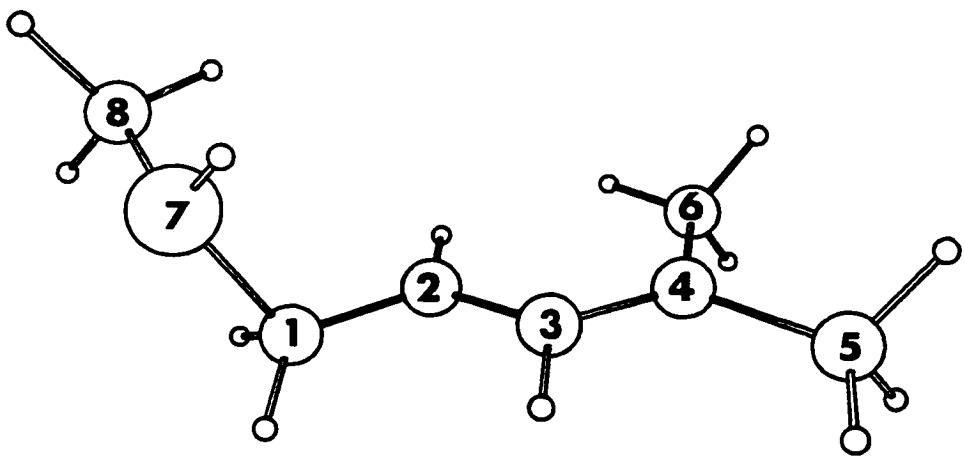

4-Methyl-1,3-Pentadiene/Methanol Distonic Radical Cation: C_4 Bonded, ($5b^{+\cdot}$)

HF/6-31G* Optimized Geometrical Parameters

Interatomic Distance (Å)		Angles (deg)		Dihedral Angles (deg)	
C_1C_2	1.389	$C_1C_2C_3$	122.9	$C_1C_2C_3C_4$	179.4
C_2C_3	1.393	$C_2C_3C_4$	125.4	$C_5C_4C_3C_2$	153.8
C_3C_4	1.477	$C_3C_4C_5$	114.6	$C_6C_4C_3C_2$	15.1
C_4C_5	1.512	$C_3C_4C_6$	118.5	$C_2C_3C_4O_7$	94.9
C_4C_6	1.509	$C_3C_4O_7$	105.3	$C_3C_4O_7C_8$	61.8
C_4O_7	1.708	$C_4O_7C_8$	123.8		
C_3O_7	2.537				
C_8O_7	1.452				

Atomic Charge and Spin Density Distribution from Mulliken Population Analysis

Atom Number	Charge[a]	Spin[a]
1	0.09	0.85
2	0.06	-0.69
3	0.05	0.83
4	0.20	-0.03
5	0.16	0.00
6	0.16	0.00
7	-0.21	0.04
8	0.48	0.00

[a]All charge and spin densities of directly bonded hydrogen atoms are summed into the carbon atoms

Total Energy (MP2/6-31G*//HF/6-31G*): -348.84514 au

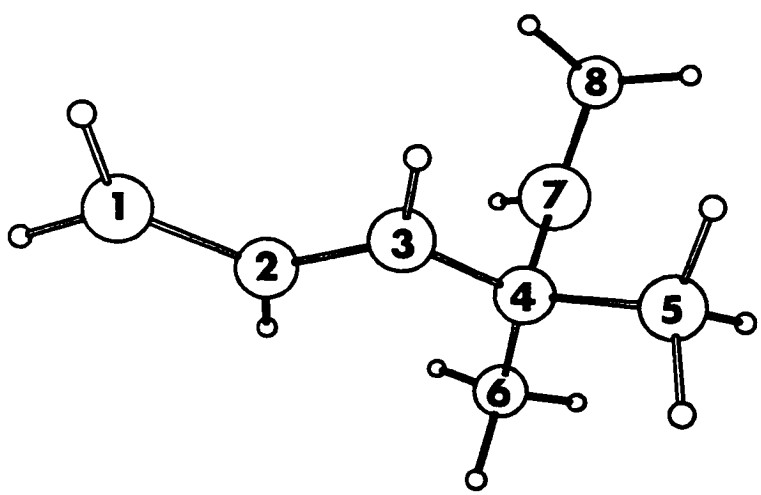

2-Methylpropene/Methanol Distonic Radical Cation: C_1 Bonded, ($8a^{+\cdot}$)

HF/6-31G* Optimized Geometrical Parameters

Interatomic Distance (Å)		Angles (deg)		Dihedral Angles (deg)	
C_1C_2	1.449	$C_1C_2C_3$	120.0	$C_1C_2C_3C_4$	174.1
C_2C_3	1.503	$C_1C_2C_4$	120.5	$C_3C_2C_1O_5$	81.1
C_2C_4	1.504	$C_3C_2C_4$	119.2	$C_6O_5C_1C_2$	179.9
C_1O_5	1.566	$C_1C_2O_5$	109.2		
C_2O_5	2.474	$C_1O_5C_6$	119.4		
C_6O_5	1.466				

Atomic Charge and Spin Density Distribution from Mulliken Population Analysis

Atom Number	Charge[a]	Spin[a]
1	0.43	-0.05
2	0.01	1.12
3	0.10	-0.06
4	0.09	-0.06
5	-0.16	0.04
6	0.52	0.01

[a]All charge and spin densities of directly bonded hydrogen atoms are summed into the carbon atoms

Total Energy (MP2/6-31G*//HF/6-31G*): -271.68225 au

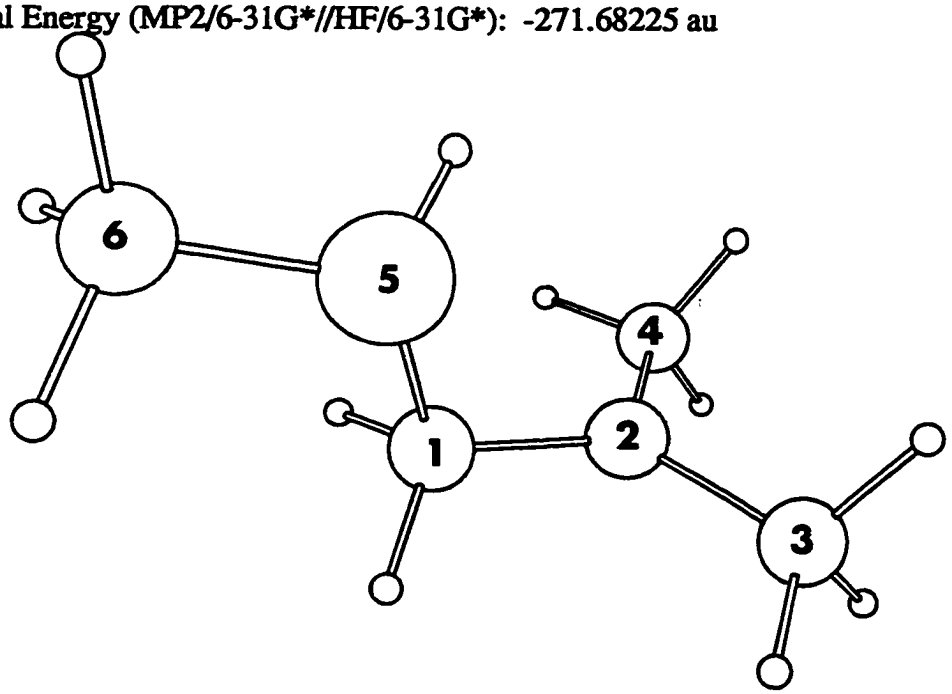

2-Methylpropene/Methanol Distonic Radical Cation: C_2 Bonded, ($8b^{+\cdot}$)

HF/6-31G* Optimized Geometrical Parameters

Interatomic Distance (Å)		Angles (deg)		Dihedral Angles (deg)	
C_1C_2	1.476	$C_1C_2C_3$	114.8	$C_1C_2C_3C_4$	-136.3
C_2C_3	1.512	$C_1C_2C_4$	115.3	$C_3C_2C_1O_5$	110.5
C_2C_4	1.512	$C_3C_2C_4$	114.3	$C_6O_5C_2C_1$	-56.4
C_1O_5	2.506	$C_1C_2O_5$	106.3		
C_2O_5	1.653	$C_2O_5C_6$	123.8		
C_6O_5	1.459				

Atomic Charge and Spin Density Distribution from Mulliken Population Analysis

Atom Number	Charge[a]	Spin[a]
1	0.14	1.00
2	0.22	-0.06
3	0.16	0.00
4	0.16	0.00
5	-0.20	0.05
6	0.50	0.00

[a]All charge and spin densities of directly bonded hydrogen atoms are summed into the carbon atoms

Total Energy (MP2/6-31G*//HF/6-31G*): -271.68459 au

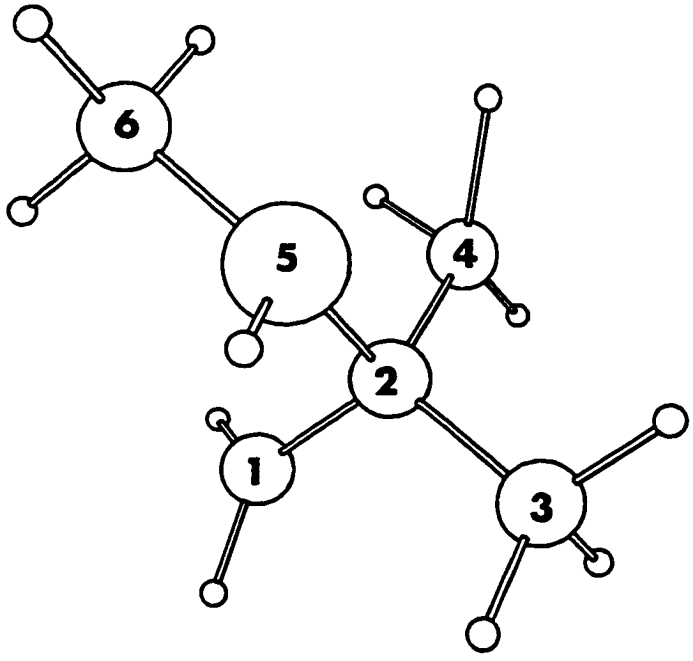

2-Methylpropene/Methanol Distonic Radical Cation: Bridged, ($8c^{+\cdot}$)

HF/6-31G* Optimized Geometrical Parameters

Interatomic Distance (Å)		Angles (deg)		Dihedral Angles (deg)	
C_1C_2	1.410	$C_1C_2C_3$	120.7	$C_1C_2C_3C_4$	179.4
C_2C_3	1.485	$C_1C_2C_4$	120.5	$C_3C_2C_1O_5$	-81.4
C_2C_4	1.485	$C_3C_2C_4$	118.8	$C_6O_5C_1C_2$	-119.3
C_1O_5	2.776	$C_2C_1O_5$	75.3		
C_2O_5	2.776	$C_1O_5C_6$	122.6		
C_6O_5	1.419				

Atomic Charge and Spin Density Distribution from Mulliken Population Analysis

Atom Number	Charge[a]	Spin[a]
1	0.33	0.68
2	0.26	0.32
3	0.19	-0.01
4	0.19	-0.01
5	-0.32	0.01
6	0.36	0.00

[a]All charge and spin densities of directly bonded hydrogen atoms are summed into the carbon atoms

Total Energy (MP2/6-31G*//HF/6-31G*): -271.67327 au

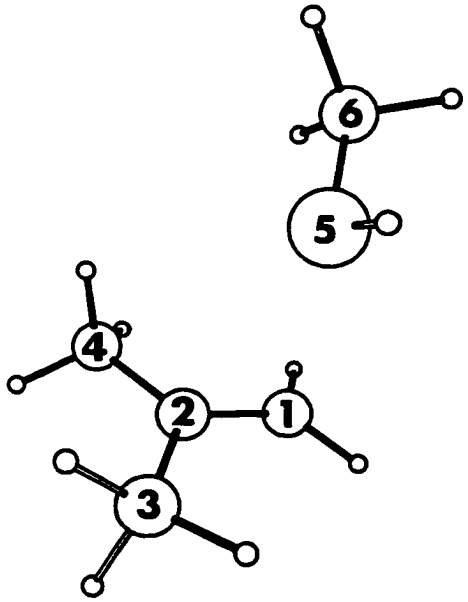

2-Methyl-2-Butene/Methanol Distonic Radical Cation: C_2 Bonded ($9a^{+\cdot}$)

HF/6-31G* Optimized Geometrical Parameters

Interatomic Distance (Å)		Angles (deg)		Dihedral Angles (deg)	
C_1C_2	1.520	$C_1C_2C_3$	114.7	$C_1C_2C_3C_4$	42.1
C_2C_3	1.488	$C_1C_2C_5$	113.4	$C_1C_2O_6C_7$	179.1
C_2C_5	1.516	$C_2C_3C_4$	123.4	$C_4C_3C_2O_6$	-68.7
C_3C_4	1.499	$C_3C_2C_5$	113.8	$C_3C_2O_6C_7$	-61.1
C_2O_6	1.580	$C_1C_2O_6$	101.9		
C_3O_6	2.434	$C_2O_6C_7$	123.7		
C_7O_6	1.462				

Atomic Charge and Spin Density Distribution from Mulliken Population Analysis

Atom Number	Charge[a]	Spin[a]
1	0.14	0.00
2	0.22	-0.07
3	0.08	1.09
4	0.09	-0.07
5	0.14	0.02
6	-0.18	0.02
7	0.51	0.01

[a]All charge and spin densities of directly bonded hydrogen atoms are summed into the carbon atoms

Total Energy (MP2/6-31G*//HF/6-31G*): -310.85828 au

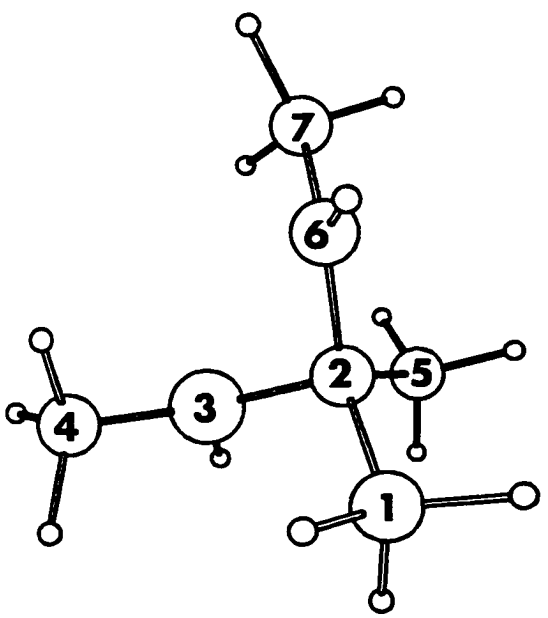

2-Methyl-2-Butene/Methanol Distonic Radical Cation: C_3 Bonded ($9b^{+\cdot}$)

HF/6-31G* Optimized Geometrical Parameters

Interatomic Distance (Å)		Angles (deg)		Dihedral Angles (deg)	
C_1C_2	1.505	$C_1C_2C_3$	119.1	$C_1C_2C_3C_4$	119.4
C_2C_3	1.483	$C_1C_2C_5$	119.4	$C_1C_2C_3O_6$	-124.4
C_2C_5	1.504	$C_2C_3C_4$	117.7	$C_2C_3O_6C_7$	65.3
C_3C_4	1.514	$C_3C_2C_5$	120.0		
C_2O_6	2.458	$C_2C_3O_6$	106.6		
C_3O_6	1.580	$C_3O_6C_7$	120.5		
C_7O_6	1.462				

Atomic Charge and Spin Density Distribution from Mulliken Population Analysis

Atom Number	Charge[a]	Spin[a]
1	0.09	-0.06
2	0.02	1.15
3	0.33	-0.08
4	0.14	0.02
5	0.09	-0.07
6	-0.17	0.03
7	0.51	0.01

[a]All charge and spin densities of directly bonded hydrogen atoms are summed into the carbon atoms

Total Energy (MP2/6-31G*//HF/6-31G*): -310.85696 au

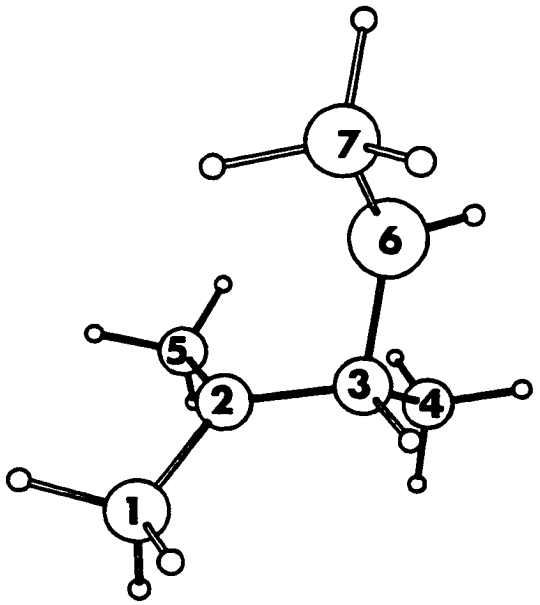

2-Methyl-2-Butene/Methanol Distonic Radical Cation: Bridged ($9c^{+\cdot}$)

HF/6-31G* Optimized Geometrical Parameters

Interatomic Distance (Å)		Angles (deg)		Dihedral Angles (deg)	
C_1C_2	1.488	$C_1C_2C_3$	120.2	$C_1C_2C_3C_4$	179.0
C_2C_3	1.411	$C_1C_2C_5$	118.0	$C_2C_3O_6C_7$	118.6
C_2C_5	1.489	$C_2C_3C_4$	126.2	$C_3C_2O_6C_7$	-89.0
C_3C_4	1.486	$C_3C_2C_5$	121.8		
C_2O_6	2.806	$C_3C_2O_6$	81.7		
C_3O_6	2.954	$C_2O_6C_7$	150.7		
C_7O_6	1.418				

Atomic Charge and Spin Density Distribution from Mulliken Population Analysis

Atom Number	Charge[a]	Spin[a]
1	0.17	-0.02
2	0.24	0.41
3	0.24	0.64
4	0.16	-0.03
5	0.17	-0.02
6	-0.32	0.01
7	0.35	0.00

[a]All charge and spin densities of directly bonded hydrogen atoms are summed into the carbon atoms

Total Energy (MP2/6-31G*//HF/6-31G*): -310.85651 au

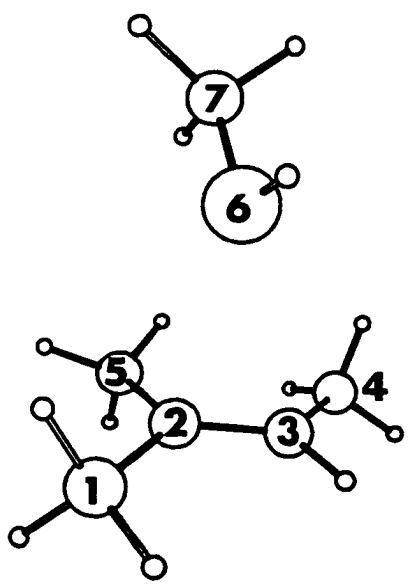

Appendix IV

Selected Geometrical Parameters, Charge and Spin Density Distributions for β-Substituted Radicals

2,4-Dimethyl-1,3-Pentadiene/Methanol β-Alkoxyalkyl Radical: C_1 Bonded, (6a•)

HF/6-31G* Optimized Geometrical Parameters

Interatomic Distance (Å)		Angles (deg)		Dihedral Angles (deg)	
C_1C_2	1.510	$C_1C_2C_3$	120.4	$C_1C_2C_3C_4$	175.8
C_2C_3	1.396	$C_2C_3C_4$	131.2	$C_5C_4C_3C_2$	174.6
C_2C_6	1.510	$C_1C_2C_6$	112.9	$C_6C_2C_1C_3$	179.3
C_3C_4	1.399	$C_3C_4C_5$	119.0	$C_7C_4C_3C_2$	-4.6
C_4C_5	1.509	$C_3C_4C_7$	126.1	$C_3C_2C_1O_8$	-5.0
C_4C_7	1.510	$C_5C_4C_7$	114.9	$C_2C_1O_8C_9$	179.6
C_1O_8	1.391	$C_2C_1O_8$	112.5		
C_2O_8	2.414	$C_1O_8C_9$	114.0		
O_8C_9	1.392				

Atomic Charge and Spin Density Distribution from Mulliken Population Analysis

Atom Number	Charge[a]	Spin[a]
1	0.32	-0.06
2	-0.02	1.00
3	0.00	-0.77
4	0.05	1.00
5	-0.01	-0.06
6	-0.01	-0.06
7	-0.02	-0.06
8	-0.62	0.00
9	0.30	0.00

[a]All charge and spin densities of directly bonded hydrogen atoms are summed into the carbon atoms

Total Energy (MP2/6-31G*//HF/6-31G*): -387.67525 au

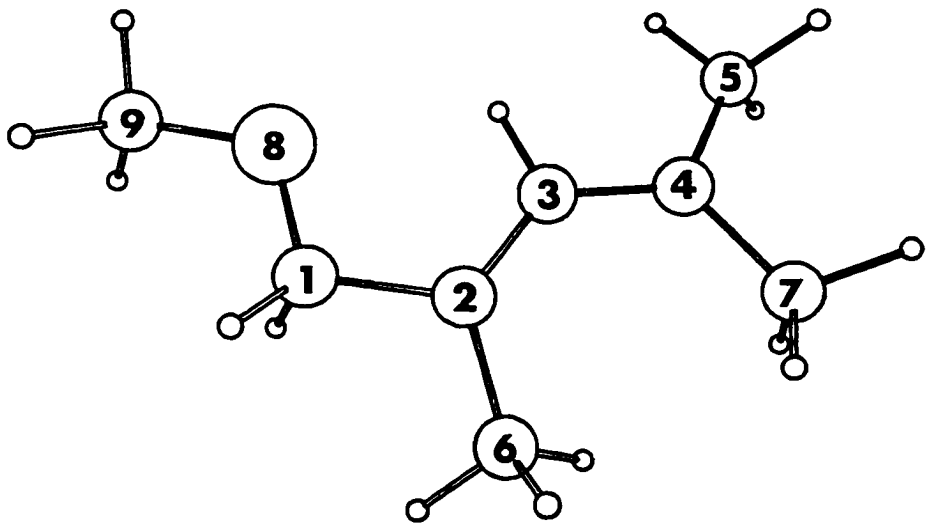

2,4-Dimethyl-1,3-Pentadiene/Methanol β-Alkoxyalkyl Radical: C_4 Bonded, (6b•)

HF/6-31G* Optimized Geometrical Parameters

Interatomic Distance (Å)		Angles (deg)		Dihedral Angles (deg)	
C_1C_2	1.388	$C_1C_2C_3$	125.8	$C_1C_2C_3C_4$	-0.3
C_2C_3	1.407	$C_2C_3C_4$	130.7	$C_5C_4C_3C_2$	54.0
C_2C_6	1.520	$C_1C_2C_6$	118.2	$C_6C_2C_1C_3$	-178.7
C_3C_4	1.523	$C_3C_4C_5$	114.1	$C_7C_4C_3C_2$	-71.2
C_4C_5	1.535	$C_3C_4C_7$	110.7	$C_2C_3C_4O_8$	176.3
C_4C_7	1.531	$C_5C_4C_7$	110.3	$C_3C_4O_8C_9$	-71.5
C_4O_8	1.419	$C_3C_4O_8$	107.7		
C_3O_8	2.376	$C_4O_8C_9$	118.7		
O_8C_9	1.395				

Atomic Charge and Spin Density Distribution from Mulliken Population Analysis

Atom Number	Charge[a]	Spin[a]
1	-0.06	0.85
2	0.08	-0.81
3	-0.04	0.98
4	0.32	-0.12
5	0.01	0.02
6	0.00	0.04
7	0.04	0.03
8	-0.65	0.00
9	0.30	0.00

[a]All charge and spin densities of directly bonded hydrogen atoms are summed into the carbon atoms

Total Energy (MP2/6-31G*//HF/6-31G*): -388.00732 au

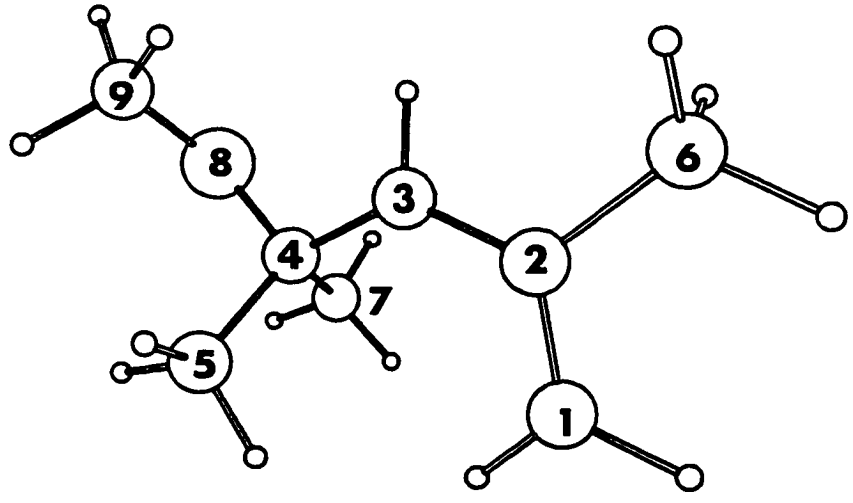

4-Methyl-1,3-Pentadiene/Methanol β-Alkoxyalkyl Radical: C_1 Bonded, (5a•)

HF/6-31G* Optimized Geometrical Parameters

Interatomic Distance (Å)		Angles (deg)		Dihedral Angles (deg)	
C_1C_2	1.509	$C_1C_2C_3$	123.0	$C_1C_2C_3C_4$	177.4
C_2C_3	1.392	$C_2C_3C_4$	127.8	$C_5C_4C_3C_2$	-0.3
C_3C_4	1.395	$C_3C_4C_5$	124.4	$C_6C_4C_3C_2$	179.9
C_4C_5	1.506	$C_3C_4C_6$	120.3	$C_3C_2C_1O_7$	27.6
C_4C_6	1.507	$C_2C_1O_7$	114.3	$C_2C_1O_7C_8$	77.0
C_1O_7	1.397	$C_1O_7C_8$	114.9		
C_2O_7	2.442				
C_8O_7	1.395				

Atomic Charge and Spin Density Distribution from Mulliken Population Analysis

Atom Number	Charge[a]	Spin[a]
1	0.33	-0.07
2	-0.07	0.94
3	0.01	-0.76
4	0.05	0.99
5	0.00	-0.06
6	-0.01	-0.05
7	-0.61	0.00
8	0.30	0.00

[a]All charge and spin densities of directly bonded hydrogen atoms are summed into the carbon atoms

Total Energy (MP2/6-31G*//HF/6-31G*): -348.51064 au

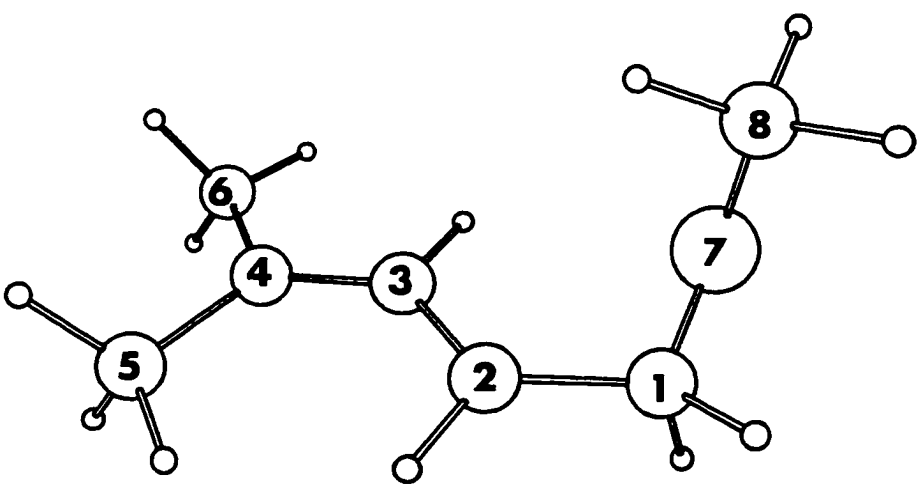

4-Methyl-1,3-Pentadiene/Methanol β-Alkoxyalkyl Radical: C_4 Bonded, (5b•)

HF/6-31G* Optimized Geometrical Parameters

Interatomic Distance (Å)		Angles (deg)		Dihedral Angles (deg)	
C_1C_2	1.392	$C_1C_2C_3$	124.0	$C_1C_2C_3C_4$	-177.2
C_2C_3	1.390	$C_2C_3C_4$	127.5	$C_5C_4C_3C_2$	12.9
C_3C_4	1.516	$C_3C_4C_5$	113.7	$C_6C_4C_3C_2$	109.9
C_4C_5	1.531	$C_3C_4C_6$	109.2	$C_2C_3C_4O_7$	-137.3
C_4C_6	1.531	$C_3C_4O_7$	109.2	$C_3C_4O_7C_8$	65.9
C_4O_7	1.417	$C_4O_7C_8$	118.3		
C_3O_7	2.391				
C_8O_7	1.396				

Atomic Charge and Spin Density Distribution from Mulliken Population Analysis

Atom Number	Charge[a]	Spin[a]
1	-0.03	0.88
2	0.03	-0.75
3	-0.01	0.93
4	0.30	-0.11
5	0.00	0.00
6	0.04	0.03
7	-0.64	0.01
8	0.30	0.00

[a]All charge and spin densities of directly bonded hydrogen atoms are summed into the carbon atoms

Total Energy (MP2/6-31G*//HF/6-31G*): -348.51259 au

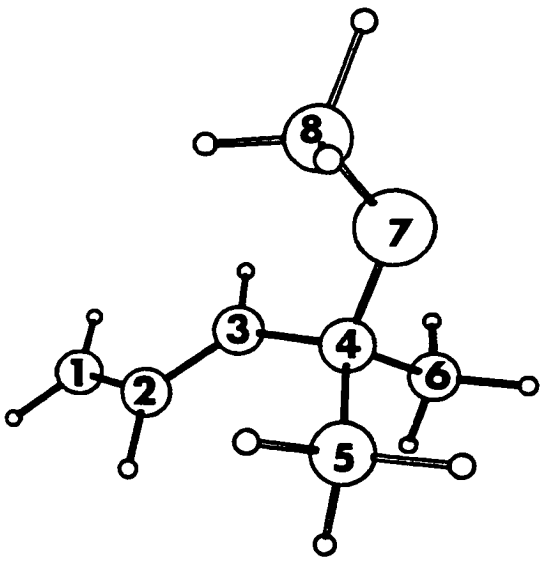

2-Methylpropene/Methanol β-Alkoxyalkyl Radical: C_1 Bonded, (8a•)

HF/6-31G* Optimized Geometrical Parameters

Interatomic Distance (Å)		Angles (deg)		Dihedral Angles (deg)	
C_1C_2	1.501	$C_1C_2C_3$	116.6	$C_1C_2C_3C_4$	151.2
C_2C_3	1.504	$C_1C_2C_4$	118.5	$C_3C_2C_1O_5$	166.3
C_2C_4	1.502	$C_3C_2C_4$	118.3	$C_6O_5C_1C_2$	-178.0
C_1O_5	1.396	$C_2C_1O_5$	110.6		
C_2O_5	2.382	$C_1O_5C_6$	114.1		
C_6O_5	1.391				

Atomic Charge and Spin Density Distribution from Mulliken Population Analysis

Atom Number	Charge[a]	Spin[a]
1	0.30	-0.07
2	0.03	1.18
3	-0.02	-0.06
4	0.01	-0.06
5	-0.61	0.01
6	0.30	0.00

[a]All charge and spin densities of directly bonded hydrogen atoms are summed into the carbon atoms

Total Energy (MP2/6-31G*//HF/6-31G*): -271.35528 au

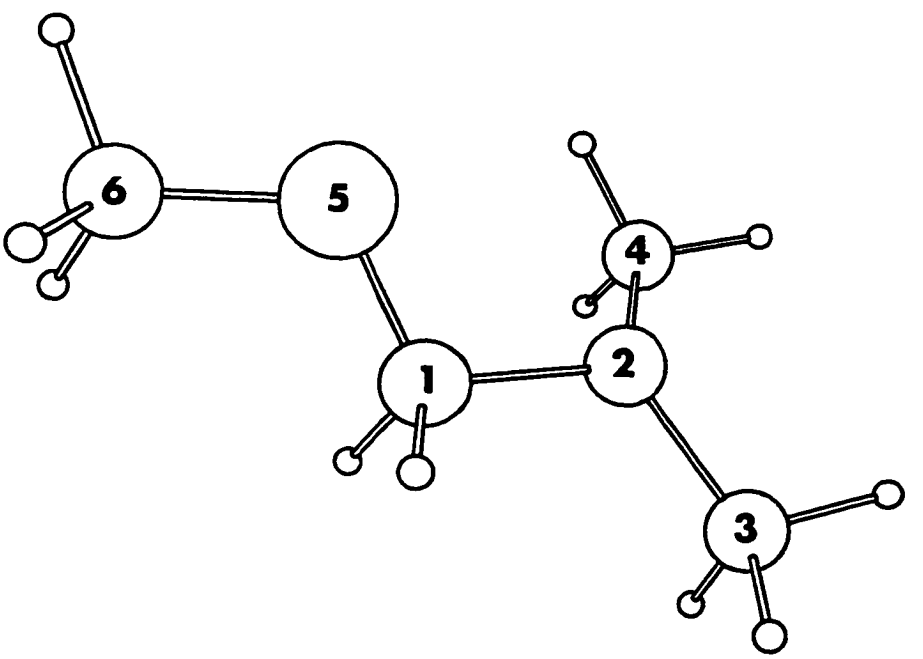

2-Methylpropene/Methanol β-Alkoxyalkyl Radical: C_2 Bonded, (8b•)

HF/6-31G* Optimized Geometrical Parameters

Interatomic Distance (Å)		Angles (deg)		Dihedral Angles (deg)	
C_1C_2	1.508	$C_1C_2C_3$	110.9	$C_6O_5C_2C_1$	-64.6
C_2C_3	1.533	$C_1C_2C_4$	110.1		
C_2C_4	1.532	$C_3C_2C_4$	109.9		
C_1O_5	2.400	$C_1C_2O_5$	110.3		
C_2O_5	1.414	$C_2O_5C_6$	118.4		
C_6O_5	1.395				

Atomic Charge and Spin Density Distribution from Mulliken Population Analysis

Atom Number	Charge[a]	Spin[a]
1	-0.01	1.07
2	0.32	-0.13
3	0.00	0.01
4	0.03	0.04
5	-0.64	0.01
6	0.30	0.01

[a]All charge and spin densities of directly bonded hydrogen atoms are summed into the carbon atoms

Total Energy (MP2/6-31G*//HF/6-31G*): -271.35479 au

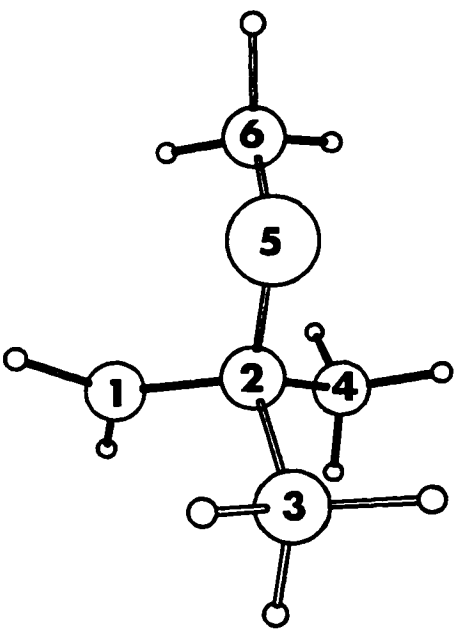

2-Methylpropene/Fluoride β-Fluoroalkyl Radical: C_1 Bonded, (8y•)

HF/6-31G* Optimized Geometrical Parameters

Interatomic Distance (Å)		Angles (deg)		Dihedral Angles (deg)	
C_1C_2	1.497	$C_1C_2C_3$	116.7	$C_1C_2C_3C_4$	-151.8
C_2C_3	1.503	$C_1C_2C_4$	118.2	$C_3C_2C_1F_5$	166.8
C_2C_4	1.502	$F_5C_1C_2$	111.0	$C_4C_2C_1F_5$	-41.2
C_1F_5	1.372				

Atomic Charge and Spin Density Distribution from Mulliken Population Analysis

Atom Number	Charge[a]	Spin[a]
1	0.41	-0.06
2	-0.01	1.18
3	-0.01	-0.06
4	0.01	-0.06
5	-0.41	0.00

[a]All charge and spin densities of directly bonded hydrogen atoms are summed into the carbon atoms

Total Energy (MP2/6-31G*//HF/6-31G*): -256.19065 au

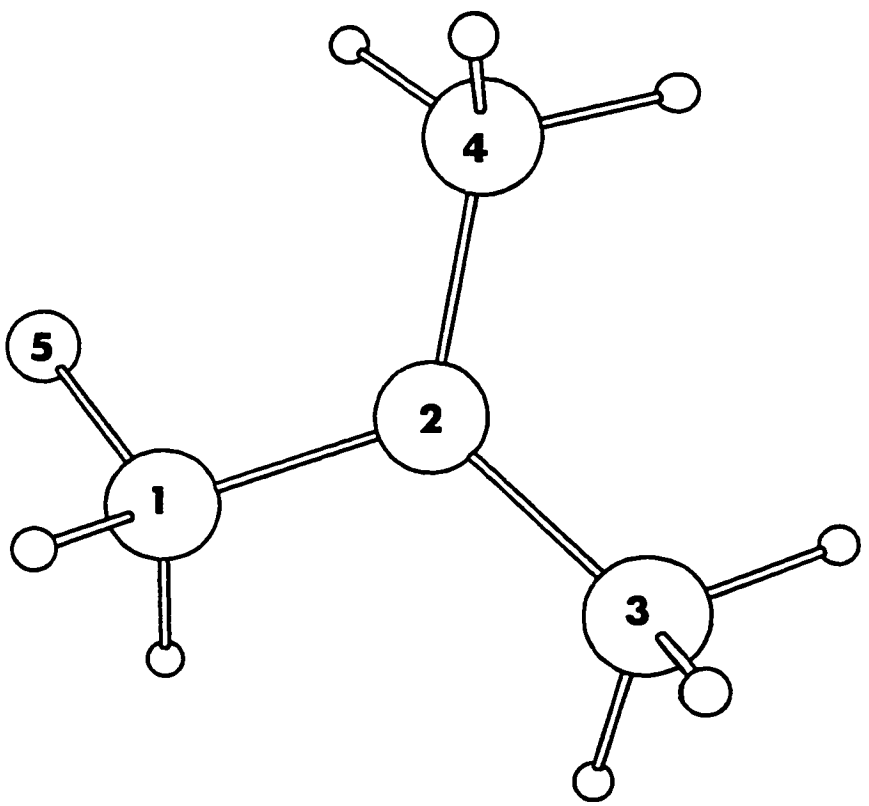

2-Methylpropene/Fluoride β-Fluoroalkyl Radical: C_2 Bonded, (8x·)

HF/6-31G* Optimized Geometrical Parameters

Interatomic Distance (Å)		Angles (deg)		Dihedral Angles (deg)	
C_1C_2	1.499	$C_1C_2C_3$	112.0	$C_1C_2C_3C_4$	126.9
C_2C_3	1.522	$C_1C_2C_4$	112.1	$HC_1C_2F_5$	33.6
C_2C_4	1.526	$F_5C_2C_1$	107.1		
C_2F_5	1.388				

Atomic Charge and Spin Density Distribution from Mulliken Population Analysis

Atom Number	Charge[a]	Spin[a]
1	-0.01	1.07
2	0.43	-0.13
3	0.01	0.03
4	0.01	0.03
5	-0.44	0.00

[a]All charge and spin densities of directly bonded hydrogen atoms are summed into the carbon atoms

Total Energy (MP2/6-31G*//HF/6-31G*): -256.19490 au

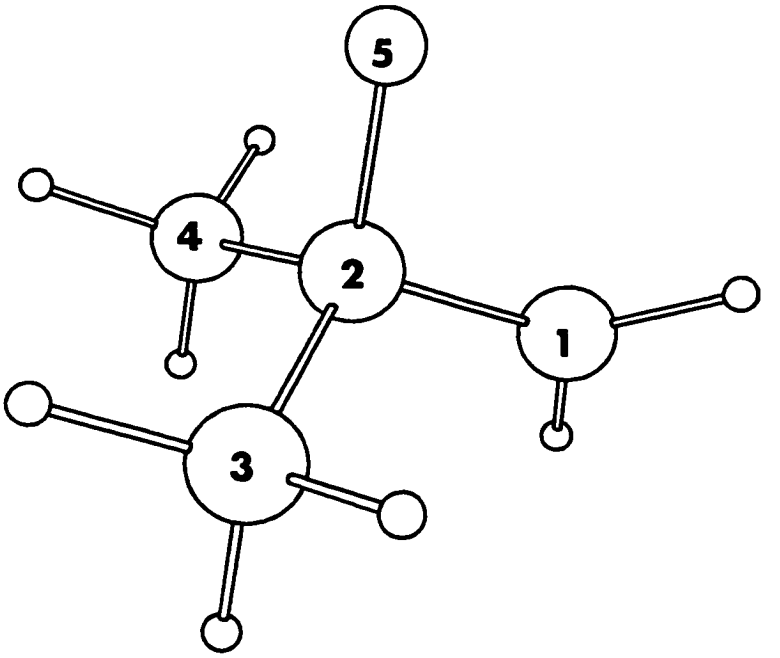

2-Methylpropene/Cyanide β-Cyanoalkyl Radical: C_1 Bonded

HF/6-31G* Optimized Geometrical Parameters

Interatomic Distance (Å)		Angles (deg)		Dihedral Angles (deg)	
C_1C_2	1.514	$C_1C_2C_3$	118.6	$C_1C_2C_3C_4$	-150.2
C_2C_3	1.503	$C_1C_2C_4$	116.1	$C_3C_2C_1C_5$	-50.5
C_2C_4	1.503	$C_3C_2C_4$	118.5	$N_6C_5C_1C_2$	146.7
C_1C_5	1.474	$C_2C_1C_5$	113.5		
C_2C_5	2.499	$C_1C_5N_6$	179.9		
C_5N_6	1.135				

Atomic Charge and Spin Density Distribution from Mulliken Population Analysis

Atom Number	Charge[a]	Spin[a]
1	0.07	-0.08
2	0.05	1.19
3	0.03	-0.06
4	0.01	-0.06
5	0.31	0.06
6	-0.47	-0.05

[a]All charge and spin densities of directly bonded hydrogen atoms are summed into the carbon atoms

Total Energy (MP2/6-31G*//HF/6-31G*): -249.18188 au

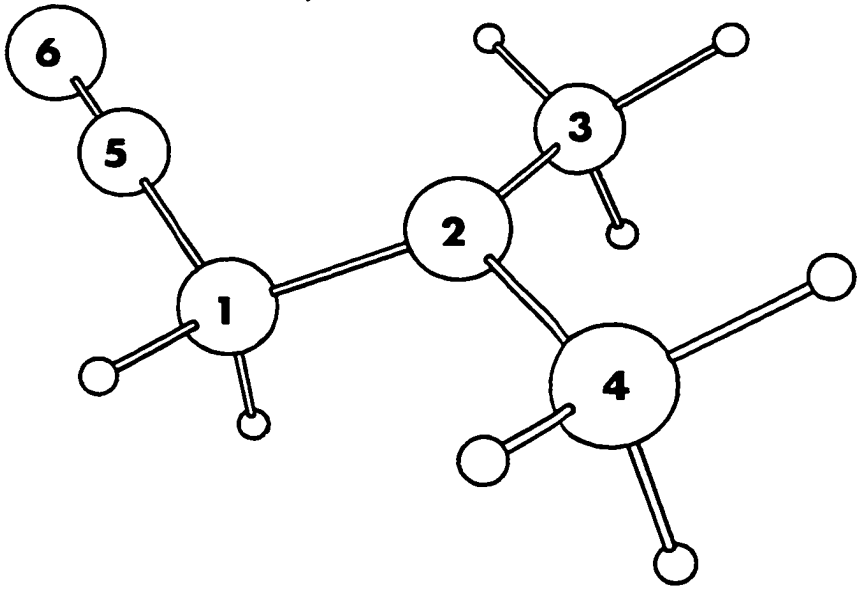

2-Methylpropene/Cyanide β-Cyanoalkyl Radical: C_2 Bonded

HF/6-31G* Optimized Geometrical Parameters

Interatomic Distance (Å)		Angles (deg)		Dihedral Angles (deg)	
C_1C_2	1.510	$C_1C_2C_3$	110.6	$C_1C_2C_3C_4$	-122.5
C_2C_3	1.545	$C_1C_2C_4$	110.5	$N_6C_5C_2C_1$	-142.4
C_2C_4	1.539	$C_3C_2C_4$	110.2		
C_2C_5	1.485	$C_1C_2C_5$	108.7		
C_1C_5	2.434	$C_2C_5N_6$	179.5		
C_5N_6	1.136				

Atomic Charge and Spin Density Distribution from Mulliken Population Analysis

Atom Number	Charge[a]	Spin[a]
1	0.06	1.07
2	-0.09	-0.14
3	0.09	0.05
4	0.08	0.01
5	0.31	0.04
6	-0.46	-0.03

[a]All charge and spin densities of directly bonded hydrogen atoms are summed into the carbon atoms

Total Energy (MP2/6-31G*//HF/6-31G*): -249.17587 au

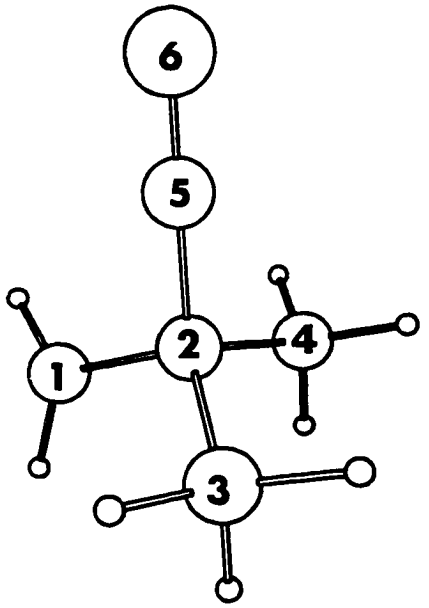

2-Methylpropene/Isocyanide β-Isocyanoalkyl Radical: C_1 Bonded

HF/6-31G* Optimized Geometrical Parameters

Interatomic Distance (Å)		Angles (deg)		Dihedral Angles (deg)	
C_1C_2	1.509	$C_1C_2C_3$	119.0	$C_1C_2C_3C_4$	-149.8
C_2C_3	1.502	$C_1C_2C_4$	115.8	$C_3C_2C_1N_5$	-47.4
C_2C_4	1.504	$C_3C_2C_4$	118.5	$C_6N_5C_1C_2$	179.3
C_1N_5	1.429	$C_2C_1N_5$	113.2		
C_2N_5	3.467	$C_1N_5C_6$	179.8		
N_5C_6	1.153				

Atomic Charge and Spin Density Distribution from Mulliken Population Analysis

Atom Number	Charge[a]	Spin[a]
1	0.29	-0.07
2	0.04	1.18
3	0.02	-0.06
4	0.00	-0.06
5	-0.40	0.03
6	0.04	0.02

[a]All charge and spin densities of directly bonded hydrogen atoms are summed into the carbon atoms

Total Energy (MP2/6-31G*//HF/6-31G*): -249.14118 au

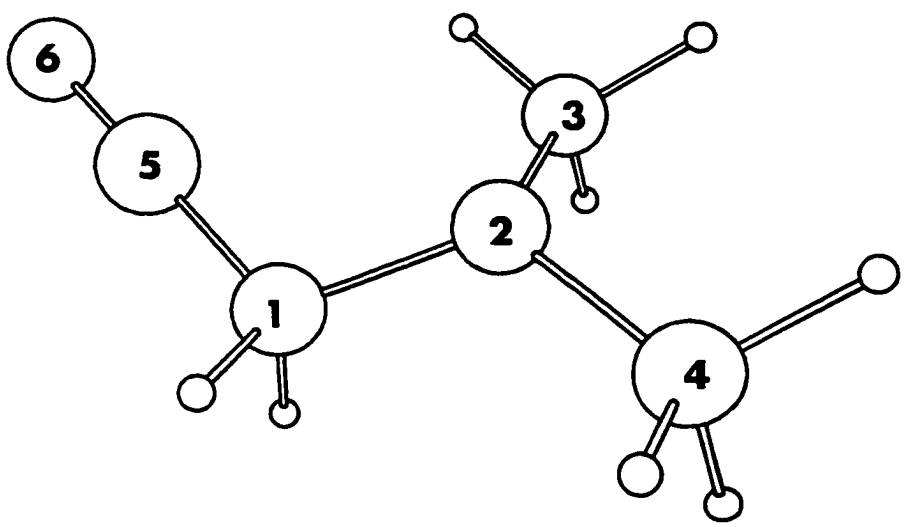

2-Methylpropene/Isocyanide β-Isocyanoalkyl Radical: C_2 Bonded

HF/6-31G* Optimized Geometrical Parameters

Interatomic Distance (Å)		Angles (deg)		Dihedral Angles (deg)	
C_1C_2	1.507	$C_1C_2C_3$	110.9	$C_1C_2C_3C_4$	-123.3
C_2C_3	1.538	$C_1C_2C_4$	110.8	$C_6N_5C_2C_1$	-169.2
C_2C_4	1.534	$C_3C_2C_4$	110.6		
C_2N_5	1.443	$C_1C_2N_5$	108.5		
C_1N_5	2.394	$C_2N_5C_6$	179.6		
N_5C_6	1.154				

Atomic Charge and Spin Density Distribution from Mulliken Population Analysis

Atom Number	Charge[a]	Spin[a]
1	0.06	1.07
2	0.13	-0.14
3	0.08	0.04
4	0.08	0.02
5	-0.38	0.02
6	0.03	-0.02

[a]All charge and spin densities of directly bonded hydrogen atoms are summed into the carbon atoms

Total Energy (MP2/6-31G*//HF/6-31G*): -249.14014 au

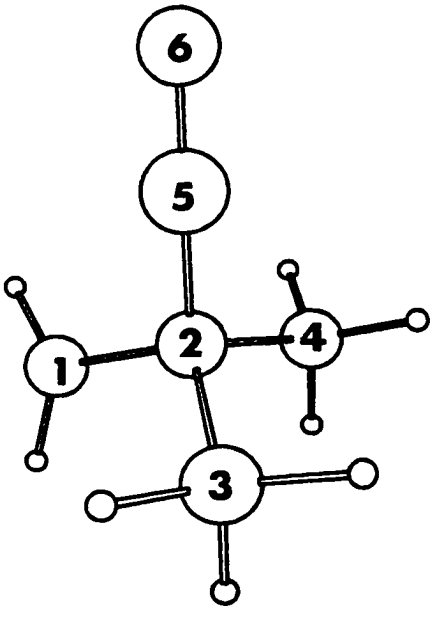

2-Methyl-2-Butene/Methanol β-Alkoxyalkyl Radical: C_2 Bonded (9a•)

HF/6-31G* Optimized Geometrical Parameters

Interatomic Distance (Å)		Angles (deg)		Dihedral Angles (deg)	
C_1C_2	1.532	$C_1C_2C_3$	110.7	$C_1C_2C_3C_4$	-66.2
C_2C_3	1.514	$C_1C_2C_5$	109.7	$C_1C_2O_6C_7$	-176.3
C_2C_5	1.532	$C_2C_3C_4$	121.8	$C_4C_3C_2O_6$	48.4
C_3C_4	1.500	$C_3C_2C_5$	110.4	$C_3C_2O_6C_7$	64.9
C_2O_6	1.416	$C_3C_2O_6$	110.8		
C_3O_6	2.413	$C_2O_6C_7$	118.3		
C_7O_6	1.395				

Atomic Charge and Spin Density Distribution from Mulliken Population Analysis

Atom Number	Charge[a]	Spin[a]
1	0.00	0.01
2	0.31	-0.13
3	0.00	1.14
4	0.01	-0.07
5	0.03	0.04
6	-0.64	0.01
7	0.30	0.00

[a]All charge and spin densities of directly bonded hydrogen atoms are summed into the carbon atoms

Total Energy (MP2/6-31G*//HF/6-31G*): -310.52614 au

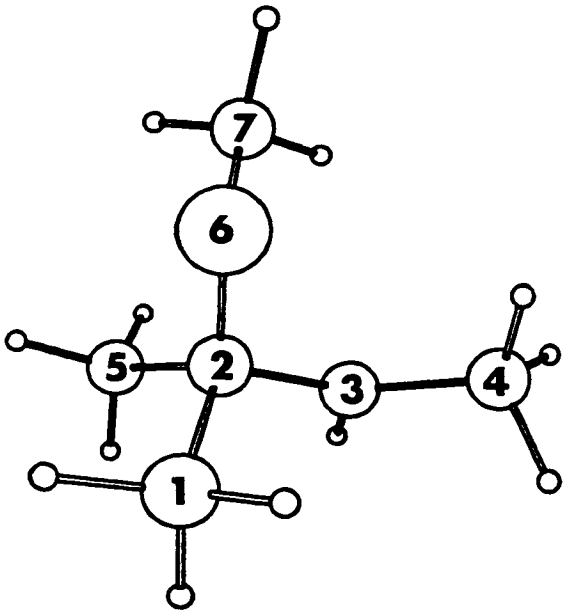

2-Methyl-2-Butene/Methanol β-Alkoxyalkyl Radical: C_3 Bonded (9b•)

HF/6-31G* Optimized Geometrical Parameters

Interatomic Distance (Å)		Angles (deg)		Dihedral Angles (deg)	
C_1C_2	1.503	$C_1C_2C_3$	118.5	$C_1C_2C_3C_4$	85.6
C_2C_3	1.513	$C_1C_2C_5$	118.0	$C_1C_2C_3O_6$	-156.5
C_2C_5	1.504	$C_2C_3C_4$	112.7	$C_5C_2C_3O_6$	48.0
C_3C_4	1.528	$C_3C_2C_5$	119.0	$C_2C_3O_6C_7$	70.6
C_2O_6	2.425	$C_2C_3O_6$	112.3		
C_3O_6	1.405	$C_3O_6C_7$	115.3		
C_7O_6	1.394				

Atomic Charge and Spin Density Distribution from Mulliken Population Analysis

Atom Number	Charge[a]	Spin[a]
1	0.00	-0.06
2	0.01	1.20
3	0.30	-0.12
4	0.02	0.04
5	-0.01	-0.06
6	-0.62	0.01
7	0.30	0.00

[a]All charge and spin densities of directly bonded hydrogen atoms are summed into the carbon atoms

Total Energy (MP2/6-31G*//HF/6-31G*): -310.52857 au

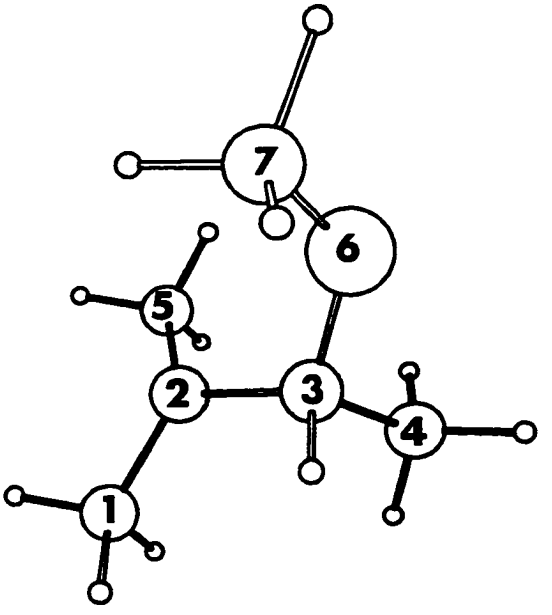

2-Methyl-2-Butene/Fluoride β-Fluoroalkyl Radical: C_2 Bonded (9x')

HF/6-31G* Optimized Geometrical Parameters

Interatomic Distance (Å)		Angles (deg)		Dihedral Angles (deg)	
C_1C_2	1.527	$C_1C_2C_3$	112.4	$C_1C_2C_3C_4$	-76.7
C_2C_3	1.504	$C_1C_2C_5$	111.9	$C_5C_2C_3C_4$	156.6
C_2C_5	1.522	$C_2C_3C_4$	121.6	$C_4C_3C_2F_6$	-39.9
C_3C_4	1.499	$C_3C_2F_6$	107.8		
C_2F_6	1.390	$C_1C_2F_6$	106.1		

Atomic Charge and Spin Density Distribution from Mulliken Population Analysis

Atom Number	Charge[a]	Spin[a]
1	0.01	0.01
2	0.42	-0.12
3	-0.01	1.14
4	0.02	-0.07
5	0.01	0.04
6	-0.44	0.01

[a]All charge and spin densities of directly bonded hydrogen atoms are summed into the carbon atoms

Total Energy (MP2/6-31G*//HF/6-31G*): -295.36617 au

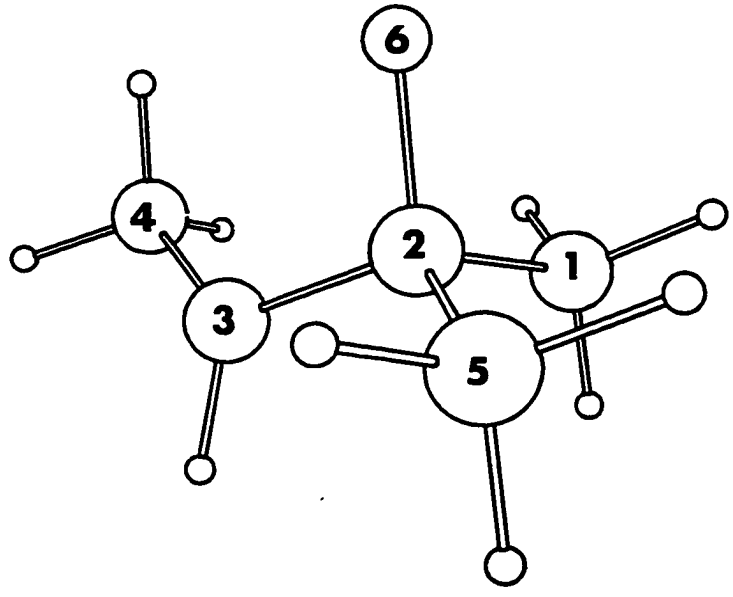

2-Methyl-2-Butene/Fluoride β-Fluoroalkyl Radical: C_3 Bonded ($9y^{\cdot}$)

HF/6-31G* Optimized Geometrical Parameters

Interatomic Distance (Å)		Angles (deg)		Dihedral Angles (deg)	
C_1C_2	1.503	$C_1C_2C_3$	117.8	$C_1C_2C_3C_4$	79.0
C_2C_3	1.503	$C_1C_2C_5$	118.6	$C_5C_2C_3C_4$	-76.7
C_2C_5	1.503	$C_2C_3C_4$	114.4	$C_1C_2C_3F_6$	-160.6
C_3C_4	1.523	$C_2C_3F_6$	109.3		
C_3F_6	1.381				

Atomic Charge and Spin Density Distribution from Mulliken Population Analysis

Atom Number	Charge[a]	Spin[a]
1	-0.01	-0.06
2	0.00	1.19
3	0.43	-0.11
4	0.00	0.04
5	0.00	-0.06
6	-0.43	0.01

[a]All charge and spin densities of directly bonded hydrogen atoms are summed into the carbon atoms

Total Energy (MP2/6-31G*//HF/6-31G*): -295.36422 au

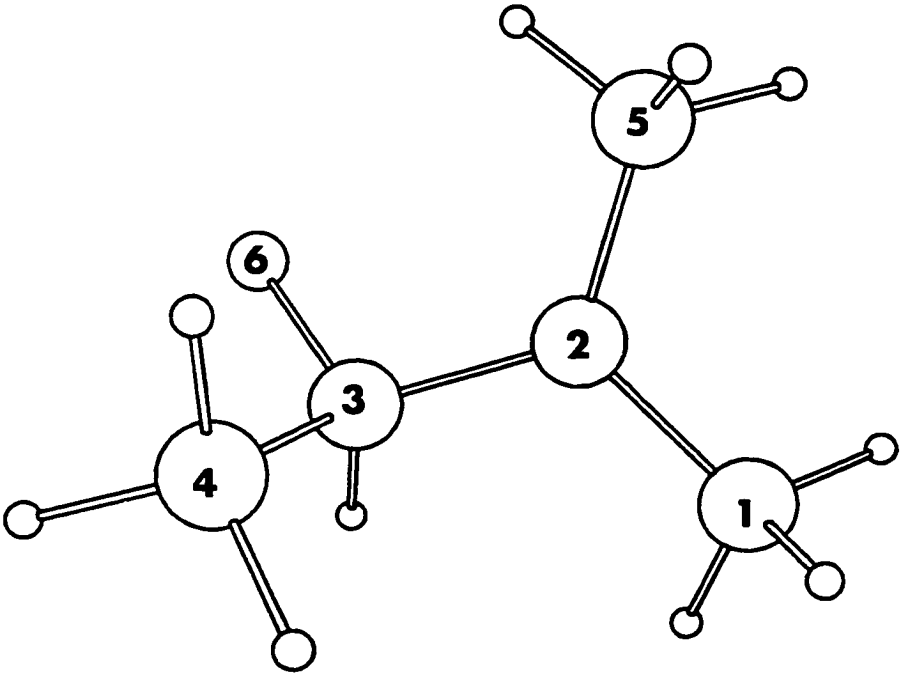

2-Methyl-2-Butene/Cyanide β-Cyanoalkyl Radical: C_2 Bonded

HF/6-31G* Optimized Geometrical Parameters

Interatomic Distance (Å)		Angles (deg)		Dihedral Angles (deg)	
C_1C_2	1.539	$C_1C_2C_3$	110.1	$C_1C_2C_3C_4$	-167.9
C_2C_3	1.517	$C_1C_2C_5$	110.0	$C_1C_2C_6N_7$	-77.4
C_2C_5	1.545	$C_2C_3C_4$	122.9	$C_4C_3C_2C_6$	-49.2
C_3C_4	1.500	$C_3C_2C_5$	111.0	$C_3C_2C_6N_7$	162.7
C_2C_6	1.486	$C_3C_2C_6$	109.4		
C_3C_6	2.452	$C_2C_6N_7$	179.4		
N_7C_6	1.136				

Atomic Charge and Spin Density Distribution from Mulliken Population Analysis

Atom Number	Charge[a]	Spin[a]
1	0.08	0.03
2	-0.10	-0.14
3	0.05	1.14
4	0.03	-0.07
5	0.08	0.03
6	0.32	0.04
7	-0.47	-0.03

[a]All charge and spin densities of directly bonded hydrogen atoms are summed into the carbon atoms

Total Energy (MP2/6-31G*//HF/6-31G*): -288.34730 au

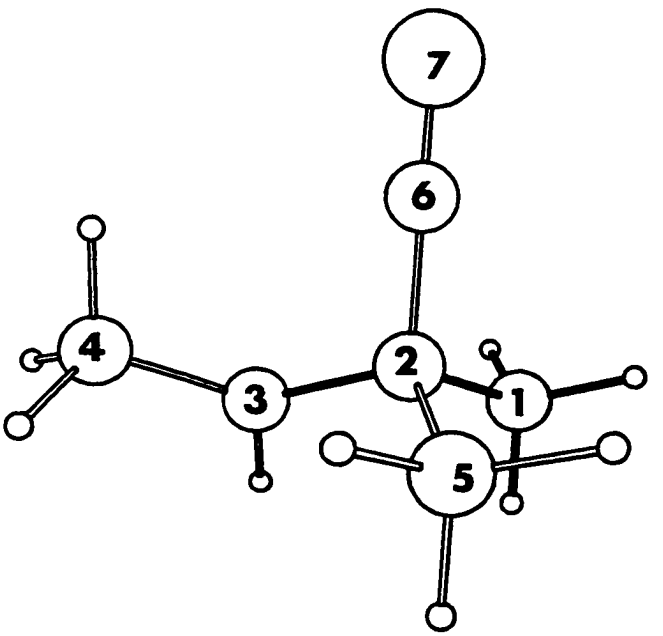

2-Methyl-2-Butene/Cyanide β-Cyanoalkyl Radical: C_3 Bonded

HF/6-31G* Optimized Geometrical Parameters

Interatomic Distance (Å)		Angles (deg)		Dihedral Angles (deg)	
C_1C_2	1.504	$C_1C_2C_3$	119.5	$C_1C_2C_3C_4$	-70.0
C_2C_3	1.518	$C_1C_2C_5$	118.1	$C_1C_2C_3C_6$	54.0
C_2C_5	1.504	$C_2C_3C_4$	113.3	$C_5C_2C_3C_6$	-151.9
C_3C_4	1.543	$C_3C_2C_5$	117.2	$C_2C_3C_6N_7$	-134.8
C_2C_6	2.474	$C_2C_3C_6$	111.2		
C_3C_6	1.480	$C_3C_6N_7$	179.4		
N_7C_6	1.136				

Atomic Charge and Spin Density Distribution from Mulliken Population Analysis

Atom Number	Charge[a]	Spin[a]
1	0.02	-0.06
2	0.06	1.20
3	-0.01	-0.13
4	0.08	0.06
5	0.01	-0.07
6	0.31	0.05
7	-0.47	-0.04

[a]All charge and spin densities of directly bonded hydrogen atoms are summed into the carbon atoms

Total Energy (MP2/6-31G*//HF/6-31G*): -288.34944 au

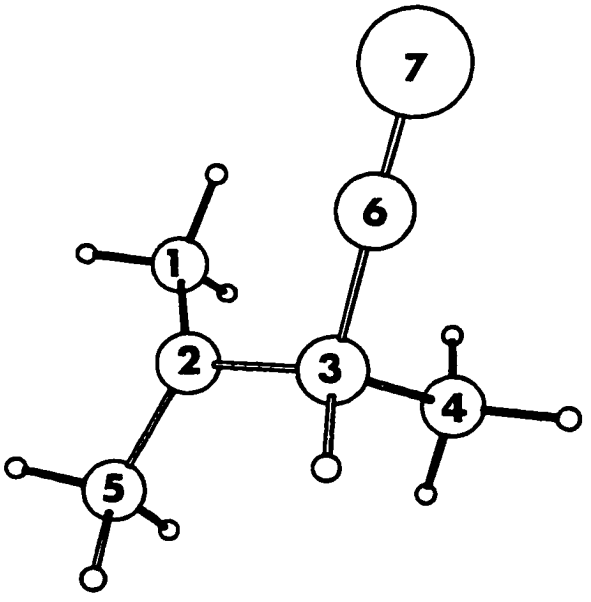

2-Methyl-2-Butene/Isocyanide β-Isocyanoalkyl Radical: C_2 Bonded

HF/6-31G* Optimized Geometrical Parameters

Interatomic Distance (Å)		Angles (deg)		Dihedral Angles (deg)	
C_1C_2	1.538	$C_1C_2C_3$	111.2	$C_1C_2C_3C_4$	-72.3
C_2C_3	1.514	$C_1C_2C_5$	110.5	$C_1C_2N_6C_7$	-37.1
C_2C_5	1.533	$C_2C_3C_4$	122.9	$C_4C_3C_2N_6$	46.4
C_3C_4	1.499	$C_3C_2C_5$	110.2	$C_3C_2N_6C_7$	-158.0
C_2N_6	1.444	$C_3C_2N_6$	109.4		
C_3N_6	2.414	$C_2N_6C_7$	179.4		
C_7N_6	1.154				

Atomic Charge and Spin Density Distribution from Mulliken Population Analysis

Atom Number	Charge[a]	Spin[a]
1	0.08	0.04
2	0.13	-0.17
3	0.05	1.14
4	0.03	-0.07
5	0.08	0.04
6	-0.40	0.02
7	0.03	-0.02

[a]All charge and spin densities of directly bonded hydrogen atoms are summed into the carbon atoms

Total Energy (MP2/6-31G*//HF/6-31G*): -288.31170 au

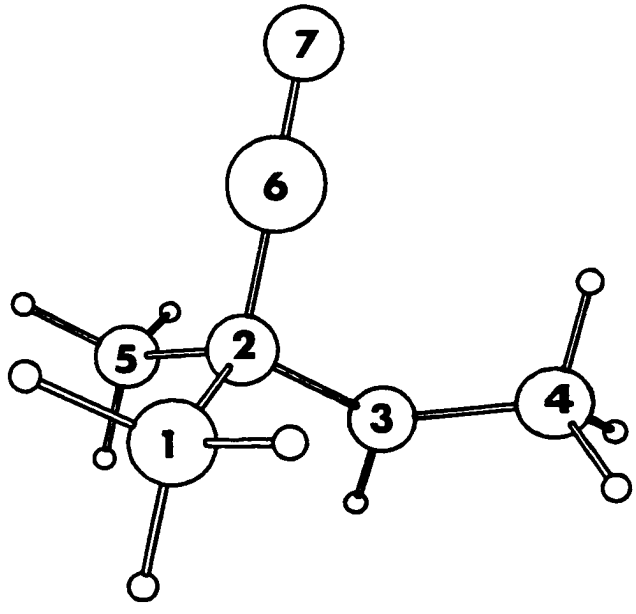

2-Methyl-2-Butene/Isocyanide β-Isocyanoalkyl Radical: C_3 Bonded

HF/6-31G* Optimized Geometrical Parameters

Interatomic Distance (Å)		Angles (deg)		Dihedral Angles (deg)	
C_1C_2	1.504	$C_1C_2C_3$	116.7	$C_1C_2C_3C_4$	158.5
C_2C_3	1.515	$C_1C_2C_5$	118.0	$C_1C_2C_3N_6$	-77.9
C_2C_5	1.505	$C_2C_3C_4$	115.0	$C_5C_2C_3N_6$	73.8
C_3C_4	1.528	$C_3C_2C_5$	119.1	$C_2C_3N_6C_7$	-16.1
C_2N_6	2.422	$C_2C_3N_6$	109.8		
C_3N_6	1.446	$C_3N_6C_7$	178.6		
C_7N_6	1.154				

Atomic Charge and Spin Density Distribution from Mulliken Population Analysis

Atom Number	Charge[a]	Spin[a]
1	0.01	-0.06
2	0.05	1.19
3	0.21	-0.12
4	0.07	0.05
5	0.02	-0.06
6	-0.39	0.03
7	0.03	-0.03

[a]All charge and spin densities of directly bonded hydrogen atoms are summed into the carbon atoms

Total Energy (MP2/6-31G*//HF/6-31G*): -288.31137 au

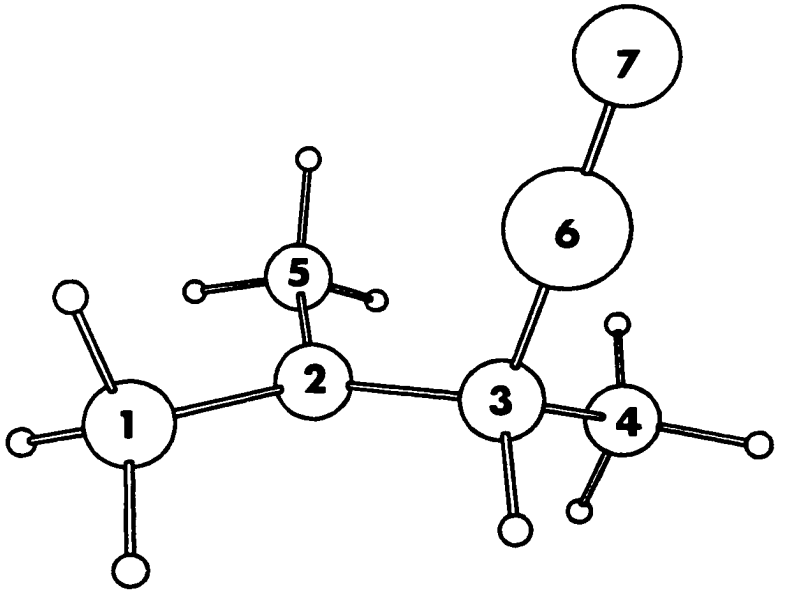

Appendix V

Selected Geometrical Parameters and Charge Density Distribution for Substituted Alkanes

2,2-Dimethyl-3-Oxabutane

HF/6-31G* Optimized Geometrical Parameters

Interatomic Distance (Å)		Angles (deg)		Dihedral Angles (deg)	
C_1C_2	1.527	$C_1C_2C_3$	103.7	$C_1C_2O_3C_4$	180.0
C_2O_3	1.416	$C_2C_3C_4$	119.7	$C_5C_2O_3C_4$	61.9
O_3C_4	1.394	$C_1C_2C_5$	109.9	$C_6C_2O_3C_4$	-62.0
C_2C_5	1.532	$C_1C_2C_6$	109.9		
C_2C_6	1.532				

Atomic Charge Density Distribution from Mulliken Population Analysis

Atom Number	Charge[a]
1	0.00
2	0.32
3	-0.64
4	0.30
5	0.03
6	0.00

[a]All charges of directly bonded hydrogen atoms are summed into the carbon atoms

Total Energy (MP2/6-31G*//HF/6-31G*): -272.01315 au

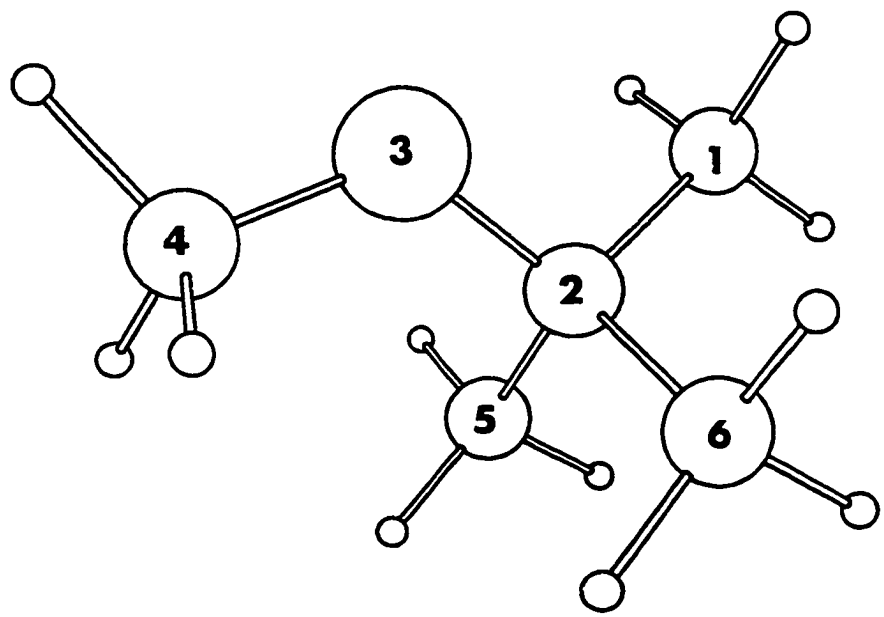

2-Oxabutane

HF/6-31G* Optimized Geometrical Parameters

Interatomic Distance (Å)		Angles (deg)		Dihedral Angles (deg)	
C_1O_2	1.391	$C_1O_2C_3$	114.2	$C_1O_2C_3C_4$	180.0
O_2C_3	1.396	$O_2C_3C_4$	108.6		
C_3C_4	1.516				

Atomic Charge Density Distribution from Mulliken Population Analysis

Atom Number	Charge[a]
1	0.30
2	-0.60
3	0.30
4	0.01

[a]All charges of directly bonded hydrogen atoms are summed into the carbon atoms

Total Energy (MP2/6-31G*//HF/6-31G*): -193.67303 au

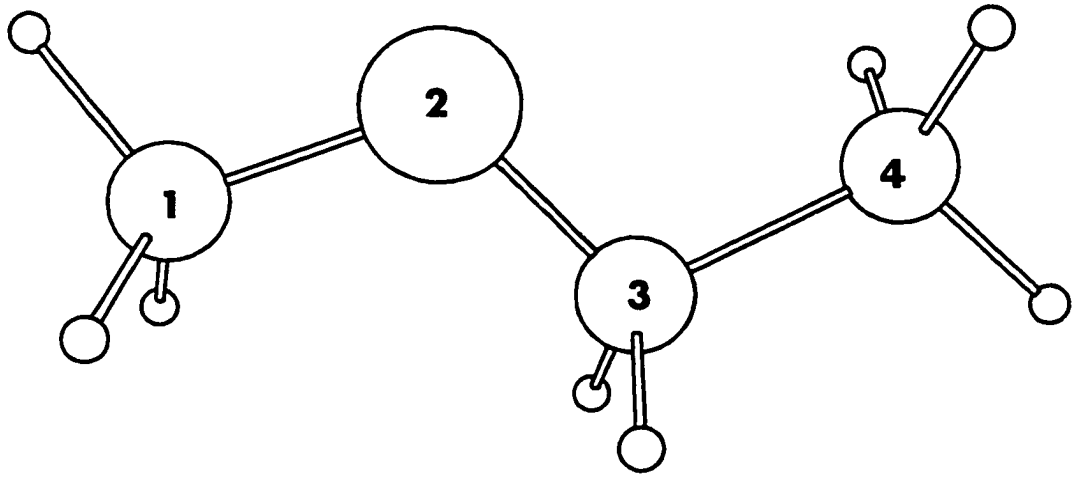

4-Methyl-2-Oxapentane

HF/6-31G* Optimized Geometrical Parameters

Interatomic Distance (Å)		Angles (deg)		Dihedral Angles (deg)	
C_1O_2	1.391	$C_1O_2C_3$	114.3	$C_1O_2C_3C_4$	-179.3
O_2C_3	1.396	$O_2C_3C_4$	109.6	$O_2C_3C_4C_5$	-174.7
C_3C_4	1.524	$C_3C_4C_5$	110.2	$O_2C_3C_4C_6$	61.2
C_4C_5	1.531	$C_3C_4C_6$	111.4		
C_4C_6	1.530				

Atomic Charge Density Distribution from Mulliken Population Analysis

Atom Number	Charge[a]
1	0.30
2	-0.62
3	0.31
4	0.00
5	0.01
6	-0.01

[a]All charges of directly bonded hydrogen atoms are summed into the carbon atoms

Total Energy (MP2/6-31G*//HF/6-31G*): -272.00731 au

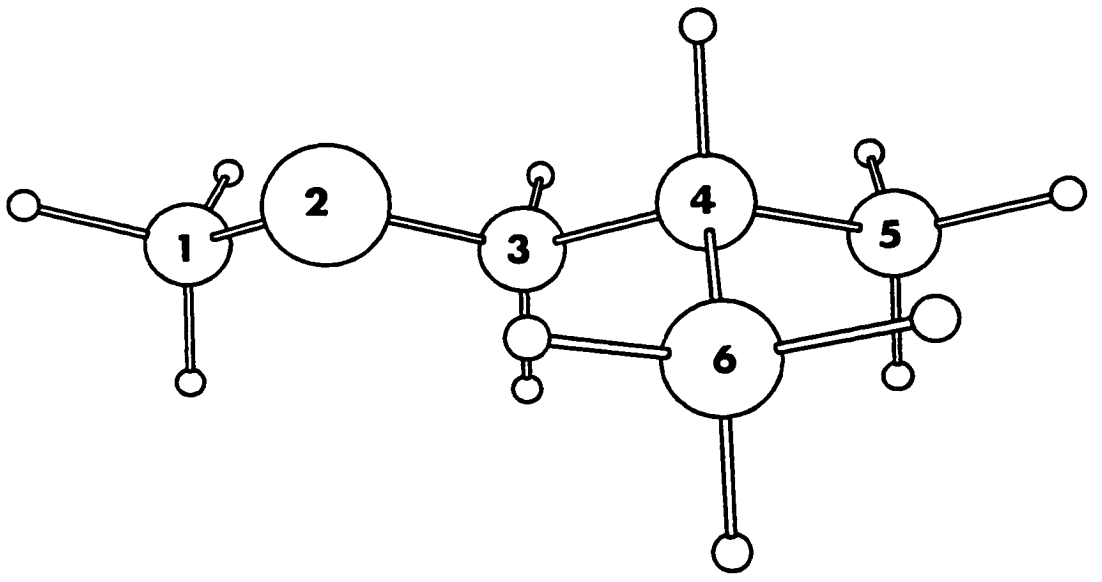

3,3-Dimethyl-2-Oxapentane

HF/6-31G* Optimized Geometrical Parameters

Interatomic Distance (Å)		Angles (deg)		Dihedral Angles (deg)	
C_1O_2	1.394	$C_1O_2C_3$	119.6	$C_1O_2C_3C_4$	66.7
O_2C_3	1.417	$O_2C_3C_4$	111.3	$O_2C_3C_4C_5$	53.3
C_3C_4	1.541	$C_3C_4C_5$	115.4	$C_1O_2C_3C_6$	-173.3
C_4C_5	1.529	$O_2C_3C_6$	103.8	$C_1O_2C_3C_7$	-55.9
C_3C_6	1.528	$C_6C_3C_7$	109.3		
C_3C_7	1.533				

Atomic Charge Density Distribution from Mulliken Population Analysis

Atom Number	Charge[a]
1	0.30
2	-0.64
3	0.32
4	-0.01
5	0.01
6	0.00
7	0.03

[a]All charges of directly bonded hydrogen atoms are summed into the carbon atoms

Total Energy (MP2/6-31G*//HF/6-31G*): -311.17824 au

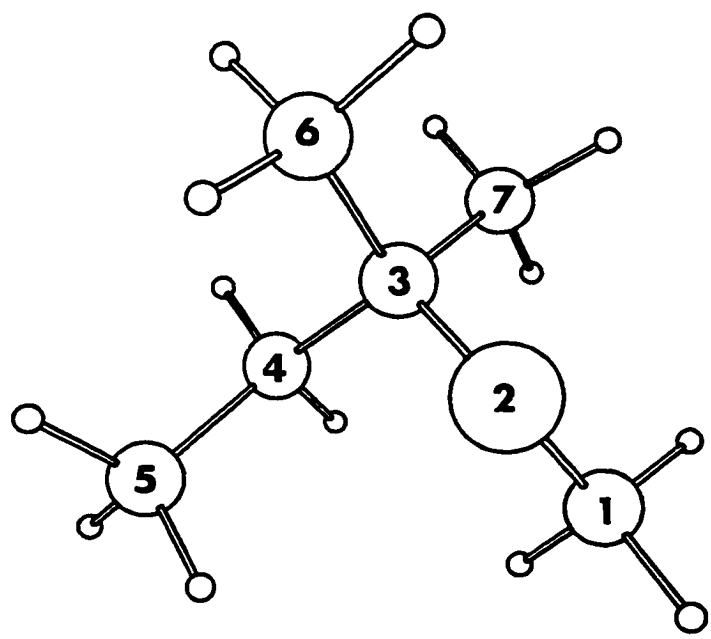

3,4-Dimethyl-2-Oxapentane

HF/6-31G* Optimized Geometrical Parameters

Interatomic Distance (Å)		Angles (deg)		Dihedral Angles (deg)	
C_1O_2	1.392	$C_1O_2C_3$	116.5	$C_1O_2C_3C_4$	-157.5
O_2C_3	1.406	$O_2C_3C_4$	107.8	$O_2C_3C_4C_5$	64.1
C_3C_4	1.536	$C_3C_4C_5$	110.7	$C_1O_2C_3C_6$	77.3
C_3C_6	1.528	$O_2C_3C_6$	111.3	$O_2C_3C_4C_7$	-60.6
C_4C_5	1.532	$C_3C_4C_7$	113.1		
C_4C_7	1.532				

Atomic Charge Density Distribution from Mulliken Population Analysis

Atom Number	Charge[a]
1	0.30
2	-0.63
3	0.32
4	-0.01
5	0.01
6	0.00
7	0.01

[a]All charges of directly bonded hydrogen atoms are summed into the carbon atoms

Total Energy (MP2/6-31G*//HF/6-31G*): -311.17633 au

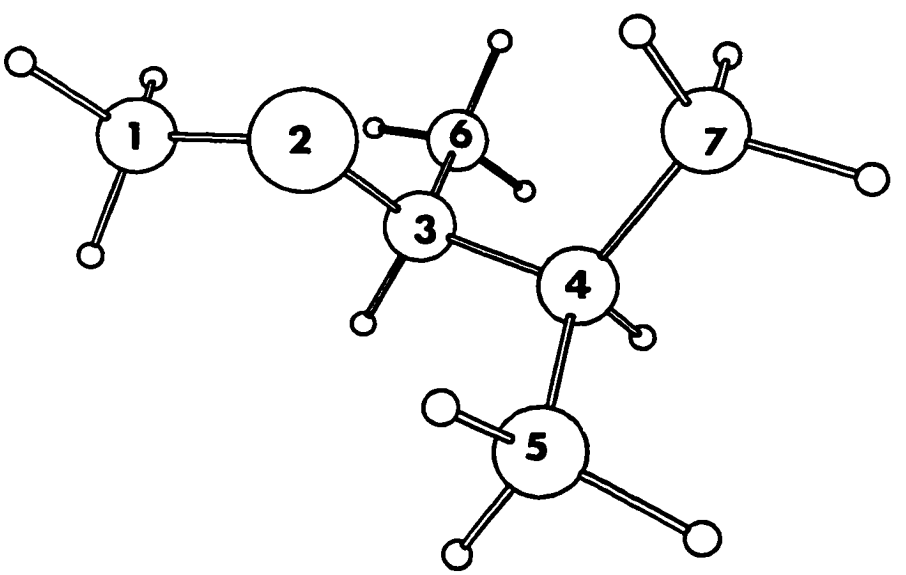

3-Methyl-2-Oxabutane

HF/6-31G* Optimized Geometrical Parameters

Interatomic Distance (Å)		Angles (deg)		Dihedral Angles (deg)	
C_1O_2	1.392	$C_1O_2C_3$	116.4	$C_1O_2C_3C_4$	77.6
O_2C_3	1.406	$O_2C_3C_4$	111.6	$C_1O_2C_3C_5$	-160.0
C_3C_4	1.527	$O_2C_3C_5$	106.6		
C_3C_5	1.521				

Atomic Charge Density Distribution from Mulliken Population Analysis

Atom Number	Charge[a]
1	0.30
2	-0.62
3	0.31
4	0.00
5	0.02

[a]All charges of directly bonded hydrogen atoms are summed into the carbon atoms

Total Energy (MP2/6-31G*//HF/6-31G*): -232.84326 au

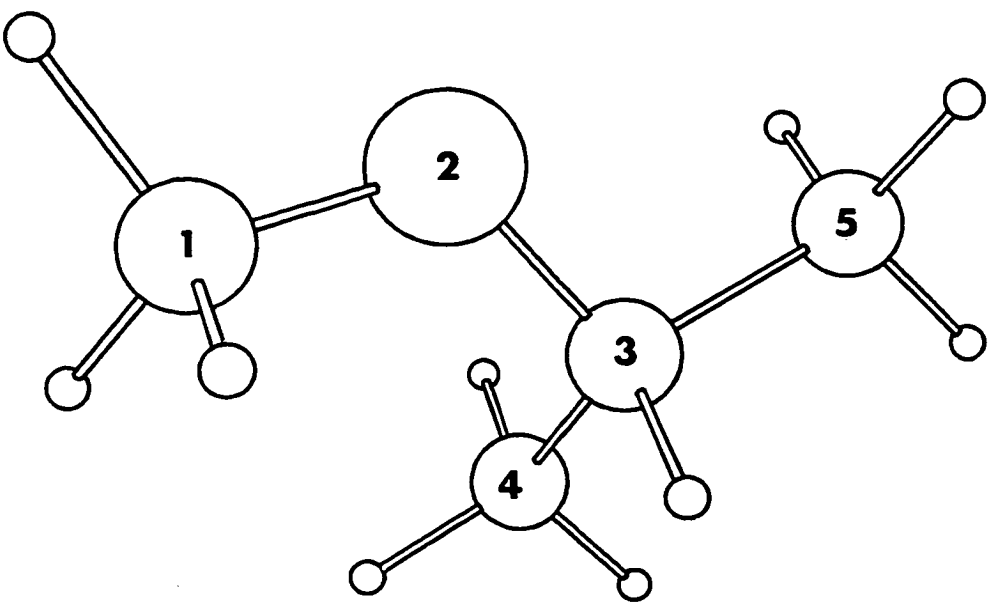

2-Fluoro-2-Methylpropane

HF/6-31G* Optimized Geometrical Parameters

Interatomic Distance (Å)		Angles (deg)		Dihedral Angles (deg)	
C_1C_2	1.521	$C_1C_2C_3$	112.2	$C_1C_2C_3C_4$	127.2
C_2C_3	1.521	$C_1C_2C_4$	112.1		
C_2C_4	1.521	$C_1C_2F_5$	106.6		
C_2F_5	1.389				

Atomic Charge Density Distribution from Mulliken Population Analysis

Atom Number	Charge[a]
1	0.01
2	0.42
3	0.01
4	0.01
5	-0.44

[a]All charges of directly bonded hydrogen atoms are summed into the carbon atoms

Total Energy (MP2/6-31G*//HF/6-31G*): -256.85596 au

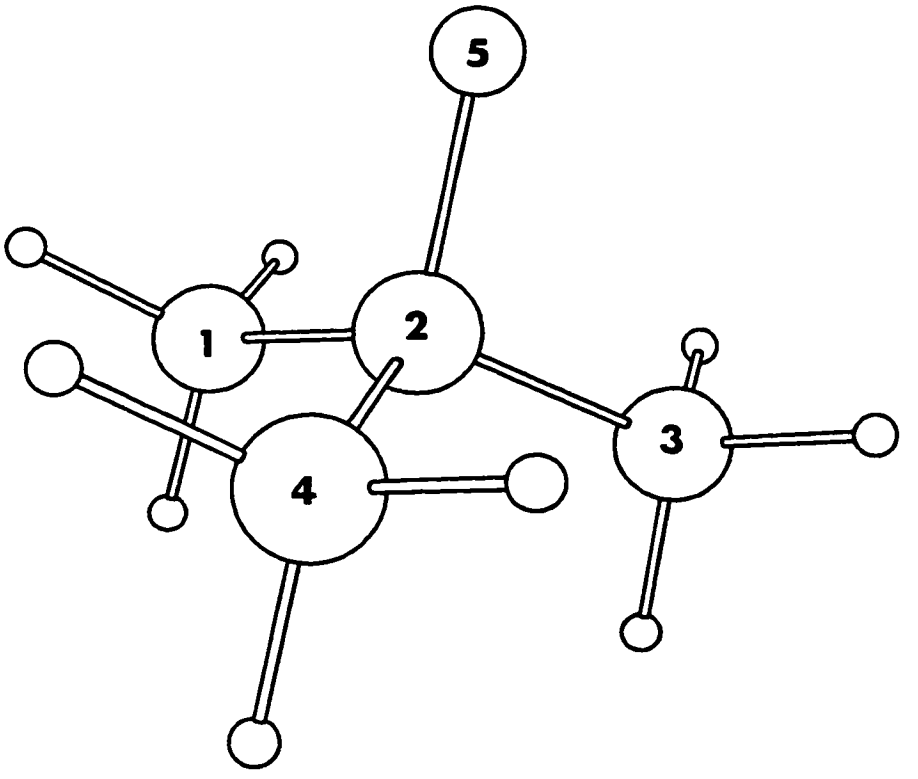

Fluoroethane

HF/6-31G* Optimized Geometrical Parameters

Interatomic Distance (Å)		Angles (deg)	
C_1C_2	1.512	$F_3C_1C_2$	109.5
C_1F_3	1.373		

Atomic Charge Density Distribution from Mulliken Population Analysis

Atom Number	Charge[a]
1	0.41
2	0.00
3	-0.41

[a]All charges of directly bonded hydrogen atoms are summed into the carbon atoms

Total Energy (MP2/6-31G*//HF/6-31G*): -178.50785 au

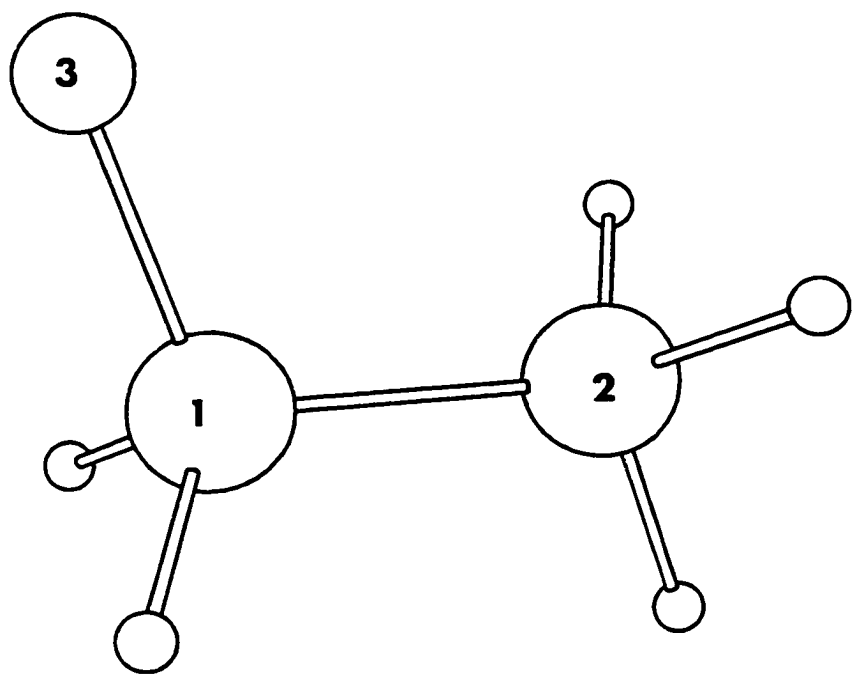

1-Fluoro-2-Methylpropane

HF/6-31G* Optimized Geometrical Parameters

Interatomic Distance (Å)		Angles (deg)		Dihedral Angles (deg)	
C_1C_2	1.519	$C_1C_2C_3$	111.0	$F_5C_1C_2C_3$	62.4
C_1F_5	1.375	$C_1C_2C_4$	111.1	$F_5C_1C_2C_4$	-62.3
C_2C_3	1.531	$F_5C_1C_2$	110.2		
C_2C_4	1.531				

Atomic Charge Density Distribution from Mulliken Population Analysis

Atom Number	Charge[a]
1	0.47
2	-0.06
3	0.02
4	0.02
5	-0.44

[a]All charges of directly bonded hydrogen atoms are summed into the carbon atoms

Total Energy (MP2/6-31G*//HF/6-31G*): -256.84252 au

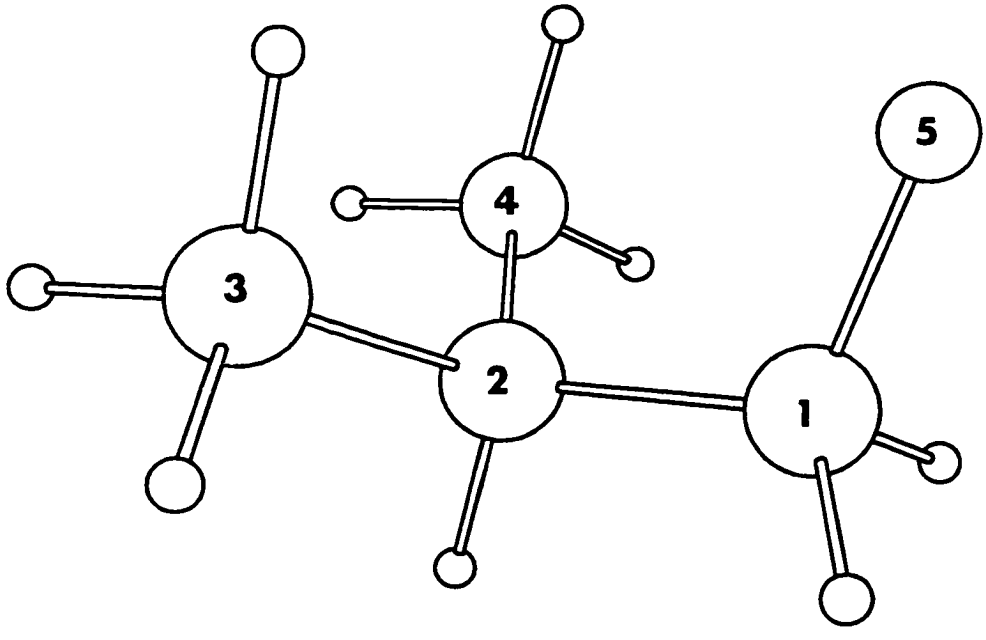

2-Fluoro-2-Methylbutane

HF/6-31G* Optimized Geometrical Parameters

Interatomic Distance (Å)		Angles (deg)		Dihedral Angles (deg)	
C_1C_2	1.522	$C_1C_2C_3$	111.2	$C_1C_2C_3C_4$	-174.1
C_2C_3	1.529	$C_1C_2C_5$	111.5	$C_5C_2C_3C_4$	59.1
C_3C_4	1.529	$C_2C_3C_4$	115.1	$F_6C_2C_3C_4$	-58.3
C_2C_5	1.522	$C_1C_2F_6$	106.4		
C_2F_6	1.391				

Atomic Charge Density Distribution from Mulliken Population Analysis

Atom Number	Charge[a]
1	0.01
2	0.42
3	0.00
4	0.01
5	0.01
6	-0.44

[a]All charges of directly bonded hydrogen atoms are summed into the carbon atoms

Total Energy (MP2/6-31G*//HF/6-31G*): -296.02090 au

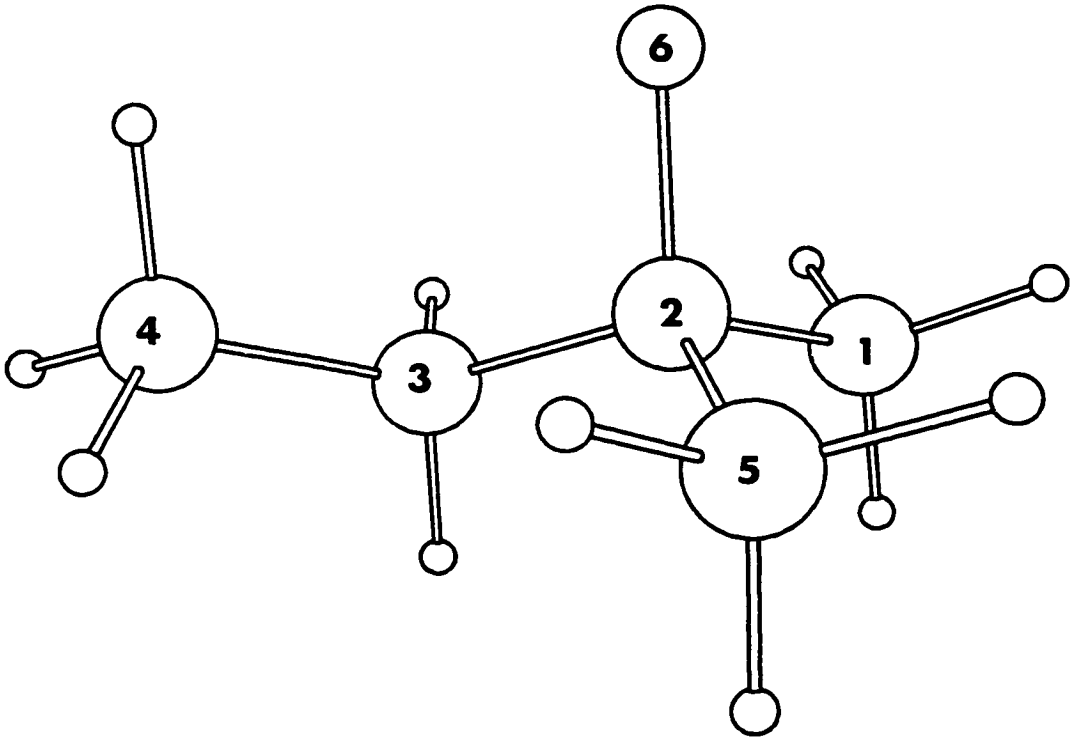

2-Fluoro-3-Methylbutane

HF/6-31G* Optimized Geometrical Parameters

Interatomic Distance (Å)		Angles (deg)		Dihedral Angles (deg)	
C_1C_2	1.517	$C_1C_2C_3$	116.0	$C_1C_2C_3C_4$	175.7
C_2C_3	1.529	$C_2C_3C_4$	110.2	$F_6C_2C_3C_4$	-63.0
C_2F_6	1.383	$C_2C_3C_5$	112.8	$F_6C_2C_3C_5$	61.3
C_3C_4	1.532	$C_4C_3C_5$	110.7		
C_3C_5	1.532	$F_6C_2C_3$	108.6		

Atomic Charge Density Distribution from Mulliken Population Analysis

Atom Number	Charge[a]
1	0.00
2	0.44
3	-0.04
4	0.01
5	0.01
6	-0.43

[a]All charges of directly bonded hydrogen atoms are summed into the carbon atoms

Total Energy (MP2/6-31G*//HF/6-31G*): -296.01499 au

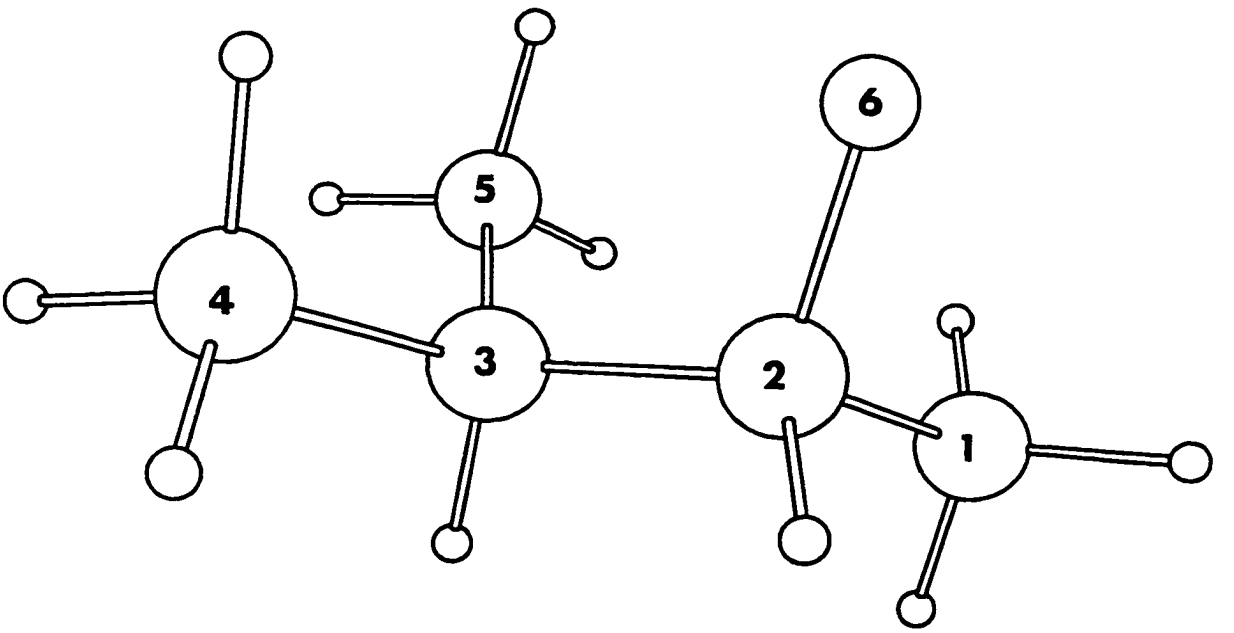

2-Fluoropropane

HF/6-31G* Optimized Geometrical Parameters

Interatomic Distance (Å)		Angles (deg)		Dihedral Angles (deg)	
C_1C_2	1.516	$C_1C_2C_3$	114.0	$C_1C_2C_3F_4$	120.0
C_2C_3	1.515	$C_1C_2F_4$	108.0		
C_2F_4	1.381				

Atomic Charge Density Distribution from Mulliken Population Analysis

Atom Number	Charge[a]
1	0.00
2	0.43
3	0.00
4	-0.43

[a]All charges of directly bonded hydrogen atoms are summed into the carbon atoms

Total Energy (MP2/6-31G*//HF/6-31G*): -217.68175 au

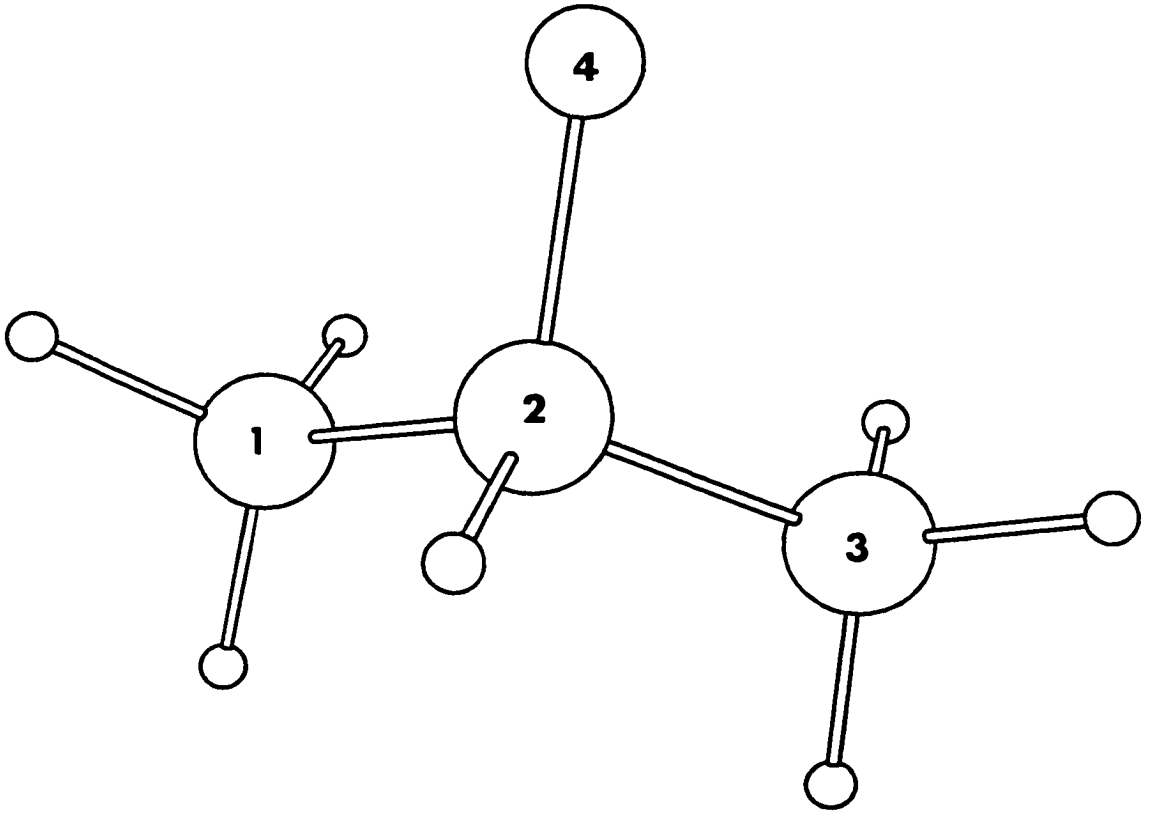

2-Cyano-2-Methylpropane

HF/6-31G* Optimized Geometrical Parameters

Interatomic Distance (Å)		Angles (deg)		Dihedral Angles (deg)	
C_1C_2	1.537	$C_1C_2C_3$	110.5	$C_1C_2C_4N_5$	97.5
C_2C_3	1.537	$C_1C_2C_6$	110.5	$C_3C_2C_4N_5$	-22.5
C_2C_4	1.485	$C_1C_2C_4$	108.4		
C_2C_6	1.537	$C_2C_4N_5$	180.0		
C_4N_5	1.136				

Atomic Charge Density Distribution from Mulliken Population Analysis

Atom Number	Charge[a]
1	0.08
2	-0.09
3	0.08
4	0.32
5	-0.46
6	0.08

[a]All charges of directly bonded hydrogen atoms are summed into the carbon atoms

Total Energy (MP2/6-31G*//HF/6-31G*): -249.83693 au

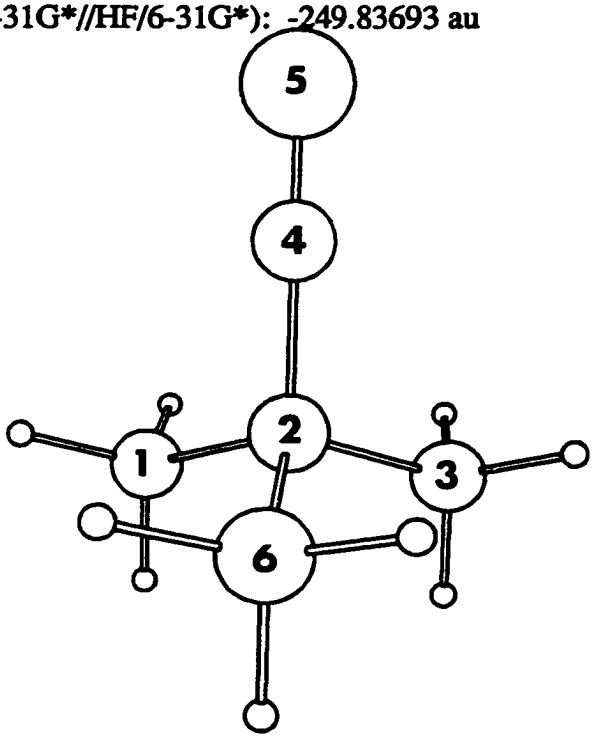

Cyanoethane

HF/6-31G* Optimized Geometrical Parameters

Interatomic Distance (Å)		Angles (deg)		Dihedral Angles (deg)	
C_1C_2	1.533	$C_3C_1C_2$	112.2	$N_4C_3C_1C_2$	0.0
C_1C_3	1.473	$C_1C_3N_4$	179.4		
C_3N_4	1.135				

Atomic Charge Density Distribution from Mulliken Population Analysis

Atom Number	Charge[a]
1	0.08
2	0.07
3	0.30
4	-0.46

[a]All charges of directly bonded hydrogen atoms are summed into the carbon atoms

Total Energy (MP2/6-31G*//HF/6-31G*): -171.49886 au

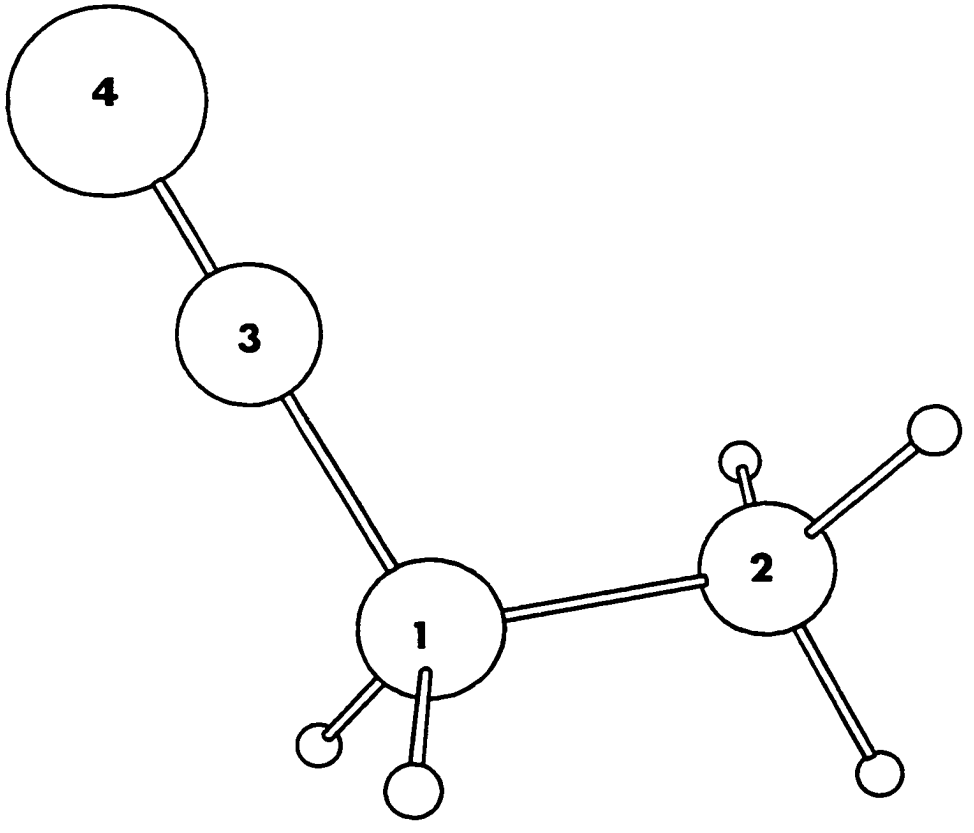

1-Cyano-2-Methylpropane

HF/6-31G* Optimized Geometrical Parameters

Interatomic Distance (Å)		Angles (deg)		Dihedral Angles (deg)	
C_1C_2	1.541	$C_1C_2C_3$	109.4	$C_4C_1C_2C_3$	174.2
C_1C_4	1.473	$C_2C_1C_4$	111.7	$C_6C_2C_1C_4$	-62.2
C_2C_3	1.530	$C_3C_2C_6$	111.3	$N_5C_4C_1C_2$	-23.0
C_2C_6	1.530	$C_1C_4N_5$	179.4		
C_4N_5	1.135				

Atomic Charge Density Distribution from Mulliken Population Analysis

Atom Number	Charge[a]
1	0.09
2	0.02
3	0.02
4	0.31
5	-0.47
6	0.03

[a]All charges of directly bonded hydrogen atoms are summed into the carbon atoms

Total Energy (MP2/6-31G*//HF/6-31G*): -249.83374 au

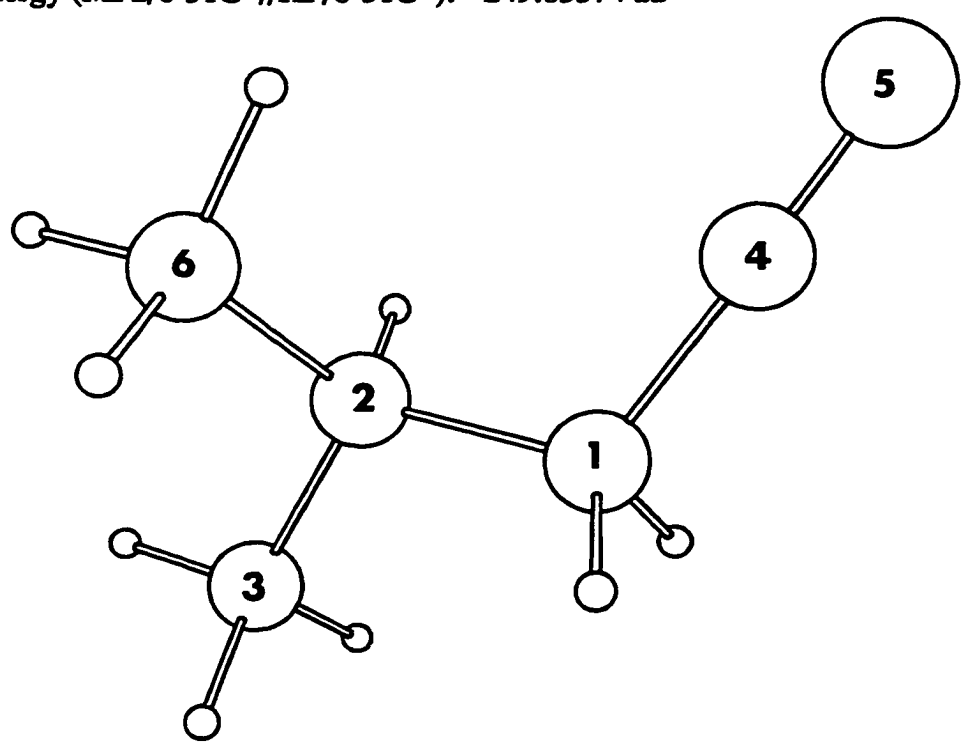

2-Cyano-2-Methylbutane

HF/6-31G* Optimized Geometrical Parameters

Interatomic Distance (Å)		Angles (deg)		Dihedral Angles (deg)	
C_1C_2	1.539	$C_1C_2C_3$	109.4	$C_1C_2C_3C_4$	-178.2
C_2C_3	1.547	$C_1C_2C_5$	108.0	$C_4C_3C_2C_5$	-60.3
C_2C_5	1.485	$C_1C_2C_7$	109.8	$C_7C_2C_3C_4$	59.8
C_2C_7	1.539	$C_2C_3C_4$	116.1	$N_6C_5C_2C_3$	-102.7
C_3C_4	1.529	$C_2C_5N_6$	179.8		
C_5N_6	1.136				

Atomic Charge Density Distribution from Mulliken Population Analysis

Atom Number	Charge[a]
1	0.08
2	-0.09
3	0.06
4	0.03
5	0.32
6	-0.47
7	0.08

[a]All charges of directly bonded hydrogen atoms are summed into the carbon atoms

Total Energy (MP2/6-31G*//HF/6-31G*): -289.00242 au

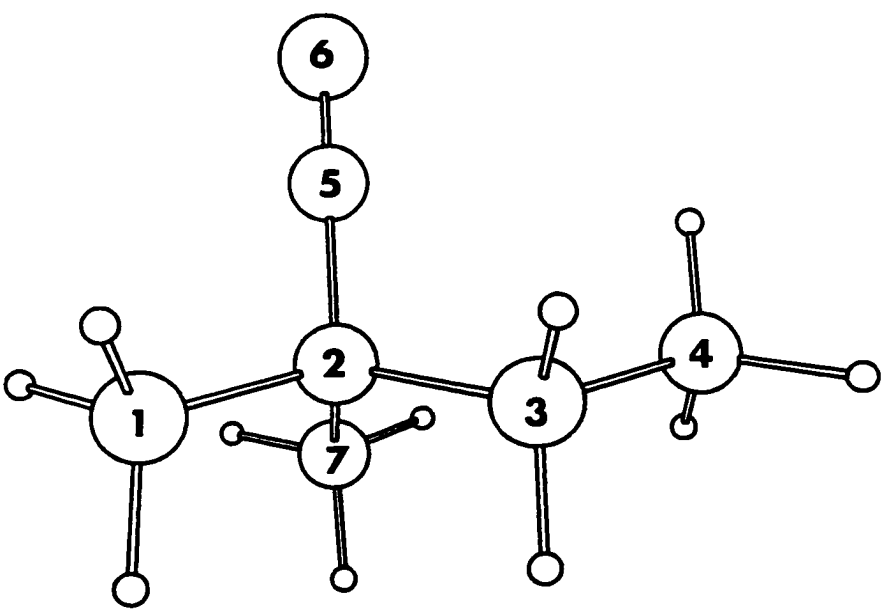

2-Cyano-3-Methylbutane

HF/6-31G* Optimized Geometrical Parameters

Interatomic Distance (Å)		Angles (deg)		Dihedral Angles (deg)	
C_1C_2	1.536	$C_1C_2C_3$	114.2	$C_1C_2C_3C_4$	171.0
C_2C_3	1.549	$C_1C_2C_5$	109.8	$C_1C_2C_3C_7$	-63.3
C_2C_5	1.480	$C_2C_3C_4$	111.1	$C_1C_2C_5N_6$	37.2
C_3C_4	1.532	$C_2C_3C_7$	113.4	$C_5C_2C_3C_4$	-64.0
C_3C_7	1.532	$C_2C_5N_6$	179.6		
C_5N_6	1.136				

Atomic Charge Density Distribution from Mulliken Population Analysis

Atom Number	Charge[a]
1	0.07
2	0.01
3	0.02
4	0.03
5	0.32
6	-0.47
7	0.03

[a]All charges of directly bonded hydrogen atoms are summed into the carbon atoms

Total Energy (MP2/6-31G*//HF/6-31G*): -289.00109 au

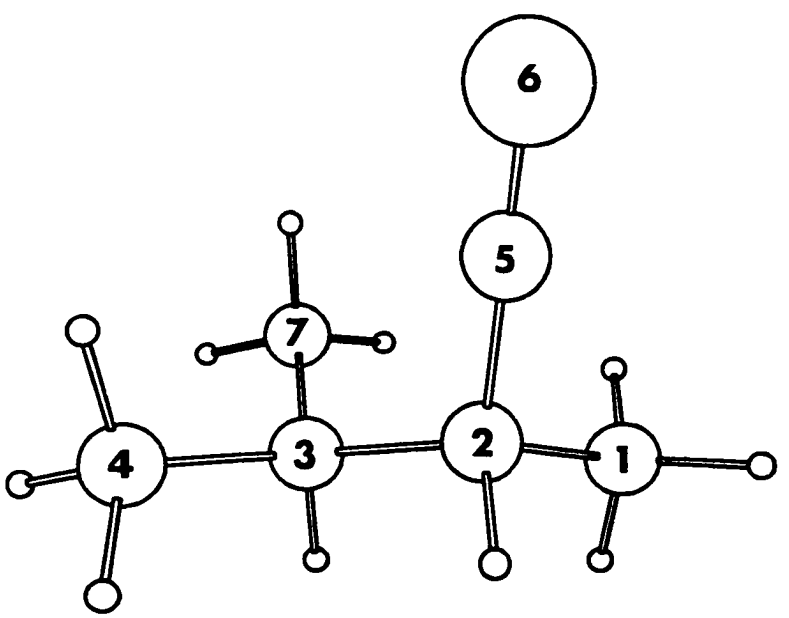

2-Cyanopropane

HF/6-31G* Optimized Geometrical Parameters

Interatomic Distance (Å)		Angles (deg)		Dihedral Angles (deg)	
C_1C_2	1.534	$C_1C_2C_3$	112.4	$C_1C_2C_4N_5$	-62.3
C_2C_3	1.534	$C_1C_2C_4$	110.2	$C_3C_2C_4N_5$	62.3
C_2C_4	1.479	$C_2C_4N_5$	179.5		
C_4N_5	1.136				

Atomic Charge Density Distribution from Mulliken Population Analysis

Atom Number	Charge[a]
1	0.07
2	0.01
3	0.07
4	0.31
5	-0.46

[a]All charges of directly bonded hydrogen atoms are summed into the carbon atoms

Total Energy (MP2/6-31G*//HF/6-31G*): -210.66679 au

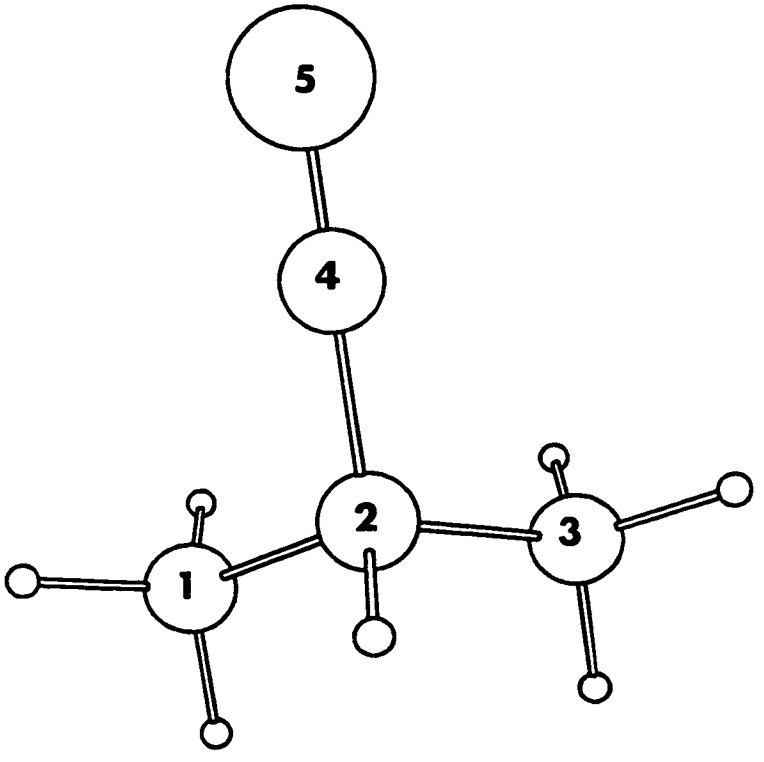

2-Isocyano-2-Methylpropane

HF/6-31G* Optimized Geometrical Parameters

Interatomic Distance (Å)		Angles (deg)		Dihedral Angles (deg)	
C_1C_2	1.532	$C_1C_2C_3$	110.8	$C_1C_2N_4C_5$	-138.0
C_2C_3	1.532	$C_1C_2C_6$	108.1	$C_3C_2N_4C_5$	-18.0
C_2N_4	1.444	$C_1C_2N_4$	110.8		
C_2C_6	1.532	$C_2N_4C_5$	180.0		
N_4C_5	1.154				

Atomic Charge Density Distribution from Mulliken Population Analysis

Atom Number	Charge[a]
1	0.07
2	0.13
3	0.07
4	-0.38
5	0.03
6	0.07

[a]All charges of directly bonded hydrogen atoms are summed into the carbon atoms

Total Energy (MP2/6-31G*//HF/6-31G*): -249.80185 au

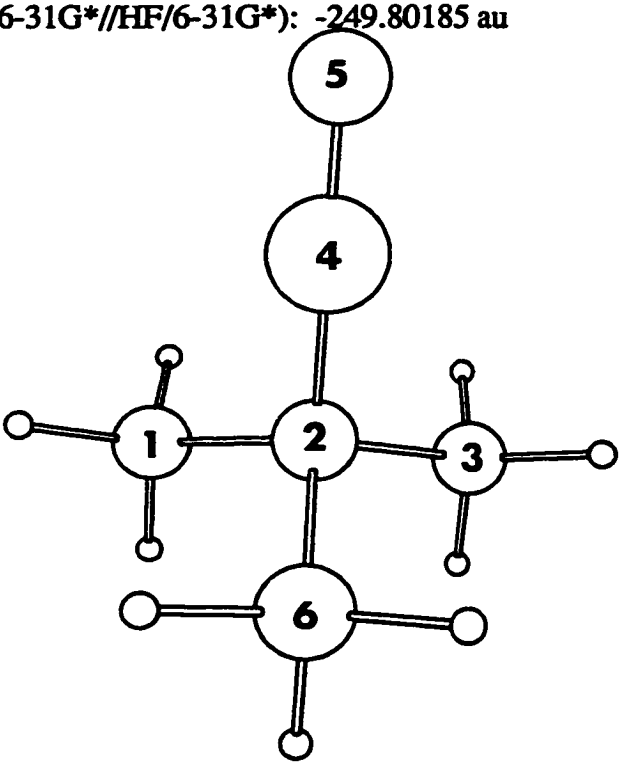

Isocyanoethane

HF/6-31G* Optimized Geometrical Parameters

Interatomic Distance (Å)		Angles (deg)		Dihedral Angles (deg)	
C_1C_2	1.524	$C_1N_3C_4$	179.3	$C_4N_3C_1C_2$	12.4
C_1N_3	1.429	$N_3C_1C_2$	111.5		
N_3C_4	1.154				

Atomic Charge Density Distribution from Mulliken Population Analysis

Atom Number	Charge[a]
1	0.29
2	0.06
3	-0.39
4	0.05

[a]All charges of directly bonded hydrogen atoms are summed into the carbon atoms

Total Energy (MP2/6-31G*//HF/6-31G*): -171.45879 au

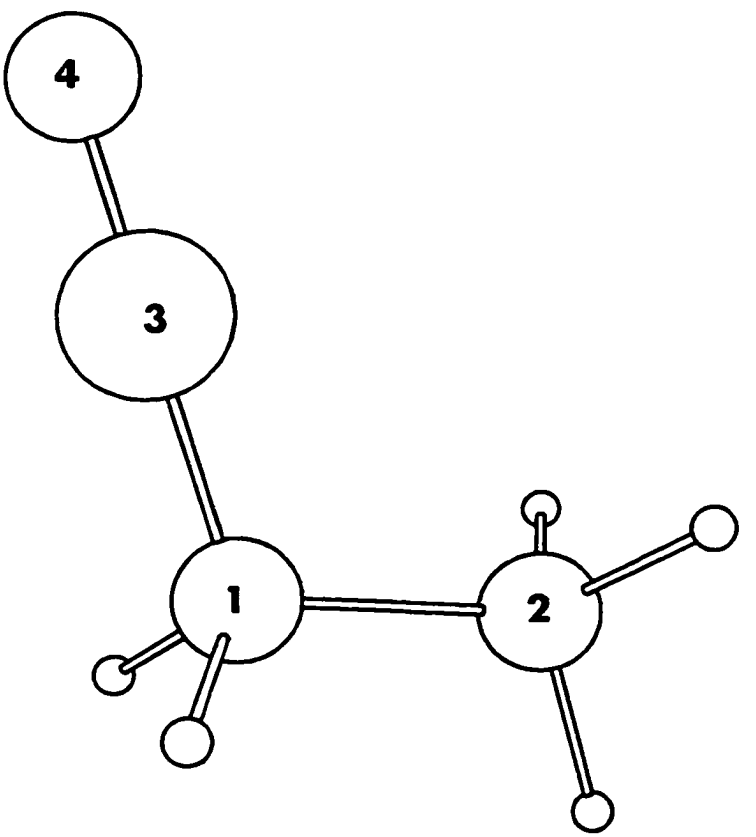

1-Isocyano-2-Methylpropane

HF/6-31G* Optimized Geometrical Parameters

Interatomic Distance (Å)		Angles (deg)		Dihedral Angles (deg)	
C_1C_2	1.534	$C_1C_2C_3$	109.2	$N_4C_1C_2C_3$	174.2
C_1N_4	1.428	$C_3C_2C_6$	111.4	$C_6C_2C_1N_4$	-62.1
C_2C_3	1.531	$N_4C_1C_2$	112.5	$C_5N_4C_1C_2$	-24.2
C_2C_6	1.530	$C_5N_4C_1$	179.5		
N_4C_5	1.154				

Atomic Charge Density Distribution from Mulliken Population Analysis

Atom Number	Charge[a]
1	0.31
2	0.01
3	0.03
4	-0.40
5	0.03
6	0.02

[a]All charges of directly bonded hydrogen atoms are summed into the carbon atoms

Total Energy (MP2/6-31G*//HF/6-31G*): -249.79364 au

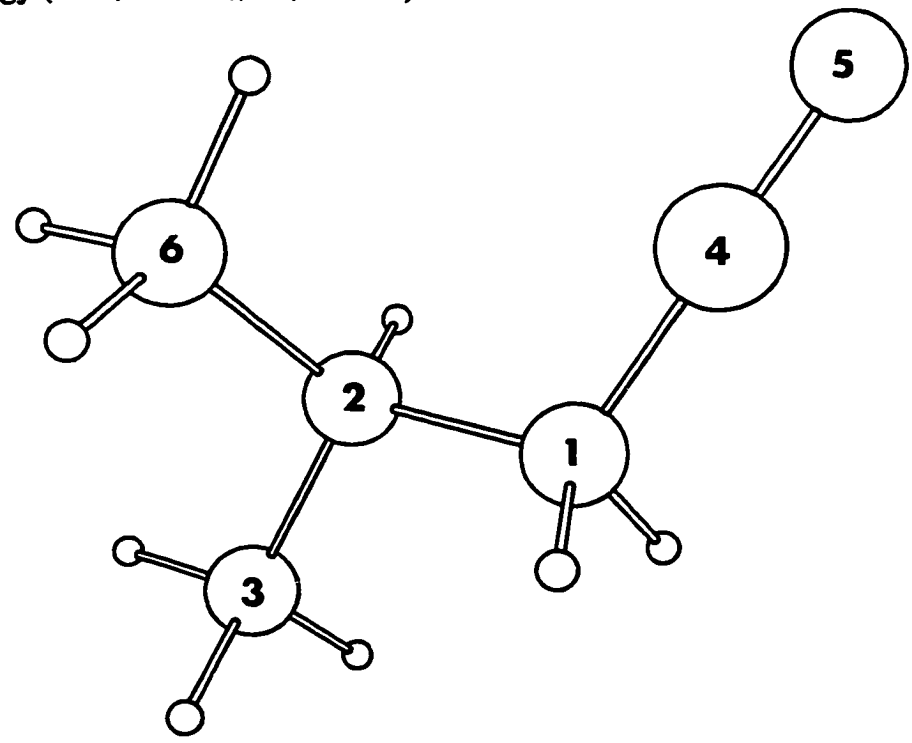

2-Isocyano-2-Methylbutane

HF/6-31G* Optimized Geometrical Parameters

Interatomic Distance (Å)		Angles (deg)		Dihedral Angles (deg)	
C_1C_2	1.533	$C_1C_2C_3$	109.7	$C_1C_2C_3C_4$	178.2
C_2C_3	1.541	$C_1C_2N_5$	107.7	$C_4C_3C_2N_5$	60.8
C_2N_5	1.444	$C_1C_2C_7$	110.2	$C_7C_2C_3C_4$	-58.7
C_2C_7	1.533	$C_2C_3C_4$	116.1	$C_6N_5C_2C_3$	167.6
C_3C_4	1.528	$C_2N_5C_6$	179.7		
N_5C_6	1.154				

Atomic Charge Density Distribution from Mulliken Population Analysis

Atom Number	Charge[a]
1	0.07
2	0.13
3	0.05
4	0.03
5	-0.38
6	0.02
7	0.07

[a]All charges of directly bonded hydrogen atoms are summed into the carbon atoms

Total Energy (MP2/6-31G*//HF/6-31G*): -288.96735 au

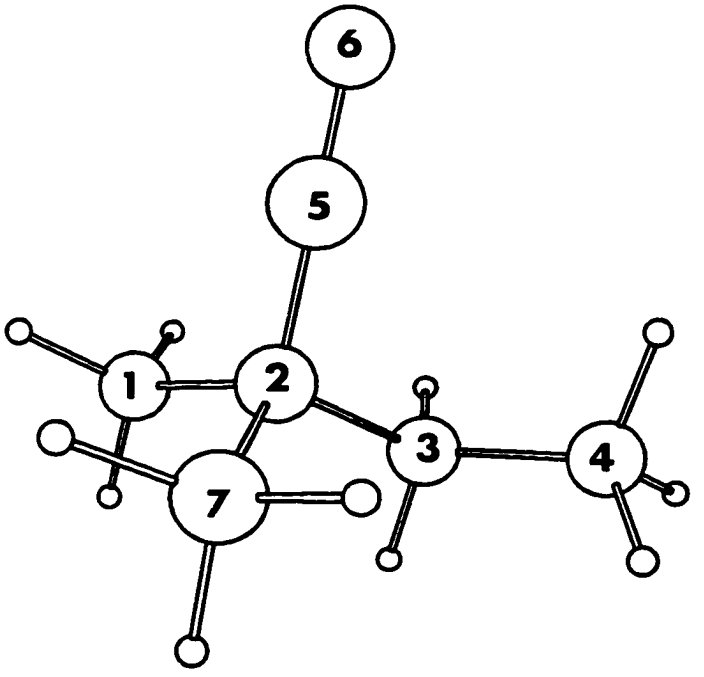

2-Isocyano-3-Methylbutane

HF/6-31G* Optimized Geometrical Parameters

Interatomic Distance (Å)		Angles (deg)		Dihedral Angles (deg)	
C_1C_2	1.529	$C_1C_2C_3$	114.4	$C_1C_2C_3C_4$	172.1
C_2C_3	1.543	$C_1C_2N_5$	109.2	$C_1C_2C_3C_7$	-62.1
C_2N_5	1.437	$C_2C_3C_4$	111.1	$C_1C_2N_5C_6$	3.3
C_3C_4	1.531	$C_2C_3C_7$	113.5	$N_5C_2C_3C_4$	-63.7
C_3C_7	1.531	$C_2N_5C_6$	179.4		
N_5C_6	1.154				

Atomic Charge Density Distribution from Mulliken Population Analysis

Atom Number	Charge[a]
1	0.06
2	0.23
3	0.01
4	0.03
5	-0.39
6	0.03
7	0.03

[a]All charges of directly bonded hydrogen atoms are summed into the carbon atoms

Total Energy (MP2/6-31G*//HF/6-31G*): -288.96373 au

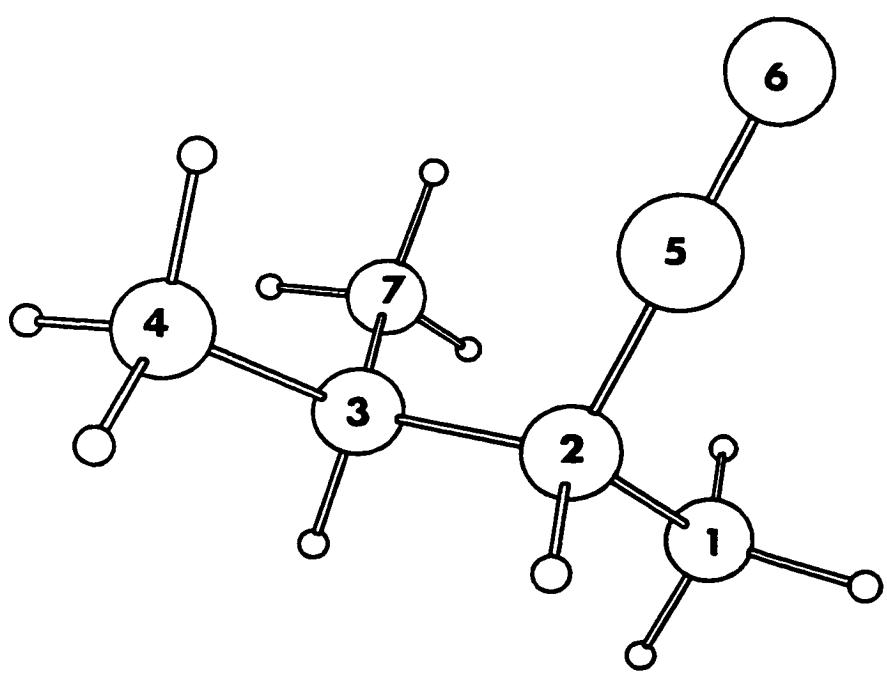

2-Isocyanopropane

HF/6-31G* Optimized Geometrical Parameters

Interatomic Distance (Å)		Angles (deg)		Dihedral Angles (deg)	
C_1C_2	1.527	$C_1C_2C_3$	112.7	$C_1C_2N_4C_5$	62.6
C_2C_3	1.527	$C_1C_2N_4$	109.6	$C_3C_2N_4C_5$	-61.6
C_2N_4	1.436	$C_2N_4C_5$	179.4		
N_4C_5	1.154				

Atomic Charge Density Distribution from Mulliken Population Analysis

Atom Number	Charge[a]
1	0.06
2	0.22
3	0.06
4	-0.39
5	0.04

[a]All charges of directly bonded hydrogen atoms are summed into the carbon atoms

Total Energy (MP2/6-31G*//HF/6-31G*): -210.62961 au

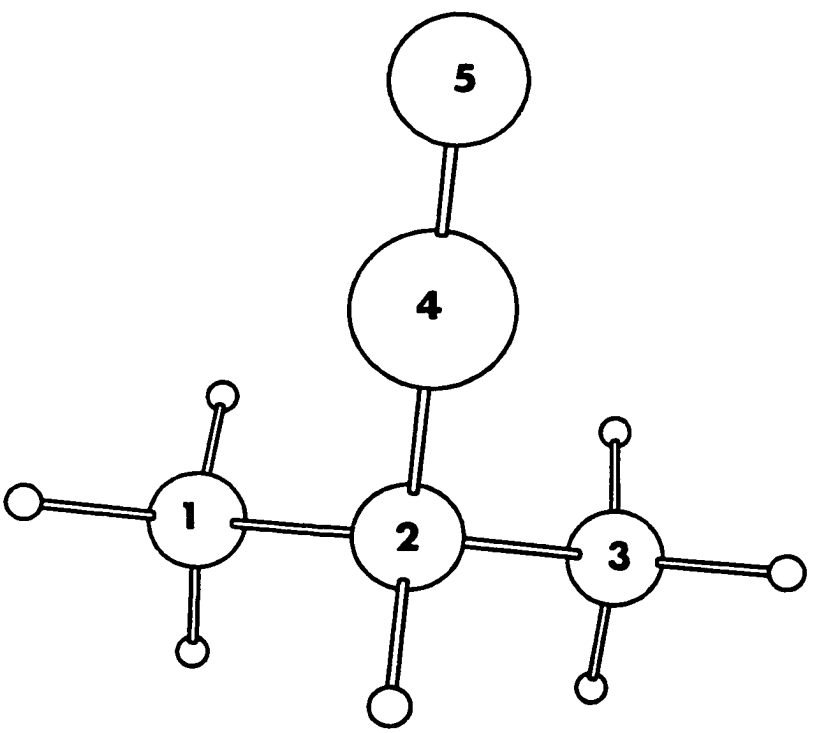

Appendix VI

Selected Geometrical Parameters, Charge and Spin Density Distributions for Alkyl Radicals

2-Methyl-2-Butenyl Radical

HF/6-31G* Optimized Geometrical Parameters

Interatomic Distance (Å)		Angles (deg)		Dihedral Angles (deg)	
C_1C_2	1.390	$C_1C_2C_3$	120.7	$C_1C_2C_3C_4$	-179.9
C_2C_3	1.402	$C_1C_2C_5$	119.6	$C_5C_2C_3C_4$	0.1
C_2C_5	1.515	$C_2C_3C_4$	124.6		
C_3C_4	1.505				

Atomic Charge and Spin Density Distribution from Mulliken Population Analysis

Atom Number	Charge[a]	Spin[a]
1	-0.06	0.86
2	0.09	-0.80
3	-0.02	0.96
4	0.00	-0.06
5	0.00	0.04

[a]All charge and spin densities of directly bonded hydrogen atoms are summed into the carbon atoms

Total Energy (MP2/6-31G*//HF/6-31G*): -195.16179 au

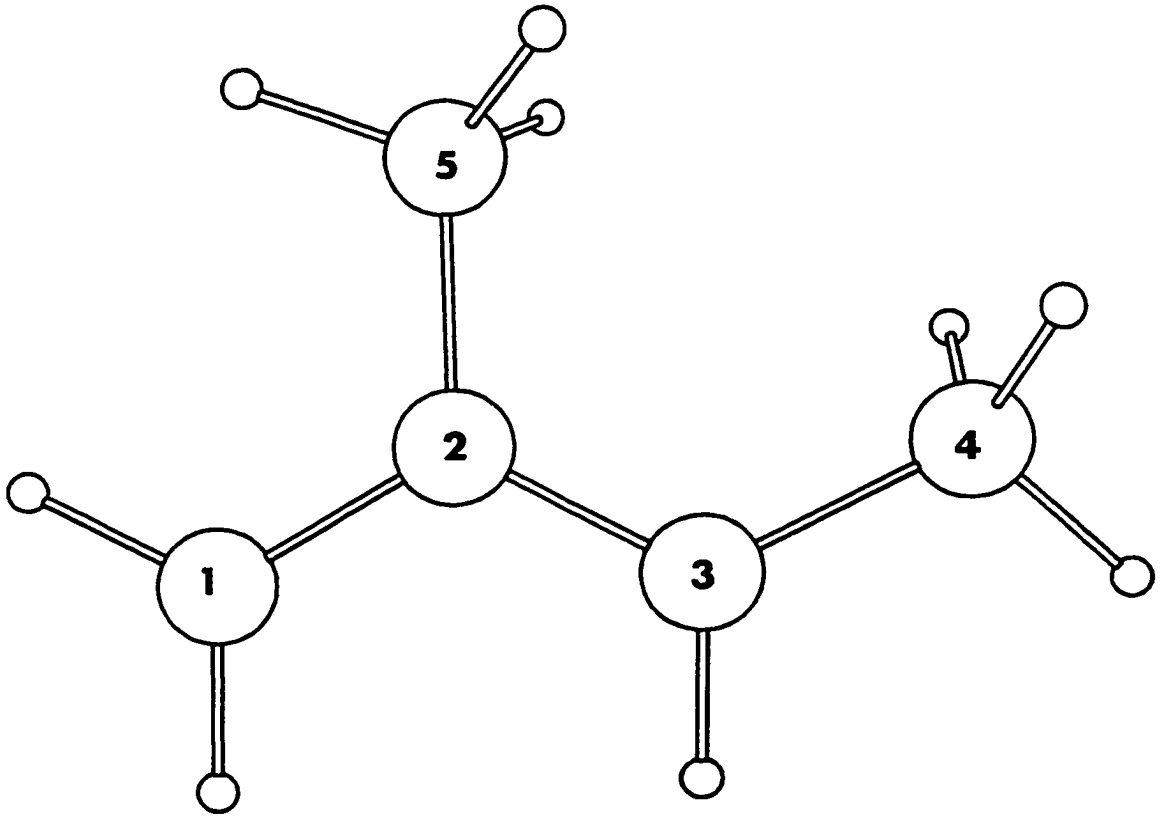

3-Methyl-2-Butenyl Radical

HF/6-31G* Optimized Geometrical Parameters

Interatomic Distance (Å)		Angles (deg)		Dihedral Angles (deg)	
C_1C_2	1.391	$C_1C_2C_3$	127.9	$C_1C_2C_3C_4$	180.0
C_2C_3	1.396	$C_2C_3C_4$	120.5	$C_1C_2C_3C_5$	0.0
C_3C_4	1.507	$C_5C_3C_4$	115.5		
C_3C_5	1.506				

Atomic Charge and Spin Density Distribution from Mulliken Population Analysis

Atom Number	Charge[a]	Spin[a]
1	-0.04	0.87
2	0.00	-0.75
3	0.05	0.99
4	-0.01	-0.05
5	0.00	-0.06

[a]All charge and spin densities of directly bonded hydrogen atoms are summed into the carbon atoms

Total Energy (MP2/6-31G*//HF/6-31G*): -195.16436 au

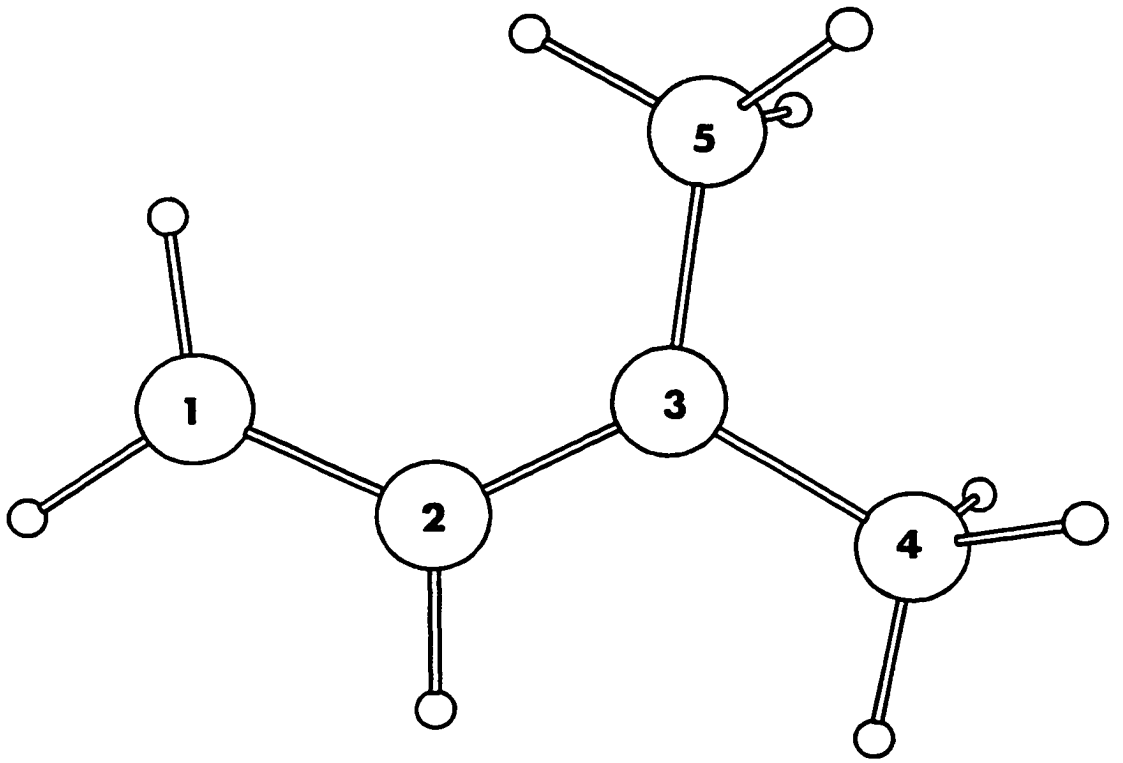

1,1,3-Trimethyl-2-Butenyl Radical

HF/6-31G* Optimized Geometrical Parameters

Interatomic Distance (Å)		Angles (deg)		Dihedral Angles (deg)	
C_1C_2	1.399	$C_1C_2C_3$	132.0	$C_1C_2C_3C_4$	-174.0
C_1C_5	1.509	$C_2C_3C_4$	119.2	$C_1C_2C_3C_7$	5.6
C_1C_6	1.510	$C_2C_3C_7$	125.9	$C_5C_1C_2C_3$	-174.0
C_2C_3	1.399	$C_5C_1C_2$	119.2	$C_6C_1C_2C_3$	5.6
C_3C_4	1.509	$C_5C_1C_6$	114.9		
C_3C_7	1.510				

Atomic Charge and Spin Density Distribution from Mulliken Population Analysis

Atom Number	Charge[a]	Spin[a]
1	0.05	1.00
2	-0.06	-0.78
3	0.05	1.00
4	-0.01	-0.06
5	-0.02	-0.06
6	-0.01	-0.06
7	-0.02	-0.06

[a]All charge and spin densities of directly bonded hydrogen atoms are summed into the carbon atoms

Total Energy (MP2/6-31G*//HF/6-31G*): -273.49859 au

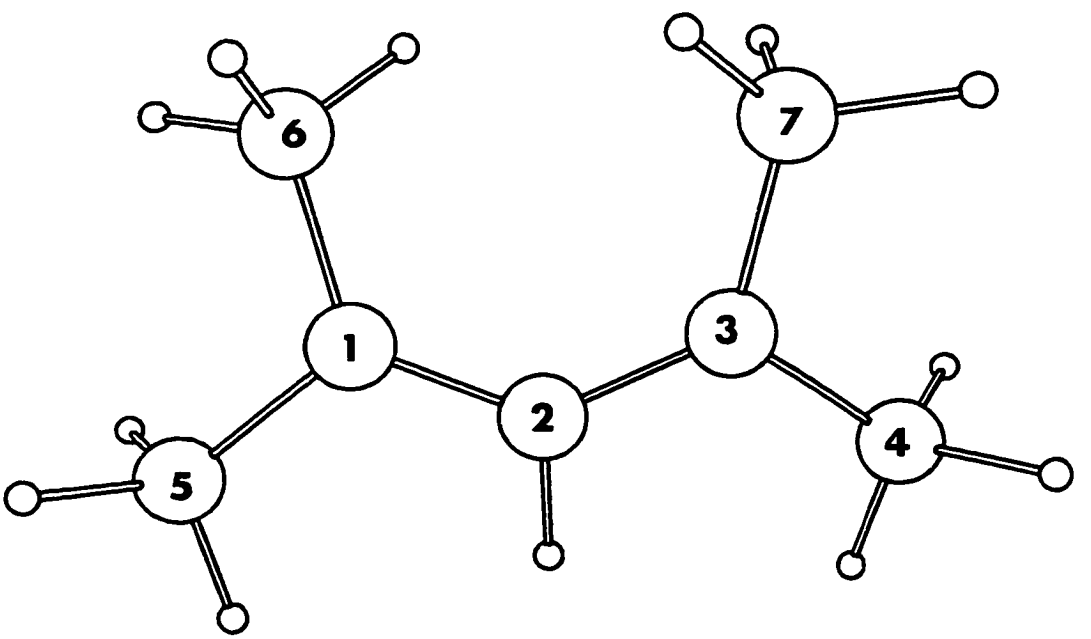

1,1-Dimethyl-2-Butenyl Radical

HF/6-31G* Optimized Geometrical Parameters

Interatomic Distance (Å)		Angles (deg)		Dihedral Angles (deg)	
C_1C_2	1.399	$C_1C_2C_3$	128.1	$C_1C_2C_3C_4$	180.0
C_1C_5	1.507	$C_2C_3C_4$	123.4	$C_5C_1C_2C_3$	180.0
C_1C_6	1.506	$C_2C_1C_6$	124.3	$C_6C_1C_2C_3$	0.0
C_2C_3	1.392	$C_5C_1C_6$	115.3		
C_3C_4	1.502				

Atomic Charge and Spin Density Distribution from Mulliken Population Analysis

Atom Number	Charge[a]	Spin[a]
1	0.05	1.00
2	-0.03	-0.76
3	0.00	0.94
4	-0.01	-0.06
5	0.00	-0.06
6	-0.01	-0.06

[a]All charge and spin densities of directly bonded hydrogen atoms are summed into the carbon atoms

Total Energy (MP2/6-31G*//HF/6-31G*): -234.33393 au

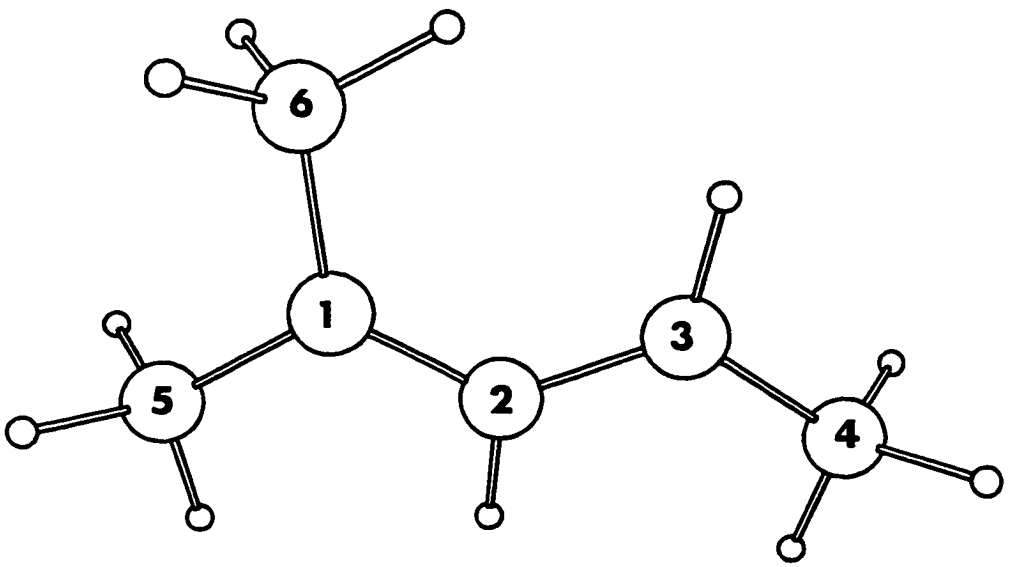

2-Butenyl Radical

HF/6-31G* Optimized Geometrical Parameters

Interatomic Distance (Å)		Angles (deg)		Dihedral Angles (deg)	
C_1C_2	1.391	$C_1C_2C_3$	124.8	$C_1C_2C_3C_4$	180.0
C_2C_3	1.391	$C_2C_3C_4$	124.3		
C_3C_4	1.501				

Atomic Charge and Spin Density Distribution from Mulliken Population Analysis

Atom Number	Charge[a]	Spin[a]
1	-0.03	0.87
2	0.03	-0.74
3	0.01	0.93
4	0.00	-0.06

[a]All charge and spin densities of directly bonded hydrogen atoms are summed into the carbon atoms

Total Energy (MP2/6-31G*//HF/6-31G*): -155.99458 au

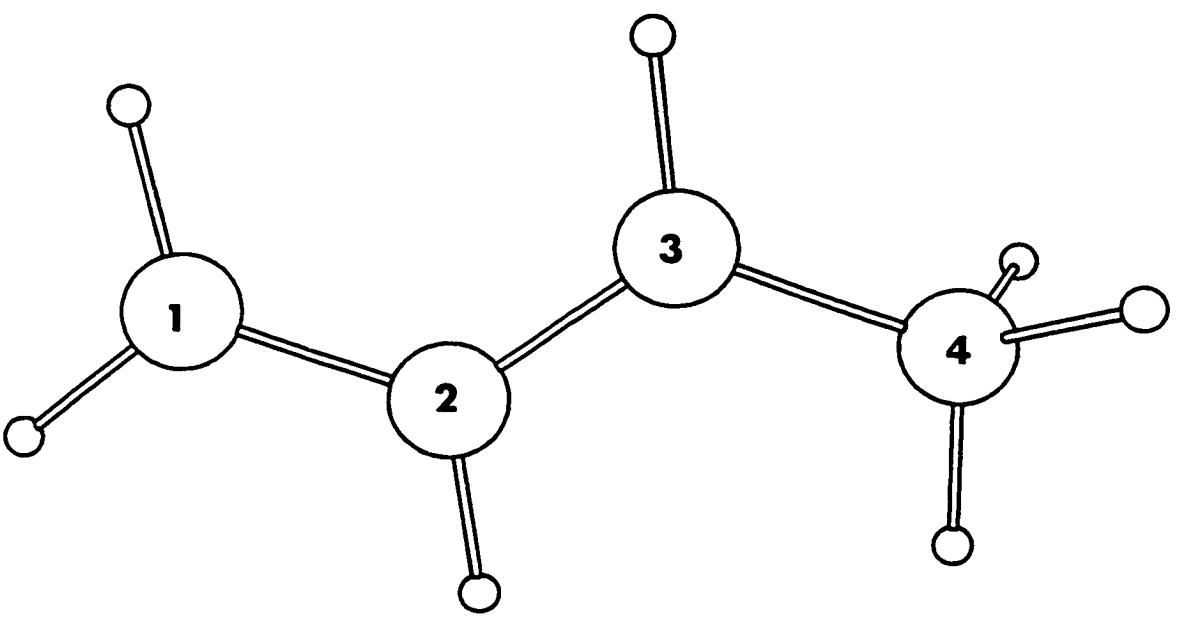

2-Methyl-1-Propyl Radical

HF/6-31G* Optimized Geometrical Parameters

Interatomic Distance (Å)		Angles (deg)		Dihedral Angles (deg)	
C_1C_2	1.505	$C_1C_2C_3$	111.2	$C_1C_2C_3C_4$	-124.3
C_2C_3	1.532	$C_1C_2C_4$	111.3		
C_2C_4	1.539				

Atomic Charge and Spin Density Distribution from Mulliken Population Analysis

Atom Number	Charge[a]	Spin[a]
1	-0.01	1.07
2	0.00	-0.13
3	0.00	0.01
4	0.00	0.05

[a]All charge and spin densities of directly bonded hydrogen atoms are summed into the carbon atoms

Total Energy (MP2/6-31G*//HF/6-31G*): -157.16933 au

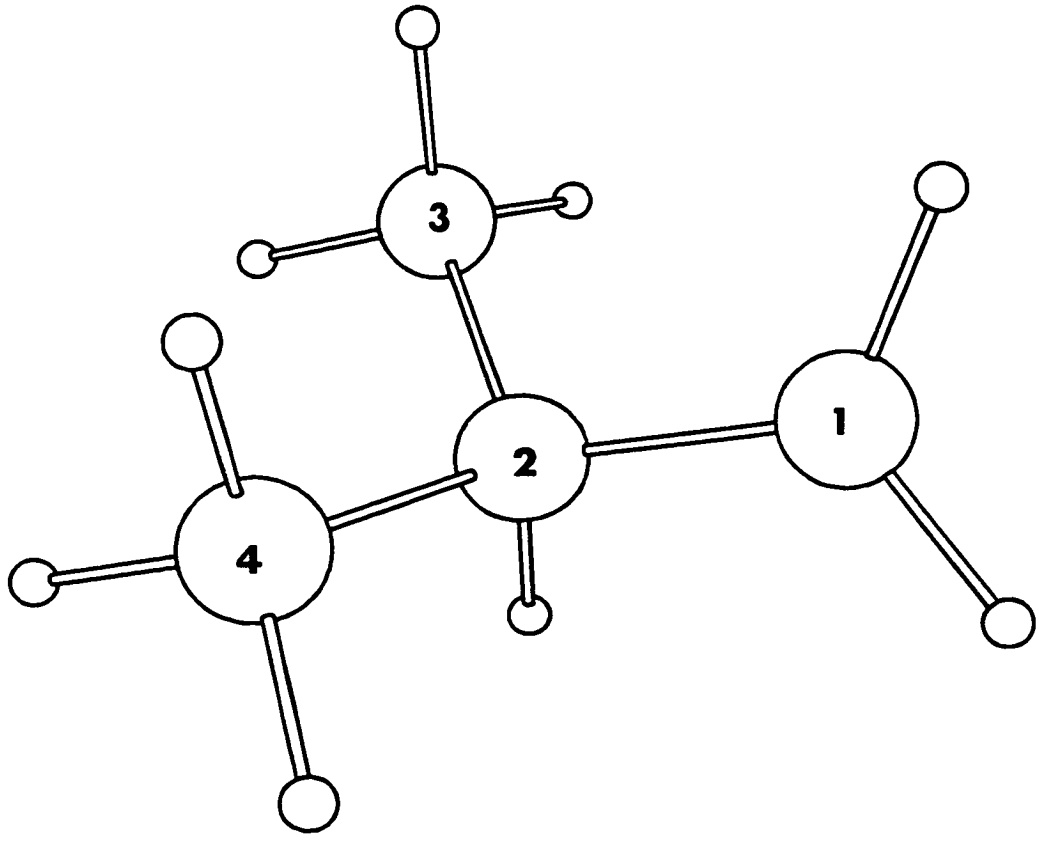

2-Methyl-2-Propyl Radical

HF/6-31G* Optimized Geometrical Parameters

Interatomic Distance (Å)		Angles (deg)		Dihedral Angles (deg)	
C_1C_2	1.504	$C_1C_2C_3$	117.9	$C_1C_2C_3C_4$	-151.8
C_2C_3	1.504	$C_1C_2C_4$	117.9		
C_2C_4	1.504	$C_3C_2C_4$	117.9		

Atomic Charge and Spin Density Distribution from Mulliken Population Analysis

Atom Number	Charge[a]	Spin[a]
1	-0.02	-0.06
2	0.05	1.18
3	-0.02	-0.06
4	-0.02	-0.06

[a]All charge and spin densities of directly bonded hydrogen atoms are summed into the carbon atoms

Total Energy (MP2/6-31G*//HF/6-31G*): -157.17849 au

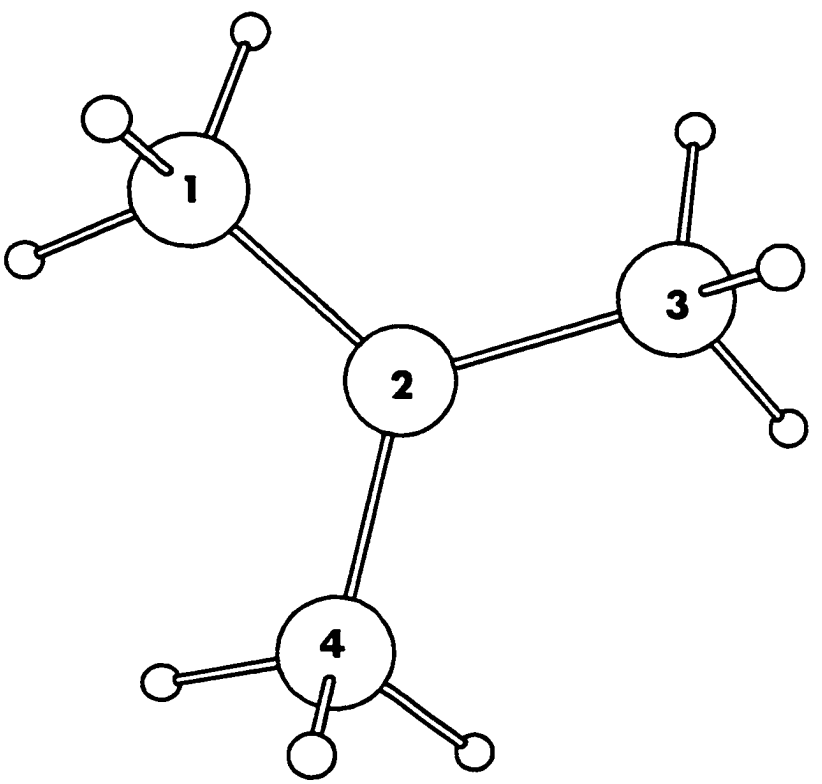

Ethyl Radical

HF/6-31G* Optimized Geometrical Parameters

Interatomic Distance (Å)	
C_1C_2	1.498

Atomic Charge and Spin Density Distribution from Mulliken Population Analysis

Atom Number	Charge[a]	Spin[a]
1	-0.01	1.07
2	-0.01	-0.07

[a]All charge and spin densities of directly bonded hydrogen atoms are summed into the carbon atoms

Total Energy (MP2/6-31G*//HF/6-31G*): -78.8.728 au

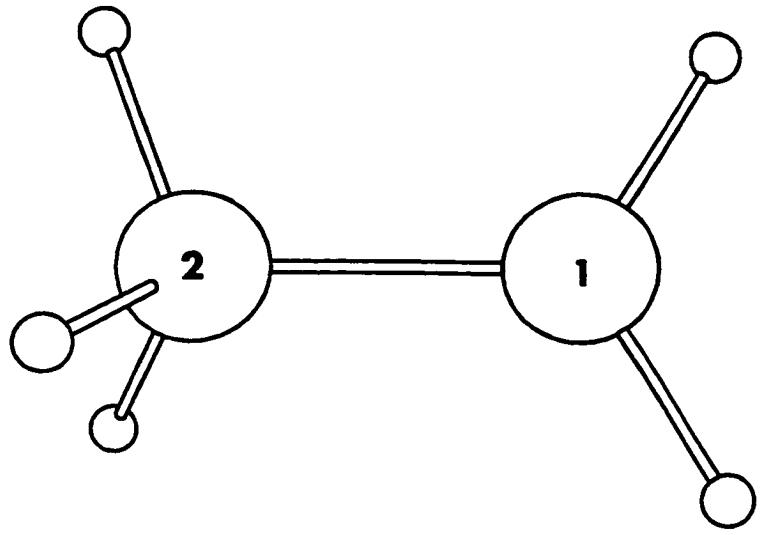

3-Methyl-2-Butyl Radical

HF/6-31G* Optimized Geometrical Parameters

Interatomic Distance (Å)		Angles (deg)		Dihedral Angles (deg)	
C_1C_2	1.501	$C_1C_2C_3$	121.6	$C_1C_2C_3C_4$	79.6
C_2C_3	1.507	$C_2C_3C_4$	111.1	$C_1C_2C_3C_5$	-159.1
C_3C_5	1.539	$C_2C_3C_5$	111.6		
C_3C_4	1.532	$C_4C_3C_5$	110.6		

Atomic Charge and Spin Density Distribution from Mulliken Population Analysis

Atom Number	Charge[a]	Spin[a]
1	-0.01	-0.07
2	0.02	1.14
3	-0.01	-0.14
4	0.00	0.01
5	0.00	0.05

[a]All charge and spin densities of directly bonded hydrogen atoms are summed into the carbon atoms

Total Energy (MP2/6-31G*//HF/6-31G*): -196.33939 au

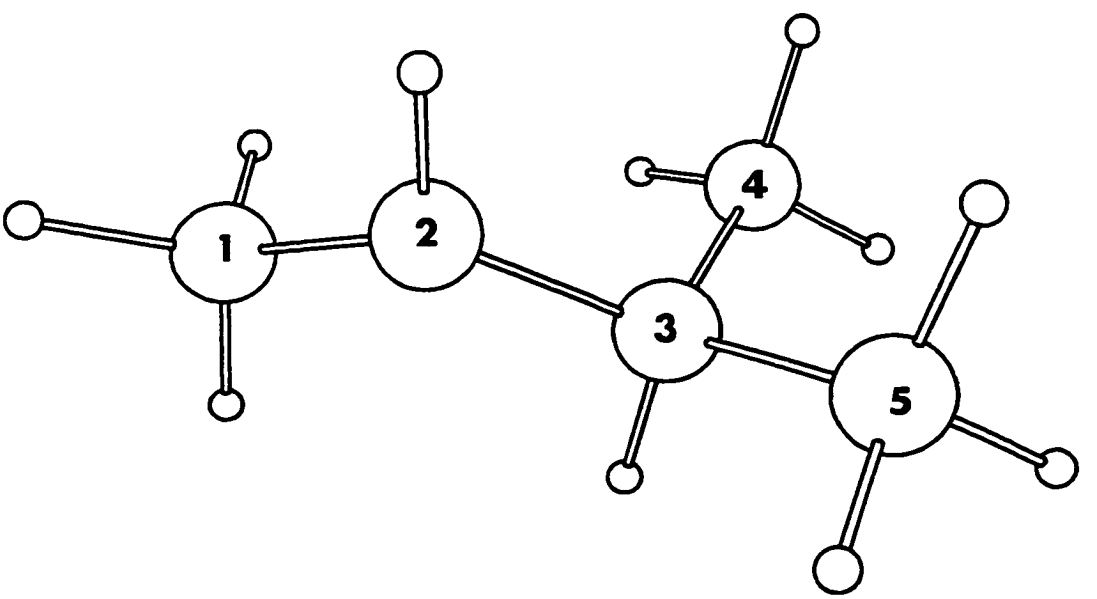

2-Methyl-2-Butyl Radical

HF/6-31G* Optimized Geometrical Parameters

Interatomic Distance (Å)		Angles (deg)		Dihedral Angles (deg)	
C_1C_2	1.504	$C_1C_2C_3$	118.8	$C_1C_2C_3C_4$	77.5
C_2C_3	1.508	$C_1C_2C_5$	117.6	$C_5C_2C_3C_4$	-77.5
C_2C_5	1.504	$C_2C_3C_4$	113.9		
C_3C_4	1.539				

Atomic Charge and Spin Density Distribution from Mulliken Population Analysis

Atom Number	Charge[a]	Spin[a]
1	-0.02	-0.06
2	0.04	1.19
3	-0.01	-0.12
4	0.00	0.05
5	-0.02	-0.06

[a]All charge and spin densities of directly bonded hydrogen atoms are summed into the carbon atoms

Total Energy (MP2/6-31G*//HF/6-31G*): -196.34313 au

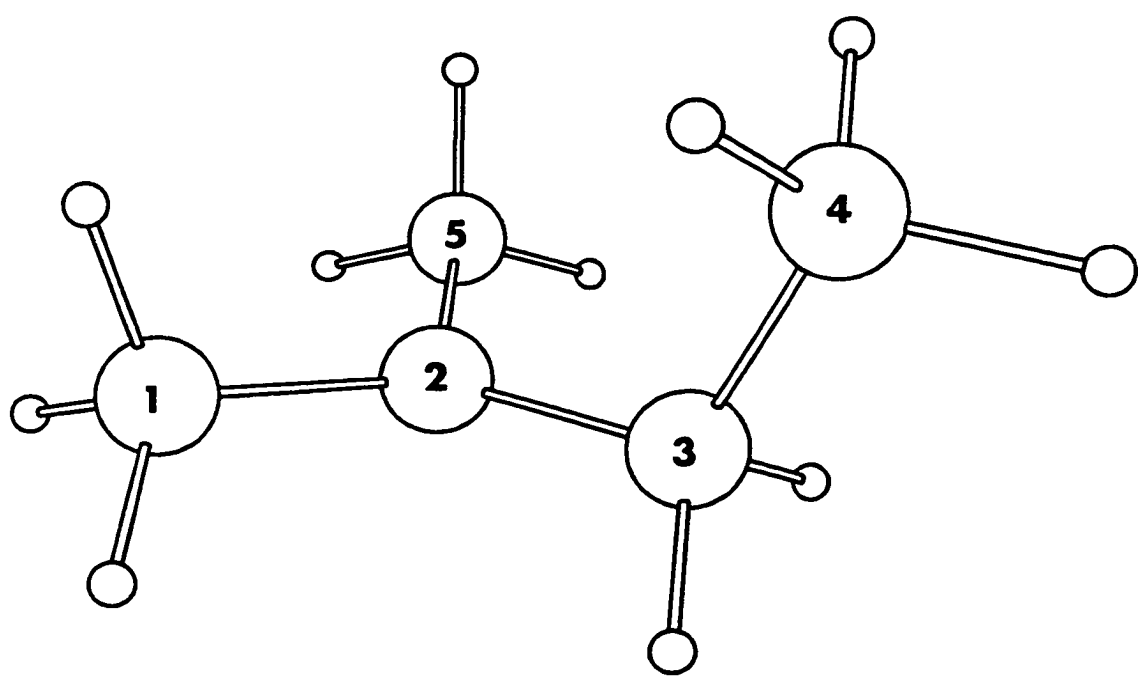

2-Propyl Radical

HF/6-31G* Optimized Geometrical Parameters

Interatomic Distance (Å)		Angles (deg)	
C_1C_2	1.500	$C_1C_2C_3$	120.3
C_2C_3	1.500		

Atomic Charge and Spin Density Distribution from Mulliken Population Analysis

Atom Number	Charge[a]	Spin[a]
1	-0.01	-0.07
2	0.02	1.13
3	-0.01	-0.07

[a]All charge and spin densities of directly bonded hydrogen atoms are summed into the carbon atoms

Total Energy (MP2/6-31G*//HF/6-31G*): -118.00703 au

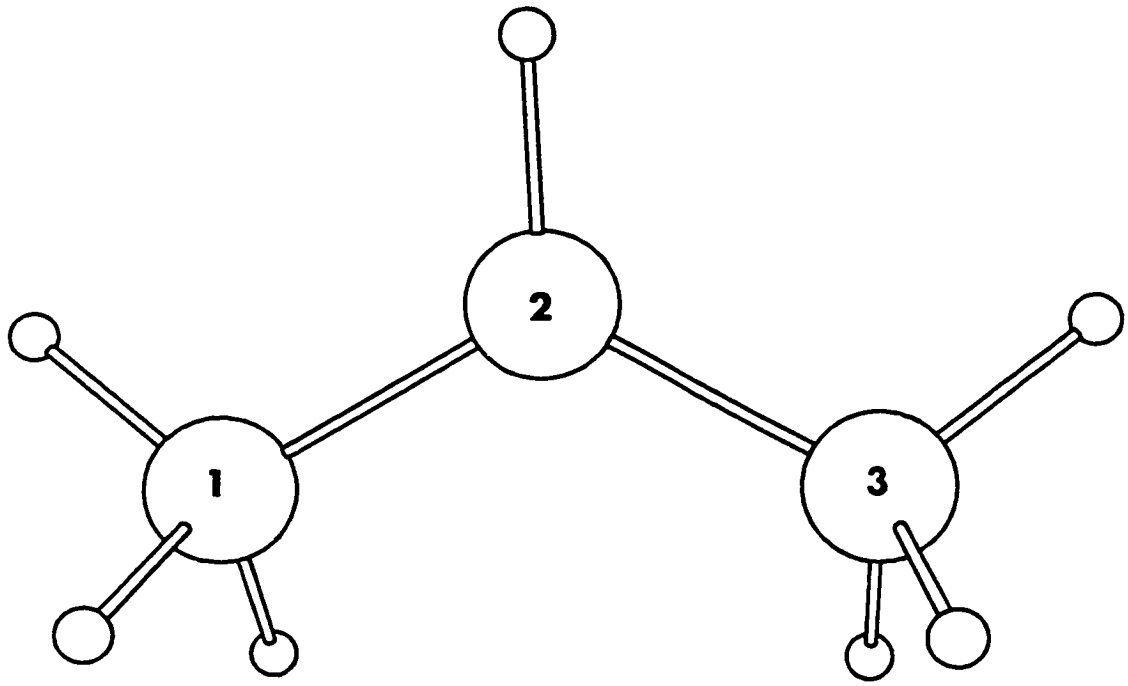

References

1. A.J. Bard, A. Ledwith and H.J. Shine. Adv. Phys. Org. Chem. **13**, 155 (1976).

2. (a) I.C. Lewis and L.S. Singer. J. Chem. Phys. **43**, 2712 (1965).
   (b) I.C. Lewis and L.S. Singer. J. Chem. Phys. **44**, 2082 (1966).
   (c) R.M. Dessau. J. Am. Chem. Soc. **92**, 6356 (1970).

3. (a) H. Wieland. Ber. **40**, 4260 (1907).
   (b) H. Wieland and E. Wecker. Ber. **43**, 699 (1910).

4. A.J. Fry. Synthetic Organic Electrochemistry. Harper and Row Publishers Inc., New York. 1972.

5. F.W. McLafferty. Interpretation of Mass Spectra 3rd ed. University Science Books, Mill Valley, California. 1980.

6. (a) M.A. Fox and M. Chanon (*editors*). Photoinduced Electron Transfer, Parts A-D. Elsevier Science Pub. Co., Amsterdam. 1988.
   (b) J. Mattay (*editor*). Topics in Current Chemistry: Photoinduced Electron Transfer I-V. **156, 158, 159, 163, 168**. Springer-Verlag, Berlin. 1990-1993.

7. (a) F. Müller and J. Mattay. Chem. Rev. **93**, 99 (1993).
   (b) A. Albini, M. Mella and M. Freccero. Tetrahedron. **50**, 575 (1994).
   (c) S. Hintz, A. Heidbreder and J. Mattay. *In* Topics in Current Chemistry: Electron Transfer II. *Edited by* J. Mattary. **177**. Springer-Verlag, Berlin. 1996. p 77.

8. J.S. Connolly (*Editor*). Photochemical Conversion and Storage of Solar Energy. Academic, New York. 1981.

9. (a) M.A. Fox and M.T. Dulay. Chem. Rev. **93**, 341 (1993).
   (b) O. Legrini, E. Oliveros and A.M. Braun. Chem. Rev. **93**, 671 (1993).

10. M.R. Wasielewski. Chem. Rev. **92**, 435 (1992).

11. R. Bonnett. Chem. Soc. Rev. **24**, 19 (1995).

12. D. Rehm and A. Weller. Isr. J. Chem. **8**, 259 (1970).

13. (a) B.E. Goodson and G.B. Schuster. J. Am. Chem. Soc. **106**, 7254 (1984).
   (b) B.E. Goodson and G.B. Schuster. Tetrahedron Lett. **27**, 3123 (1986).

14. (a) M.A. Fox. Chem. Rev. **79**, 253 (1979).
   (b) E. Krogh and P. Wan. *In* Photoinduced Electron Transfer, Topics in Current Chemistry. *Edited by* J. Mattay. **156**. Springer-Verlag, Berlin. 1990. p. 93.

15. (a) R.A. Marcus. Ann. Rev. Phys. Chem. **15**, 155 (1964).
   (b) R.A. Marcus. J. Chem. Phys. **43**, 679 (1965).
   (c) J. Ulstrup and J. Jortner. J. Chem. Phys. **63**, 4358 (1975).
   (d) T. Kakitani and N. Mataga. Chem. Phys. **93**, 381 (1985).

16. (a) H.D. Roth and M.L.M. Schilling. J. Am. Chem. Soc. **102**, 4303 (1980).
(b) H. Suzuki, K. Ogawa, T. Shida and A. Kira. Bull. Chem. Soc. Jpn. **56**, 66 (1983).
(c) T. Bally, S. Nitsche, K. Roth and E. Haselbach. J. Phys. Chem. **89**, 2528 (1985).
(d) T. Majima, C. Pac and H. Sakurai. Chem. Lett. 1133 (1979).

17. (a) T.R. Evans, R.W. Wake and M.M. Sifain. Tetrahedron Lett. 701 (1973).
(b) N.J. Peacock and G.B. Schuster. J. Am. Chem. Soc. **105**, 3632(1983).
(c) H.D. Roth, M.L.M. Schilling and K. Raghavachari. J. Am. Chem. Soc. **106**, 253 (1984).
(d) T. Miyashi, K. Wakamatsu, T. Akiya, K. Kikuchi and T. Mukai. J. Am. Chem. Soc. **109**, 5270 (1987).

18. (a) D.R. Arnold and S.A. Mines. Can. J. Chem. **65**, 2312 (1987).
(b) D.R. Arnold and S.A. Mines. Can. J. Chem. **67**, 689 (1989).
(c) A.L. Perrott and D.R. Arnold. Can. J. Chem. **70**, 272 (1992).

19. (a) A.L. Perrott, H.J.P. de Lijser, and D.R. Arnold. Can J. Chem. **75**, 184 (1997).
(b) D.R. Arnold, X. Du, and H.J.P. de Lijser. Can. J. Chem. **73**, 522 (1995).
(c) D.R. Arnold and X. Du. J. Am. Chem. Soc. **111**, 7666 (1989).

20. (a) D.R. Arnold, K.A. McManus and X. Du. Can. J. Chem. **72**, 415 (1994).
(b) D.A. Connor, D.R. Arnold, P.K. Bakshi and T.S. Cameron. Can J. Chem. **73**, 762 (1995).
(c) K.A. McManus and D.R. Arnold. Can. J. Chem. **73**, 2158 (1995).
(d) D.R. Arnold, D.A. Connor, K.A. McManus, P.K. Bakshi and T.S. Cameron. Can. J. Chem. **74**, 602 (1996).

21. (a) R.A. Neunteufel and D.R. Arnold. J. Am. Chem. Soc. **95**, 4080 (1973).
(b) R.M. Borg, D.R. Arnold and T.S. Cameron. Can. J. Chem. **62**, 1785 (1984).
(c) D.R. Arnold and M.S. Snow. Can. J. Chem. **66**, 3012 (1988).
(d) D.R. Arnold, X. Du and K. M. Henseleit. Can. J. Chem. **69**, 839 (1991).
(e) K. McMahon and D. R. Arnold. Can. J. Chem. **71**, 450 (1993).
(f) K.A. McManus and D.R. Arnold. Can. J. Chem. **72**, 2291 (1994).
(g) D.R. Arnold, X. Du and J. Chen. Can. J. Chem. **73**, 307 (1995).

22. (a) H.D. Roth. Acc. Chem. Res. **20**, 343 (1987).
(b) N.L. Bauld, D.J. Bellville, R. Pabon, R. Chelsky and G. Green. J. Am. Chem. Soc. **105**, 2378 (1983).
(c) R.A. Pabon and N.L. Bauld. J. Am. Chem. Soc. **106**, 1145 (1984).
(d) M. Kojima, A. Kakehi, A. Ishida and S. Takamuku. J. Am .Chem. Soc. **118**, 2612 (1996).
(e) F.D. Lewis and M. Kojima. J. Am. Chem. Soc. **110**, 8664 (1988).

23. (a) W. Markovnikov. Ann. Chem. Pharm. **153**, 256 (1870).
(b) H.J. Lucas and A.Y. Jameson. J. Am. Chem. Soc. **46**, 2475 (1924).
(c) J. March. Advanced Organic Chemistry 4th ed. Wiley-Interscience, Toronto. 1992. pp.750-753.

24. J. March. Advanced Organic Chemistry 4th ed. Wiley-Interscience, Toronto. 1992. p. 763.

25. J.A. Marshall. Acc. Chem. Res. **2**, 33 (1969).

26. C.M. Sharts and W.A. Sheppard. Org. React. **21**, 125 (1974).

27. For reviews on fluorinating agents see:
(a) A. Haas and M. Lieb. Chimia. **39**, 134 (1985).
(b) W. Dmowski. J. Fluorine Chem. **32**, 255 (1986).
(c) H. Vyplel. Chimia. **39**, 305 (1985).
(c) O.A. Mascaretti. Aldrichimica Acta. **26**, 47 (1993).
(d) J.A. Wilkinson. Chem. Rev. **92**, 505 (1992).

28. (a) M. Maeda, M. Abe and M. Kojima. J. Fluorine Chem. **34**, 337 (1987).
(b) F. Camps, E. Chamorro, V. Gasol and A. Guerrero. J. Org. Chem. **54**, 4294 (1989).

29. S. Stavber, M. Zupan, A.J. Poss and G.A. Shia. Tetrahedron Lett. **36**, 6769 (1995).

30. (a) S. Stavber and M. Zupan. J. Org. Chem. **52**, 919 (1987).
(b) N.S. Zefirov, V.V. Zhdankin, A.S. Koz'min, A.A. Fainzilberg, A.A. Gakh, B.I. Ugrak and S.V. Romaniko. Tetrahedron. **44**, 6505 (1988).

31. (a) M.W. Wong, A. Pross and L. Radom. J. Am. Chem. Soc. **116**, 11938 (1994).
(b) M.W. Wong, A. Pross and L. Radom. J. Am. Chem. Soc. **116**, 6284 (1994).
(c) M.W. Wong, A. Pross and L. Radom. J. Am. Chem. Soc. **115**, 11050 (1993).
(d) M.W. Wong, A. Pross and L. Radom. Isr. J. Chem. **33**, 415, (1993).
(d) K. Heberger and A. Lopata. J. Chem. Soc., Perkin Trans. 2. 91 (1995).

32. (a) J.M. Tedder and J.C. Walton. Tetrahedron. **36**, 701 (1980).
(b) J.M. Tedder. Angew. Chem. Int. Ed. Engl. **21**, 401 (1982).
(c) B. Giese. Angew. Chem. Int. Ed. Engl. **22**, 753 (1983).

33. (a) M.S. Kharasch and F.R. Mayo. J. Am. Chem. Soc. **55**, 2468 (1933).
(b) F.R. Mayo and C. Walling. Chem. Rev. **27**, 351 (1940).

34. (a) M. Fagnoni, M. Mella and A. Albini. J. Am. Chem. Soc. **117**, 7877 (1995).
(b) M. Mella, M. Fagnoni and A. Albini. J. Org. Chem. **59**, 5614 (1994).

35. (a) M. Kojima, A. Ishida, S. Takamuku, Y. Wada and S. Yanagida. Chem. Lett. 1897 (1994).
(b) Y. Inoue, T. Okano, N. Yamasaki and A. Tai. J. Chem. Soc., Chem. Commun. 718 (1993).
(c) A. Ishida, T. Uesugi and S. Takamuku. Bull. Chem. Soc. Jpn. **66**, 1580 (1993).
(d) K. Mizuno, I. Nakanishi, N. Ichinose and Y. Otsuji. Chem. Lett. 1095 (1989).
(e) A.J. Maroulis and D.R. Arnold. Synthesis. 819 (1979).

36. A.J. Maroulis, Y. Shigemitsu and D.R. Arnold. J. Am. Chem. Soc. **100**, 535 (1978).

37. (a) R. Kojima, T. Yamashita, K. Tanabe, T. Shiragami, M. Yasuda and K. Shima. J. Chem. Soc., Perkin Trans. 1. 217 (1997).
(b) M. Yasuda, T. Isami, J. Kubo, M. Mizutani, T. Yamashita and K. Shima. J. Org. Chem. **57**, 1350 (1992).
(c) T. Yamashita, K. Shiomori, M. Yasuda, K. Shima. Bull. Chem. Soc. Jpn. **64**, 366 (1991).

38. (a) L.J. Johnston and N.P. Schepp. Pure & Appl. Chem. **67**, 71 (1995).
(b) L.J. Johnston and N.P. Schepp. J. Am. Chem. Soc. **115**, 6564 (1993).

39. (a) H. Zipse. J. Am. Chem. Soc. **117**, 11798 (1995).
(b) R. Postma, P.J.A. Ruttink, B. Van Baar, J.K. Terlouw, J.L. Holmes and P.C. Burgers. Chem. Phys. Lett. **123**, 409 (1986).
(c) W.J. Bouma, R.H. Nobes and L. Radom. J. Am. Chem. Soc. **105**, 1743 (1983).
(d) B.T. Golding and L. Radom. J. Am. Chem. Soc. **98**, 6331 (1976).
(e) J. Fossey and J.-Y. Nedelec, Tetrahedron. **37**, 2967 (1981).
(f) P. George, J.P. Glusker, C.W. Bock. J. Am. Chem. Soc. **117**, 10131 (1995).

40. T. Majima, C. Pac, A. Nakasone and H. Sakurai. J. Am. Chem. Soc. **103**, 4499 (1981).

41. D.R. Arnold and X. Du. Can. J. Chem. **72**, 403 (1994).

42. (a) N. Hirota, H. Ohya-Nishiguchi, A. Oku and A. Terahara. J. Phys. Chem. **90**, 1564 (1986).
(b) O.W. Howarth and G.K. Fraenkel. J. Chem. Phys. **52**, 6258 (1970).
(c) T. Bally, K. Roth and R. Straub. J. Am. Chem. Soc. **110**, 1639 (1988).

43. S. Shaik, A.C. Reddy, A. Ioffe, J.P. Dinnocenzo, D. Danovich and J.K. Cho. J. Am. Chem. Soc. **117**, 3205 (1995).

44. For an in depth discussion of theoretical methods and basis sets see:
(a) W.J. Hehre, L. Radom, P.v.R. Schleyer and J.A. Pople. Ab Initio Molecular Orbital Theory. Wiley-Interscience, New York. 1987.
(b) P.C. Hariharan and J.A. Pople. Theor. Chim. Acta. **28**, 213 (1973).

45. G.S. Hammond. J. Am. Chem. Soc. **77**, 334 (1955).

46. T.H. Lowry and K. Schueller-Richardson. Mechanism and Theory in Organic Chemistry 3rd ed. Harper and Row Publishers Inc., New York. 1987.

47. M.J. Frisch, G.W. Trucks, H.B. Schlegel, P.M.W. Gill, B.G. Johnson, M.W. Wong, J.B. Foresman, M.A. Robb, M. Head-Gordon, E.S. Replogle, R. Gomperts, J.L. Andres, K. Raghavachari, J.S. Binkley, C. Gonzalez, R.L. Martin, D.J. Fox, D.J. Defrees, J. Baker, J.P. Stewart and J.A. Pople. *GAUSSIAN* 92/DFT, Revision F.2; Gaussian, Inc.: Pittsburgh PA, 1993.

48. C. Møller and M.S. Plesset. Phys. Rev. **46**, 618 (1934).

49. (a) H.B. Schlegel. J. Chem. Phys. **77**, 3676 (1982).
(b) H.B. Schlegel. J. Comput. Chem. **3**, 214 (1982).

50. (a) R.S. Mulliken. J. Chem. Phys. **23**, 1833 (1955).
(b) R.S. Mulliken. J. Chem. Phys. **23**, 1841 (1955).

51. International Encyclopedia of Chemical Science. D. van Nostrand Company. Inc.: Toronto. 1964. p. 622.

52. (a) G. Bieri, F. Burger, E. Heilbronner and J.P. Maier. Helv. Chim. Acta. **60**, 2213 (1977).

(b) P. Masclet, D. Grosjean, G. Mouvier and J. Dubois. J. Electron Spectrosc. Relat. Phenom. 2, 225 (1973).
(c) M. Beez, G. Bieri. H. Bock and E. Heilbronner. Helv. Chem. Acta. **56**, 1028 (1973).
(d) D. Klapstein. St. Francis Xavier University, Antigonish, NS, Canada. unpublished results.

53. (a) J. Fujisawa, T. Takayanagi, S. Sato and K. Shimokoshi. Bull. Chem. Soc. Jpn. **61**, 1527 (1988).
(b) C. Dass, D.A. Peake and M.L. Gross. Org. Mass. Spectrom. **21**, 741 (1986).

54. A.V. Cunliffe and R.K. Harris. Org. Magn. Reson. **6**, 121 (1974).

55. H. Guo and M. Karplus. J. Mol. Struct. (Theochem), **260**, 347 (1992).

56. (a) W.J. Leigh, C.J. Bradaric, C. Kerst and J. H. Banisch. Organometallics, **15**, 2246 (1996).
(b) C.J. Bradaric and W.J. Leigh. J. Am. Chem. Soc. **118**, 8971 (1996).

57. F.H. Allen and A.J. Kirby. J. Am. Chem. Soc. **106**, 6197 (1984).

58. E.R. Banks, D.W.A. Sharp and J.C. Tatlow (*Editors*). Fluorine: The First Hundred Years. Elsevier Sequoia, New York. 1986.

59. D.R. Arnold, K.A. McManus, and M.S.W. Chan. Can. J. Chem. **75**, 1055 (1997).

60. A. Skancke. "The Effect of Fluorine as a Substituent on Selected Properties of Neutral and Charged Aromatic Systems." *In* Fluorine-Containing Molecules: Structure, Reactivity, Synthesis, and Applications. *Edited by* J.F. Liebman, A. Greenberg and W.R. Dolbier. VCH Publishers, Inc., New York. 1988, Chapter 3.

61. (a) J.K. Kochi. Free Radicals, Vol. II. John Wiley & Sons, Toronto. 1973. Chapter 26.
(b) D.J. Edge and J.K. Kochi. J. Am. Chem. Soc. **94**, 6485 (1972).
(c) D.J. Edge and J.K. Kochi. Tetrahedron Lett. 2427 (1972).

62. D.P. Cox, J. Terpinski and W. Lawrynowicz. J. Org. Chem. **49**, 3216 (1984).

63. J. H. Clark. Chem. Rev. **80**, 429 (1980).

64. (a) J.M. Gerdes, R.N. Keil, A.T. Shulgin and C.A. Mathis. J. Fluorine Chem. **78**, 121 (1996).
(b) J.-I. Hayami, N. Ono and A. Kaji. Tetrahedron Lett. 2727, (1970).

65. D.R. Arnold, P.C. Wong, A. J. Maroulis and T.S. Cameron. Pure & Appl. Chem. **52**, 2609 (1980).

66. A.M. de P. Nicholas and D.R. Arnold. Can. J. Chem. **60**, 2165 (1982).

67. H.J.P. de Lijser and D.R. Arnold. Submitted to J. Org. Chem.

68. T.-L. Ho. Hard and Soft Acids and Bases Principle in Organic Chemistry. Academic Press, New York. 1977. Chapter 2.

69. (a) Y. Li and J.N.S. Evans. J. Am. Chem. Soc. **117**, 7756 (1995).
(b) F. Méndez and J.L. Gázquez. J. Am. Chem. Soc. **116**, 9298 (1994).

70. M.J. Frisch, G.W. Trucks, H.B. Schlegel, P.M.W. Gill, B.G. Johnson, M.A. Robb, J.R. Cheeseman, T. Keith, G.A. Petersson, J.A. Montgomery, K. Raghavachari, M.A. Al-Laham, V.G. Zakrzewski, J.V. Ortiz, J.B. Foresman, J. Cioslowski, B.B. Stefanov, A. Nanayakkara, M. Challacombe, C.Y. Peng, P.Y. Ayala, W. Chen, M.W. Wong, J.L. Andres, E.S. Replogle, R. Gomperts, R.L. Martin, D.J. Fox, J.S. Binkley, D.J. Defrees, J. Baker, J.P. Stewart, M. Head-Gordon, C. Gonzalez, and J.A. Pople, *GAUSSIAN* 94, Revision B.2; Gaussian, Inc., Pittsburgh PA, 1995.

71. Purchased from Harrison Research, Palo Alto, CA.

72. L.H. Harwood. Aldrichimica Acta. **18**, 25 (1985).

73. K. Nakanishi, K. Mizuno and Y. Otsuji. Bull. Chem. Soc. Jpn. **66**, 2371 (1993).

74. (a) J.A.M. Simões, A. Greenberg and J.F. Liebman (*Editors*). Energetics of Organic Free Radicals. Chapman & Hall, New York. 1996.
(b). W.A. Pryor. Frontiers of Free Radical Chemistry. Academic Press, Toronto. 1980.
(c) J.K. Kochi. Free Radicals. Vol. I and II. John Wiley & Sons, Toronto. 1973.

75. (a) D.V. Avila, K.U. Ingold, J. Lusztyk, W.R. Dolbier and H.-Q. Pan. J. Am. Chem. Soc. **115**, 1577 (1993).
(b) D.V. Avila, K.U. Ingold, J. Lusztyk, W.R. Dolbier and H.-Q. Pan. J. Org. Chem. **61**, 2027 (1996).
(c) K. Heberger, M. Walbiner and H. Fischer. Angew. Chem. Int. Ed. Engl. **31**, 635 (1992).
(d) A. Citterio, R. Sebastiano, A. Marion and R. Santi. J. Org. Chem. **56**, 5328 (1991).

76. K. Heberger, H. Fischer. Int. J. Chem. Kinet. **25**, 249 (1993).

77. D.R. Lide (*Editor*). C.R.C. Handbook of Chemistry and Physics (76th ed. 1995-1996). CRC Press, Inc. New York. 1995.

78. Y.-R Luo and S.W. Benson. J. Phys. Chem. **92**, 5255 (1988).

79. (a) Y.-R. Luo and S.W. Benson. J. Phys. Chem. **93**, 3304 (1989).
(b) Y.-R. Luo and S.W. Benson. J. Phys. Chem. **93**, 3306 (1989).
(c) Y.-R. Luo and S.W. Benson. Acc. Chem. Res. **25**, 375 (1992).

80. Y.-R Luo and S.W. Benson. J. Phys. Chem. **94**, 914 (1990).

81. N. Laurencelle and P.D. Pacey. J. Am. Chem. Soc. **115**, 625 (1993).

IMAGE EVALUATION TEST TARGET (QA-3)

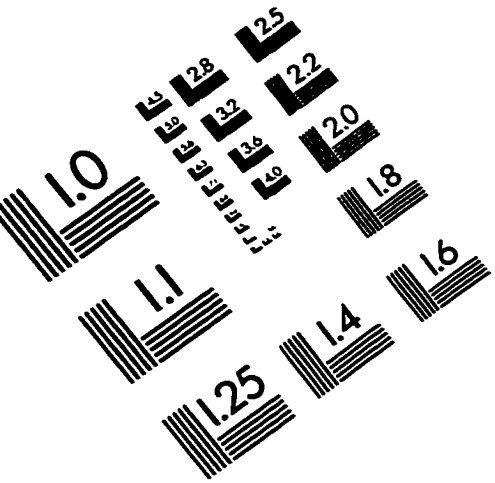

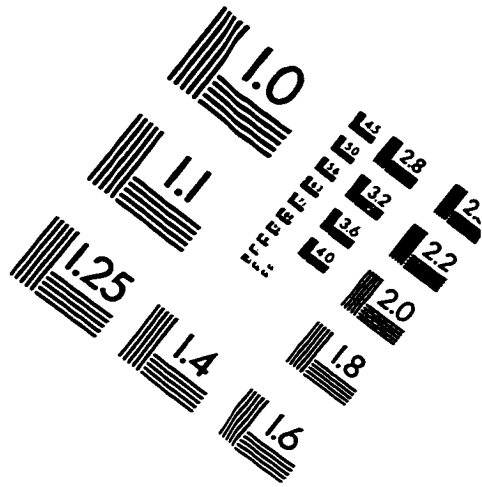

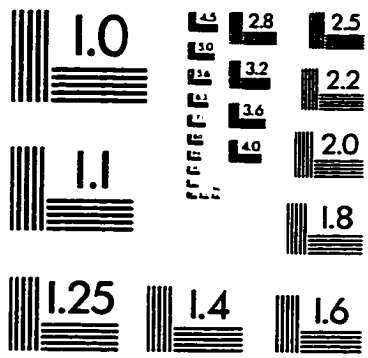

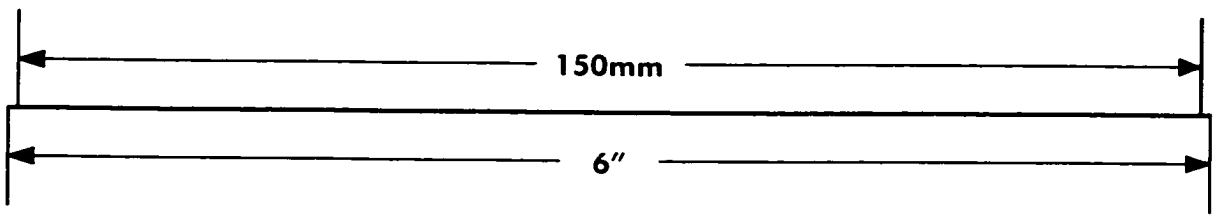

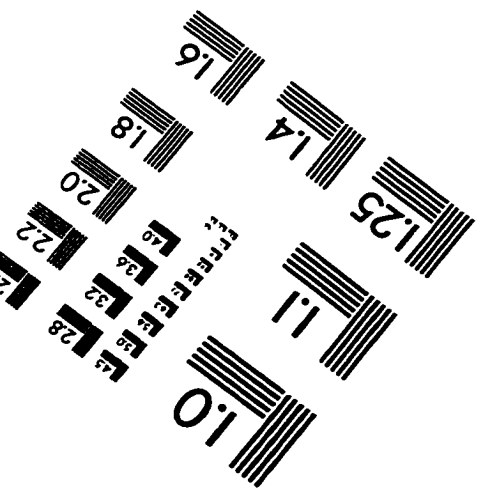

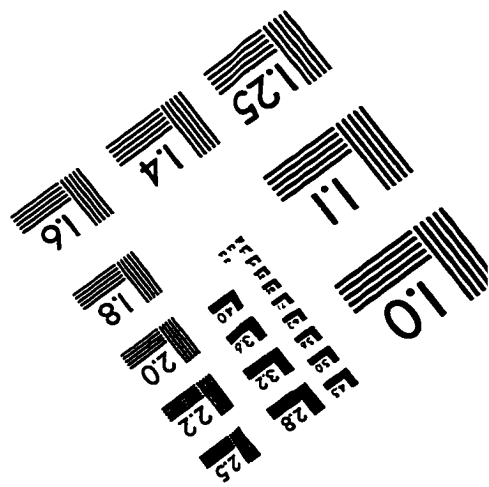

APPLIED IMAGE, Inc
1653 East Main Street
Rochester, NY 14609 USA
Phone: 716/482-0300
Fax: 716/288-5989